

# **INVESTIGATION OF ATMOSPHERIC OZONE IMPACTS OF SELECTED PESTICIDES**

Final Report to the

California Air Resources Board  
Contract No. 04-334

By

William P. L. Carter, and Irina L. Malkina

January 10, 2007

Center for Environmental Research and Technology  
College of Engineering  
University of California  
Riverside, California 92521

## ABSTRACT

An experimental and modeling study was carried out to assess the ground-level atmospheric ozone impacts of representative pesticide-related VOCs. Environmental chamber experiments were carried out to develop and evaluate mechanisms for methyl isothiocyanate (MITC), S-ethyl N,N-di-n-propyl thiocarbamate (EPTC), 1,3-dichloropropenes, kerosene, and carbon disulfide. The first four are important compounds in the California pesticide emissions inventory where ozone impact data are not available, and carbon disulfide is a known pesticide degradation product. In addition, results of previous experiments on the pesticide chloropicrin were used to evaluate an updated mechanism for this compound. Chamber data were also used to derive rate constants for the reactions of OH radicals with the MITC and EPTC, with the results indicating rate constants of  $1.72 \times 10^{-12}$  and  $2.21 \times 10^{-11} \text{ cm}^3 \text{ molec}^{-1} \text{ s}^{-1}$ , respectively, which are both somewhat different from previously measured values. The UCR EPA environmental chamber was employed, and most experiments were “incremental reactivity” experiments to determine effects of adding the test compounds to experiments simulating representative ambient chemical conditions. These employed  $\text{NO}_x$  levels of 25-30 ppb and at reactive organic gas (ROG)/ $\text{NO}_x$  ratios representing maximum incremental reactivity (MIR) and  $\text{NO}_x$ -limited conditions. Mechanisms for the compounds studied were developed based on available information in the literature and the results of the chamber experiments, and the mechanism for chloropicrin was updated. Mechanisms for other thiocarbamates were estimated based on the mechanism derived for EPTC. The SAPRC-99 mechanism was used as the starting point, to which an updated chlorine mechanism was added so the reactions of the chlorine-containing compounds could be modeled. It was necessary to adjust uncertain portions of the mechanisms for MITC,  $\text{CS}_2$ , and EPTC to give predictions that were consistent with the chamber data, and it was also necessary for the 1,3-dichloropropene mechanism to include an explicit representation of chloroacetaldehyde undergoing photolysis to form chlorine atoms at near-unit quantum yields to simulate the reactivity data for these compounds. The experiments with kerosene were found to be consistent with the predictions of the model derived from the available compositional data without the need for adjustments. The mechanisms were then used to derive quantitative ozone impacts for these and other pesticide compounds in the MIR and other incremental reactivity scales. The MIR values derived (in units of grams  $\text{O}_3$  per gram VOC) were 1,3-dichloropropenes: 5.4; chloropicrin: 2.2; EPTC and pebulate: 1.8; kerosene and molinate: 1.7; thiobencarb: 0.7; MITC: 0.35; and  $\text{CS}_2$ : 0.25-0.28. (For comparison, the mixture used to represent reactive VOCs from all sources has an MIR of 3.7, and ethane has an MIR of 0.3). In addition, relative impacts of these compounds on particulate matter (PM) formation were determined, with kerosene having the greatest PM impact on a mass basis, followed by the sulfur-containing compounds, and with the 1,3-dichloropropenes having no PM impact. Areas of uncertainties and needs for future research are discussed.

## **ACKNOWLEDGEMENTS AND DISCLAIMERS**

This work was funded by the California Air Resources Board (CARB) through contract number 04-334. The EPTC sample studied for this project was provided by the Gowan Company, the Telone II soil fumigant (1,3-dichloropropene) sample was provided by Dow AgroSciences, the kerosene sample used for this project were provided by Harkrider Distribution Company in Houston, Texas, and the analyses of the kerosene sample were carried out by ExxonMobil Process Research Labs in Baton Rouge, Louisiana. We thank these companies for their assistance with this project. Helpful discussions with the CARB project officer, Dr. Dongmin Luo, other members of the CARB staff, Randy Segawa and other members of the California Department of Pesticide Regulation staff, and with Arlean M. Rohde of ExxonMobil chemical company concerning the materials that were studied are gratefully acknowledge. We also thank Roger Atkinson of the Air Pollution Research Center at the University of California at Riverside for helpful discussions concerning the atmospheric chemistry of some of the compounds studied.

The environmental chamber experiments for this project were carried out at the College of Engineering Center for Environmental Research and Technology (CE-CERT) primarily by Irina Malkina and Kurt Bumiller with the assistance of Bethany Warren. Valuable assistance in carrying out the experiments was also provided by Dennis Fitz, Charles Bufalino, and John Pisano of CE-CERT. Mr. Dennis Fitz also provided valuable assistance in administering this project.

Although this work was funded by the CARB, the contents of this report reflect only the opinions and conclusions of the primary author. Mention of trade names and commercial products does not constitute endorsement or recommendation for use.

## TABLE OF CONTENTS

EXECUTIVE SUMMARY .....	1
Methods and Results .....	3
INTRODUCTION .....	6
Introduction and Background .....	6
Background .....	6
Volatile Organic Compounds in Pesticides .....	7
Overall Approach .....	12
EXPERIMENTAL METHODS.....	15
Chamber Description.....	15
Analytical Instrumentation .....	17
Sampling methods .....	21
Characterization Methods.....	21
Experimental Procedures.....	22
Materials .....	23
MODELING METHODS .....	24
Base Mechanism.....	24
Standard Chemical Mechanism .....	24
Adjusted Base Mechanism.....	24
Representation of Chlorine Chemistry.....	25
Representation of Chamber Conditions.....	26
Mechanisms for Test Compounds .....	27
Methyl Isothiocyanate (MITC) .....	27
Carbon Disulfide.....	36
S-Ethyl N,N-di-n-Propyl Thiocarbamate (EPTC) and Other Thiocarbamates .....	37
1,3-Dichloropropenes.....	41
Chloropicrin .....	49
Kerosene .....	49
Atmospheric Reactivity Simulations .....	54
RESULTS AND DISCUSSION .....	55
Characterization Results .....	55
Arc Light Characterization .....	55
Blacklight Characterization .....	55
Chamber Effects Characterization .....	57
Background PM Characterization.....	58
Results of Injection Tests .....	59
OH Radical Rate Constant Determinations .....	60
Mechanism Evaluation Results .....	65
Methyl Isothiocyanate (MITC) .....	69
Carbon Disulfide.....	72
S-Ethyl N,N-di-n-Propyl Thiocarbamate (EPTC) .....	74
1,3-Dichloropropenes.....	77
Chloropicrin .....	81
Kerosene .....	81

## TABLE OF CONTENTS (continued)

PM Impact Results .....	85
Atmospheric Reactivity Calculations .....	87
DISCUSSION AND CONCLUSIONS .....	90
REFERENCES .....	94
APPENDIX A. REPRESENTATION OF ATMOSPHERIC CHLORINE REACTIONS .....	100
Mechanism Listing .....	100
Estimation of Chlorine + VOC Mechanisms.....	113
References .....	119
APPENDIX B. MECHANISMS FOR KEROSENE CONSTITUENTS .....	121
APPENDIX C. CHAMBER EXPERIMENT LISTING.....	127

## LIST OF TABLES

Table E-1.	Summary of pesticide compounds and calculated ozone impacts in the MIR scale. ....	2
Table 1.	Pesticide speciation profile from the 2000 California VOC emissions inventory.....	8
Table 2.	List of analytical and characterization instrumentation for the UCR EPA chamber.....	18
Table 3.	List of model species added to the mechanism to represent the atmospheric reactions of the pesticide compounds modeled for this project.....	28
Table 4.	Reactions and kinetic parameters added to the mechanism to represent the atmospheric reactions of the pesticide compounds modeled for this project.....	29
Table 5.	Absorption cross sections used for the photolysis reactions added to the mechanism to represent the atmospheric reactions of the pesticide compounds modeled for this project. ....	33
Table 6.	Mechanisms for reactions of HS, HSO, and HSO <sub>2</sub> radicals under atmospheric conditions, and current IUPAC recommended rate constants.....	35
Table 7.	Summary of overall processes for the reactions of OH with various thiocarbamates .....	42
Table 8.	Rate constants used in the model simulations of the atmospheric or environmental chamber reactivities of the 1,3-dichloropropenes. ....	44
Table 9.	Mechanism derived for the atmospheric reactions of the 1,3-dichloropropenes.....	45
Table 10.	Products predicted to be formed in the various overall reactions of the 1,3-dichloropropenes, their estimated yields, and their representation in the mechanism used in the model simulations. ....	47
Table 11.	Composition derived of kerosene sample studied for this project. Derived from data provided by ExxonMobil (2006).....	50
Table 12.	Distribution of chemical categories assigned to the kerosene sample and compounds used to represent these categories for modeling purposes. ....	51
Table 13.	Distributions of types of aromatics assumed for estimating aromatic compositions of kerosene, and methods used for representing them in model calculations. ....	53
Table 14.	Data used for OH radical rate constant determinations for the MITC reactivity experiments. ....	62
Table 15.	Data used for OH radical rate constant determinations for the EPTC reactivity experiments. ....	63
Table 16.	Data used for to test the consistency of the results of the dichloropropene reactivity experiments with measurements of the OH + dichloropropene rate constants .....	66
Table 17.	Summary of initial concentrations and selected gas-phase results of the incremental reactivity experiments. ....	68
Table 18.	Summary of initial concentrations and selected gas-phase results of the dichloropropene - NO <sub>x</sub> and dichloropropene - NO <sub>x</sub> + propane experiments. ....	69

## LIST OF TABLES (continued)

Table 19.	Selected results of PM number and volume measurements made during the incremental reactivity experiments carried out for this project.....	86
Table 20.	Calculated atmospheric ozone impacts of the selected pesticide-related compounds and mixtures in the MIR, MOIR, and EBIR incremental reactivity scales.....	88
Table A-1.	List of model species in the SAPRC-99 mechanism as expanded to represent atmospheric chlorine chemistry. The new model species used to represent chlorine chemistry are underlined. ....	101
Table A-2.	Reactions added to the SAPRC-99 mechanism to represent atmospheric chlorine chemistry. ....	104
Table A-3.	Absorption cross sections and quantum yields for the photolysis reactions used in the representation of atmospheric chlorine chemistry.....	109
Table A-4.	List of compounds used to derive mechanistic parameters for the reactions of Cl atoms with lumped parameter species in the SAPRC-99 mechanism.....	111
Table A-5.	Rate constants for reactions with chlorine atoms for organic compounds represented in the SAPRC-99 mechanism, or used to derive parameters for group-additivity estimates, for which measurement data are available. ....	114
Table A-6.	Group additivity rate constants and factors used for estimating rates of abstraction reactions by Cl atoms.....	116
Table A-7.	Group additivity rate constants and factors used for estimating rates of addition of Cl atoms to double bonds.....	116
Table A-8.	Branching ratio assignments for chlorine-substituted alkoxy radicals that had to be made in order to generate mechanisms for the reactions of chlorine for the representative alkenes. ....	118
Table B-1.	Representations of the compounds used to represent the constituents of kerosene in the SAPRC-99 mechanism.....	121
Table C-1.	Summary chamber experiments relevant to this project. ....	127

## LIST OF FIGURES

Figure 1.	Schematic of the UCR EPA environmental chamber reactors and enclosure. ....	16
Figure 2.	Spectrum of the argon arc light source used in the UCR EPA chamber. Blacklight and representative solar spectra, with relative intensities normalized to give the same NO <sub>2</sub> photolysis rate as that for the UCR EPA spectrum, are also shown. ....	16
Figure 3.	Absorption cross sections for chloroacetaldehyde and absorption cross sections and action spectra for propionaldehyde. ....	48
Figure 4.	Plots results of NO <sub>2</sub> actinometry experiments vs. EPA run number using the arc light source in its current power setting and configuration. ....	56
Figure 5.	Plots of light intensity data used to assign NO <sub>2</sub> photolysis rates for the blacklight light source. ....	57
Figure 6.	Plots of best fit HONO offgasing parameters against UCR EPA run number. (Data from Carter (2004), with results of newer experiments for this project added.) ....	58
Figure 7.	Plots of 5-hour PM volume measured in pure air irradiations in the UCR EPA chamber through the time of the experiments for this project. ....	59
Figure 8.	Plots of estimated fractions of kerosene or EPTC injected into the gas phase in representative injection tests. ....	60
Figure 9.	Plots of Equation (II) for the data from the MITC and EPTC reactivity experiments, assuming no losses of the test compounds by photolysis or other processes. ....	64
Figure 10.	Plots of Equation (II) for the data from the MITC reactivity experiments, assuming that MITC undergoes loss by photolysis with photolysis rates calculated using the absorption cross sections of Alvarez et al (1994) and assuming unit quantum yields. ....	64
Figure 11.	Plots of Equation (II) for the data from the dichloropropene reactivity experiments, assuming no losses of the test compounds other processes. ....	67
Figure 12.	Experimental and calculated concentration-time plots for $\Delta([O_3]-[NO])$ and IntOH for the incremental reactivity experiments with MITC. ....	70
Figure 13.	Experimental and calculated concentration-time plots for formaldehyde for the incremental reactivity experiments with MITC that had formaldehyde data. ....	71
Figure 14.	Experimental and alternative model calculations of concentration-time plots for change in $\Delta([O_3]-[NO])$ for the incremental reactivity experiments with MITC. ....	72
Figure 15.	Experimental and calculated concentration-time plots for $\Delta([O_3]-[NO])$ and IntOH for the incremental reactivity experiments with CS <sub>2</sub> . ....	73
Figure 16.	Experimental and calculated concentration-time plots for $\Delta([O_3]-[NO])$ , IntOH and (where experimental data available) formaldehyde for the incremental reactivity experiments with EPTC. ....	75
Figure 17.	Experimental and calculated concentration-time plots for changes in $\Delta([O_3]-[NO])$ , IntOH and (where experimental data available) formaldehyde for the incremental reactivity experiments with EPTC. ....	76



## LIST OF FIGURES (continued)

Figure 18.	Experimental and calculated concentration-time plots for selected species in the dichloropropene - NO <sub>x</sub> experiments.....	78
Figure 19.	Experimental and calculated concentration-time plots for selected species in the dichloropropene + propane - NO <sub>x</sub> experiments.....	79
Figure 20.	Experimental and calculated concentration-time plots for $\Delta([O_3]-[NO])$ , IntOH, and IntCl for the incremental reactivity experiments with the dichloropropenes.....	80
Figure 21.	Experimental and calculated concentration-time plots for selected species in the chloropicrin + alkane - NO <sub>x</sub> environmental chamber experiments carried out by Carter et al (1997a,b). ....	82
Figure 22.	Experimental and calculated concentration-time plots for $\Delta([O_3]-[NO])$ , Integrated OH, and Integrated Cl in the chloropicrin incremental reactivity environmental chamber experiments carried out by Carter et al (1997a,b). ....	83
Figure 23.	Experimental and calculated concentration-time plots for changes in $\Delta([O_3]-[NO])$ and IntOH for the incremental reactivity experiments with kerosene.....	84

## EXECUTIVE SUMMARY

### Background

Pesticides are widely used in agricultural operations in California and in addition to their other environmental impacts they may also be emitted into the atmosphere and contribute to the formation of ground-level ozone. Because ground-level ozone continues to be a problem in many areas of California, the California Air Resources Board (ARB) and the California Department of Pesticide Regulation need a means to quantify the ozone impacts of pesticide compounds that are used in the state. The only practical way to do this is to conduct airshed model calculations to predict the effects of the pesticides on ozone, which mechanisms for the pesticides' atmospheric reactions, as well as models for airshed conditions.

However, airshed model calculations are no more reliable than the chemical mechanisms upon which they are based. While the initial atmospheric reaction rates for many VOCs are reasonably well known or at least can be estimated, for most VOCs the subsequent reactions of the radicals formed are complex and have uncertainties that can significantly affect predictions of atmospheric impacts. Laboratory studies can reduce these uncertainties, but for most VOCs they will not provide the needed information in the time frame required for current regulatory applications. For this reason, environmental chamber experiments and other experimental measurements of reactivity are necessary to test and verify the predictive capabilities of the chemical mechanisms used to calculate atmospheric reactivities. They provide the only means to assess as a whole all the many mechanistic factors that might affect reactivity, including the role of products or processes that cannot be studied directly using currently available techniques. Because of this, the ARB and others have funded programs of environmental chamber studies to provide data needed to reduce uncertainties in ozone impact assessments of the major classes of VOCs present in emissions.

Although progress has been made in developing methods to estimate and quantify relative ozone impacts of the major classes of VOCs present in vehicle emissions and solvents, the ozone impacts of many of the compounds used in pesticides are either unknown or very uncertain. Table E-1 shows the VOC speciation profile that is used to represent pesticide emissions in the 2000 California VOC emissions inventory. The approximate mass fractions, which represent the relative amounts of each compound that are estimated to be emitted, are also shown, and the compounds are listed in order of decreasing amounts emitted. The volatility and the estimated ozone impacts of the compounds are also given on the table. The ozone impacts are expressed in terms of the MIR reactivity scale, which is used in California vehicle and architectural coatings regulations (CARB 1993, 2000). The reactivity estimates for the compounds that are not underlined were calculated using the existing SAPRC-99 mechanism (Carter, 2000a) and are from previous reactivity tabulations that have already been submitted to the CARB (2003a). For the underlined compounds there was no chemical mechanism and therefore no ozone impact estimate, prior to this study.

It can be seen that for a substantial number of the pesticides listed in Table E-1 there was no chemical mechanism or quantitative ozone impact estimate prior to this study. The objective of the project discussed in this report was to derive the mechanisms and make the reactivity estimates for these representative pesticide compounds where this was needed. This requires environmental chamber experiments to develop and evaluate the predictive capabilities of the mechanisms for representative compounds. Based on the above considerations, and after discussions with the staff of the CARB and the California Department of Pesticide Regulations, it was decided that the highest priority compounds to study for assessing ozone impacts of pesticides are MITC, the 1,3-dichloropropenes, kerosene, EPTC and carbon disulfide. The results for EPTC were also useful as a basis for estimating ozone impacts of the

Table E-1. Summary of pesticide compounds and calculated ozone impacts in the MIR scale.

Compound or Mixture	Mass fract. [a]	V.P. (ppm) [b]	MIR [c]	Source of MIR or comment * = Studied experimentally
Methyl bromide	25.3%	High	≤0.03 [d]	Previously estimated
<u>MITC (methyl isothiocyanate)</u>	17.8%	High	<u>0.35</u>	<u>Unknown prior to this work *</u>
<u>1,3-Dichloropropenes [e]</u>	11.3%	High	<u>4.64</u>	<u>Unknown prior to this work *</u>
Chloropicrin	8.6%	High	<u>2.18</u>	<u>Updated for this work</u>
Aromatic 200 solvent	4.8%	High		Depends on composition
Xylene range solvent	4.6%	High		Depends on composition
<u>Molinate</u>	3.3%	7.4	<u>1.68</u>	<u>Unknown prior to this work</u>
<u>Kerosene</u>	1.7%	[f]	<u>1.71</u>	<u>Unknown prior to this work *</u>
Chlorpyrifos	1.7%	0.03		Low volatility
Methylisobutyl ketone	0.8%	High	4.28	Previously calculated
Glyphosate, isopropylamine salt	0.7%	Low		Not volatile
Acrolein	0.7%	High	7.55	Previously calculated
Glycerine	0.5%	0.22	3.26	Previously calculated
Propylene glycol	0.5%	170	2.74	Previously calculated
<u>Thiobencarb</u>	0.5%	0.03	<u>0.72</u>	<u>Unknown prior to this work</u>
N-Methyl pyrrolidinone	0.5%	454	2.55	Previously calculated
<u>S-ethyl N,N-dipropyl thiocarbamate (EPTC)</u>	0.5%	32	<u>1.82</u>	<u>Unknown prior to this work *</u>
Oxyfluorfen	0.5%	0.0003		Low volatility
<u>Pebulate</u>	0.4%	116	<u>1.84</u>	<u>Unknown prior to this work</u>
Pendimethalin	0.4%	0.04		Low volatility
Oryzalin	0.3%	0.00001		Not volatile
Trifluralin	0.2%	0.06		Low volatility
Aliphatic solvent	0.2%	High		Depends on composition
Oxydemeton-methyl	0.2%	0.04		Low volatility
Carbon disulfide	[g]	High	0.28	This work
Base ROG Mixture [h]	-	High	3.71	Previously calculated
Ethane [j]	-	High	0.31	Previously calculated
Methane	-	High	0.014	Previously calculated

[a] Mass Fraction of compound in total pesticide VOC profile. Data provided by the CARB staff in October, 2004. The unidentified fraction is not shown.

[b] Vapor pressures at 25°C obtained from the Syracuse Research Corporation (SRC) online physical properties database at <http://www.syrres.com/esc/physdemo.htm>. “High” means that the vapor pressure is greater than 1000 ppm. “Low” means probably has negligible volatility.

[c] Calculated ozone reactivity in grams O<sub>3</sub> per gram VOC in the Carter (1994a) MIR scale.

[d] Mechanism is highly uncertain. Estimated upper limit MIR is given (Carter, 2000a, 2003a).

[e] MIR calculated based on MIR's calculated for cis and trans isomer, assuming 56% cis and 44% trans, based on initial concentrations in the environmental chamber experiments.

[f] Sufficient to inject at least 95% into the gas phase in the experiments for this project.

[g] Expected to be a pesticide degradation product.

[h] Mixture used to represent reactive organic gas (ROG) emissions from all sources for the purpose of calculating atmospheric ozone impacts (Carter, 1994a).

[j] Ethane has been used by the EPA to define the borderline between reactive and negligible reactive for VOC exemption purposes.

other thiocarbamates listed in Table E-1. Chloropicrin had been studied previously, but its mechanism was out-of-date and the existing chamber data were used to evaluate an updated mechanism for this compound. The results of experiments, mechanism development, and model analyses of ozone impacts of these materials are discussed in this report.

## Methods and Results

The environmental chamber experiments were carried out in the state-of-the art UCR-EPA chamber, which was developed recently under EPA funding to permit mechanism evaluations at lower reactant concentrations than previously possible. This chamber was used in previous CARB-funded studies of low-NO<sub>x</sub> mechanism evaluation and in evaluations of impacts of coatings VOC emissions. The experimental procedures were the same as used in the previous studies of coatings VOC emissions (Carter and Malkina, 2005; Carter et al, 2005a). This primarily involved conducting “incremental reactivity” experiments where the effects of adding the test compounds or mixtures to irradiations of “base case” reactive organic gas (ROG) - NO<sub>x</sub> mixtures designed to represent ambient chemical conditions. To obtain data for mechanism evaluation under differing chemical conditions, experiments were carried out at two different base case ROG/NO<sub>x</sub> ratios. In addition to measurements of O<sub>3</sub> impacts, measurements were made of impacts of adding the test compound on particulate matter (PM) formation. Information was also obtained concerning the rate constants for the reactions of MITC and EPTC with OH radicals, based on rates of consumption of these compounds in the chamber with m-xylene, a reference compound with a well-known OH radical rate constant.

Chemical mechanisms or representations were developed for the compounds or mixtures that were experimentally studied, and the results of the experiments were used to evaluate the mechanisms and improve their predictive capabilities. The SAPRC-99 mechanism used to calculate existing reactivity scales was used as the starting point, but an updated representation of chlorine chemistry, which is documented in Appendix A to this report, was developed to adequately represent the impacts of the dichloropropenes and chloropicrin. Adjustments had to be made to uncertain portions of the mechanisms for MITC, carbon disulfide, and EPTC in order to obtain satisfactory fits for these compounds, and an explicit representation of the 1,3-dichloropropene product chloroacetaldehyde was needed in the mechanism to correctly predict these compounds' reactivity. Estimated mechanisms for the other thiocarbamates were developed based on the mechanism for EPTC that fit the chamber data.

The mechanisms developed for this project were then used to calculate MIR and other reactivity scales, using the same procedures, scenarios and base case mechanism as used to calculate the existing MIR scale used in California. The results are shown on as the underlined values on Table E-1, and are discussed in the following section.

Although this was not a primary objective of this study, information was also obtained concerning the PM impacts of the representative pesticide materials studied. Kerosene had the greatest PM impact on a mass basis, forming about 5 times more PM on a mass basis than the aromatic-containing hydrocarbon solvents studied for the coatings reactivity project (Carter et al, 2005a). This is consistent with the much higher molecular weight range of the constituents of this mixture. On the other hand, the dichloropropenes had essentially no PM impact, which is also consistent with expectations based on their mechanisms, which predict only high volatility products. All the sulfur-containing compounds studied had measurable PM impacts, with the impacts of the three being generally comparable. In the case of MITC and CS<sub>2</sub> this can be attributed to the formation of SO<sub>2</sub> in the oxidation mechanisms (which reacts to form non-volatile sulfuric acid), but in the case of EPTC it appears likely that other condensable products also contribute to PM formation.

## Discussion and Recommendations

This project has been successful in its objective of reducing uncertainties in atmospheric impacts of many types of pesticide-related VOCs used in California, and has resulted in quantitative estimates of ozone impacts of most of the compounds in the California pesticide emissions profile. The major gaps are complex mixtures whose compositions were not specified, or compounds of such low volatility that their availability for participation in gas-phase ozone formation is highly uncertain. There are uncertainties in some of the new ozone impact estimates, and additional data would be useful to reduce these uncertainties. However, for the compounds that were studied experimentally the predictions of the mechanisms developed in this work were sufficiently consistent with the experimental data obtained for this project (or the previous experiments on chloropicrin) that they can be considered a useful basis for estimates of atmospheric ozone impacts. In any case, the level of uncertainty in these estimates is considerably less than would be the case previously, where in most cases quantitative ozone impacts were not available.

Except for kerosene, the compounds studied for this project are representatives of chemical classes whose ozone impacts have not been studied previously. There have been experimental measurements of some of the primary atmospheric rate constants and some limited product data is available in some cases, but in all cases the initially estimated mechanisms did not perform satisfactorily in simulating the chamber data, and adjustments had to be made. In the case of the sulfur-containing compounds the adjustments reflect uncertain aspects of the mechanism where additional study would be useful to reduce uncertainties in the mechanisms, and therefore their predictions of atmospheric ozone impacts. In the case of dichloropropenes, the adjustments made reflect the level of detail that is necessary to be included in lumped mechanisms to obtain satisfactory representations of atmospheric reactivities of chlorinated compounds. Although the adjusted mechanisms simulate the data reasonably well, there are some inconsistencies in predictions of some aspects of the data that suggest that further refinements may be appropriate.

The updated mechanism for chloropicrin was found to give good simulations of the chamber data obtained previously. Since chloropicrin has a relatively simple mechanism for chlorine formation, the good performance of the mechanism in simulating the data in these experiments therefore not only tends to validate the chloropicrin mechanism, it also lends support to the predictive capability of the overall chlorine mechanism that is presented in Appendix A of this report.

Although no new mechanisms had to be developed to successfully simulate the ozone impacts measured for kerosene, studies with this mixture were useful in extending the range of types of hydrocarbon mixtures for which experimental evaluation data are available to mixture with much higher molecular weight constituents. Despite the greater uncertainties in deriving specific compositions for heavier mixtures, and the greater uncertainties in the estimated mechanisms involved, the model was able to simulate the kerosene experiments at least as well, and in some cases better, than was the case for the lighter hydrocarbon mixtures studied for the coatings project. In addition, the calculated MIR agreed with the MIR estimated with the CARB “binning” method developed for the aerosol coatings regulation (Kwok et al, 2000, CARB, 2000) within the range that is observed for lighter mixtures when we reviewed the “binning” method as part of our previous study of coatings reactivity (Carter and Malkina, 2005). Therefore, use of this “binning” method is probably appropriate in cases where detailed compositional data are not available.

As indicated above, as a result of this project we were able to derive quantitative estimates of the ozone impacts of most of the pesticides in the California pesticide profile in the MIR and other reactivity scales. The results indicate a relatively wide range of ozone impacts of the pesticide compounds, as might be expected considering the wide range of chemicals involved. The most reactive is acrolein, which is

about twice as reactive as the base ROG, the mixture of reactive organic gases used to represent emissions from all sources, followed by the 1,3-dichloropropenes and methyl isobutyl ketone, which are also more reactive than this mixture. The least reactive is methyl bromide, which has a highly uncertain mechanism but has an upper limit reactivity below that of ethane, the compound the EPA has used as the borderline for defining negligible reactivity for exemption decisions. Whether it is more or less reactive than methane is uncertain, and would require experimental data to determine. Carbon disulfide may also be somewhat less reactive than ethane (on a mass basis), but the difference between the two is probably within the uncertainty of the CS<sub>2</sub> mechanism. Most of the other pesticides have reactivities between those of ethane and the base ROG.

Other than complex mixtures with unspecified compositions (for which the CARB “binning” method can probably be employed), the only compounds on the California pesticide profile list on Table E-1 which reactivity estimates were not made are all have estimated vapor pressures of less than ~30 ppb at 25°C, which suggests that they may not have sufficient volatility to participate in gas-phase reactions. The least volatile of these should probably not be included in VOC emissions profiles at all. However, the semi-volatiles might exist at least to some extent in the gas phase, depending on partitioning and other considerations, and therefore may undergo reaction. However, experimentally studying gas-phase reactions of such compounds would be very difficult in practice, and modeling their atmospheric impacts probably would require appropriate representation of the heterogeneous partitioning processes they probably also undergo. This is beyond the scope of this project, but is an appropriate study for future research.

Finally, it should be noted that the mechanisms for the test compounds are not the only significant source of uncertainty in model predictions of atmospheric ozone impacts. As discussed in previous reports to the CARB, uncertainties in the aromatic photooxidation mechanisms lead to uncertainties in the representation of the base case conditions that would affect predictions of atmospheric reactivity and also complicates the use of incremental reactivity chamber data for mechanism evaluation. We are currently developing an updated version of the SAPRC mechanism, with a major objective of addressing this problem. However, progress to date suggests that at least some of the problems with the aromatics mechanisms may not be resolved in the near term.

Another problem that needs to be addressed is limitations in the environmental chamber database in evaluating mechanisms for the impacts of the reactions of the secondary products. A modeling analysis indicates that chamber experiments such as used in this and previous projects are much less sensitive to the effects on ozone of the reactions of the VOCs' oxidation products than is calculated to be the case for the atmosphere. This means that an important aspect of the mechanism affecting predictions of ozone in the atmosphere is not being adequately tested, and may not be giving correct predictions in airshed models. This may be applicable to some of the pesticide-related compounds studied for this project, particularly EPTC and kerosene. A project concept to address this has been submitted to the CARB

## INTRODUCTION

### Introduction and Background

#### Background

Pesticides are widely used in agricultural operations in California and in addition to their other environmental impacts they may also be emitted into the atmosphere and contribute to the formation of ground-level ozone. Because ground-level ozone continues to be a problem in many areas of California, the California Air Resources Board (ARB) and the California Department of Pesticide Regulation need a means to quantify the ozone impacts of pesticide compounds that are used in the state. Because VOCs can react in the atmospheres at different rates and with different mechanisms, the different types of VOCs can vary significantly in their effects on air quality. An ability to quantify the effects of emissions of different types of VOCs on ozone formation is useful for assessing relative ozone impacts of various emissions sources such as pesticide use, and for developing cost-effective ozone control strategies. The effect of a VOC on ozone formation in a particular environment can be measured by its “incremental reactivity”, which is defined as the amount of additional ozone formed when a small amount of the VOC is added to the environment, divided by the amount added. Although this can be measured in environmental chamber experiments, incremental reactivities in such experiment cannot be assumed to be the same as incremental reactivities in the atmosphere (Carter and Atkinson, 1989; Carter et al., 1995a). This is because it is not currently practical to duplicate in an experiment all the environmental factors that affect relative reactivities; and, even if it were, the results would only be applicable to a single type of environment. The only practical means to assess atmospheric reactivity, and how it varies among different environments, is to estimate its atmospheric ozone impacts using airshed models.

However, airshed model calculations are no more reliable than the chemical mechanisms upon which they are based. Although several chemical mechanisms are used in airshed modeling applications in the United States (Gery et al, 1989; Stockwell et al, 1990, 1997; Carter, 2000a,b), the SAPRC-99 mechanism (Carter, 2000a) is considered to represent the current state of the art for model simulations of ozone impacts of individual VOCs. This is because it is the only one of these mechanisms that is designed to separately represent the reactions of several hundreds of different types of VOCs, while most other mechanisms use a limited number of “lumped species” to represent a broad classes of compounds assumed to have similar reactivity. The only other currently available state of the art mechanism that can be used to assess impacts of multiple VOCs is the European “Master Chemical Mechanism” (MCM) (Jenkin et al, 1997, 2003; Saunders et al, 2003, MCM, 2004), which explicitly represents the tropospheric degradations of over 130 volatile organic compounds. However, this mechanism is not widely used in the United States because it is not compatible with the multi-cell grid models that are currently used for regulatory applications in this country. For that reason, most of the discussion and analysis in this report will focus on use of the current version of the SAPRC-99 mechanism.

While the initial atmospheric reaction rates for many VOCs are reasonably well known or at least can be estimated, for most VOCs the subsequent reactions of the radicals formed are complex and have uncertainties that can significantly affect predictions of atmospheric impacts. Laboratory studies can reduce these uncertainties, but for most VOCs they will not provide the needed information in the time frame required for current regulatory applications. For this reason, environmental chamber experiments and other experimental measurements of reactivity are necessary to test and verify the predictive capabilities of the chemical mechanisms used to calculate atmospheric reactivities. They provide the only means to assess as a whole all the many mechanistic factors that might affect reactivity, including the role of products or processes that cannot be studied directly using currently available techniques. Because of

this, the ARB and others have funded programs of environmental chamber studies to provide data needed to reduce uncertainties in ozone impact assessments of the major classes of VOCs present in emissions, and the development of the SAPRC-99 is based extensively on these data.

Although progress has been made in developing methods to estimate and quantify relative ozone impacts of the major classes of VOCs present in vehicle emissions and solvents, but the ozone impacts of many of the compounds used in pesticides are either unknown or very uncertain. The VOCs present in pesticides used in California, and the extent of our knowledge and ability to represent their atmospheric ozone impacts, are discussed in the following section.

### **Volatile Organic Compounds in Pesticides**

Table 1 shows the VOC speciation profile that is used to represent pesticide emissions in the 2000 California VOC emissions inventory. The approximate mass fractions, which represent the relative amounts of each compound that are estimated to be emitted, are also shown, with the compounds listed in order of decreasing amounts emitted. The chemical structure, volatility, and the representation of the compounds in the current SAPRC-99 mechanism, and the SAPRC-99 uncertainty classification, if applicable, are also shown. It is immediately apparent that most of the pesticide VOCs listed on Table 1 are either not represented in the current mechanism or are represented in a highly approximate and uncertain manner. Footnotes to the table indicate the meanings of the uncertainty classifications used. Note that if there is no SAPRC-99 model species indicated for a compound in Table 1, then there is presently no way to estimate the ozone impact of the compound, except by using highly lumped mechanisms whose applicability is subject to significant uncertainty.

The first compound on the list is methyl bromide, which is currently represented using a “placeholder” mechanism that probably does not correctly represent its mechanistic reactivity. However, the rate constant for its reaction with OH radicals, which is expected to be its major atmospheric fate, has been measured to be only  $4 \times 10^{-14} \text{ cm}^3 \text{ molec}^{-1} \text{ s}^{-1}$ , indicating that regardless of its mechanism it may have only a relatively low impact on  $\text{O}_3$ . Therefore, studies of the atmospheric ozone impact of this compound is not considered to be a priority for atmospheric ozone impact assessment.

After methyl bromide the most important compound according to Table 1 is methyl isothiocyanate (MITC). Although no environmental chamber data are available for this compound, there have been studies of its environmental fate (Wales, 2002, and references therein). Geddes et al (1995) determined that MITC undergoes photodecomposition in simulated sunlight with a half life of about one day, suggesting that its atmospheric reactivity is probably non-negligible. However, the impacts of the subsequent reactions on  $\text{O}_3$  formation has not been determined.

The next compound after MITC on Table 1 is 1,3-dichloropropene, which actually is a mixture of two isomers, cis and trans. Although a gas-phase mechanisms for ozone reactivity assessment have not been developed for these compounds, as discussed by Finlayson-Pitts and Pitts (1997) there are kinetic and product data available for their atmospheric reactions.

The other previously unstudied compounds listed on Table 1 consist of various sulphur-, nitrogen- and in some cases chlorine- and phosphorous-containing compounds with varying degrees of volatility. The most volatile of these are the thiocarbamates molinate, EPTC and pebulate. Kwok et al (1992) obtained reasonably comprehensive kinetic and some mechanistic information on EPTC and also dimethylthiocarbamate and cycloate, a compound similar to EPTC except with the propyl groups on the N replaced by cyclohexyl and ethyl groups. Although molinate and pebulate were not studied, the data for the other compounds can provide a basis for estimating rate constants and mechanism for thiocarbamates



Table 1. Pesticide speciation profile from the 2000 California VOC emissions inventory.


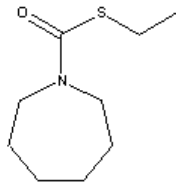
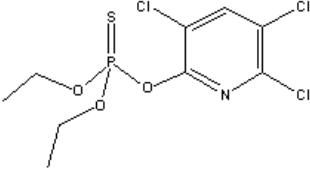
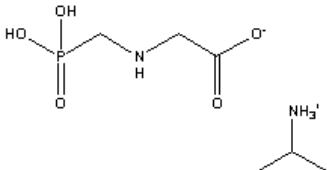
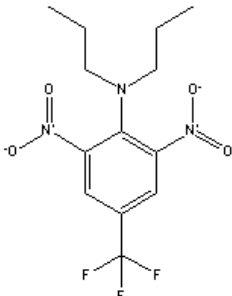
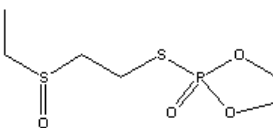
Compound or Mixture [a]	CAS #	Mass fract. [a]	Vapor Pressure (ppm) [b]	SAPRC-99 [c] Model Species	Unc. Code	Structure [d]
methyl bromide	74-83-9	25.3%	high	ME-BR	6	CH <sub>3</sub> Br
MITC (methyl isothiocyanate)	556-61-6	17.8%	high			CH <sub>3</sub> NCS
1,3-dichloropropene	542-75-6	11.3%	high			
chloropicrin	76-06-2	8.6%	high	CCL <sub>3</sub> NO <sub>2</sub>	[e]	CCl <sub>3</sub> NO <sub>2</sub>
aromatic 200 solvent		4.8%		Mixture [f]		Aromatic hydrocarbon mixture
xylene range solvent		4.6%		Mixture [f]		Aromatic hydrocarbon mixture
molinate	2212-67-1	3.3% [g]	7.4			
kerosene		1.7%		Mixture [f]		Alkane and aromatic hydrocarbon mixture
chlorpyrifos	2921-88-2	1.7%	0.03			
methylisobutyl ketone	108-10-1	0.8%	high	MIBK	2	CH <sub>3</sub> C(O)CH <sub>2</sub> CH(CH <sub>3</sub> )CH <sub>3</sub>
glyphosate, isopropylamine salt	38641-94-0	0.7%	[h]	NONVOL	[j]	
acrolein	107-02-8	0.7%	high	ACROLEIN	3	CH <sub>2</sub> =CHCHO
glycerine	56-81-5	0.5%	0.22	GLYCERL	2	HOCH <sub>2</sub> CH(OH)CH <sub>2</sub> OH
propylene glycol	57-55-6	0.5%	170	PR-GLYCL	3 [k]	CH <sub>3</sub> CH(OH)CH <sub>2</sub> OH

Table 1 (continued)

Compound or Mixture [a]	CAS #	Mass fract. [a]	Vapor Pressure (ppm) [b]	SAPRC-99 [c]		Structure [d]
				Model Species	Unc. Code	
thiobencarb	28249-77-6	0.5%	0.03			
N-methyl pyrrolidinone	872-50-4	0.5%	454	NMP	2	
S-ethyl N,N-di-n-propyl thiocarbamate (EPTC)	759-94-4	0.5%	32			
oxyfluorfen	42874-03-3	0.5%	0.0003	NONVOL	[j]	
pebulate	1114-71-2	0.4%	116			
pendimethalin	40487-42-1	0.4%	0.04			
oryzalin	19044-88-3	0.3%	0.00001	NONVOL	[j]	

Table 1 (continued)

Compound or Mixture [a]	CAS #	Mass fract. [a]	Vapor Pressure (ppm) [b]	SAPRC-99 [c]		Structure [d]
				Model Species	Unc. Code	
trifluralin	1582-09-8	0.2%	0.06			
aliphatic solvent		0.2%		Mixture [f]		Alkane hydrocarbon mixture
oxydemeton-methyl	301-12-2	0.2%	0.04			

[a] Mass Fraction of compound in total pesticide VOC profile. Data provided by Frank Spurlock of the California Department of Pesticide Regulation on October 18 to the staff of the California Air Resources Board and provided to us by Dongmin Luo of the CARB. The unidentified fraction, which consists of 13.9% of the mass of the profile, is not shown.

[b] Vapor pressure in mm Hg at 25°C obtained from the Syracuse Research Corporation (SRC) online physical properties database. Available at <http://www.syrres.com/esc/physdemo.htm>, accessed October, 2004. Converted to ppm using 1315 ppm per torr. “High” means that the vapor pressure is greater than 1000 ppm.

[c] Model species used to represent compound in the current SAPRC-99 mechanism and assigned uncertainty code. If these compounds are blank then the compound is not currently represented in the mechanism. The uncertainty codes used in the current mechanism are as follows:

1. Considered to be relatively uncertain, or some uncertainties but reactivity is not expected to change significantly.
2. Uncertain mechanism may change somewhat if refined, but change is expected to be less than a factor of two.
3. Uncertain and may change if compound is studied (or studied further) or estimation methods are updated. Change in atmospheric reactivity calculations could be as much as a factor of two.
4. Uncertain and is expected to change if compound is studied or estimation methods are updated. It is recommended that uncertainty adjustments be employed in regulatory applications.
5. Non-negligible chance of the estimate being incorrect in significant respects. It is recommended that uncertainty adjustments be employed in regulatory applications.
6. Current mechanism is probably incorrect, but biases in atmospheric reactivity predictions are unknown. Uncertainty adjustments should be employed in regulatory applications.

[d] Structure graphics obtained from the ChemFinder online database (<http://chemfinder.cambridgesoft.com>)

Table 1 (continued)

- [e] This compound is not part of the standard SAPRC-99 mechanism because it requires chlorine chemistry to be represented. No uncertainty code assigned, but it is probably equivalent to 2 or 3 when chlorine chemistry is implemented.
- [f] The model species representation depends on the composition of the mixture. The SAPRC-99 mechanism has model species for the various alkanes and aromatics that can be contained in the mixture. See text for a discussion of the uncertainties in representing these mixtures in model calculations.
- [g] Use of this compound is being phased out.
- [h] Vapor pressure data not available from the SRC online database.
- [j] This compound is represented as non-volatile in the current emissions speciation database (Carter, 2006).
- [k] The uncertainty classification has been increased because of inconsistencies in model predictions of results of recent environmental chamber experiments (Carter et al, 2005a).

in general. The rate constants they obtained indicate that these compounds should have non-negligible atmospheric reactivity.

The compounds that have been studied, in order of mass fraction, are chloropicrin (Carter et al, 1997a,b), methyl isobutyl ketone (Carter et al, 2000a), acrolein (Carter, 2000a), propylene glycol (Carter et al, 1997c, 2005a), and N-methyl pyrrolidinone (Carter et al, 1996a). An estimated mechanism for glycerol was derived using the mechanism generation system (Carter, 2000a), and although no experimental data exist to support this mechanism its uncertainty is not considered to be on the same order as those for the other compounds discussed below.

The issue of volatility needs to be taken into account in considering (a) whether it is feasible to carry out environmental chamber experiments suitable for mechanism evaluation and (b) whether the compound actually exists in sufficient concentration in the atmosphere to participate in ozone formation. Although an assessment of availability issues is beyond the scope of this project, we suspect that if a compound is sufficiently volatile that it is feasible to carry out gas-phase environmental chamber experiments suitable for evaluation of ozone formation mechanisms, it is likely to undergo such gas-phase reactions in the environment. Note that the inverse is not necessarily true. The surface/volume ratio in even the largest chambers is much greater than in the atmosphere, and semi-volatile or “sticky” compounds that go to the walls in chamber experiments may still react in the gas phase in the environment.

Although we have not investigated the limit of low vapor pressure for compounds for chamber studies, from a thermodynamic standpoint we would place the absolute lower limit at about 0.1 ppm at ambient temperatures (25°C). Concentration in this range are usually necessary to see a measurable effect on environmental chamber experiments. This rules out chamber studies of chlorpyrifos, glyphosate isopropylamine salt, thiobencarb, oxyfluorfen, pendimethalin, oryzalin, trifluralin, and oxydemeton-methyl, and suggests that experiments with glycerine (which is expected to be very “sticky” in addition to having borderline volatility) are unlikely to be successful.

In addition to individual compounds, the table indicates that a number of hydrocarbon mixtures, such as “Aromatic 200” and “kerosene” are also present in pesticides used in California. Estimates of ozone impacts of such materials require a knowledge of the composition of the mixture as well as appropriate representations of the atmospheric reactions of the constituents, and thus there are two sources of uncertainty in these cases. Hydrocarbon mixtures are also used in coatings applications, and for

this reason atmospheric ozone impacts of many representative hydrocarbon mixtures have already been studied (Carter and Malkina, 2005). However, hydrocarbon mixtures used in coatings applications are generally lighter than those used in pesticides, and uncertainties in chemical composition and also in chemical mechanisms generally increase as the molecular weight ranges of the mixtures increase. This is particularly the case for the aromatics, where ozone reactivities can vary significantly from isomer to isomer, and where data for higher molecular weight isomers are highly limited (Carter, 2000a). Of the hydrocarbon mixtures listed on Table 1, those with the most uncertain ozone impacts are probably Aromatic 200 and kerosene.

Many of the pesticides listed on Table 1 are either nonvolatile or have very low volatility, which means that probably reaction of the compound itself is not important in affecting atmospheric ozone. However, when assessing the atmospheric impacts of pesticide use, it is also important to consider impacts of volatile products that might be formed when pesticides break down in the soil. Among the known pesticide breakdown products is carbon disulfide (CS<sub>2</sub>), which is highly volatile and likely to be emitted into the atmosphere if formed, but which is not represented in current mechanisms. Other volatile breakdown products may also contribute to ozone formation, and this may be appropriate to examine in future studies.

Based on the above considerations, and after discussions with the staff of the CARB and the California Department of Pesticide Regulations, it was decided that the highest priority compounds to study for assessing ozone impacts of pesticides are MITC, the 1,3-dichloropropenes, kerosene, EPTC and carbon disulfide. The results for EPTC may also be useful as a basis for estimating ozone impacts of the other thiocarbamates listed in Table 1. The results of experiments, mechanism development, and model analyses of ozone impacts of these materials are discussed in this report.

## **Overall Approach**

The chamber experiments were carried out in the UCR EPA chamber, which was developed under EPA funding for more precise mechanism evaluation at lower and more atmospherically representative pollutant levels than previously possible (Carter et al, 1999; Carter, 2002; Carter et al 2005b). Results of earlier experiments carried out in this chamber, including characterization results that are applicable to this study, are given in previous reports or publications (Carter, 2004; Carter and Malkina, 2005; Carter et al, 2005a,b). The approach employed followed that used in our previous studies of architectural coating VOC reactivity, as discussed previously (Carter and Malkina, 2005; Carter et al, 2005a).

As discussed in more detail previously (Carter and Malkina, 2005), the primary objective of these experiments with respect to ozone formation is not to directly measure atmospheric ozone reactivity, but to provide data to test the ability of chemical mechanisms used in models to predict their ozone impacts in the atmosphere. If the mechanism can be shown to adequately simulate the relevant impacts of the VOC in well-characterized environmental chamber experiments with a range of chemical conditions representative of the atmosphere, one has increased confidence in the predictive capabilities of the model when applied to atmospheric scenarios. If the mechanism performance in simulating the experiments is less than satisfactory, then the need to improve the mechanism is indicated, and one has decreased confidence in its predictions of atmospheric reactivity.

The most realistic chemical environment in this regard is one where the test compounds or mixtures react in the presence of the other pollutants present in the atmosphere. Therefore, most of the environmental chamber experiments for this and the coatings VOC reactivity programs consisted of

measurements of “incremental reactivity” of the subject compounds or solvents under various conditions. These involve two types of irradiations of model photochemical smog mixtures. The first is a “base case” experiment where a mixture of reactive organic gases (ROGs) representing those present in polluted atmospheres (the “ROG surrogate”) is irradiated in the presence of oxides of nitrogen ( $\text{NO}_x$ ) in air. The second is the “test” experiment that consists of duplicating the base case irradiation except that the VOC whose reactivity is being assessed is added. The differences between the results of these experiments provide a measure of the atmospheric impact of the test compound. These results can be used to test a chemical mechanism’s to predict the compound’s atmospheric impacts under the chemical conditions of the experiment.

Base case experiments to simulate ambient chemical environments require choice of an appropriate reactive organic gas (ROG) surrogate mixture to represent the reactive organics that are important in affecting ozone formation in the urban atmospheres. For this and the coatings reactivity projects, we continued to use a modified version of the 8-component “full surrogate” that was employed in our previous reactivity studies for the initial reactivity studies for this project. This is because as discussed previously (Carter et al, 1995a) use of this surrogate gives a reasonably good representation of ambient anthropogenic VOC emissions as represented in current models, and use of more detailed mixtures would not give significantly different reactivity results. However, because of experimental problems, for this and many of the experiments in the coatings project the formaldehyde was removed from the surrogate and the initial concentrations of the other ROG components were increased by 10% to make up for the reactivity. Model calculations indicate that this surrogate modification should not have significant effects on experimental incremental reactivity results (Carter and Malkina, 2005). Target and average measured compositions of the ROG surrogates for the reactivity experiments for coatings projects are given by Carter and Malkina (2005). The target concentrations used in the experiments for this program were the same.

In order to provide data to test mechanism impacts of the test compounds or mixtures under differing atmospheric conditions, the incremental reactivity experiments for this and the coatings projects were carried out using two different standard conditions of  $\text{NO}_x$  availability relevant to VOC reactivity assessment. Probably the most relevant for California regulatory applications is “maximum incremental reactivity” (MIR) conditions, which are relatively high  $\text{NO}_x$  conditions where ozone formation is most sensitive to VOC emissions. However, it is also necessary to provide data to test mechanism predictions under lower  $\text{NO}_x$  conditions, since different aspects of the mechanisms are important when  $\text{NO}_x$  is limited. The  $\text{NO}_x$  levels that define the boundary line between VOC-sensitive, MIR-like conditions and  $\text{NO}_x$ -limited (and therefore  $\text{NO}_x$ -sensitive) conditions is that which yields the maximum ozone concentrations for the given level of ROGs, or the conditions of the “maximum ozone incremental reactivity” (MOIR) scale. Therefore, experiments with  $\text{NO}_x$  levels that are approximately half that for MOIR conditions might provide an appropriate test of the mechanism under  $\text{NO}_x$ -limited conditions. This is referred to as “MOIR/2” conditions in the subsequent discussion. If  $\text{NO}_x$  levels are reduced significantly below this, the experiment becomes less sensitive to VOC levels and thus less relevant to VOC reactivity assessment.

The conditions of  $\text{NO}_x$  availability are determined by the ROG/ $\text{NO}_x$  ratios in the base case incremental reactivity experiments. In order to completely fix the conditions of these experiments, it is also necessary to specify a desired absolute  $\text{NO}_x$  level. In order to determine this, we sought input from the CARB staff concerning the  $\text{NO}_x$  levels they would consider to be appropriate to use for reactivity studies in the new chamber (Carter and Malkina, 2005). Based on their input, and model simulations of reactivity characteristics in our chamber, it was determined that the nominal initial concentrations of the MIR base case experiment would consist of ~30 ppb  $\text{NO}_x$  and ~0.5 ppmC ROG surrogate, and the

MOIR/2 experiment would consist of ~25 ppb NO<sub>x</sub> and ~1 ppmC ROG surrogate (Carter and Malkina, 2005). These were therefore the two standard base cases for all the incremental reactivity experiments discussed in this report.

In order to provide additional mechanism evaluation data for dichloropropenes, we also carried out several experiments where these compounds were irradiated in the presence of NO<sub>x</sub> without any added base ROG. Propane was added in some experiments with these compounds to assess the role of Cl atoms that may be formed, since it reacts rapidly with Cl atoms but not rapidly with OH or other reactive radicals present in the system. Such experiments were not considered useful for the other test compounds in this study because they were not expected to have sufficiently large internal radical sources for such data to be useful. NO<sub>x</sub>-air irradiations of compounds that lack large internal radical sources tend to be too sensitive to chamber effects to be useful for mechanism evaluation (Carter et al, 1982, Carter and Lurmann, 1991).

A number of other control and characterization experiments were also carried out in order to adequately characterize the conditions of the chamber for mechanism evaluation and background particulate matter (PM). These experiments are discussed where applicable in the results and modeling methods sections.

The SAPRC-99 mechanism, as documented by Carter (2000a) was used as the starting point for the mechanism development aspect of the project. However, it is necessary to include chlorine chemistry to model the reactions of the chloropropenes, and also to update the reactivity of chloropicrin for the purpose of this project. The appropriate chlorine and ClO<sub>x</sub> reactions were added to the mechanism for the purpose of this project, updated as part of our ongoing project to update the SAPRC mechanism (Carter, 2003b).

## EXPERIMENTAL METHODS

### Chamber Description

All of the environmental chamber experiments for this project were carried out using the UCR EPA chamber. This chamber was constructed under EPA funding to address the needs for an improved environmental chamber database for mechanism evaluation (Carter et al, 1999, Carter, 2002). The objectives, design, construction, and results of the initial evaluation of this chamber facility are described in more detail elsewhere (Carter et al, 1999, Carter, 2002; Carter, 2004, Carter et al, 2005b). A description of the chamber is also given below.

The UCR EPA chamber consists of two ~85,000-liter Teflon® reactors located inside a 16,000 cubic ft temperature-controlled “clean room” that is continuously flushed with purified air. The clean room design is employed in order to minimize background contaminants into the reactor due to permeation or leaks. The primary light source consists of a 200 KW argon arc lamp with specially designed UV filters that give a UV and visible spectrum similar to sunlight. This light source was used for most but not all of the experiments discussed in this report. Banks of blacklights are also present to serve as a backup light source for experiments where blacklight irradiation is sufficient. This was used for some of the later experiments for this project because of problems with the primary light source, and because use of blacklights was judged to be sufficient to satisfy the objectives of this project for the particular compounds being studied. The interior of the enclosure is covered with reflective aluminum panels in order to maximize the available light intensity and to attain sufficient light uniformity, which is estimated to be  $\pm 10\%$  or better in the portion of the enclosure where the reactors are located (Carter, 2002). A diagram of the enclosure and reactors is shown in Figure 1, and spectra of the light sources are shown in Figure 2.

The dual reactors are constructed of flexible 2 mil Teflon® film, which is the same material used in the other UCR Teflon chambers used for mechanism evaluation (e.g., Carter et al, 1995b; Carter, 2000a, and references therein). A semi-flexible framework design was developed to minimize leakage and simplify the management of large volume reactors. The Teflon film is heat-sealed into separate sheets for the top, bottom, and sides (the latter sealed into a cylindrical shape) that are held together and in place using bottom frames attached to the floor and moveable top frames. The moveable top frame is held to the ceiling by cables that are controlled by motors that raise the top to allow the reactors to expand when filled or lower the top to allow the volume to contract when the reactors are being emptied or flushed. These motors in turn are controlled by pressure sensors that raise or lower the reactors as needed to maintain slight positive pressure. During experiments the top frames are slowly lowered to maintain continuous positive pressure as the reactor volumes decrease due to sampling or leaks. The experiment is terminated once the volume of one of the reactor reaches about 1/3 the maximum value, where the time this took varied depending on the amount of leaks in the reactor, but was greater than the duration of most of the experiments discussed in this report. Since at least some leaks are unavoidable in large Teflon film reactors, the constant positive pressure is important to minimize the introduction of enclosure air into the reactor that may otherwise result.

As indicated in Figure 1, the floor of the reactors has openings for a high volume mixing system for mixing reactants within a reactor and also for exchanging reactants between the reactors to achieve equal concentrations in each. This utilizes four 10” Teflon pipes with Teflon-coated blowers and flanges



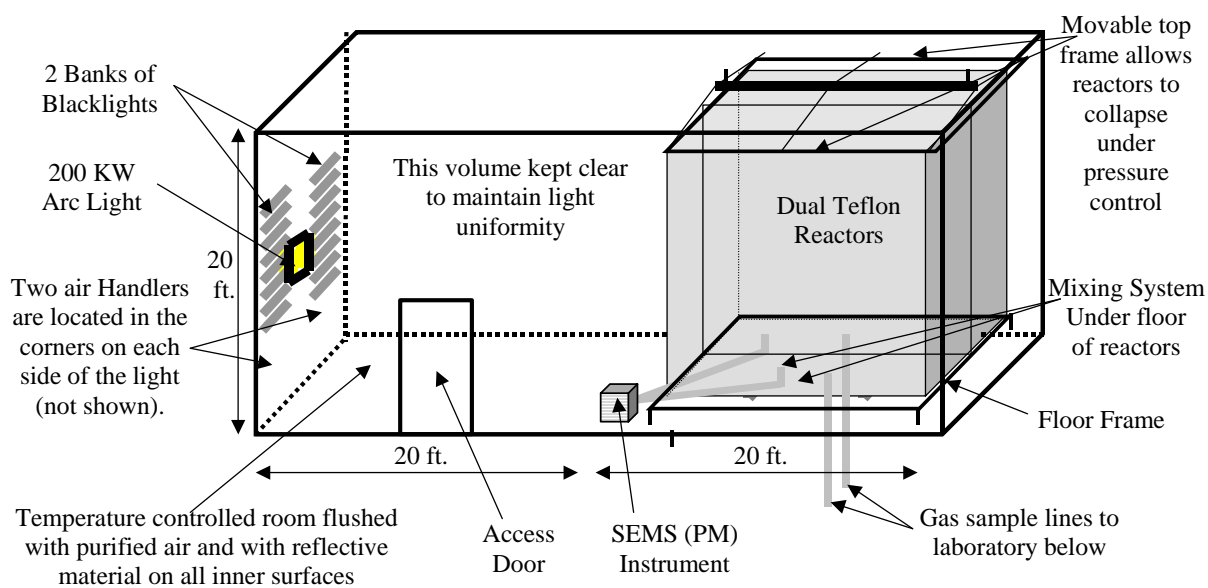


Figure 1. Schematic of the UCR EPA environmental chamber reactors and enclosure.

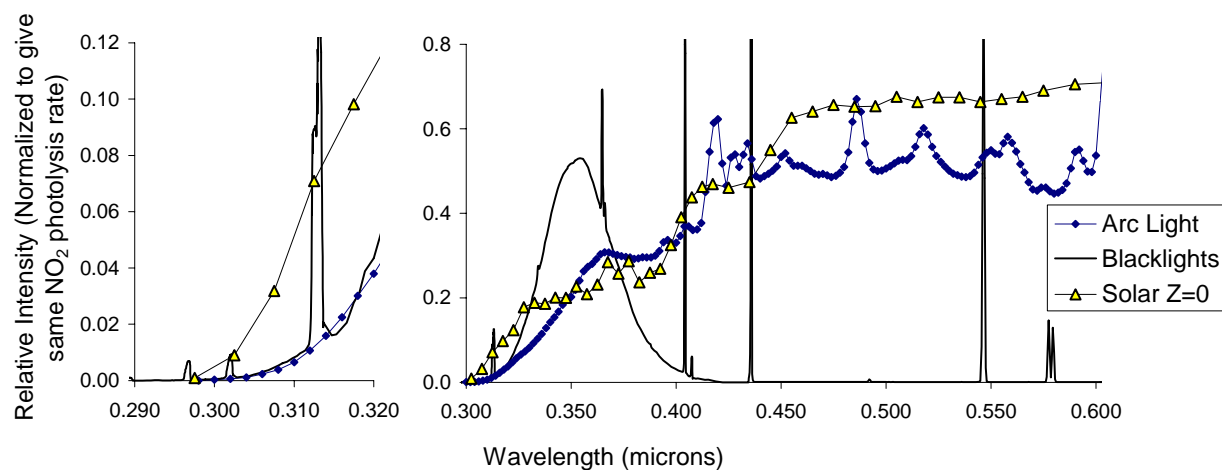


Figure 2. Spectrum of the argon arc light source used in the UCR EPA chamber. Blacklight and representative solar spectra, with relative intensities normalized to give the same  $\text{NO}_2$  photolysis rate as that for the UCR EPA spectrum, are also shown.

to either blow air from one side of a reactor to the other, or to move air between each of the two reactors. Teflon-coated air-driven metal valves are used to close off the openings to the mixing system when not in use, and during the irradiation experiments.

An AADCO air purification system that provides dry purified air at flow rates up to 1500 liters  $\text{min}^{-1}$  is used to supply the air to flush the enclosure and to flush and fill the reactors between experiments. The air is further purified by passing it through cartridges filled with Purafil® and heated Carulite 300® which is a Hopcalite® type catalyst and also through a filter to remove particulate matter. The measured  $\text{NO}_x$ , CO, and non-methane organic concentrations in the purified air were found to be less than the detection limits of the instrumentation employed (see Analytical Equipment, below).

The chamber enclosure is located on the second floor of a two-floor laboratory building that was designed and constructed specifically to house this facility (Carter et al, 2002). Most of the analytical instrumentation is located on the ground floor beneath the chamber, with sampling lines leading down as indicated in Figure 1.

### Analytical Instrumentation

Table 2 gives a listing of the analytical and characterization instrumentation whose data were utilized for this project. Other instrumentation was available and used for some of these experiments, as discussed by Carter 2002a, but the data obtained were not characterized for modeling and thus not used in the mechanism evaluations for this project. The table includes a brief description of the equipment, species monitored, and their approximate sensitivities, where applicable. These are discussed further in the following sections.

Ozone, CO, NO, and  $\text{NO}_y$  were monitored using commercially available instruments as indicated in Table 2. A second ozone analyzer, based on the chemiluminescence method, was utilized in some experiments, and its data were consistent with the UV absorption instrument listed in Table 2. The instruments were spanned for NO,  $\text{NO}_2$ , and CO and zeroed prior to most experiments using the gas calibration system indicated in Table 2, and a prepared calibration gas cylinder with known amounts of NO and CO.  $\text{O}_3$  and  $\text{NO}_2$  spans were conducted by gas phase titration using the calibrator during this period. Span and zero corrections were made to the NO,  $\text{NO}_2$ , and CO data as appropriate based on the results of these span measurements, and the  $\text{O}_3$  spans indicated that the UV absorption instrument was performing within its specifications.

As discussed by Carter (2002), Tunable Diode Laser Absorption Spectroscopy (TDLAS) systems are available at our laboratories, with the potential for monitoring up to four different species, though only formaldehyde data were used in this project. TDLAS analysis is described in detail elsewhere (Hastie et al., 1983; Schiff et al., 1994) and is based on measuring single rotational - vibrational lines of the target molecules in the near to mid infrared using laser diodes with very narrow line widths and tunability. The sample for analysis is flushed through closed absorption cells with multi-pass optics held at low pressure ( $\sim 25$  Torr) to minimize spectral broadening. Because of the narrow bandwidth of the diode lasers required to get the highly species-specific measurement, usually separate diode lasers are required for each compound being monitored. Unfortunately, because of instrument problems TDLAS formaldehyde data were available for only a few experiments carried out for this project.

The TDLAS formaldehyde measurements were calibrated using a formaldehyde permeation source that in turn was calibrated based on Wet chemical calibration procedure using Purpald reagent (Jacobsen and Dickinson, 1974; Quesenberry and Lee, 1996; NIOSH, 1994).

Table 2. List of analytical and characterization instrumentation for the UCR EPA chamber.

Type	Model or Description	Species	Sensitivity	Comments
Ozone Analyzer	Dasibi Model 1003-AH. UV absorption analysis. Also, a Monitor Labs Chemiluminescence Ozone Analyzer Model 8410 was used as a backup.	O <sub>3</sub>	2 ppb	Standard monitoring instrument.
NO - NO <sub>y</sub> Analyzer	Teco Model 42 C with external converter. Chemiluminescent analysis for NO, NO <sub>y</sub> by catalytic conversion.	NO NO <sub>y</sub>	1 ppb 1 ppb	Useful for NO and initial NO <sub>2</sub> monitoring. Converter close-coupled to the reactors so the “NO <sub>y</sub> ” channel should include HNO <sub>3</sub> as well as NO <sub>2</sub> , PANs, organic nitrates, and other species converted to NO by the catalyst.
CO Analyzer	Thermo Environmental Instruments Inc. Model 48 C	CO	50 ppb	Standard monitoring instrument
TDLAS #2	Purchased from Unisearch Inc. for this chamber. See Carter (2002). Data transmitted to DAC system using RS-232.	HCHO	~ 1 ppb	Formaldehyde data from this instrument are considered to be interference-free. This instrument was only operational for a few of the experiments discussed in this report.
GC-FID #1	HP 5890 Series II GC with dual columns, loop injectors and FID detectors. Controlled by computer interfaced to network.	VOCs	~10 ppbC	30 m x 0.53 mm GS-Alumina column used for the analysis of light hydrocarbons such as ethylene, propylene, n-butane and trans-2-butene and 30 m x 0.53 mm DB-5 column used for the analysis of C <sub>5+</sub> alkanes and aromatics, such as toluene and m-xylene, and also used for MITC and the dichloropropenes. Loop injection is suitable for low to medium volatility VOCs that are not too “sticky” to pass through valves.
GC-FID #2	HP 5890 Series II GC with dual columns and FID detectors, one with loop sampling and one set up for Tenax cartridge sampling. (Only the Tenax cartridge system used for this project.) Controlled by computer interfaced to network.	VOCs	1 ppbC	Tenax cartridge sampling used for low volatility or moderately “sticky” VOCs that cannot go through GC valves but can go through GC columns. 30 m x 0.53 mm DB-5 column. Used to as the primary method to analyze EPTC, and data was also obtained for MITC and the dichloropropenes, though the GC-FID #1 (loop) analysis was used as the primary method for those compounds.
Total Sulfur Analyzer	Meloy Labs Sulfur Dioxide Analyzer SA 285E	Sulfur cmpds.	~ 1 ppb	Assumed to have the same response to all gas-phase S-containing compounds regardless of compound. Calibrated using SO <sub>2</sub> . Used during most of the CS <sub>2</sub> experiments for this project.

Table 2 (continued)

Type	Model or Description	Species	Sensitivity	Comments
Total Hydrocarbon analyzer, FID	Ratfisch Instruments, Model RS 55CA	VOCs	50 ppbC	Standard commercial instrument. Used for preliminary EPTC and kerosene injection tests only.
Gas Calibrator	Model 146C Thermo Environmental Dynamic Gas Calibrator	N/A	N/A	Used for calibration of NO <sub>x</sub> and other analyzers. Instrument acquired early in project and under continuous use.
Data Acquisition System	Windows PC with custom LabView software, 16 analog input, 40 I/O, 16 thermocouple, and 8 RS-232 channels.	N/A	N/A	Used to collect data from most monitoring instruments and control sampling solenoids. In-house LabView software was developed using software developed by Sonoma Technology for ARB for the Central California Air Quality Study as the starting point.
Temperature sensors	Various thermocouples, radiation shielded thermocouple housing	Temperature	~0.1 °C	Primary measurement is thermocouples inside reactor. However, comparison with temperature measurements in the sample line suggest that irradiative heating may bias these data high by ~2.5°C. See text.
Humidity Monitor	General Eastern HYGRO-M1 Dew Point Monitor	Humidity	Dew point range: -40 - 50°C	Instrument performs as expected, but dew point below the performance range for most of the experiments discussed in this report, except for those with added humidity.
Spectroradiometer	LiCor LI-1800 Spectroradiometer	300-850 nm Light Spectrum	Adequate	Resolution relatively low but adequate for this project. Used to obtain relative spectrum. Also gives an absolute intensity measurement on surface useful for assessing relative trends.
QSL Spherical Irradiance Sensor	Biospherical QSL-2100 PAR Irradiance Sensor. Responds to 400-700 nm light.	Spherical Broad-band Light Intensity	Adequate	Provides a measure of absolute intensity and light uniformity that is more directly related to photolysis rates than light intensity on surface. Gives more precise measurement of light intensity trends than NO <sub>2</sub> actinometry, but is relatively sensitive to small changes in position.
Scanning Electrical Mobility Spectrometer (SEMS)	TSI 3080L column, TSI 3077 <sup>85</sup> Kr neutralizer, and TSI 3760A CPC. Instrument design, control, and operation Similar to that described in Cocker et al. (2001)	Aerosol number and size distributions	Adequate	Provides information on size distribution of aerosols in the 28-730 nm size range, which accounts for most of the aerosol mass formed in our experiments. Data can be used to assess effects of VOCs on secondary PM formation.

Organic reactants other than formaldehyde were measured by gas chromatography with FID detection as described elsewhere (Carter et al, 1995b); see also Table 2. The surrogate gaseous compounds ethylene, propylene, n-butane and trans-2-butene were monitored by using 30 m megabore GS-Alumina column and the loop sampling system. The second signal of the same GC outfitted with FID, loop sampling system and 30 m megabore DB-5 column was used to analyze surrogate liquid components toluene, n-octane and m-xylene. The sampling methods employed for injecting the sample with the test compounds on the GC column depended on the volatility or “stickiness” of the compounds. For analyses of more volatile species such as MITC and the chloropropenes the same loop method was suitable.

Low volatility, more “sticky” test compounds such as Texanol were monitored on a second GC-FID using the Tenax cartridge sampling system. During the experiments discussed in this report this GC was outfitted with a 30 m DB-5 megabore column, which was used as the primary method in the analysis of EPTC, and as a secondary method in the analysis of MITC.

Both the GC instruments were controlled and their data were analyzed using HPChem software installed on a dedicated PC. The GC's were spanned using the prepared calibration cylinder with known amounts of ethylene, propane, propylene, n-butane, n-hexane, toluene, n-octane and m-xylene in ultrapure nitrogen. Analyses of the span mixture were conducted approximately every day an experiment was run, and the results were tracked for consistency.

The surrogate components analyzed by the above system were calibrated by repeated analysis of a standard mixture containing these compounds, and verified by injecting and sampling known amounts of the compound in calibration chamber of known volume. The amounts of gaseous compounds injected were determined by vacuum methods, using an MKS Baratron precision pressure gauge, and bulbs of known volume, determined by weighing when filled with water. The amounts of liquid compounds injected were determined by measuring amounts injected using microliter syringes. The volumes of the calibration chambers were determined by injecting and analyzing compounds whose analyses have been calibrated previously.

The dichloropropene and (in part) the EPTC analyses were calibrated as discussed above for the liquid surrogate components. The EPTC analysis was also calibrated based on the injections of EPTC into the reactor during the experiments, based on the volume of liquid injected and the calculated volumes of the reactors. The MITC analysis could not be calibrated by this method because it is a solid at room temperature. Instead, it was calibrated in conjunction with the environmental chamber experiments, where known amounts were injected into the reactor using vacuum methods as discussed below. The reactor volumes were determined by injection and analysis of known amounts of the surrogate components and NO<sub>x</sub> during the experiments, and varied relatively little from experiment to experiment.

Carbon disulfide does not give a sufficient response on our GC-FID systems to be suitable for analysis by this method. Instead, a total sulfur analyzer (described on Table 2) was used for most experiments with this compound. This was calibrated using a calibration cylinder for SO<sub>2</sub> and other compounds purchased from Praxair. Although MITC and EPTC also contain sulfur, this instrument was not used because of limited availability, and because the GC analysis was considered to be sufficient.

Although the components of kerosene give a response on the GC-FID systems, the results are not suitable for quantitative analysis. A total carbon analyzer (described on Table 2) was used in injection tests for kerosene, carried out as described below for the purpose of developing and evaluating methods of injection into the gas phase. However, this analyzer was not sufficiently sensitive to be useful for qualitative analysis during the chamber experiments. Therefore, as was the case in our studies of other petroleum distillates in our coatings project (Carter and Malkina, 2005), it was necessary to assume that the injection of kerosene into the chamber was sufficiently complete so that the amount present in the gas

phase was the same as the calculated amount injected. This is discussed further in the “Results of Injection Tests” section, below.

As indicated in Table 2, aerosol number and size distributions were also measured in conjunction with our experiments. The instrumentation employed is similar to that described by Cocker et al. (2001), and is the same as employed in our previous studies of coatings VOCs (Carter et al, 2005a). Particle size distributions are obtained using a scanning electrical mobility spectrometer (SEMS) (Wang and Flagan, 1990) equipped with a 3077 <sup>85</sup>Kr charger, a 3081L cylindrical long column, and a 3760A condensation particle counter (CPC). Flow rates of 2.5 LPM and 0.25 LPM for sheath and aerosol flow, respectively, are maintained using Labview 6.0-assisted PID control of MKS proportional solenoid control valves. Both the sheath and aerosol flow are obtained from the reactor enclosure. The data inversion algorithm described by Collins et al (2002) converts CPC counts versus time to particle size distribution.

Most of the instruments other than the GCs and aerosol instrument were interfaced to a PC-based computer data acquisition system under the control of a LabView program written for this purpose. The TDLAS instruments were controlled by their own computers, but the data obtained were sent to the LabView data acquisition system during the course of the experiments using RS-232 connections. These data, and the GC data from the HP ChemStation computer, were collected over the CE-CERT computer network and merged into Excel files that are used for applying span, zero, and other corrections, and preparation of the data for modeling.

## **Sampling methods**

Samples for analysis by the continuous monitoring instrument were withdrawn alternately from the two reactors and zero air, under the control of solenoid valves that were in turn controlled by the data acquisition system discussed above. For most experiments the sampling cycle was 5 minutes for each reactor, the zero air, or (for control purpose) the chamber enclosure. The program controlling the sampling sent data to the data acquisition program to indicate which state was being sampled, so the data could be appropriately apportioned when being processed. Data taken less than 3-4 minutes after the sample switched were not used for subsequent data processing. The sampling system employed is described in more detail by Carter (2002).

Samples for GC analysis of surrogate compounds were taken at approximately 20-minute intervals directly from each of the reactors through the separate sample lines attached to the bottom of the reactors. The GC sample loops were flushed for a desired time with the air from reactors using pump. In the analyses using the Tenax system the 100 ml sample was collected directly from the reactors onto Tenax-GC solid adsorbent cartridge and then placed in series with the GC column, thermally desorbed at 300 C and cryofocused on the column. 100 ml gas-tight, all-glass syringe was used to collect Tenax sample. Additional sampling lines were attached to the bottom of each reactor for the Tenax sample collection, and their length was minimized to avoid possible losses.

## **Characterization Methods**

Use of chamber data for mechanism evaluation requires that the conditions of the experiments be adequately characterized. This includes measurements of temperature, humidity, light and wall effects characterization. Wall effects characterization is discussed in detail by Carter (2004) and updated by Carter and Malkina (2005) and most of that discussion is applicable to the experiments for this project. The instrumentation used for the other characterization measurements is summarized in Table 2, above, and these measurements are discussed further below.

Temperature was monitored during chamber experiments using calibrated thermocouples attached to thermocouple boards on our computer data acquisition system. The temperature in each of the reactors was continuously measured using relatively fine gauge thermocouples that were located ~1' above the floor of the reactors. These thermocouples were not shielded from the light, though it was hoped that irradiative heating would be minimized because of their small size. Experiments where the thermocouple for one of the reactors was relocated to inside the sample line indicated that radiative heating is probably non-negligible, and that a correction needs to be made for this by subtracting ~2.5°C from the readings of the thermocouples in the reactors. This is discussed by Carter (2004).

Light Spectrum and Intensity. The spectrum of the light source in the 300-850 nm region was measured using a LiCor LI-1800 spectroradiometer, which is periodically calibrated at the factory. Spectroradiometer readings were taken several times during a typical experiment, though the relative spectra were found to have very little variation during the course of these experiments. Changes in light intensity over time were measured using a PAR spherical irradiance sensor that was located immediately in front of the reactors. In addition, NO<sub>2</sub> actinometry experiments were carried out periodically using the quartz tube method of Zafonte et al (1977) modified as discussed by Carter et al (1995b). In most cases the quartz tube was located in front of the reactors near where the PAR sensor was located. Since this location is closer to the light than the centers of the reactors, the measurement at this location is expected to be biased high, so the primary utility of these data are to assess potential variation of intensity over time. However, several special actinometry experiments were conducted where the quartz tube was located inside the reactors, to provide a direct measurement of the NO<sub>2</sub> photolysis rates inside the reactors. The actinometry results obtained for the experiments of interest are discussed later in this report.

## **Experimental Procedures**

The reaction bags were collapsed to the minimum volume by lowering the top frames, and then emptying and refilling them at least six times after each experiment, and then filling them with dry purified air on the nights before experiments. Span measurements were generally made on the continuous instruments prior to injecting the reactants for the experiments. The reactants were then injected through Teflon injection lines (that are separate from the sampling lines) leading from the laboratory below to the reactors. The common reactants were injected in both reactors simultaneously, and were mixed by using the reactor-to-reactor exchange blowers and pipes for 10 minutes. The valves to the exchange system were then closed and the other reactants were injected to their respective sides and mixed using the in-reactor mixing blowers and pipes for 1 minute. The contents of the chamber were then monitored for at least 30 minutes prior to irradiation, and samples were taken from each reactor for GC analysis.

Once the initial reactants are injected, stabilized, and sampled, the light or lights employed (argon arc or blacklights) are turned on to begin the irradiation. During the irradiation the contents of the reactors are kept at a constant positive pressure by lowering the top frames as needed, under positive pressure control. The reactor volumes therefore decrease during the course of the experiments, in part due to sample withdrawal and in part due to small leaks in the reactor. A typical irradiation experiment ended after about 6 hours, by which time the reactors are typically down to about half their fully filled volume. Larger leaks are manifested by more rapid decline of reactor volumes, and the run is aborted early if the volume declines to about 1/3 the maximum. This was not the case for the experiments discussed in this report. After the irradiation the reactors were emptied and filled six times as indicated above.

The procedures for injecting the various types of reactants were as follows. The NO, NO<sub>2</sub> and MITC were prepared for injection using a vacuum rack. Known pressures of NO, measured with MKS Baratron capacitance manometers, were expanded into Pyrex bulbs with known volumes, which were then filled with nitrogen (for NO or MITC) or purified air (for NO<sub>2</sub>). In order to maintain constant NO/NO<sub>2</sub> ratios the same two bulbs of specified volume were utilized in most of experiments. The

contents of the bulbs were then flushed into the reactor(s) with nitrogen. Some of the gaseous reactants such as propylene and n-butane (other than for surrogate experiments) were prepared for injection using a high vacuum rack as well. For experiments with added CO, the CO was purified by passing it through an in-line activated charcoal trap and flushing it into the reactor at a known rate for the amount of time required to obtain the desired concentration. Measured volumes of volatile liquid reactants were injected, using a micro syringe, into a 2 ft long Pyrex injection tube surrounded with heat tape and equipped with one port for the injection of the liquid and other ports to attach bulbs with gas reactants. For injections into both reactors (e.g, the NO<sub>x</sub> and base ROG surrogate components in incremental reactivity experiments), one end of the injection tube was attached to the “Y”-shape glass tube (equipped with stopcocks) that was connected to reactors and the other end of injection tube was connected to a nitrogen source. The injections into a single reactor (e.g., for MITC in the reactivity experiments) was similar except the “Y” tube was not used.

The procedures for injection of the hydrocarbon surrogate components were as follows. A cylinder containing n-butane, trans-2-butene, propylene and ethylene in nitrogen, was used for injecting the gaseous components of the surrogate. The cylinder was attached to the injection system and a gas stream was introduced into reactors at controlled flow for certain time to obtain desired concentrations. A prepared mixture with the appropriate ratios of toluene, n-octane and m-xylene was utilized for injection of these surrogate components, using the procedures as discussed above for pure liquid reactants. All the gas and liquid reactants intended to be the same in both reactors were injected at the same time. The injection consisted of opening the stopcocks and flushing the contents of the bulbs and the liquid reactants with nitrogen, with the liquid reactants being heated slightly using heat that surrounded the injection tube. The flushing continued for approximately 10 minutes.

The liquid test compounds were injected, using a microsyringe, into a glass injection tube leading into the reactor to be employed for the compound. For the chloropropenes and CS<sub>2</sub> the procedures were the same as used for the liquid hydrocarbon surrogate components. For EPTC and kerosene, which are less volatile, the glass injection tube was heated to about 100°C, the injection lines into the reactors, which were wrapped with heat tape, were heated to ~75-90°C, and the samples were flushed into the reactor for at least an hour. As discussed below in the “Results of Injection Tests” section, tests were carried out to determine the extent to which these samples were injected into the gas phase using this method. The results indicated that at essentially all of the liquid EPTC and at least 90% of the liquid kerosene was injected into the gas phase using this procedure.

## Materials

The sources of the NO, CO and the various base case surrogate compounds came from various commercial vendors as employed in previous projects at our laboratory. The MITC was purchased from Aldridge Chemicals, and had a stated purity of 97%. The dichloropropenes used were in a “Telone II” sample provided by Dow AgroSciences LLC, of Indianapolis, IN, and it had a stated content of 95.5% active ingredients, and an identification number of TSN104897. This contained a mixture of isomers as discussed in the “Results” section of this report. The EPTC “Technical” sample was provided by Gowan Company of Yuma, AZ, and had a stated active ingredient content of 98.8% and a sample identification number of MB0473-3. The carbon disulfide sample was from Fisher Scientific, with a stated purity of >99.9%. No significant impurities were detected in any of the GC analyses of these samples.

The kerosene sample used in this project was provided by Harkrider Distribution Company of Houston, TX, at the request of ExxonMobil Chemical Company, also of Houston. A lot number or other identification was not provided. After conducting the chamber experiments and retaining a portion of this sample for potential future use, the remaining sample was sent to ExxonMobil Process Research Labs in Baton Rouge, LA for compositional analysis.



## MODELING METHODS

### Base Mechanism

#### Standard Chemical Mechanism

The starting point for the chemical mechanism evaluated in this work is the SAPRC-99 mechanism as documented by Carter (2000a). A complete listing of this mechanism is given by Carter (2000a) and in subsequent reports from our laboratory where this mechanism was used, all of which are available on our web site<sup>1</sup>. Files and software implementing this chemical mechanism are also available at our web site<sup>2</sup>, with the chemical mechanism simulation computer programs available there being essentially the same as those employed in this work. Changes have been made to the mechanisms of some individual VOCs due to subsequent experimental studies and reactivity assessment projects (Carter, 2003a), though none of those VOCs were studied in this project. The mechanisms used for test compounds studied for this project are discussed later in this section.

As discussed previously (Carter, 2000a,b), the SAPRC-99 mechanism consists of a “base mechanism” that represents the reactions of the inorganic species and common organic products and lumped organic radical model species and “operators”, and separate mechanisms for the initial reactions of the many types other organic compounds that are not in the base mechanism. The compounds, or groups of compounds, that are not included in the base mechanism but for which mechanism assignments have been made, are referred to as detailed model species. The latter include all the base ROG surrogate constituents and compounds whose reactivities were evaluated in this work. These compounds can either be represented explicitly, with separate model species with individual reactions or sets of reactions for each, or using lumped model species similar to those employed in the “fixed parameter” version of SAPRC-99 (Carter, 2000b). The latter approach is useful when modeling complex mixtures in ambient simulations or simulations of experiments with complex mixtures, but the other approach, representing each compound explicitly, is more appropriate when evaluating mechanisms for individual compounds or simple mixtures. This is because the purpose of mechanism evaluations against chamber data is to assess the performance of the mechanism itself, not to assess the performance lumping approaches. The latter is most appropriately assessed by comparing simulations of explicit and condensed versions of the same mechanism in ambient simulations.

In view of this, all of the organic constituents of the base ROG surrogate were represented explicitly using separate model species for each compound. In addition, the individual test compounds were also represented explicitly when simulating experiments with those compounds. This gives the least approximate representation of the atmospheric reactions of these compounds within the framework of the SAPRC-99 mechanism. The mechanisms for the individual test compounds are discussed separately later in this section.

#### Adjusted Base Mechanism

As discussed by Carter (2004) and Carter and Malkina (2005), the standard SAPRC-99 mechanism has a consistent bias to underpredict  $O_3$  formation in the surrogate -  $NO_x$  irradiations at the lower ROG/ $NO_x$  ratios. This bias showed up in a consistent underprediction of  $O_3$  in the base case of the

---

<sup>1</sup> These reports can be downloaded from <http://www.cert.ucr.edu/~carter/bycarter.htm>.

<sup>2</sup> Files and software implementing the SAPRC-99 mechanism are available at <http://www.cert.ucr.edu/~carter/SAPRC99.htm>.

standard MIR incremental reactivity experiment for this project. This bias should to some extent cancel out when modeling incremental reactivities because incremental reactivities are differences, and a similar bias would also occur to some extent in the added VOC test experiment. However, the addition of the test compound would change the effective ROG/NO<sub>x</sub> ratio, and therefore the magnitude of the underprediction bias may be different than in the base case. Also, the bias means that the model is not correctly simulating the chemical environment in which the VOC is reacting, and could result in inaccurate predictions of the impacts of the reactions of the test compounds, even if their mechanisms are correct. Worse, the possibility of errors in the base case simulation compensating for errors in the mechanism of the test compounds can not necessarily be ruled out.

To address this, it is necessary to provide an alternative approach for evaluating the model performance for the test compounds where the biases in the simulations of the base case is removed or at least modified. Therefore, as part of our previous study of coatings VOC reactivity (Carter and Malkina, 2005; Carter et al, 2005a) we developed an adjusted version of the base mechanism where the bias is removed. This adjustment involved increasing the yields of the aromatic fragmentation products AFG2 and AFG3 for toluene and m-xylene by a factor of 1.75, and increasing the rate constant for the reaction of the aromatic fragmentation product AFG1 by a factor of 10. These adjustments remove the underprediction bias in the model simulations of NO oxidation and O<sub>3</sub> formation in the MIR experiments without significantly impacting the ability of the model to simulate the MOIR/2 and other low NO<sub>x</sub> experiments, as shown by Carter and Malkina (2005), and also in the Results section, below.

Although this adjustment to the mechanism for toluene and m-xylene mechanisms in the base ROG improved the simulations of the base case experiments used in this and the CARB project (Carter and Malkina, 2005), it also resulted in significant overpredictions of O<sub>3</sub> formation rates in many of the aromatics - NO<sub>x</sub> experiments that were well simulated by the standard SAPRC-99 mechanism (see Carter and Malkina, 2005, Carter et al, 2005a for examples). The unadjusted mechanism also performed better in simulations of the base case for the earlier incremental reactivity experiments carried out at higher NO<sub>x</sub> levels in older UCR chambers (Carter et al, 1995b). Therefore, this adjusted base aromatics mechanism is not a “better” mechanism for these aromatics, it just has biases and problems that are different from the standard version.

The results of model simulations of incremental reactivity experiments using this mechanism, compared with those using the standard base mechanism, have been shown previously (Carter and Malkina, 2005; Carter et al, 2005a), and results of simulations of the base case experiments carried out for this study are similar. Carter and Malkina (2005) and Carter et al (2005a) also evaluated the mechanisms for the test compounds with both versions of the base mechanism, to provide useful information on effects of the base mechanism biases on results of incremental reactivity simulations for the test compounds of interest. The results indicated that the biases in the incremental reactivity results (the model predictions of the differences between the base case and the added test compound experiments) were not significantly different in the standard compared to the adjusted mechanisms. Therefore, to simplify the presentation in this report, except for a few illustrative examples the model simulations of the UCR EPA incremental reactivity experiments utilize primarily the adjusted base mechanism.

### **Representation of Chlorine Chemistry**

In order to represent the atmospheric reactions of chlorine-containing compounds whose reactions may result in the release of chlorine atoms, it is necessary to include in the mechanism a representation of the reactions of chlorine atoms and the ClO<sub>x</sub> species they form. Although chlorine chemistry is not part of the standard SAPRC-99 mechanism as documented by Carter (2000a), previous versions of the SAPRC mechanism included chlorine chemistry for the purpose of evaluating mechanisms for trichloroethylene (Carter et al, 1996b) and chloropicrin (Carter et al, 1997a,b). However, these

mechanisms were developed prior to the development of SAPRC-99 and are therefore somewhat out-of-date.

Therefore, an updated version of atmospheric chlorine chemistry, which was developed as part of our project to update the overall SAPRC mechanism (Carter, 2003b), was utilized for modeling the atmospheric reactions of the chlorine-containing pesticides for this project. This mechanism as utilized for this project is documented in Appendix A to this report. Note that the development of the updated SAPRC mechanism is still underway, and portions of the chlorine mechanism, particularly the representation of reactions of Cl with individual VOCs, is subject to change. The final report on the mechanism update project, which is expected around the end of 2006 or early 2007, should be consulted for the final version.

## **Representation of Chamber Conditions**

The procedures used in the model simulations of the environmental chamber experiments for this project were based on those discussed in detail by Carter (2004) and were employed in the studies of Carter and Malkina (2005) and Carter et al (2005a), except as indicated below. Carter (2004) should be consulted for details of the characterization model and chamber effects parameters employed. The temperatures used when modeling were the averages of the temperatures measured in the reactors, corrected as discussed by Carter (2004). The light intensity and spectrum for the arc light experiments was assumed to be constant, and a constant NO<sub>2</sub> photolysis rate of 0.260 min<sup>-1</sup> was used, as indicated by the results of the actinometry measurements discussed in the “Characterization Results” section, below. The arc light spectral distribution used by Carter (2004) was also used in this work because the spectral distribution measurements made during the experiments indicated no significant changes with time. The light intensity for the black light experiments varied with time, and the NO<sub>2</sub> photolysis rate for those experiments was derived as discussed in the “Characterization Results” section, below. The blacklight spectral distribution given by Carter et al (1995b) was found to be appropriate for the blacklights in this chamber and was therefore used when modeling the blacklight runs discussed in this report.

The chamber effects parameters used when modeling the experiments in this chamber were the same as those given by Carter (2004) except for the HONO offgasing parameters, which were derived based on results of characterization runs carried out in conjunction with these experiments. As discussed by Carter (2004), the chamber effects model currently used for this chamber represents both the chamber radical source and background NO<sub>x</sub> offgasing by HONO offgasing, whose magnitude is determined by the chamber effects parameter RN-I, which is the ratio of the HONO offgasing rate to the NO<sub>2</sub> photolysis rate. The RN-I parameter that best fits the characterization data tends to vary over time depending on the conditions of the chamber, and the results of the characterization experiments applicable to modeling the experiments discussed in this report, and the assignment of the RN-I values used, are given in the Characterization Results section, below.

The initial reactant concentrations used in the model simulations were based on the measured values except for kerosene, for which the amount injected had to be derived from the volume of liquid injected and the calculated or estimated volume of the reactors. The assumption of complete or near-complete injection was supported by results of injection tests carried out with these materials, as discussed below. The volumes of the reactors were determined in separate experiments where known amounts of materials were injected and analyzed in the gas-phase. Although the reactors are flexible, their initial volumes were very consistent from run to run because of the use of the pressure control system when filling the reactor to its maximum volume prior to the reactant injections (see Chamber Description section, above, and Carter, 2004). (Note that the calibration of the EPTC analysis is also based in part of results of injections into the reactors during the experiments, based on assuming complete injection.)

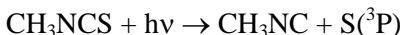
## Mechanisms for Test Compounds

Table 3 and Table 4 give the model species and reactions used for the atmospheric reactions of the pesticide compounds represented in model simulations carried out for this project, and Table 5 gives the absorption cross sections of the photoreactive species involved. Footnotes to Table 4 document the choices of the rate constants and the reactions used. These include representative compounds methyl isothiocyanate (MITC), carbon disulfide, S-ethyl N,N-di-n-propyl thiocarbamate (EPTC), and the 1,3-dichloropropenes that were studied in the chamber experiments for this project, and the additional representative pesticide compounds whose atmospheric reactivities were also calculated for this project. The compounds listed include those that were studied in the chamber experiments for this project, and volatile pesticide compounds listed in Table 1 whose atmospheric ozone impacts were assessed for this project.

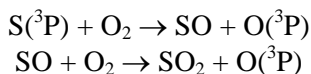
Most of the individual compounds used to represent the constituents of kerosene are already included in the SAPRC-99 mechanism as documented (Carter, 2000a), but some compounds may have been added subsequently so a complete listing of their reactions is given in Appendix B to this report. The main issue with representing kerosene and other complex hydrocarbon mixtures in atmospheric model simulations is the choice of compounds used to represent the mixture. This is discussed in the subsection for kerosene, below.

### Methyl Isothiocyanate (MITC)

Available information concerning the reactions of MITC in air are discussed by Wales (2002). Geddes et al (1995) studied the gas-phase photolysis of MITC and found that it underwent loss by photolysis with a half-life of about one day under ambient conditions, and formed a variety of products, including methyl isocyanide ( $\text{CH}_3\text{NC}$ ) and  $\text{SO}_2$ , in addition to other products whose formations can be attributed to heterogeneous hydrolysis processes. The photolysis reaction was studied in more detail by Alvarez (1993) and Alvarez and Moore (1994), who measured the absorption cross sections for MITC, and obtained data indicating that the primary photolysis process is



with a quantum yield of  $0.98 \pm 0.24$ . Under atmospheric conditions, the primary fate of S atoms is expected to be reaction with  $\text{O}_2$ , forming SO, which is also expected to primarily react with  $\text{O}_2$ .



(SO will also react with  $\text{O}_3$  and  $\text{NO}_2$ , but based on the IUPAC (2006) rate constant recommendations the reaction with  $\text{O}_2$  would dominate as long as the concentration of  $\text{NO}_2$  is below about 100 ppb.)

The MITC absorption cross sections used for modeling purposes, based on the data of Alvarez (1993) and Alvarez and Moore (1994) are given in Table 5. Their data also indicate essentially unit quantum yields, which is also assumed in the model. Based on this and the measured light source spectra of our chamber experiments, we obtain ratios of photolysis rates for MITC relative to  $\text{NO}_2$  of  $2.19 \times 10^{-4}$  and  $4.00 \times 10^{-4}$ , for the arc light and blacklight experiments respectively. These correspond to MITC photolysis rates of  $6.45 \times 10^{-5} \text{ min}^{-1}$  for the arc light experiments and  $5.31 - 5.40 \times 10^{-5} \text{ min}^{-1}$  for the blacklight runs. For actinic fluxes calculated for atmospheric conditions with direct overhead sunlight (Peterson, 1976) the calculated photolysis rate is  $4.5 \times 10^{-4} \text{ min}^{-1}$  ( $8.5 \times 10^{-4}$  relative to  $\text{NO}_2$ ).

For modeling purposes, we assume that the overall process of the MITC photolysis under atmospheric conditions is

Table 3. List of model species added to the mechanism to represent the atmospheric reactions of the pesticide compounds modeled for this project.

Type and Name	Description
<u>Pesticide compounds studied for this project</u>	
MITC	Methyl isothiocyanate
CS <sub>2</sub>	Carbon disulfide
EPTC	S-ethyl N,N-di-n-propyl thiocarbamate
T13DCP	Trans 1,3-dichloropropene
C13DCP	Cis 1,3-dichloropropene
<u>Other representative pesticide compounds modeled</u>	
MOLINATE	Molinate
PEBULATE	Pebulate
THIOCARB	thiobencarb
CCL <sub>3</sub> NO <sub>2</sub>	Chloropicrin
<u>Reactive pesticide product species added to mechanism</u>	
OCS	OCS molecules. (Treated as unreactive)
CLCHO	Formyl Chloride. (Treated as unreactive)
CL <sub>2</sub> CO	Phosgene. (Treated as unreactive)
CLCCHO	Chloroacetaldehyde
<u>Reactive intermediate radicals</u>	
HS	HS Radicals
HSO	HSO Radicals
R <sub>2</sub> NCOS.	C <sub>3</sub> H <sub>7</sub> N(C <sub>3</sub> H <sub>7</sub> )C(O)S· Radicals. (Steady state approximation employed)
R <sub>2</sub> NCOSO.	C <sub>3</sub> H <sub>7</sub> N(C <sub>3</sub> H <sub>7</sub> )C(O)SO· Radicals. (Steady state approximation employed)
<u>Species used to represent overall thiocarbamate reactions. (Steady state approximation employed)</u>	
EPTC-1	CH <sub>3</sub> CH <sub>2</sub> CH(·)N(C <sub>3</sub> H <sub>7</sub> )C(O)SC <sub>2</sub> H <sub>5</sub> radicals and subsequent processes. Also used to represent reactions at other positions of the molecule besides at or by the N or the S.
PBLA-1A	Radicals formed from OH reaction with pebulate, molinate, or thiobencarb, respectively, that represent an analogue to EPTC-1.
PBLA-1B	
MOLI-1	
THCB-1	C <sub>3</sub> H <sub>7</sub> N(C <sub>3</sub> H <sub>7</sub> )C(O)S(OH)C <sub>2</sub> H <sub>5</sub> radicals and subsequent processes.
EPTC-2	
PBLA-2	
MOLI-2	
THCB-2	C <sub>3</sub> H <sub>7</sub> N(C <sub>3</sub> H <sub>7</sub> )C(O)SCH(·)CH <sub>3</sub> radicals and subsequent processes.
EPTC-3	
PBLA-3	
MOLI-3	
THCB-3	Radicals formed from OH reaction with pebulate, molinate, or thiobencarb, respectively, that represent an analogue to EPTC-3.

Table 4. Reactions and kinetic parameters added to the mechanism to represent the atmospheric reactions of the pesticide compounds modeled for this project.

Label	Reaction and Products [a]	Rate Parameters [b]			Refs & Notes [c]	
		k(298)	A	Ea		
<u>Reactions of Methyl Isothiocyanate</u>						
MIOH	MITC + HO. = XC + HS	1.72e-12			1	
MIHV	MITC + HV = XC + SO2 + #2 O3P		Phot Set= MITC			2
SH01	HS + O3 = HSO + O2	3.32e-12	8.50e-12	0.56	3	
SH02	HS + NO2 = HSO + NO	6.49e-11	2.90e-11	-0.48	3	
SH03	HSO + O3 = #.55 {HS + O2 + O2} + #.45 {HO2. + SO2}	1.10e-13			3	
SH04	HSO + NO2 = NO + HO2. + SO2	9.60e-12			3	
SHX1	HS + O2 = HO2. + SO2	1.00e-20			4	
SHX2	HSO + O2 = HO2. + SO2 + O3P	1.00e-17			5	
<u>Reactions of Carbon Disulfide</u>						
CSOH	CS2 + HO. = HO2. + SO2 + OCS	2.76e-12			6	
CSHV	CS2 + HV = OCS + SO2 + O3P		Phot Set= CS2, qy= 0 - 1.2e-2			7
<u>Reactions of S-Ethyl N,N-di-n-propyl thiocarbamate</u>						
EPOH	EPTC + HO. = #.59 EPTC-1 + #.205 {EPTC-2 + EPTC-3}	2.12e-11			1,8	
EPr1	EPTC-1 = #.2 RO2-N. + #.8 {RO2-R. + R2O2. + CCHO + PROD2} + #1.4 XC + XN		Fast		8	
EPr2	EPTC-2 = PROD2 + HO2. + #3 XC + XN		Fast		8	
EPr3	EPTC-3 = #.2 {RO2-N. + XN} + #.8 {R2O2. + CCHO + R2NCOS.} + #.6 XC		Fast		8	
EPS1	R2NCOS. + NO2 = R2NCOSO. + NO	6.00e-11			9	
EPS2	R2NCOS. + O3 = R2NCOSO. + O2	4.90e-12			9	
EPS3	R2NCOSO. + NO2 = RCO-O2. + SO2 + NO + #4 XC + XN	1.20e-11			10	
EPS4	R2NCOSO. + O3 = RCO-O2. + SO2 + O2 + #4 XC + XN	4.10e-13			10	
EPN3	EPTC + NO3 = HNO3 + #.6 EPTC-1 + #.4 EPTC-3	9.20e-15			11	
<u>Reactions of Pebulate</u>						
pbOH	PEBULATE + HO. = #.4 PBLA-1A + #.21 PBLA-1B + #.195 {PBLA-2 + PBLA-3}	2.26e-11			12	
pbr1a	PBLA-1A = #.23 RO2-N. + #.77 {RO2-R. + R2O2. + RCHO + PROD2} + #1.69 XC + XN		Fast		13,14	
pbr1b	PBLA-1B = #.23 RO2-N. + #.77 {RO2-R. + R2O2. + HCHO + PROD2} + #3.23 XC + XN				13,14	
pbr2	PBLA-2 = PROD2 + HO2. + #4 XC + XN		Fast		15	
pbr3	PBLA-3 = #.23 {RO2-N. + XN} + #.77 {R2O2. + RCHO + R2NCOS.} + #.92 XC		Fast		14,16	
pbN3	PEBULATE + NO3 = HNO3 + #.3 PBLA-1A + #.3 PBLA-1B + #.4 PBLA-3	9.20e-15			17	

Table 4 (continued)

Label	Reaction and Products [a]	Rate Parameters [b]			Refs & Notes [c]
		k(298)	A	Ea	
<u>Reactions of Molinate</u>					
moOH	MOLINATE + HO. = #.64 MOLI-1 + #.18 {MOLI-2 + MOLI-3}	2.42e-11			12
mor1	MOLI-1 = #.2 RO2-N. + #.8 {RO2-R. + R2O2. + RCHO} + #5.4 XC + XN		Fast		18
mor2	MOLI-2 = PROD2 + HO2. + #3 XC + XN		Fast		15
mor3	MOLI-3 = #.2 {RO2-N. + XN} + #.8 {R2O2. + CCHO + R2NCOS.} + #.6 XC		Fast		16
moN3	MOLINATE + NO3 = HNO3 + #.6 MOLI-1 + #.4 MOLI-3	9.20e-15			17
<u>Reactions of Thiobencarb</u>					
tcOH	THIOCARB + HO. = #.53 THCB-1 + #.235 {THCB-2 + THCB-3}	1.87e-11			12,19
tcr1	THCB-1 = #.23 RO2-N. + #.77 {RO2-R. + R2O2. + HCHO} + #9.85 XC + XN		Fast		13,14
tcr2	THCB-2 = PROD2 + HO2. + #6 XC + XN		Fast		15
tcr3	THCB-3 = #.23 {RO2-N. + XN} + #.77 {R2O2. + BALD + R2NCOS.} + #-.16 XC		Fast		14,16
tcN3	THIOCARB + NO3 = HNO3 + #.6 THCB-1 + #.4 THCB-3	9.20e-15			17
<u>Reactions of the 1,3-Dichloropropenes</u>					
tpOH	T13DCP + HO. = RO2-R. + CLCCHO + CLCHO	1.44e-11			20,21
cpOH	C13DCP + HO. = RO2-R. + CLCCHO + CLCHO	8.45e-12			20,21
tpO3	T13DCP + O3 = #.057 HO. + #.057 RO2-CL. + #.057 CO + #.057 HCHO + #.5 CLCCHO + #.5 CLCHO + #.444 RCO-OH + #.054 XC	3.10e-19	6.64e-15	5.91	20,22
cpO3	C13DCP + O3 = #.057 HO. + #.057 RO2-CL. + #.057 CO + #.057 HCHO + #.5 CLCCHO + #.5 CLCHO + #.444 RCO-OH + #.054 XC	1.50e-19	3.22e-15	5.91	20,22
tpN3	T13DCP + NO3 = #.949 NO2 + #.051 RO2-N. + #.949 R2O2. + #.949 CLCCHO + #.949 CLCHO + #.051 XN + #-.153 XC	9.13e-17			20,23
cpN3	C13DCP + NO3 = #.949 NO2 + #.051 RO2-N. + #.949 R2O2. + #.949 CLCCHO + #.949 CLCHO + #.051 XN + #-.153 XC	5.57e-18			20,23
tpOP	T13DCP + O3P = MEK + #-1 XC	1.30e-12			20,24
cpOP	C13DCP + O3P = MEK + #-1 XC	4.79e-13			20,24
tpCL	T13DCP + CL. = #.474 RO2-R. + #.051 RO2-N. + #.474 RO2-CL. + #.474 CLCCHO + #.474 CLCHO + #1.27 XC	8.58e-11			20,25
cpCL	C13DCP + CL. = #.474 RO2-R. + #.051 RO2-N. + #.474 RO2-CL. + #.474 CLCCHO + #.474 CLCHO + #1.27 XC	8.58e-11			20,25

Table 4 (continued)

Label	Reaction and Products [a]	Rate Parameters [b]			Refs & Notes [c]
		k(298)	A	Ea	
<u>Reactions of Chloroacetaldehyde</u>					
clp2	CLCCHO + HV = HO2. + CO + HCHO + RO2-CL.		Phot Set= CLCCHO		26
clp3	CLCCHO + HO. = RCO-O2. + #-1 XC	3.10e-12			27
clp4	CLCCHO + CL. = HCL + RCO-O2. + #-1 XC	1.29e-11			27
<u>Reactions of Chloropicrin</u>					
CPHV	CCL3NO2 + HV = NO2 + RO2-CL. + XC		Phot Set= CLPICRIN, qy= 8.7e-1		28

[a] Format of reaction listing: “=” separates reactants from products; “#*number*” indicates stoichiometric coefficient, “#*coefficient* { *product list* }” means that the stoichiometric coefficient is applied to all the products listed.

[b] Except as indicated, the rate constants are given by  $k(T) = A \cdot (T/300)^B \cdot e^{-E_a/RT}$ , where the units of k and A are  $\text{cm}^3 \text{ molec}^{-1} \text{ s}^{-1}$ , Ea are  $\text{kcal mol}^{-1}$ , T is  $^{\circ}\text{K}$ , and  $R=0.0019872 \text{ kcal mol}^{-1} \text{ deg}^{-1}$ . The following special rate constant expressions are used:

Phot Set = *name*: The absorption cross sections and quantum yields for the photolysis reaction are given in Table A-5, where “*name*” indicates the photolysis set used. If a “qy=*number*” notation is given, the number is the overall quantum yield, which is assumed to be wavelength independent.

Fast: Represented as fast and as the only fate of the reactant, which is treated in steady state. Equivalent to replacing all reactions forming this reactant with the products of this reaction.

[c] Footnotes documenting sources of rate constants and mechanisms are as follows.

- 1 Rate constants derived from chamber data from this study.
- 2 Based on data from Alvarez (1993) and Alvarez and Moore (1994). Absorption cross sections given in Table 5.
- 3 Based on current IUPAC (2006) recommendations
- 4 Added at or below the upper limit rate constant to avoid problems in simulations where both NO<sub>2</sub> and O<sub>3</sub> are low. These are not expected to be important under conditions of the experiments and scenarios simulated for this project.
- 5 Rate constant set at a sufficiently high value so that this reaction is the major fate of HSO, but still below the IUPAC (2006)-recommended upper limit. It is necessary for the model to predict that this reaction dominates over competing processes to be consistent with the chamber data; see text. Note that this is used for MITC Mechanism “B”. Mechanism “A”, which is not used for the atmospheric reactivity simulations because its predictions are inconsistent with the chamber data obtained for this project, uses a rate constant of  $1 \times 10^{-20} \text{ cm}^3 \text{ molec}^{-1} \text{ s}^{-1}$ , which is sufficiently low that this reaction is unimportant in the chamber simulations.
- 6 Mechanism is complex and depends on pressure, temperature, and O<sub>2</sub> content. Rate constant given is for 1 atm air and 298K only, and derived from the IUPAC (2006) rate constants recommended for CS<sub>2</sub> and HOCS<sub>2</sub>, the species assumed to be initially formed in the reaction.
- 7 Absorption cross sections from current IUPAC (2006) recommendation, and are given in Table 5. Quantum yield is IUPAC (2006) upper limit recommendation, but the possibility of a lower quantum yield cannot be ruled out by the data. Chamber and atmospheric reactivity simulations are carried out using both this upper limit and zero overall quantum yield.
- 8 EPTC-1 through EPTC-3 represents radicals formed by reactions at various positions of the molecule, as indicated in Table 7 and in the discussion of the thiocarbamate mechanisms.
- 9 Rate constant and mechanism based on IUPAC (2006) recommendations for CH<sub>3</sub>S·.



Table 4 (continued)

- 10 Rate constant and mechanism based on IUPAC (2006) recommendations for  $\text{CH}_3\text{SO}\cdot$ .
- 11 Rate constant from Kwok et al (1992). Mechanism is assumed to be analogous to the OH reaction except that the analogue to the addition reaction does not occur.
- 12 Mechanism and rate constant estimated by analogy with EPTC. Rate constant estimated by assuming that rate constant for reaction at the positions next to the N and next to or on the S are the same as for the analogous reactions of EPTC. Rate constants for reactions at the other positions are estimated using the group-additivity methods in the SAPRC-99 estimation system (Carter, 2000a). The product species shown have analogous meanings and mechanisms as EPTC-1 through 3. Their relative rates of formation are based on the estimated rates of reactions at the various positions of the molecule, with model species-1 being used to represent reactions at other positions besides those next to or on the N or S, as assumed in the case of EPTC. See Table 7.
- 13 Analogous to the reactions of EPTC-1 except that different aldehydes are expected to be formed in the decomposition reactions. See Table 7.
- 14 A higher overall nitrate yield is estimated (Carter, 2000a) for the peroxy intermediates than is the case for EPTC because of the greater number of carbons. The nitrate yields for aromatic compounds are probably less than for the corresponding alkane, so we assume approximately the same overall nitrate yields for the C12 radicals formed from thiocarb as the C10 radicals formed from pebulate.
- 15 Same as the representation of EPTC-2, with the sulfoxide product formed also represented by PROD2. See Table 7.
- 16 Analogous to the reactions of EPTC-3 except that different aldehyde products may be formed in the decomposition reaction. See Table 7.
- 17 Same rate constant and analogous mechanism as used for EPTC.
- 18 Analogous to the reactions of EPTC-1 except that a dialdehyde product is expected to be formed in the decomposition reaction, rather than two separate aldehyde molecules. The dialdehyde is represented by RCHO. See Table 7.
- 19 Reaction on the Cl-substituted aromatic is assumed to be relatively minor and is ignored for mechanistic or kinetic estimates.
- 20 Mechanism derived from detailed mechanism given in Table 9 and products represented as shown on Table 10.
- 21 Rate constant from Tuazon et al (1988).
- 22 Rate constant at 298K measured by Tuazon et al (1984). Temperature dependence estimated by assuming that the A factor is the same as that for trans or cis-2-butene.
- 23 Rate constant estimated from the correlation between the OH and NO<sub>3</sub> rate constants, as discussed by Carter (2000a).
- 24 Estimated from the correlation between the OH and O(<sup>3</sup>P) rate constants (Carter 2000a).
- 25 Rate constant estimated using group-additivity methods as discussed in Appendix A.
- 26 Absorption cross sections from NASA (2006), and are given in Table 5. Unit quantum yields assumed. See text for a discussion of the mechanism.
- 27 Rate constants from Scollard et al (1993). Represented as forming same products as corresponding reaction of propionaldehyde.
- 29 Absorption cross sections, overall quantum yield, and best fit mechanism discussed by Carter et al (1997a,b). Assumes photolysis forms  $\text{CCl}_3\cdot$ , which forms  $\text{CCl}_3\text{O}\cdot$  after an NO to NO<sub>2</sub> conversion, then decomposes to  $\text{Cl}_2\text{CO}$  and Cl atoms.  $\text{Cl}_2\text{CO}$  is treated as unreactive.

Table 5. Absorption cross sections used for the photolysis reactions added to the mechanism to represent the atmospheric reactions of the pesticide compounds modeled for this project.

Phot Set = CS2				Phot Set = CLCCHO				Phot Set = CLPICRIN			
Wl.	Abs.	Wl.	Abs.	Wl.	Abs.	Wl.	Abs.	Wl.	Abs.	Wl.	Abs.
285	1.58e-21	329	2.85e-20	285	4.55e-20	322	3.26e-20	286	1.44e-19	340	5.20e-21
286	2.09e-21	330	3.80e-20	286	4.64e-20	323	2.49e-20	288	1.34e-19	342	4.80e-21
287	2.54e-21	331	1.30e-20	287	4.80e-20	324	2.11e-20	290	1.23e-19	344	4.36e-21
288	3.09e-21	332	3.06e-20	288	4.99e-20	325	1.92e-20	292	1.10e-19	346	4.00e-21
289	4.45e-21	333	1.55e-20	289	5.03e-20	326	1.87e-20	294	9.82e-20	348	3.68e-21
290	4.38e-21	334	1.51e-20	290	5.20e-20	327	1.87e-20	296	8.71e-20	350	3.34e-21
291	6.35e-21	335	1.38e-20	291	4.95e-20	328	1.70e-20	298	7.57e-20	352	3.05e-21
292	6.40e-21	336	8.61e-21	292	4.94e-20	329	1.92e-20	300	6.44e-20	354	2.70e-21
293	8.78e-21	337	1.38e-20	293	5.14e-20	330	1.64e-20	302	5.47e-20	356	2.51e-21
294	8.01e-21	338	5.91e-21	294	5.48e-20	331	1.52e-20	304	4.68e-20	358	2.30e-21
295	1.14e-20	339	1.12e-20	295	5.47e-20	332	1.68e-20	306	3.97e-20	360	1.54e-21
296	1.13e-20	340	4.89e-21	296	5.64e-20	333	1.42e-20	308	3.33e-20	362	2.13e-21
297	1.86e-20	341	3.86e-21	297	5.56e-20	334	1.36e-20	310	2.79e-20	364	1.78e-21
298	2.29e-20	342	5.73e-21	298	5.75e-20	335	1.06e-20	312	2.36e-20	366	1.25e-21
299	2.02e-20	343	3.87e-21	299	5.63e-20	336	7.47e-21	314	2.03e-20	368	1.28e-21
300	1.88e-20	344	5.56e-21	300	5.57e-20	337	6.22e-21	316	1.77e-20	370	1.04e-21
301	3.27e-20	345	3.53e-21	301	5.10e-20	338	5.02e-21	318	1.55e-20	372	1.08e-21
302	3.17e-20	346	3.50e-21	302	4.92e-20	339	4.11e-21	320	1.38e-20	374	7.13e-22
303	3.13e-20	347	3.28e-21	303	5.01e-20	340	3.40e-21	322	1.23e-20	376	6.96e-22
304	4.44e-20	348	1.09e-21	304	5.30e-20	341	2.81e-21	324	1.10e-20	378	5.85e-22
305	4.46e-20	349	3.68e-21	305	5.27e-20	342	2.47e-21	326	9.94e-21	380	5.57e-22
306	3.66e-20	350	2.39e-21	306	5.48e-20	343	2.13e-21	328	8.98e-21	382	4.66e-22
307	5.12e-20	351	1.27e-21	307	5.34e-20	344	1.90e-21	330	8.18e-21	384	4.68e-22
308	7.10e-20	352	2.55e-21	308	5.44e-20	345	1.59e-21	332	7.54e-21	386	1.70e-22
309	4.93e-20	353	6.60e-22	309	5.37e-20	346	1.36e-21	334	6.82e-21	388	5.02e-22
310	8.84e-20	354	1.72e-21	310	5.03e-20	347	9.77e-22	336	6.27e-21	390	3.50e-22
311	5.61e-20	355	2.47e-21	311	4.61e-20	348	7.91e-22	338	5.69e-21	392	-
312	6.69e-20	356	5.20e-22	312	3.92e-20	349	6.23e-22				
313	8.15e-20	357	1.33e-21	313	3.71e-20	350	5.45e-22	<div>Phot Set = MITC</div>			
314	7.84e-20	358	5.50e-22	314	3.73e-20	351	5.58e-22	Wl.	Abs.		
315	9.44e-20	359	5.90e-22	315	3.96e-20	352	6.03e-22	285.6	3.44e-20		
316	7.04e-20	360	1.19e-21	316	3.85e-20	353	6.33e-22	290.0	2.66e-20		
317	9.46e-20	361	4.20e-22	317	4.16e-20	354	5.65e-22	297.5	1.70e-20		
318	7.16e-20	362	4.80e-22	318	3.84e-20	355	3.77e-22	302.5	1.23e-20		
319	9.80e-20	363	2.10e-22	319	3.78e-20	356	2.39e-22	307.5	8.52e-21		
320	4.52e-20	364	3.70e-22	320	3.84e-20	357	1.23e-22	312.5	5.63e-21		
321	6.12e-20	365	1.20e-22	321	3.43e-20	358	-	317.5	3.48e-21		
322	4.22e-20	366	3.60e-22					322.5	1.96e-21		
323	5.18e-20	367	2.30e-22					327.5	9.60e-22		
324	3.52e-20	368	2.00e-22					332.5	4.00e-22		
325	8.63e-20	369	1.10e-22					337.5	1.70e-22		
326	5.02e-20	370	1.80e-22					340.0	-		
327	3.48e-20	371	-								
328	2.85e-20										

Wavelengths in nm and absorption cross sections are in  $\text{cm}^{-2}$ .



$\text{CH}_3\text{NC}$  is assumed to be relatively unreactive on the time scale of the experiments and its subsequent reactions are ignored. Although  $\text{SO}_2$  is represented in the base SAPRC-99 mechanism, its formation is also not expected to have a significant contribution to the ozone reactivity of MITC. (It will impact the reactivity with respect to PM formation, as discussed below in the “PM Impact Results” section.) On the other hand, the major fate of  $\text{O}(^3\text{P})$  is reaction with  $\text{O}_2$  to form  $\text{O}_3$ , and thus this photolysis promotes  $\text{O}_3$  formation, though this is not a radical initiation process.

MITC is also expected to react in the atmosphere primarily with OH radicals. This reaction was studied by Sommerlade et al (2006), who obtained a rate constant of  $1.28 \times 10^{-12} \text{ cm}^3 \text{ molec}^{-1} \text{ s}^{-1}$  at 70 torr and 298K. This rate constant is sufficiently high that the reaction with OH would be expected to be an important loss process for MITC under the conditions of our experiments and atmospheric simulations. A measurement of this rate constant was also obtained in the experiments carried out for this project, as discussed in the “OH Radical Rate Constant Determination” section, below. The results indicated a rate constant for the reaction of OH with MITC of  $1.72 \times 10^{-12} \text{ cm}^3 \text{ molec}^{-1} \text{ s}^{-1}$ , assuming that MITC undergoes photolysis in our experiments at rates estimated as discussed above. (If photolysis is assumed to be negligible, the OH derived rate constant is 16% higher, though the data are equally well fit in either case.) This is about 34% higher than the rate constant of Sommerlade et al (2006), but is not necessarily inconsistent with this result if the reaction is pressure dependent. Because of this possibility of pressure dependence, the rate constant obtained in our study, which was obtained at atmospheric pressure, was used as the basis for modeling.

We could find no information concerning the mechanism of the OH reaction. Sommerlade et al (2006) postulated that the initial reaction is OH addition to the unsaturated carbon center, followed by elimination of HS.



This is a reasonable mechanism and we also assume that this is the case for this work. Note that the initial process is an addition reaction, so the reaction could well be pressure dependent, explaining the difference between the rate constant measured in this work and that of Sommerlade et al (2006), who measured the rate constant at 70 torr. For modeling purposes we assume that  $\text{CH}_3\text{NCO}$  is relatively unreactive on the time scale of the experiments (and the one day atmospheric reactivity calculations) and its subsequent reactions are ignored.

There is information available concerning the subsequent reactions for the HS radical under atmospheric conditions, but not enough to completely constrain the mechanism for atmospheric modeling purposes. The reactions expected to occur, based on current IUPAC (2006) evaluations where available or our estimates otherwise, are listed on Table 6. Other reactions may be occurring with these species, but those listed on Table 6 are considered to be the most likely to be non-negligible under atmospheric or simulated atmospheric conditions. The main uncertainty appears to be the possible reaction of HSO with  $\text{O}_2$ , for which only an upper limit rate constant of  $2 \times 10^{-17} \text{ cm}^3 \text{ molec}^{-1} \text{ s}^{-1}$ . If this reaction occurs with a rate constant at or near this upper limit, this would be the major fate of HSO, but the actual rate constant may well be orders of magnitude lower, if it occurs at all.

For mechanism evaluation purposes, we consider two alternative mechanisms, based on the assumed rate constant for  $\text{HSO} + \text{O}_2$ . In Mechanism “A” we assume that the reaction is unimportant under atmospheric conditions, and use a rate constant that is sufficiently low that it is negligible as long as at least some  $\text{NO}_2$  or  $\text{O}_3$  is present. In conditions where reaction with  $\text{NO}_2$  dominates over reaction with  $\text{O}_3$  (which is calculated to be the case in our incremental reactivity chamber experiments), the net effect of the MITC reaction is conversion of two molecules of  $\text{NO}_2$  to NO and formation of  $\text{HO}_2$ . Since  $\text{HO}_2$  reacts

Table 6. Mechanisms for reactions of HS, HSO, and HSO<sub>2</sub> radicals under atmospheric conditions, and current IUPAC recommended rate constants.

Reaction	k (300K) (cm <sup>3</sup> molec <sup>-1</sup> s <sup>-1</sup> )	References and notes [a]
HS + O <sub>3</sub> → HSO + O <sub>2</sub>	3.74e-12	k(T)=9.5e-13 exp(280/T) [IUPAC SOx36 11/19/01]
HS + NO <sub>2</sub> → HSO + NO	6.45e-11	k(T)=2.9e-11 exp(-240/T) [IUPAC SOx36 11/19/01]
HS + O <sub>2</sub> → HSO <sub>2</sub> [b]	1.0e-20 [c]	k < 4e-19 IUPAC SOx35 [IUPAC SOx39 11/19/01]
HSO + O <sub>3</sub> → 0.55 {HS + 2 O <sub>2</sub> } + 0.45 {HSO <sub>2</sub> + O <sub>2</sub> }	1.0e-13	Mechanism k(298) rate constant based on IUPAC recommendation [IUPAC SOx40 11/19/01]
HSO + NO <sub>2</sub> → HSO <sub>2</sub> + NO	9.6e-12	Recommended k(298) [IUPAC SOx42 11/19/01]
HSO + O <sub>2</sub> → HO <sub>2</sub> + SO [d]	Varied A: 1.0e-20 B: 1.0e-17	k < 2e-17 [IUPAC SOx39 11/19/01]. “A” and “B” refer to alternative mechanisms that are examined. See text.
HSO <sub>2</sub> + O <sub>2</sub> → HO <sub>2</sub> + SO <sub>2</sub>	Fast [c]	Expected to be the only fate of HSO <sub>2</sub>
SO + O <sub>2</sub> → SO <sub>2</sub> + O( <sup>3</sup> P)	Fast [c]	Assumed to dominate over competing reactions based on IUPAC recommendations [IUPAC SOx44, SOx45, SOx46 11/20/01]

[a] IUPAC (2006) recommended rate constant temperature dependence, evaluation sheet number, and date given where applicable. Names and dates of IUPAC datasheets are indicated.

[b] This is the expected mechanism, but it has not been experimentally verified.

[c] Reaction is included at rate constant below the recommended upper limit to provide a sink for the species in cases where both NO<sub>2</sub> and O<sub>3</sub> are low. Rate constant set such that the reaction is negligible under the conditions of the experiments modeled in this report.

[d] The mechanism for this reaction, if it occurs, is unknown. This is the expected mechanism, either as a concerted process or following the formation of an adduct that subsequently decomposes. The concerted reaction is estimated to be endothermic by ~6 kcal/mole (NASA, 2006), but this is not inconsistent with the reaction occurring at its upper limit rate constant of 2 x 10<sup>-17</sup> cm<sup>3</sup> molec<sup>-1</sup> s<sup>-1</sup> if the A factor > 3 x 10<sup>-13</sup> cm<sup>3</sup> molec<sup>-1</sup> s<sup>-1</sup>. The A factor is probably similar to that for HCO + O<sub>2</sub>, which is 5.2 x 10<sup>-12</sup> cm<sup>3</sup> molec<sup>-1</sup> s<sup>-1</sup> (NASA, 2006).

[c] These reactions are assumed to be the only fate of these species and these species are replaced by the products formed in the model simulations. Reactions forming HSO<sub>2</sub> or SO are represented as forming HO<sub>2</sub> and SO<sub>2</sub> or SO<sub>2</sub> and O(<sup>3</sup>P), respectively, instead.

primarily with NO to form OH and NO<sub>2</sub> when NO<sub>x</sub> is present, the net effect becomes re-formation of OH and one NO<sub>2</sub> to NO conversion. Since NO to NO<sub>2</sub> conversions is the process that forms O<sub>3</sub> in this system, this in effect is the same as the destruction of one molecule of O<sub>3</sub> for each molecule of MITC that reacts. Under low NO<sub>x</sub> conditions where the reactions of HS and HSO may dominate, the overall process becomes somewhat more complex, but the net effect is also the destruction of O<sub>3</sub> when MITC reacts.

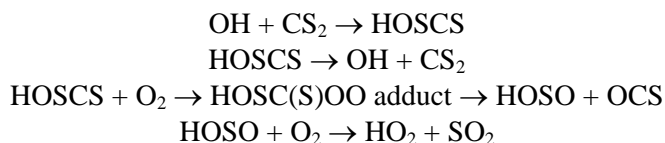
In alternative Mechanism “B” we assume that the reaction of HSO with O<sub>2</sub> occurs with a rate constant of 1 x 10<sup>-17</sup> cm<sup>3</sup> molec<sup>-1</sup> s<sup>-1</sup>, which, though still lower than the recommended upper limit, is sufficiently rapid that reaction with O<sub>2</sub> is the major fate for HSO under the conditions of our experiments and in most atmospheric conditions. This leads to a mechanism where the reaction of MITC with OH has

a net positive impact on O<sub>3</sub> formation. Although the reactions of HS either destroy a molecule of O<sub>3</sub> (either directly or by the conversion of NO<sub>2</sub> to NO), this effect is cancelled out by the formation of O(<sup>3</sup>P) from the SO formed in the HSO + O<sub>2</sub> reaction, since O(<sup>3</sup>P) reacts primarily with O<sub>2</sub> to form O<sub>3</sub>. The formation of HO<sub>2</sub> in the HSO + O<sub>2</sub> reaction causes the additional NO to NO<sub>2</sub> conversion that gives the overall process a net impact on O<sub>3</sub> formation.

The results of the model simulations of the MITC chamber experiments are discussed in the “Incremental Reactivity and Mechanism Evaluation Results” section, below. Since the results indicate that only Mechanism “B” is consistent with the chamber data, this is the only mechanism used in the atmospheric reactivity simulations discussed near the end of the report, and is the basis of the MITC mechanism given in Table 4, above.

### Carbon Disulfide

Under atmospheric conditions, the main reaction of CS<sub>2</sub> is expected to be reaction with OH radicals. This reaction has been extensively studied, but the mechanism is complex and the kinetics under atmospheric conditions is somewhat uncertain. The available data are discussed in both the NASA (2006) and IUPAC (2006) evaluations, and the reader is referred to those discussions for details. The reaction is slow in the absence of O<sub>2</sub> but occurs in the presence of O<sub>2</sub> and exhibits temperature and pressure dependence. The mechanism appears to be a reversible addition of an HOSCS adduct, which either decomposes back to reactants or reacts with O<sub>2</sub>. The available theoretical and experimental data as discussed by NASA (2006) indicate that the mechanism is primarily.



with the overall process being



This is the process that is assumed in the mechanism.

Despite the extensive studies of this reaction, there is some uncertainty concerning the rate of the overall reaction under atmospheric conditions. The NASA (2006) evaluation recommends using a rate constant of  $1.2 \times 10^{-12} \text{ cm}^3 \text{ molec}^{-1} \text{ s}^{-1}$  as the rate constant for the overall process under atmospheric conditions at 298K. However, this overall rate constant can also be calculated from the NASA (2006) and IUPAC (2006)-recommended rate constants and equilibrium constant for the reaction of OH with CS<sub>2</sub> forming HOCS<sub>2</sub>, and the reaction of HOCS<sub>2</sub> with O<sub>2</sub>. Using the NASA (2006)-recommended rate and equilibrium constants, the effective rate constant for 298K and 1 atm air is  $2 \times 10^{-12} \text{ cm}^3 \text{ molec}^{-1} \text{ s}^{-1}$ , while using the IUPAC (2006)-recommended rate constants this effective atmospheric rate constant is  $2.76 \times 10^{-12} \text{ cm}^3 \text{ molec}^{-1} \text{ s}^{-1}$ . The measured values of the effective rate constant for atmospheric conditions also varies approximately within this range (see, for example, data tabulated by Hynes et al, 1988). Therefore, for the purpose of mechanism evaluation we consider the OH rate constant variable within the range of  $1.2$  to  $2.76 \times 10^{-12} \text{ cm}^3 \text{ molec}^{-1} \text{ s}^{-1}$ . However, as discussed in the Mechanism Evaluation Results section, below, the data are best fit using the high rate constant, so this is the value incorporated in the mechanism and used in the atmospheric reactivity calculations, as indicated in Table 4, above.

CS<sub>2</sub> also absorbs light in the 290-330 nm range, which means that the possibility of photolysis also needs to be considered. Recommended absorption cross sections for CS<sub>2</sub> from the current IUPAC recommendation (IUPAC, 2006) are shown on Table 5. These are used in the model calculations for this work. OCS is observed as a product in this photolysis, and IUPAC (2006) gives a recommended quantum

yield of 0.012 for OCS formation. However, they state that this “might best be considered an upper limit since the observed slow oxidation of the CS<sub>2</sub> could have been due, at least in part, to other mechanisms, possibly involving excited CS<sub>2</sub>.” The co-product is not known, but it is likely to be SO, formed in a possible reaction with excited CS<sub>2</sub> and O<sub>2</sub>. Under atmospheric conditions the primary fate of SO is reaction with O<sub>2</sub> to form SO<sub>2</sub> and O(<sup>3</sup>P), which gives the following overall process for the photolysis reaction:



For modeling purposes, we consider alternatives with and without this photolysis reaction, with the quantum yield ranging from 0 to 0.012.

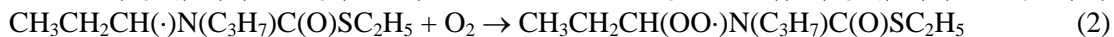
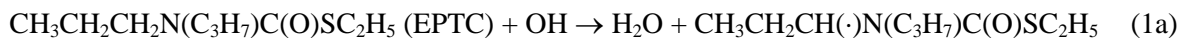
### S-Ethyl N,N-di-n-Propyl Thiocarbamate (EPTC) and Other Thiocarbamates

A reasonably comprehensive study of the gas-phase atmospheric chemistry of EPTC and several other thiocarbamates was carried out by Kwok et al (1992). The major atmospheric loss processes were found to be reaction with OH and NO<sub>3</sub> radicals, and the rate constants and mechanistic information were obtained for these reactions, as discussed below. The data indicate that the major atmospheric loss process would be reaction with OH radicals, but reaction with NO<sub>3</sub> is also represented in the mechanism developed for this work. Only upper limit rate constants or rates were obtained for reaction with O<sub>3</sub> and photolysis, so these reactions are assumed to be negligible in the mechanism.

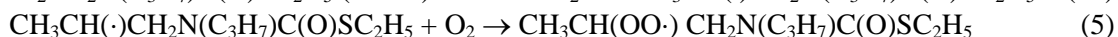
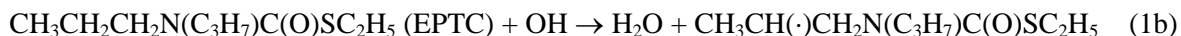
#### Reaction of EPTC with OH

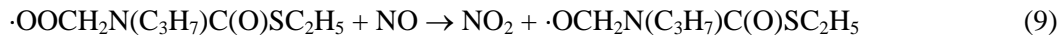
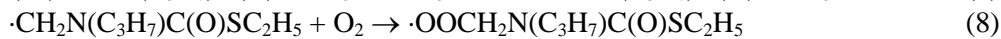
The rate constant for the reaction of OH radicals with EPTC was measured by Kwok et al (1992) to be  $3.18 \pm 0.49 \times 10^{-11} \text{ cm}^3 \text{ molec}^{-1} \text{ s}^{-1}$ . However, as part of this work we obtained a somewhat lower rate constant of  $2.12 \pm 0.25 \times 10^{-11} \text{ cm}^3 \text{ molec}^{-1} \text{ s}^{-1}$ , based on its rate of consumption in the incremental reactivity experiments relative to m-xylene. Note that if there were non-negligible consumption of EPTC by reactions with NO<sub>3</sub> radicals or some heterogeneous loss process in our experiments, the rate constant derived from our data would be biased high, not low. The only way we could obtain a low rate constant for EPTC would be if there were some loss process for m-xylene in our experiments other than reaction with OH radicals, and this would have been evident long before now if that were the case. The OH + m-xylene rate constant, used as the basis to obtain the absolute rate constants in our study, is also believed to be sufficiently well characterized so it is not a significant source of uncertainty (Atkinson and Arey, 2003); Atkinson, personal communication (2006). Therefore, for modeling our data, and also for the atmospheric ozone impact estimates, we use the lower rate constant as measured in this work.

The major product observed by Kwok et al (1992) in the reaction of OH radicals with EPTC was S-ethyl-N-formyl-N-propylthiocarbamate, or HC(O)N(C<sub>3</sub>H<sub>7</sub>)C(O)SC<sub>2</sub>H<sub>5</sub>, for which a yield of 0.45±0.08 was derived. This could arise from the following series of reactions, initiated by reaction of OH at the 3-position of a propyl group:



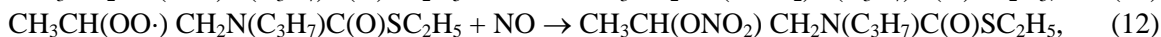
This product could also be formed following reaction of OH at the 2-position of the propyl group:





The ethyl radicals formed in Reaction (4) react primarily to ultimately form acetaldehyde and HO<sub>2</sub>, following an NO to NO<sub>2</sub> conversion, so the overall effect of each of the above two sequences of reactions is the same.

Competing reactions could be nitrate formation formed from the reaction of NO with the peroxy radicals formed in the sequence above,



There are also possible competing reactions of the alkoxy radicals shown above, though reaction of CH<sub>3</sub>CH<sub>2</sub>CH(O·)N(C<sub>3</sub>H<sub>7</sub>)C(O)SC<sub>2</sub>H<sub>5</sub> or CH<sub>3</sub>CH(O·)CH<sub>2</sub>N(C<sub>3</sub>H<sub>7</sub>)C(O)SC<sub>2</sub>H<sub>5</sub> with O<sub>2</sub> can be ruled out because of the failure of Kwok et al (1992) to observe the corresponding ketone products, which should have been detected with the methods used. Decomposition forming the N-centered radical or 1,5-H shift isomerization are possible, but we assume that the decomposition that is supported by the product data is the major process. However, this possibility of these competing alkoxy radical reactions can be considered an area of uncertainty in the EPTC mechanism.

Based on organic nitrate yields from other radicals, or adjustments to fit chamber data for a number of compounds, the SAPRC-99 mechanism estimation procedures predict that the nitrate yield,  $k_{11}/(k_3+k_{11})$  and  $k_{12}/(k_6+k_{12})$  for the radicals formed as shown above would be about 20%. However, this estimate is uncertain, and the assumed nitrate yield can have a significant effect on predictions of overall reactivity, since nitrate formation is a sink for both radicals and NO<sub>x</sub>, and this could be treated as an adjustable parameter when the mechanism is evaluated against the chamber data. Such adjustment was not indicated in this case, however.

Thus, the overall effects of the reactions at the 2- and 3-positions of the propyl group, reactions (1a) and (1b) is assumed to be formation of S-ethyl-N-formyl-N-propylthiocarbamate in an 80% yield, with 20% formation of the 2- or 3-nitrato compounds shown above. Since the former product is observed to be formed in a ~45% yield, this means that Reactions (1a) + (1b) are occurring 45%/85% = 56% of the time. Since the overall OH rate constant is assumed to be  $2.12 \times 10^{-11} \text{ cm}^3 \text{ molec}^{-1} \text{ s}^{-1}$ , and the rate constant for reaction at the 2-position (Reaction 1b) is estimated to be  $2.3 \times 10^{-12} \text{ cm}^3 \text{ molec}^{-1} \text{ s}^{-1}$  from existing structure-reactivity methods (Carter, 2000a, Kwok and Atkinson, 1995), then the rate constant for reaction at the 3-position, adjacent to the -NCO group, (reaction 1a), is estimated to be  $56\% \times 2.12 \times 10^{-11} - 2.3 \times 10^{-12} = 9.6 \times 10^{-12} \text{ cm}^3 \text{ molec}^{-1} \text{ s}^{-1}$ . This is used for estimation of rate constants for analogous reactions adjacent to the -NCO group for the other thiocarbamates, as discussed below.

Since reactions (1a) + (1b) account for ~56% of the overall reaction, reactions at other positions of the EPTC molecule must be occurring the remaining ~44% of the time. Based on existing structure-reactivity estimates (Carter, 2000a, Kwok and Atkinson, 1995), reaction at the methyl groups is estimated to occur with a rate constant of  $\sim 5 \times 10^{-13} \text{ cm}^3 \text{ molec}^{-1} \text{ s}^{-1}$ , or about 3% of the time. The net effects of these reactions are expected to be similar to reactions (1a) + (1b) as discussed above, and for modeling purposes these minor routes are lumped with reactions (1a) + (1b), so its overall yield is increased to 59%.

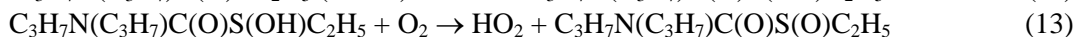
In terms of SAPRC-99 model species, the overall process these reactions is represented as (see also Table 4):



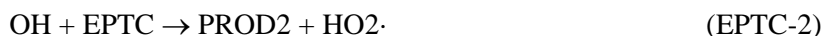
As discussed by Carter (2000a), “PROD2” is the lumped model species is used to represent moderately reactive oxidation products. In this case PROD2 is used to represent  $\text{HC(O)N(C}_3\text{H}_7\text{)C(O)SC}_2\text{H}_5$ . “CCHO” is the model species for acetaldehyde;  $\text{RO2-R}\cdot$  is the model species representing reactions of peroxy radicals that react with NO to form  $\text{HO}_2$ ;  $\text{R2O2}\cdot$  is the model species representing extra NO to  $\text{NO}_2$  conversions in multi-step processes, and  $\text{RO2-N}\cdot$  represents reactions of peroxy radicals with NO forming organic nitrates.

The remaining ~41% of the reaction of OH radicals with EPTC could be abstraction from the  $\text{CH}_2$  adjacent to the S-atom, or addition of OH to the S-atom, analogous to reactions of other sulfide compounds, or (most likely) both. The mechanisms for these reactions are uncertain, as is the relative importance of each. Based on an examination of reactions of other S-containing compounds such as dimethyl sulfide (IUPAC, 2006, and references therein), the following speculative (and probably oversimplified) mechanisms are derived.

The addition reaction at S is assumed to proceed as follows:

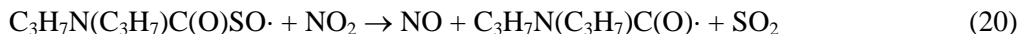
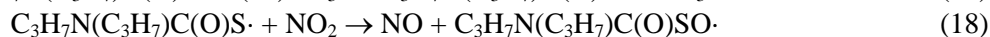
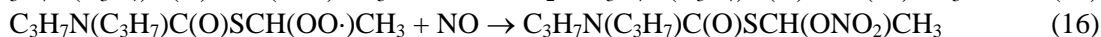
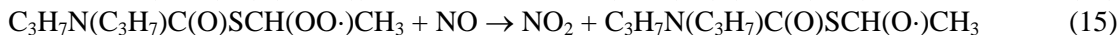


This reaction may well be much more complex, but this simple process is reasonable and is assumed for our analysis. In terms of SAPRC-99 model species, this can be represented as



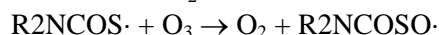
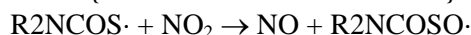
where in this case “PROD2” is used to represent  $\text{C}_3\text{H}_7\text{N(C}_3\text{H}_7\text{)C(O)S(O)C}_2\text{H}_5$ .

The reaction at the  $\text{CH}_2$  next to S is assumed to proceed as follows.

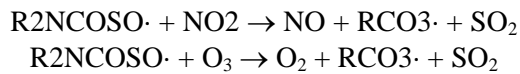


The nitrate formation is assumed to occur with the same relative rate as assumed for the analogous reactions of the other radicals, discussed above, i.e.,  $k_{16}/(k_{15}+k_{16}) \approx 20\%$ . Based on IUPAC (2006) recommendations for analogous reactions of  $\text{CH}_3\text{S}\cdot$  and  $\text{CH}_3\text{SO}\cdot$ , we assume that  $k_{18} \approx 6 \times 10^{-11} \text{ cm}^3 \text{ molec}^{-1} \text{ s}^{-1}$ ,  $k_{19} \approx 4.9 \times 10^{-12} \text{ cm}^3 \text{ molec}^{-1} \text{ s}^{-1}$ ,  $k_{20} \approx 1.2 \times 10^{-11} \text{ cm}^3 \text{ molec}^{-1} \text{ s}^{-1}$ , and  $k_{21} \approx 4.1 \times 10^{-13} \text{ cm}^3 \text{ molec}^{-1} \text{ s}^{-1}$ .

In terms of SAPRC-99 model species, the reactions initiated by (1d) can be represented as follows, where “R3NCOS $\cdot$ ” and “R3NCOSO $\cdot$ ” are new model species added to represent the reactions of  $\text{C}_3\text{H}_7\text{N(C}_3\text{H}_7\text{)C(O)S}\cdot$  and  $\text{C}_3\text{H}_7\text{N(C}_3\text{H}_7\text{)C(O)SO}\cdot$ , respectively. The rate constants for the reactions of these new species are as indicated above (see also Table 4).





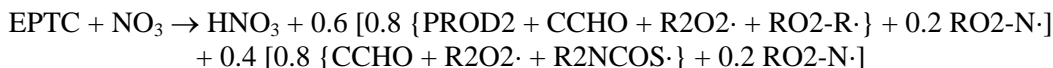


The model species  $\text{R2O2}\cdot$ ,  $\text{RO2-N}\cdot$ , and  $\text{CCHO}$  have the same meaning as indicated above. The  $\text{C}_3\text{H}_7\text{N}(\text{C}_3\text{H}_7)\text{C}(\text{O})\cdot$  radicals formed in Reactions (20) and (21) are assumed to add  $\text{O}_2$  to form  $\text{C}_3\text{H}_7\text{N}(\text{C}_3\text{H}_7)\text{C}(\text{O})\text{OO}\cdot$ , which is assumed to react in a manner analogous to acyl peroxy radicals such as  $\text{RC}(\text{O})\text{OO}\cdot$ , and is therefore represented by “ $\text{RCO3}\cdot$ ”, the generic model species used to represent such radicals in the SAPRC-99 mechanism. The new model species  $\text{R2NCOS}\cdot$  and  $\text{R2NCOSO}\cdot$  are assumed to react sufficiently rapidly that the steady state approximation can be employed. Note that this mechanism requires either  $\text{NO}_2$  or  $\text{O}_3$  to be present, but this is the case in all the chamber or atmospheric reactivity simulations carried out for this project.

Note that the overall processes designated EPTC-1, EPTC-2, and EPTC-3 are expected to have quite different effects on  $\text{O}_3$  reactivity, so their relative importances can be significant. The relative importance of EPTC-1 is set at 59%, based on the considerations discussed above. The relative importance of addition to the S-atom (EPTC-2) or abstraction from the  $\text{CH}_2$  next to the S (EPTC-3), is unknown, and thus the  $k_{1b}/k_{1c}$  ratio is treated as an adjustable parameter in the model simulations of the chamber experiments, discussed below. The results indicate that the best fits to the data are obtained if it is assumed that  $k_{1b} \approx k_{1c}$ , so this is what is assumed for purposes of estimating mechanisms for other thiocarbamates. Since the overall rate  $\text{OH} + \text{EPTC}$  rate constant is  $2.12 \times 10^{-11} \text{ cm}^3 \text{ molec}^{-1} \text{ s}^{-1}$  and reactions (1b) and (1c) are assumed to be equally important and together occur ~21% of the time, this yields estimates of  $k_{1b} \approx k_{1c} \approx 4.4 \times 10^{-12} \text{ cm}^3 \text{ molec}^{-1} \text{ s}^{-1}$ .

### Reaction of EPTC with $\text{NO}_3$

Although the reaction with  $\text{NO}_3$  is not expected to be a major loss process for EPTC, it may be non-negligible under some circumstances and is represented in our model calculations. Kwok et al (1992) measured an  $\text{NO}_3 + \text{EPTC}$  rate constant of  $9.2 \times 10^{-15} \text{ cm}^3 \text{ molec}^{-1} \text{ s}^{-1}$  at 298K, and this is used in the mechanism for this work. The product data suggest that reaction at the 3-position, analogous to Reaction (1), above except forming  $\text{HNO}_3$  instead of  $\text{H}_2\text{O}$ , occurs about half of the time, essentially the same relative yield as the corresponding OH reaction. We assume therefore that the mechanism of the  $\text{NO}_3$  reaction is analogous to the OH reaction, discussed above, except that the analogue to the addition reaction (Reaction 11, above) does not occur. In terms of SAPRC-99 or the new model species discussed above, the representation is:



This is uncertain, but test calculations indicate that the model predictions are much less sensitive to assumptions concerning the mechanism of the  $\text{NO}_3$  reaction than is the case for the OH reaction.

### Reactions of Other Thiocarbamates.

As shown on Table 3 and Table 4 mechanisms for the other thiocarbamate pesticides pebulate, molinate, and thiobencarb are also derived as part of this project. (The structures of these compounds are shown on Table 1.) Based on the data of Kwok et al (1992) for other thiocarbamates we assume that reaction with OH and  $\text{NO}_3$  radicals are the only atmospherically important loss processes. Since we could find no data for these reactions, the rate constants are estimated from the estimated rate constants from the reactions at the various positions of the molecule, which are based largely on the rate constants derived for the corresponding reactions of EPTC.

Table 7 summarizes the rate constants and overall processes assumed for the reactions of the various thiocarbamates with OH radicals. As indicated in the footnotes to the table, the rate constants for abstraction next to the NC(O) group, addition to the S atom, or abstraction next to the SC(O) group, are assumed to be the same as derived for EPTC, and the other rate constants are estimated using structure-reactivity methods (Carter, 2000a). The mechanisms for the various reactions are assumed to be analogous to the corresponding reactions for EPTC, though in general slightly different products are formed, as indicated on the table. The representation of these reactions in the mechanism that corresponds to these overall processes, and estimated rate constants and branching ratios, are given in Table 4 above, with footnotes to Table 7 indicating the model species used to represent the various products or radicals predicted to be formed.

The reactions with NO<sub>3</sub> are assumed to occur by abstractions adjacent to the N or S groups, yielding the same products and radicals as formed in the corresponding reaction with OH radicals, except that HNO<sub>3</sub> is formed instead of H<sub>2</sub>O. We assume that the rate constants for reactions at these positions for all four of these thiocarbamates, i.e., they have the same rate constants and analogous mechanisms as the corresponding reactions of EPTC. The representations of these reactions based on this assumption are shown on Table 4.

### **1,3-Dichloropropenes**

The 1,3-dichloropropenes are expected to react in the atmosphere primarily with OH radicals and (to a lesser extent) with O<sub>3</sub> and (at nighttime) with NO<sub>3</sub> radicals, but under conditions of the chamber experiments the reactions with O(<sup>3</sup>P) and Cl atoms also need to be considered. The rate constants for the reactions of both isomers with OH radicals and O<sub>3</sub> have been measured, but those for the other reactions had to be estimated, using procedures associated with the SAPRC-99 mechanism generation and estimation system, updated for chlorine systems as discussed in Appendix A. The rate constants used in our model simulations are summarized in Table 8. Footnotes to the table indicate the sources for the measured rate constants and the estimation methods used for the rate constants that had to be estimated.

The detailed mechanisms assumed for the various reactions of the dichloropropenes are given in Table 9, with the assumptions made concerning the various branching ratios documented in footnotes to the table. The products predicted to be formed in these overall reactions their estimated yields, and their representation in the mechanism used in the model calculations for this study, are summarized on Table 10. These mechanisms were derived using the SAPRC-99 mechanism generation system (Carter, 2000a), with additions for chlorine reactions made as discussed in Appendix A to this report. Several alkoxy radical reactions branching ratios could not be derived using this system, so estimates or assumptions had to be made as to which of the competing processes is dominant. These are indicated on footnotes to the table.

The major reactive (or potentially reactive) products formed in the 1,3-dichloropropene reactions that may not be adequately represented in the current SAPRC-99 mechanism are formyl chloride and chloroacetaldehyde. Libuda et al (1990) found that formyl chloride does not react with OH radicals, reacts relatively slowly with Cl atoms, and has absorption cross sections that indicate photolysis is relatively slow under atmospheric conditions. Therefore, this product is treated as unreactive in the simulations in this work. The standard procedure in the SAPRC-99 mechanism is to represent higher saturated aldehydes such as chloroacetaldehyde by the “RCHO” model species, whose mechanism is based on that assumed for propionaldehyde. However, as discussed in the “Incremental Reactivity and Mechanism Evaluation Results” section, below, using this representation results in significant underprediction of the overall reactivity observed in all the dichloropropene experiments, and also significantly underpredicts the apparent chlorine levels formed in the experiments. No other reasonable modifications to the mechanism

Table 7. Summary of overall processes for the reactions of OH with various thiocarbamates

Reaction	kOH ( $\text{cm}^3 \text{ molec}^{-1} \text{ s}^{-1}$ )	Ratio	Radicals and products (excluding nitrates)	Nitrate yields [c]	Rep'n [a]	Notes [b]
EPTC – $\text{C}_3\text{H}_7\text{N}(\text{C}_3\text{H}_7)\text{C}(\text{O})\text{SC}_2\text{H}_5$						
Adjacent to N	9.63e-12	45%	$\text{HO}_2 + \text{HC}(\text{O})\text{N}(\text{C}_3\text{H}_7)\text{C}(\text{O})\text{SC}_2\text{H}_5 + \text{CH}_3\text{CHO} + 2 (\text{NO} \rightarrow \text{NO}_2)$	20%	EPTC-1	1
Addition to S	4.38e-12	21%	$\text{HO}_2 + \text{C}_3\text{H}_7\text{N}(\text{C}_3\text{H}_7)\text{C}(\text{O})\text{S}(\text{O})\text{C}_2\text{H}_5$	0%	EPTC-2	1
Adjacent to S	4.38e-12	21%	$\text{C}_3\text{H}_7\text{N}(\text{C}_3\text{H}_7)\text{C}(\text{O})\text{S}\cdot + \text{CH}_3\text{CHO} + (\text{NO} \rightarrow \text{NO}_2)$	20%	EPTC-3	1
Other	2.81e-12	13%	Various (11% same as adjacent to N)	20%	EPTC-1	1
Total kOH	2.12e-11					
Pebulate – $\text{C}_4\text{H}_9 \text{N}(\text{C}_2\text{H}_5)\text{C}(\text{O})\text{SC}_3\text{H}_7$						
adjacent to N	4.81e-12	21%	$\text{HO}_2 + \text{C}_2\text{H}_5\text{CHO} + \text{HC}(\text{O})\text{N}(\text{C}_2\text{H}_5)\text{C}(\text{O})\text{SC}_3\text{H}_7 + 2 (\text{NO} \rightarrow \text{NO}_2)$	23%	PBLA-1A	2,3,4,5
	4.81e-12	21%	$\text{HO}_2 + \text{HCHO} + \text{HC}(\text{O})\text{N}(\text{C}_4\text{H}_9)\text{C}(\text{O})\text{SC}_3\text{H}_7$	23%	PBLA-1B	2,3,4
Addition to S	4.38e-12	19%	$\text{HO}_2 + \text{C}_4\text{H}_9\text{N}(\text{C}_2\text{H}_5)\text{C}(\text{O})\text{S}(\text{O})\text{C}_3\text{H}_9$	0%	PBLA-2	2,4
Adjacent to S	4.38e-12	19%	$\text{C}_4\text{H}_9\text{N}(\text{C}_2\text{H}_5)\text{C}(\text{O})\text{S}\cdot + \text{C}_2\text{H}_5\text{CHO} + (\text{NO} \rightarrow \text{NO}_2)$	23%	PBLA-3	2,4,6
Other	4.25e-12	19%	Various (5% same as adjacent to N)		PBLA-1A	7
Total kOH	2.26e-11					
Molinate – cyclo- $(\text{CH}_2)_6\text{N}-\text{C}(\text{O})\text{SC}_2\text{H}_5$						
Adjacent to N	9.63e-12	40%	$\text{HO}_2 + \text{HCO}(\text{CH}_2)_5\text{N}(\text{CHO})\text{C}(\text{O})\text{SC}_2\text{H}_5 + 2 (\text{NO} \rightarrow \text{NO}_2)$	20%	MOLI-1	2,5
Addition to S	4.38e-12	18%	$\text{HO}_2 + \text{cyclo}-(\text{CH}_2)_6\text{NC}(\text{O})\text{S}(\text{O})\text{C}_2\text{H}_6$		MOLI-2	2,4
Adjacent to S	4.38e-12	18%	$\text{cyclo}-(\text{CH}_2)_6\text{N}-\text{C}(\text{O})\text{S}\cdot + \text{CH}_3\text{CHO} + (\text{NO} \rightarrow \text{NO}_2)$	20%	MOLI-3	2,6
Other	5.85e-12	24%	Various	20%	MOLI-1	7
Total kOH	2.42e-11					
Thiobencarb – p- $\text{C}_2\text{H}_5\text{N}(\text{C}_2\text{H}_5)\text{C}(\text{O})\text{SCH}_2\text{-Bz-Cl}$						
Adjacent to N	9.63e-12	51%	$\text{HO}_2 + \text{p-HC}(\text{O})\text{N}(\text{C}_2\text{H}_5)\text{C}(\text{O})\text{SCH}_2\text{-Bz-Cl} + \text{HCHO} + 2 (\text{NO} \rightarrow \text{NO}_2)$	23%	THCB-1	2,4,8
Addition to S	4.38e-12	23%	$\text{HO}_2 + \text{p-C}_2\text{H}_5\text{N}(\text{C}_2\text{H}_5)\text{C}(\text{O})\text{S}(\text{O})\text{CH}_2\text{-Bz-Cl}$		THCB-2	2,4
Adjacent to S	4.38e-12	23%	$\text{C}_2\text{H}_5\text{N}(\text{C}_2\text{H}_5)\text{C}(\text{O})\text{S}\cdot + \text{p-HCO-Bz-Cl} + (\text{NO} \rightarrow \text{NO}_2)$	23%	THCB-3	2,6,8,9
On Aromatic	0		Unknown			10
Other	3.42e-13	2%	$\text{HO}_2 + \text{p-HCON}(\text{C}_2\text{H}_5)\text{C}(\text{O})\text{SCH}_2\text{-Bz-Cl} + \text{HCHO} + 2 (\text{NO} \rightarrow \text{NO}_2)$	23%	THCB-1	7,8
Total kOH	1.87e-11					

Table 7 (continued)

[a] Representation of this process is shown for the reaction of the indicated model species on Table 4

[b] Documentation notes

- 1 See text for the discussion of the EPTC mechanism and its representation.
- 2 Total rate constants for abstraction adjacent to the N, addition to the S, or abstraction adjacent to the S are assumed to be the same as for the corresponding reaction of EPTC.
- 3 Reactions at the different positions next to the N yield different products, as shown. Equal probability for reaction at each position assumed.
- 4  $\text{HC(O)N(C}_2\text{H}_5\text{)C(O)SC}_3\text{H}_7$ ,  $\text{HC(O)N(C}_4\text{H}_9\text{)C(O)SC}_3\text{H}_7$ ,  $\text{C}_4\text{H}_9\text{N(C}_2\text{H}_5\text{)C(O)S(O)C}_3\text{H}_9$ , cyclo- $(\text{CH}_2)_6\text{NC(O)S(O)C}_2\text{H}_6$ , p-HCON(C<sub>2</sub>H<sub>5</sub>)C(O)SCH<sub>2</sub>-Bz-Cl and p-C<sub>2</sub>H<sub>5</sub>N(C<sub>2</sub>H<sub>5</sub>)C(O)S(O)CH<sub>2</sub>-Bz-Cl are represented by PROD2 in the mechanism.
- 5 Propionaldehyde and  $\text{HCO(CH}_2)_5\text{N(CHO)C(O)SC}_2\text{H}_5$  are represented by RCHO in the mechanism.
- 6  $\text{C}_4\text{H}_9\text{N(C}_2\text{H}_5\text{)C(O)S}\cdot$ , cyclo- $(\text{CH}_2)_6\text{N-C(O)S}\cdot$ , and  $\text{C}_2\text{H}_5\text{N(C}_2\text{H}_5\text{)C(O)S}\cdot$  are represented by R2NCOS $\cdot$  in the mechanism. See above and Table 4 for its reactions.
- 7 The rate constants for reactions at the positions of the molecule except for adjacent or on the N or S (or on the aromatic ring in the case of thiobencarb) can be estimated using the structure-reactivity methods implemented in the SAPRC-99 mechanism generation system (Carter, 2000a). The subsequent reactions of the radicals formed are assumed to have either the same or similar overall effects on reactivity as those following the abstraction adjacent to the N, as assumed to be the case for the EPTC mechanism (see text), and are thus represented by the same overall process.
- 8 The overall nitrate yields for molinate and pebulate are derived from the estimation methods in the SAPRC-99 mechanism generation system, as was the case for EPTC. No procedures exist for systematically estimating nitrate yields from aromatic-containing peroxy radicals such as those predicted to be formed from thiobencarb. The nitrate yields for aromatic compounds are probably less than for the corresponding alkane, so we assume approximately the same overall nitrate yields for the C<sub>12</sub> radicals formed from thiocarb as the C<sub>10</sub> radicals formed from pebulate.
- 9 p-HCO-Bz-Cl is represented by BALD (benzaldehyde and other aromatic aldehydes) in the mechanism.
- 10 The chlorine substitution is assumed to slow down addition of OH radicals to the aromatic ring sufficiently so that this process is unimportant compared to the competing reaction.

[c] Overall nitrate yields for peroxy radicals formed in the EPTC,

Table 8. Rate constants used in the model simulations of the atmospheric or environmental chamber reactivities of the 1,3-dichloropropenes.

Reaction	Rate constant (cm <sup>3</sup> molec <sup>-1</sup> s <sup>-1</sup> )		Reference or Notes
	Trans	Cis	
OH	1.44e-11	8.45e-12	Measured by Tuazon et al (1988). Temperature dependence ignored.
O <sub>3</sub>	6.64e-15 x exp(-2742/T) = 7.12e-19 @ 300K	3.22e-15 x exp(-2972/T) = 1.60e-19 @ 300K	Rate constant at 298K measured by Tuazon et al (1984). Temperature dependence estimated by assuming that the A factor is the same as that for trans or cis-2-butene.
NO <sub>3</sub>	9.13e-17	5.57e-18	Estimated from the correlation between the OH and NO <sub>3</sub> rate constants, as discussed by Carter (2000a). Temperature dependence (which is probably non-negligible) is ignored.
O( <sup>3</sup> P)	1.30e-12	4.79e-13	Estimated from the correlation between the OH and O( <sup>3</sup> P) rate constants, as discussed by Carter (2000a). Temperature dependence is ignored.
Cl	8.58e-11	8.58e-11	Estimated using group-additivity methods as discussed in Appendix A.

to increase the reactivity and chlorine levels, such as assuming high Cl atom yields in the OH or O<sub>3</sub> reactions, resulted in satisfactory simulations of the chamber data if this representation is used.

Fortunately, there is information concerning the atmospheric reactions of chloroacetaldehyde, and it appears to be quite different in reactivity than propionaldehyde as represented in the SAPRC-99 mechanism. Figure 5 shows a comparison of the absorption cross sections measured by chloroacetaldehyde (NASA, 2006), in comparison with the absorption cross section and action spectrum as recommended by IUPAC (2006) for propionaldehyde and the action spectrum used for the “RCHO” model species in SAPRC-99. It can be seen that chloroacetaldehyde has higher absorption cross sections in the >300 nm wavelength region important for solar (and environmental chamber) photolysis than that for propionaldehyde. Although no information is apparently available concerning the quantum yield for chloroacetaldehyde photolysis, this suggests that chloroacetaldehyde may photolyze significantly more rapidly than propionaldehyde as represented by the SAPRC-99 model species RCHO.

There is some discrepancy in the literature concerning the quantum yields for propionaldehyde photolysis. The SAPRC-99 mechanism is based on earlier recommendations that the quantum yield fell off at the higher wavelengths, yielding an action spectrum significantly lower than the absorption cross sections, as shown on Figure 5. However, more recent, more direct measurements result in a current IUPAC (2006) recommendation to assume unit quantum yields at wavelengths above 296 nm, giving an action spectrum equal to the absorption cross section, as shown on the figure. This will probably be the representation used when the SAPRC mechanism is updated, but this has not yet been implemented in the mechanism used for this project.

If chloroacetaldehyde also has high quantum yields for photodecomposition, the calculated atmospheric photolysis rate would be 4-5 times higher than that used for RCHO in the SAPRC-99

Table 9. Mechanism derived for the atmospheric reactions of the 1,3-dichloropropenes.

	Reaction	Note	Branching Rxn	Ratios Total
<u>Reaction with OH</u>				
1	1,3-Dichloropropenes + OH $\rightarrow$ HOCH(Cl)CH( $\cdot$ )CH <sub>2</sub> Cl	1	50%	50%
2	1,3-Dichloropropenes + OH $\rightarrow$ HOCH(CH <sub>2</sub> Cl)CH( $\cdot$ )Cl		50%	50%
3	HOCH(Cl)CH( $\cdot$ )CH <sub>2</sub> Cl + O <sub>2</sub> $\rightarrow$ HOCH(Cl)CH(OO $\cdot$ )CH <sub>2</sub> Cl			50%
4	HOCH(Cl)CH(OO $\cdot$ )CH <sub>2</sub> Cl + NO $\rightarrow$ NO <sub>2</sub> + HOCH(Cl)CH(O $\cdot$ )CH <sub>2</sub> Cl			50%
5	HOCH(Cl)CH(O $\cdot$ )CH <sub>2</sub> Cl $\rightarrow$ HCOCH <sub>2</sub> Cl + HOCH( $\cdot$ )Cl	2		50%
6	HOCH( $\cdot$ )Cl + O <sub>2</sub> $\rightarrow$ HCOCl + HO <sub>2</sub> $\cdot$			50%
7	HOCH(CH <sub>2</sub> Cl)CH( $\cdot$ )Cl + O <sub>2</sub> $\rightarrow$ HOCH(CH <sub>2</sub> Cl)CH(OO $\cdot$ )Cl			50%
8	HOCH(CH <sub>2</sub> Cl)CH(OO $\cdot$ )Cl + NO $\rightarrow$ NO <sub>2</sub> + HOCH(CH <sub>2</sub> Cl)CH(O $\cdot$ )Cl			50%
9	HOCH(CH <sub>2</sub> Cl)CH(O $\cdot$ )Cl $\rightarrow$ HCOCl + HOCH( $\cdot$ )CH <sub>2</sub> Cl	2		50%
10	HOCH( $\cdot$ )CH <sub>2</sub> Cl + O <sub>2</sub> $\rightarrow$ HCOCH <sub>2</sub> Cl + HO <sub>2</sub> $\cdot$			50%
<u>Reaction with O<sub>3</sub></u>				
1	1,3-Dichloropropenes + O <sub>3</sub> $\rightarrow$ CHOO[excited]-Cl + HCOCH <sub>2</sub> Cl	1	50%	50%
2	1,3-Dichloropropenes + O <sub>3</sub> $\rightarrow$ CHOO[excited]-CH <sub>2</sub> Cl + HCOCl		50%	50%
	CHOO[excited]-CH <sub>2</sub> Cl	3		
3	+ M $\rightarrow$ CHOO[stab]-CH <sub>2</sub> Cl + M		89%	44%
4	$\rightarrow$ $\cdot$ CH <sub>2</sub> Cl + CO + OH		11%	6%
5	CHOO[stab]-CH <sub>2</sub> Cl + H <sub>2</sub> O $\rightarrow$ HOC(O)CH <sub>2</sub> Cl + H <sub>2</sub> O	4		44%
6	$\cdot$ CH <sub>2</sub> Cl + O <sub>2</sub> $\rightarrow$ $\cdot$ OOCH <sub>2</sub> Cl			6%
7	$\cdot$ OOCH <sub>2</sub> Cl + NO $\rightarrow$ NO <sub>2</sub> + $\cdot$ OCH <sub>2</sub> Cl			6%
8	$\cdot$ OCH <sub>2</sub> Cl $\rightarrow$ HCHO + Cl $\cdot$	5		6%
<u>Reaction with NO<sub>3</sub></u>				
1	1,3-Dichloropropenes + NO <sub>3</sub> $\rightarrow$ O <sub>2</sub> NOCH(Cl)CH( $\cdot$ )CH <sub>2</sub> Cl	1	50%	50%
2	1,3-Dichloropropenes + NO <sub>3</sub> $\rightarrow$ O <sub>2</sub> NOCH(CH <sub>2</sub> Cl)CH( $\cdot$ )Cl		50%	50%
3	O <sub>2</sub> NOCH(Cl)CH( $\cdot$ )CH <sub>2</sub> Cl + O <sub>2</sub> $\rightarrow$ O <sub>2</sub> NOCH(Cl)CH(OO $\cdot$ )CH <sub>2</sub> Cl			50%
	O <sub>2</sub> NOCH(Cl)CH(OO $\cdot$ )CH <sub>2</sub> Cl	6		
4	+ NO $\rightarrow$ O <sub>2</sub> NOCH(Cl)CH(ONO <sub>2</sub> )CH <sub>2</sub> Cl		5%	3%
5	+ NO $\rightarrow$ NO <sub>2</sub> + O <sub>2</sub> NOCH(Cl)CH(O $\cdot$ )CH <sub>2</sub> Cl		95%	47%
6	O <sub>2</sub> NOCH(Cl)CH(O $\cdot$ )CH <sub>2</sub> Cl $\rightarrow$ HCOCH <sub>2</sub> Cl + O <sub>2</sub> NOCH( $\cdot$ )Cl	2		47%
7	O <sub>2</sub> NOCH( $\cdot$ )Cl $\rightarrow$ NO <sub>2</sub> + HCOCl			47%
8	O <sub>2</sub> NOCH(CH <sub>2</sub> Cl)CH( $\cdot$ )Cl + O <sub>2</sub> $\rightarrow$ O <sub>2</sub> NOCH(CH <sub>2</sub> Cl)CH(OO $\cdot$ )Cl			50%
	O <sub>2</sub> NOCH(CH <sub>2</sub> Cl)CH(OO $\cdot$ )Cl	6		
9	+ NO $\rightarrow$ O <sub>2</sub> NOCH(Cl)CH(ONO <sub>2</sub> )CH <sub>2</sub> Cl		5%	3%
10	+ NO $\rightarrow$ NO <sub>2</sub> + O <sub>2</sub> NOCH(CH <sub>2</sub> Cl)CH(O $\cdot$ )Cl		95%	47%
11	O <sub>2</sub> NOCH(CH <sub>2</sub> Cl)CH(O $\cdot$ )Cl $\rightarrow$ HCOCl + O <sub>2</sub> NOCH( $\cdot$ )CH <sub>2</sub> Cl	2		47%
12	O <sub>2</sub> NOCH( $\cdot$ )CH <sub>2</sub> Cl $\rightarrow$ NO <sub>2</sub> + HCOCH <sub>2</sub> Cl			47%
<u>Reaction with O(<sup>3</sup>P)</u>				
1	1,3-Dichloropropenes + O( <sup>3</sup> P) $\rightarrow$ Cl-CH <sub>2</sub> CH*OCH*-Cl	7	76%	76%
2	1,3-Dichloropropenes + O( <sup>3</sup> P) $\rightarrow$ Cl-CH <sub>2</sub> CH <sub>2</sub> C(O)Cl		12%	12%
3	1,3-Dichloropropenes + O( <sup>3</sup> P) $\rightarrow$ Cl-CH <sub>2</sub> C(O)CH <sub>2</sub> Cl		12%	12%

Table 9 (continued)

Reaction		Note	Branching Ratios Rxn	Total
Reaction with Cl				
1	1,3-Dichloropropenes + Cl. $\rightarrow$ Cl-CH <sub>2</sub> CH(·)CH(Cl)Cl	1	50%	50%
2	1,3-Dichloropropenes + Cl. $\rightarrow$ Cl-CH <sub>2</sub> CH(Cl)CH(·)Cl		50%	50%
3	Cl-CH <sub>2</sub> CH(·)CH(Cl)Cl + O <sub>2</sub> $\rightarrow$ Cl-CH <sub>2</sub> CH(OO·)CH(Cl)Cl			50%
	Cl-CH <sub>2</sub> CH(OO·)CH(Cl)Cl	6		
4	+ NO $\rightarrow$ O <sub>2</sub> NOCH(CH <sub>2</sub> Cl)CH(Cl)Cl		5%	3%
5	+ NO $\rightarrow$ NO <sub>2</sub> + Cl-CH <sub>2</sub> CH(O·)CH(Cl)Cl		95%	47%
6	Cl-CH <sub>2</sub> CH(O·)CH(Cl)Cl + O <sub>2</sub> $\rightarrow$ Cl-CH <sub>2</sub> C(O)CH(Cl)Cl + HO <sub>2</sub> ·	8		47%
7	Cl-CH <sub>2</sub> CH(Cl)CH(·)Cl + O <sub>2</sub> $\rightarrow$ Cl-CH <sub>2</sub> CH(Cl)CH(OO·)Cl			50%
	Cl-CH <sub>2</sub> CH(Cl)CH(OO·)Cl	6		
8	+ NO $\rightarrow$ O <sub>2</sub> NOCH(Cl)CH(Cl)CH <sub>2</sub> Cl		5%	3%
9	+ NO $\rightarrow$ NO <sub>2</sub> + Cl-CH <sub>2</sub> CH(Cl)CH(O·)Cl		95%	47%
10	Cl-CH <sub>2</sub> CH(Cl)CH(O·)Cl $\rightarrow$ HCOCH(Cl)CH <sub>2</sub> Cl + Cl.	5		47%

## Notes:

1. Equal addition at each position around the double bond is assumed. Abstraction reactions by OH or NO<sub>3</sub> radicals are assumed to be minor and are ignored. Abstraction reactions by Cl atoms are estimated to occur less than 1% of the time and are also ignored.
2. Branching ratios for this radical could not be estimated using the current SAPRC-99 mechanism generation estimation methods (Carter, 2000a). This decomposition is assumed to dominate over competing reactions.
3. Branching ratios based on estimates for CH<sub>3</sub>CH<sub>2</sub>CHOO. Model simulations of 1-butene runs are best fit if radical formation is assumed to be small. Major route is assumed to be stabilizations. Total radical formation adjusted to fit results of 1-butene - NO<sub>x</sub> experiments. Note that this underpredicts the observed OH yields from 1-butene.
4. Reaction with H<sub>2</sub>O forming acid is assumed to be the major fate of stabilized Crigee biradicals under atmospheric conditions.
5. Branching ratios for this radical could not be estimated using the current SAPRC-99 mechanism generation estimation methods (Carter, 2000a). Decompositions forming chlorine atoms are assumed to dominate over competing processes.
6. Alkyl nitrate yields using the general SAPRC-99 estimation procedure, which is based on the number of carbons in the peroxy radical (Carter, 2000a).
7. Product distribution as derived using the general SAPRC-99 estimation procedure for higher alkenes (Carter, 2000a). Model simulations of of alkene-NO<sub>x</sub> chamber runs are more self-consistent and are fit with more reasonable parameters for other processes if radical formation from O<sup>3</sup>P reactions from C<sub>3+</sub> alkenes is assumed to be negligible. Product distribution estimated.
8. Reaction with O<sub>2</sub> assumed to be favored over decomposition on the basis of estimates for CH<sub>3</sub>C(O·)CH<sub>3</sub> and the expectation that Cl-substitution makes radicals less stable.

Table 10. Products predicted to be formed in the various overall reactions of the 1,3-dichloropropenes, their estimated yields, and their representation in the mechanism used in the model simulations.

Reaction	Yield	Product or Process	Model Species
OH	100%	HCOCH <sub>2</sub> Cl	CLCCHO [a]
	100%	HCOCi	CLCHO [b]
	100%	NO to NO <sub>2</sub> conversion → HO <sub>2</sub> ·	RO2-R.
O3	50%	HCOCH <sub>2</sub> Cl	CLCCHO [a]
	50%	HCOCi	CLCHO [b]
	44.4%	HOC(O)CH <sub>2</sub> Cl	RCO-OH [b]
	5.7%	HCHO	HCHO
	5.7%	CO	CO
	5.7%	OH	HO.
	5.7%	NO to NO <sub>2</sub> conversion → Cl.	RO2-CL.
NO3	94.9%	HCOCH <sub>2</sub> Cl	CLCCHO [a]
	94.9%	HCOCi	CLCHO [b]
	5.1%	O <sub>2</sub> NOCH(Cl)CH(ONO <sub>2</sub> )CH <sub>2</sub> Cl	RO2-N.
	94.9%	NO <sub>2</sub>	NO2
	94.9%	NO to NO <sub>2</sub> Conversion	R2O2.
O3P	76%	Cl-CH <sub>2</sub> CH*OCH*-Cl	MEK
	12%	Cl-CH <sub>2</sub> CH <sub>2</sub> C(O)Cl	MEK
	12%	Cl-CH <sub>2</sub> C(O)CH <sub>2</sub> Cl	MEK
Cl	47.4%	HCOCH(Cl)CH <sub>2</sub> Cl	CLCCHO [c]
	47.4%	Cl-CH <sub>2</sub> C(O)CH(Cl)Cl	CLCHO [b]
	2.6%	O <sub>2</sub> NOCH(CH <sub>2</sub> Cl)CH(Cl)Cl	RO2-N.
	2.6%	O <sub>2</sub> NOCH(Cl)CH(Cl)CH <sub>2</sub> Cl	RO2-N.
	47.4%	NO to NO <sub>2</sub> conversion → HO <sub>2</sub> ·	RO2-R.
	47.4%	NO to NO <sub>2</sub> conversion → Cl.	RO2-CL.

[a] This model species had to be added to the mechanism to account for the observed reactivity of the 1,3-dichloropropenes. See text.

[b] Treated as unreactive in the model simulations.

[c] This is assumed to have similar reactivity characteristics as chloroacetaldehyde (CLCCHO).



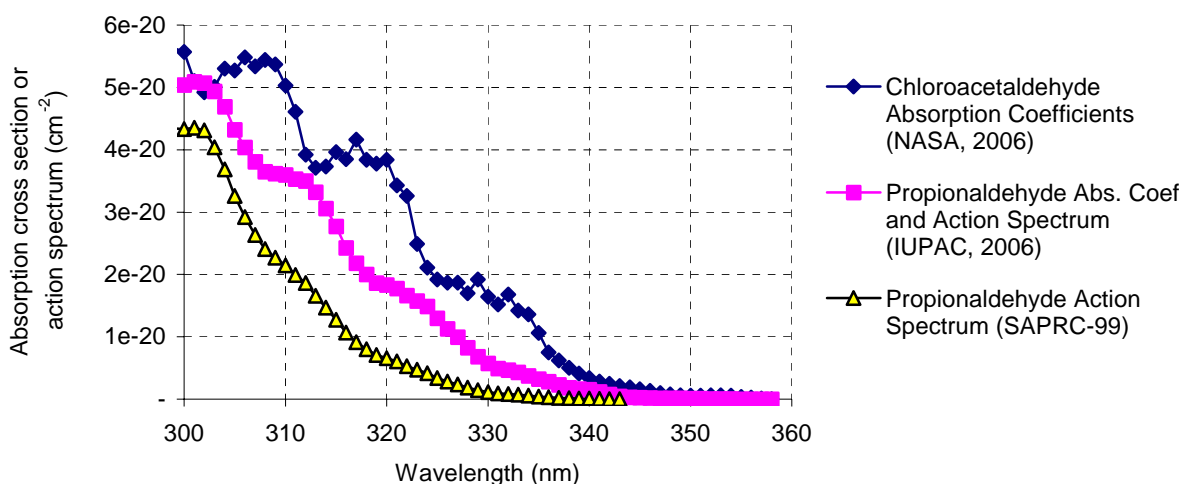
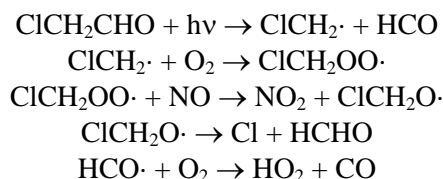


Figure 3. Absorption cross sections for chloroacetaldehyde and absorption cross sections and action spectra for propionaldehyde.

mechanism, and 2-3 times higher than propionaldehyde if the IUPAC (2006)-recommended quantum yields are assumed. The mechanism for the chloroacetaldehyde photolysis reaction is expected to be



This overall process is represented in terms of SAPRC-99, added chlorine mechanism model species as



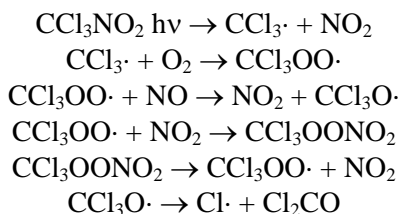
where “RO<sub>2</sub>-Cl·” represents peroxy radicals that form Cl atoms after an NO to NO<sub>2</sub> conversion (see Appendix A for a discussion of the species and reactions added to SAPRC-99 to represent chlorine chemistry). As discussed below, including this reaction with assumed quantum yields results in much better simulations of the chamber experiments. Reducing the chloroacetaldehyde quantum yields below unity results in underpredictions of reactivity in the 1,3-dichloropropene experiments, so unit quantum yields are assumed in the mechanism. The absorption cross sections used in the model simulations are given in Table 5.

Chloroacetaldehyde also reacts with OH radicals and Cl atoms, with rate constants of  $3.1 \times 10^{-12}$  and  $1.29 \times 10^{-11} \text{ cm}^3 \text{ molec}^{-1} \text{ s}^{-1}$ , respectively (Scollard et al, 1993). These are considerably lower than the rate constants of  $2.0 \times 10^{-11}$  and  $1.23 \times 10^{-10} \text{ cm}^3 \text{ molec}^{-1} \text{ s}^{-1}$  used for RCHO in the current mechanism (Carter, 2000a; see also Appendix A). These lower rate constants make photolysis of chloroacetaldehyde all more important in affecting model simulations. The mechanism for these reactions are assumed to be analogous to that used for propionaldehyde, with formation of a peroxyacetyl radical, RC(O)OO·, whose reactions ultimately form a PAN analogue, dominating. In order to avoid adding additional model species

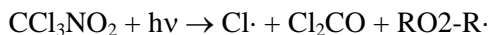
in the mechanism to represent these relatively unimportant processes, these reactions represented in the mechanism as forming the same products as the corresponding reactions of propionaldehyde.

### Chloropicrin

The ozone impacts of chloropicrin,  $\text{CCl}_3\text{NO}_2$ , have been studied previously in environmental chamber experiments by Carter et al (1997a,b), and a photooxidation mechanism for chloropicrin was developed that was consistent with the chamber data. The only significant consumption process for chloropicrin is photolysis, and in order to simulate the results of the chamber experiments the major process was assumed to be primarily formation of  $\text{NO}_2$  and  $\text{CCl}_3\cdot$  radicals, which subsequently react to form phosgene,  $\text{Cl}_2\text{CO}$ , and chlorine atoms.



Although Carter et al (1997a) uses a more explicit mechanism that includes the reversible formation of  $\text{CCl}_3\text{OONO}_2$ , the peroxyxynitrate decomposition is sufficiently rapid that the overall process can be represented more simply as



where  $\text{RO}_2\text{-R}\cdot$  is the SAPRC-99 model species used to represent formation of peroxy radicals that react to convert NO to  $\text{NO}_2$ . The absorption cross sections for chloropicrin were measured by Carter et al (1997a,b), and are given in Table 5, and an overall quantum yield of 0.85 was assumed in the photodecomposition reaction. This mechanism, as used in the model simulations discussed in this report, is included in Table 4, above.

Since the overall representation of the chloropicrin reaction was simplified and the mechanisms for the reactions of the other species were updated since the work of Carter et al (1997a,b), the current mechanism was re-evaluated using the chloropicrin chamber experiments of Carter et al (1997a,b). The results are included in the “Incremental Reactivity and Mechanism Evaluation Results” section, below.

### Kerosene

Kerosene is a complex mixture consisting primarily of higher molecular weight alkanes and aromatics. Although there are uncertainties in the mechanisms for some of these compounds (particularly aromatics and to a lesser extent branched alkanes), methods exist for representing their atmospheric reactions that generally give reasonably good simulations of environmental chamber reactivity data provided that adequate compositional information is available (e.g., Carter and Malkina, 2005; Carter, 2000a). Therefore, the main issue in terms of predicting the reactivity of kerosene is deriving an appropriate chemical composition for this purpose.

Since our laboratory is not experienced in speciating complex liquid hydrocarbon samples, ExxonMobil chemical company offered to support this project by conducting an analysis of the kerosene sample used in our chamber experiments. A portion of the sample used in our experiments was sent to ExxonMobil Process Laboratories in Baton Rouge, LA, who conducted an analysis using gas chromatography with a flame ionization detector (GC-FID), gas chromatography/mass spectrometry (GC/MS), and supercritical fluid chromatography (SFC). The compositions derived from the GC-FID and GC-MS data are summarized on Table 11. The SFC data indicated that the sample consisted of 75%,

Table 11. Composition derived of kerosene sample studied for this project. Derived from data provided by ExxonMobil (2006).

Carbons	Total	Normal Alkanes	Branched Alkanes	Cyclic Alkanes			Aromatics
				1 Ring	2 Rings	3+ Rings	
6	0.0	0.01	0.01				
7	0.1	0.04	0.09	0.01			
8	1.1	0.21	0.36	0.42			0.06
9	4.0	0.84	0.80	1.67			0.68
10	12.7	2.16	3.09	4.80	0.55		2.11
11	17.2	2.20	4.14	5.64	2.08		3.13
12	16.2	2.06	3.36	2.96	4.30		3.56
13	16.0	1.85	3.78	3.29	4.15	0.28	2.68
14	12.7	1.37	2.77	2.34	3.36	0.38	2.43
15	10.1	1.09	2.20	1.66	3.43	0.11	1.63
16	5.2	0.62	0.72	0.88	1.33	0.65	0.98
17	2.6	0.32	0.71	0.53	0.55	0.17	0.37
18	1.5	0.11	0.85	0.21	0.22	0.03	0.05
19	0.4	0.03	0.27	0.10	0.03	0.00	
20	0.1	0.01	0.07	0.03	0.01		
21	0.0	0.00	0.02	0.01	0.00		
22	0.0	0.00	0.01	0.00	0.00		
Total	100	12.9	23.2	24.5	20.0	1.6	17.7

21.4%, 3.7%, and 0.2% saturates, 1-ring aromatics, 2-ring aromatics, and 3-ring aromatics, respectively (ExxonMobil, 2006). Although the aromatic fractions from the SFC and GC methods were somewhat different, the GC data were used as the primary quantification method in our analysis because of their greater level of detail. However, the SFC data were useful for speciating the aromatics, as indicated below.

Table 11 indicates that >80% of the kerosene sample consists of various normal, branched, and cyclic alkanes, with carbon number ranging from 6 to 22. The SAPRC-99 mechanism has estimated mechanisms for all of the normal alkanes through n-hexadecane, and for representative branched and cyclic alkane isomers through C<sub>16</sub> (Carter, 2000a, 2003a). The normal alkanes through C<sub>16</sub> are represented explicitly, and the branched and cyclic alkanes are represented using selected isomers, as indicated on Table 12. For carbon numbers greater than C<sub>16</sub>, the model species used for C<sub>16</sub> are used on a mole per mole basis. This is based on the assumption that beyond a certain carbon number, the overall mechanisms are very similar. Note that since the representation is on a mole-for-mole basis, the molecular weight of the actual carbon number is used when determining the number of moles of C<sub>16</sub> compound to use when representing a given weight fraction of C<sub>17+</sub> compound. Table 12 shows the number of moles of each type of alkane category derived from the weight fraction data in Table 11, and the specific chemical compounds whose mechanisms are used to represent their atmospheric reactions. The mechanisms of these compounds are in Appendix B to this report. Most of these are from Carter (2000a), but some alkanes may have been added subsequently, and estimated using the same procedures as used by Carter (2000a) to derive mechanisms for all alkanes.

Table 11 also indicates that approximately 18% of the kerosene sample also consists of various C<sub>8</sub> - C<sub>18</sub> aromatics. The SAPRC-99 mechanism has explicit mechanisms for benzene and all the

Table 12. Distribution of chemical categories assigned to the kerosene sample and compounds used to represent these categories for modeling purposes.

Category	Moles / kg	Representation
<u>Alkanes</u>		
Normal C6	0.001	n-Hexane
Normal C7	0.004	n-Heptane
Normal C8	0.018	n-Octane
Normal C9	0.066	n-Nonane
Normal C10	0.152	n-Decane
Normal C11	0.141	n-Undecane
Normal C12	0.121	n-Dodecane
Normal C13	0.100	n-Tridecane
Normal C14	0.069	n-Tetradecane
Normal C15	0.051	n-Pentadecane
Normal-C16+	0.046	n-Hexadecane
Branched C6	0.001	0.5 2,3-Dimethyl Butane + 0.25 3-Methylpentane + 0.25 2-Methyl Pentane
Branched C7	0.009	0.5 2,4-Dimethyl Pentane + 0.25 3-Methyl Hexane + 0.25 2-Methyl Hexane
Branched C8	0.032	0.5 2,4-Dimethyl Hexane + 0.25 4-Methyl Heptane + 0.25 2-Methyl Heptane
Branched C9	0.062	0.5 2,4-Dimethyl Heptane + 0.25 4-Methyl Octane + 0.25 2-Methyl Octane
Branched C10	0.217	0.5 2,6-Dimethyl Octane + 0.25 4-Methyl Nonane + 0.25 2-Methyl Nonane
Branched C11	0.265	0.5 2,6-Dimethyl Nonane + 0.25 4-Methyl Decane + 0.25 3-Methyl Decane
Branched C12	0.198	0.5 3,6-Dimethyl Decane + 0.25 5-Methyl Undecane + 0.25 3-Methyl Undecane
Branched C13	0.205	0.5 3,6-Dimethyl Undecane + 0.25 5-Methyl Dodecane + 0.25 3-Methyl Dodecane
Branched C14	0.140	0.5 3,7-Dimethyl Dodecane + 0.25 6-Methyl Tridecane + 0.25 3-Methyl Tridecane
Branched C15	0.103	0.5 3,7-Dimethyl Tridecane + 0.25 6-Methyl Tetradecane + 0.25 3-Methyl Tetradecane
Branched C16+	0.108	0.5 4,8-Dimethyl Tetradecane + 0.25 7-Methyl Pentadecane + 0.25 3-Methyl Pentadecane
Monocyclic C7	0.001	Methyl cyclohexane
Monocyclic C8	0.038	Ethyl cyclohexane
Monocyclic C9	0.132	0.5 Propyl Cyclohexane + 0.5 1-Ethyl-4-Methyl Cyclohexane
Monocyclic C10	0.342	0.34 Butyl Cyclohexane + 0.33 1-Methyl-3-Isopropyl Cyclohexane + 0.33 1,4-Diethyl-Cyclohexane
Monocyclic C11	0.365	0.34 Pentyl Cyclohexane + 0.33 1,3-Diethyl-5-Methyl Cyclohexane + 0.33 1-Ethyl-2-Propyl Cyclohexane

Table 12 (continued)

Category	Moles / kg	Representation
<u>Alkanes</u>		
Monocyclic C12	0.176	0.34 Hexyl Cyclohexane + 0.33 1,3,5-Triethyl Cyclohexane + 0.33 1-Methyl-4-Pentyl Cyclohexane
Monocyclic C13	0.181	0.34 Heptyl Cyclohexane + 0.33 1,3-Diethyl-5-Propyl Cyclohexane + 0.33 1-Methyl-2-Hexyl-Cyclohexane
Monocyclic C14	0.119	0.34 Octyl Cyclohexane + 0.33 1,3-Dipropyl-5-Ethyl Cyclohexane + 0.33 trans 1-Methyl-4-Heptyl Cyclohexane
Monocyclic C15	0.079	0.34 Nonyl Cyclohexane + 0.33 1,3,5-Tripropyl Cyclohexane + 0.33 1-Methyl-2-Octyl Cyclohexane
Monocyclic C16+	0.075	0.34 Decyl Cyclohexane + 0.33 1,3-Propyl-5-Butyl Cyclohexane + 0.33 1-Methyl-4-Nonyl Cyclohexane
Bicyclic C10	0.039	Same as Monocyclic C10
Bicyclic C11	0.137	Same as Monocyclic C11
Bicyclic C12	0.258	Same as Monocyclic C12
Bicyclic C13	0.230	Same as Monocyclic C13
Bicyclic C14	0.173	Same as Monocyclic C14
Bicyclic C15+	0.258	Same as Monocyclic C15+
Polycyclic C13	0.015	Same as Monocyclic C13
Polycyclic C14	0.020	Same as Monocyclic C14
Polycyclic C15+	0.043	Same as Monocyclic C15+
<u>Aromatics</u>		
Ethylbenzene	0.005	Ethylbenzene
C9+ Monosubstituted Benzenes	0.020	n-Propyl Benzene
C8+ Disubstituted Benzenes	0.095	0.34 m-Xylene + 0.33 o-Xylene + 0.33 p-Xylene
C9+ Polysubstituted Benzenes	0.792	0.34 1,3,5-Trimethyl Benzene + 0.33 1,2,3-Trimethyl Benzene + 0.33 1,2,4-Trimethyl Benzene
Indans and Tetralins	0.100	Tetralin
Naphthalene	0.004	Naphthalene
Methyl Naphthalenes	0.012	Methyl Naphthalene
C12+ Naphthalenes	0.046	0.5 Methyl naphthalene + 0.5 2,3-Dimethyl naphthalene

methylbenzenes through C<sub>9</sub>, as well as ethylbenzene, tetralin, naphthalene, 2,3-dimethylnaphthalene, and (by interpolation of the naphthalene and 2,3-dimethylnaphthalene mechanisms) that were derived based on fits of parameterized mechanisms to environmental chamber data (Carter, 2000a). Since (unlike the case for the alkanes) general estimation methods do not exist for aromatics, all the other aromatics have to be represented by assuming the same per-molecule reactivity as the most similar compound for which a mechanism is derived. This approach was found to give moderately good simulations of reactivities observed in environmental chamber experiments with Aromatics 100, which consists of primarily C<sub>9</sub>-C<sub>10</sub> alkylbenzenes. However, more than 80% of the aromatics in kerosene are C<sub>11</sub> or greater, so the appropriateness of this representation is much more uncertain.

Based on analyses of various petroleum distillate samples, primarily by Censullo et al (2002), Carter and Malkina (2005) derived distributions of various types of C<sub>8</sub>-C<sub>11</sub> aromatics for the purpose of deriving atmospheric reactivities. These are summarized on Table 13, which also shows the distributions of aromatic carbon numbers for the kerosene sample studied in this project, and also the methods used to represent them in the model calculations. Because of limited compositional data for mixtures of C<sub>12+</sub> aromatics, Carter and Malkina (2005) had no distribution assignments for carbon numbers greater than 12. The distributions for the C<sub>12+</sub> aromatics were therefore estimated by extrapolation from those for C<sub>≤11</sub>, with the fractions of indans, tetralins, and naphthalenes assumed to level off in order to be consistent with the SFC data provided by ExxonMobil (2006). The corresponding representation in terms of moles of detailed model species with assigned mechanisms for this kerosene sample is given in Table 12.

Table 13. Distributions of types of aromatics assumed for estimating aromatic compositions of kerosene, and methods used for representing them in model calculations.

Carbons	Weight Percent in Kerosene	Weight Percents Assumed for Unspecified Mixtures					Note
		Alkylbenzenes [a]			Indans and Tetralins [b]	Naphthalenes [c]	
		Mono-	Di-	Poly-			
8	0.4	89	11				[d]
9	4	9	30	56	5		[d]
10	12	6	32	51	8	3	[d]
11	18	2	7	75	10	6	[d]
12	20		4	79	10	7	[e,f]
13	15		2	81	10	7	[e,f]
14-18	31			83	10	7	[f]

[a] Differentiated by number of alkyl substituents on the benzene ring, with “polyalkyl” referring to 3 or more substituents. C<sub>8+</sub> mono-, di- and polyalkylbenzenes are represented by ethylbenzene, a mixture of xylenes, and a mixture of trimethylbenzenes, respectively.

[b] Represented using the mechanism of tetralin, the only compound of this type for which a mechanism is derived.

[c] C<sub>10</sub>, C<sub>11</sub>, and C<sub>12+</sub> naphthalenes are represented by naphthalene, methyl naphthalene, and a mixture of methyl naphthalene and 2,3-dimethylnaphthalene, respectively.

[d] As assumed derived for hydrocarbon reactivity analysis by Carter and Malkina (2005)

[e] Di- and polyalkylbenzene fractions extrapolated from C<sub>8</sub>-C<sub>11</sub>.

[f] Indan, tetralins, and naphthalene fractions are assumed not to increase significantly from those for C<sub>11</sub> aromatics, except with a slight increase in naphthalenes to give a total of 15% for the kerosene sample.

The results of the tests of the injection method used in the kerosene experiments suggests that perhaps ~5% of the kerosene sample may not be injected into the gas phase in our experiments. To evaluate the effects of this possibility on the model simulations of the chamber experiments, an alternative kerosene composition was derived with 5% of the least volatile mass removed. “Least volatile” was defined as having the highest boiling points according to the carbon number vs. boiling point assignments used by Carter and Malkina (2005) for estimating compositions based on boiling point ranges. For this kerosene sample, the least volatile 5% consisted of all the C<sub>16+</sub> aromatics, all the C<sub>17+</sub> normal and cyclic alkanes, and all the C<sub>18+</sub> branched alkanes. In model simulations where this was removed the moles of model species used to represent these compounds were reduced accordingly, and the moles of the model species used to represent the less volatile constituents were unchanged.

Because the model simulations based on the compositions given in Table 12 gave reasonably good fits to the chamber data, and removing the least volatile 5% of the mass was found to have relatively little effect on the simulations, the effects of alternative assumptions concerning the composition of the kerosene sample or using alternative mechanisms or representations of the constituents were not examined.

### **Atmospheric Reactivity Simulations**

Conducting atmospheric reactivity model simulations were carried out to derive MIR and other atmospheric reactivity values for the selected pesticides whose ozone impacts are evaluated for this project. The scenarios and methods used were the same as those used when calculating the MIR and other atmospheric ozone reactivity scales, and were described previously (Carter, 1994a,b 2000a). The base ROG constituents were represented using the lumping procedures incorporated in the condensed version of the SAPRC-99 mechanism (Carter, 2000b), and individual compounds whose reactivities were being assessed were represented explicitly. The mechanisms used for the pesticide-related test compounds employed in these calculations are given in Table 4 and Table 5, above. The mechanisms used in the atmospheric reactivity for the chlorine-containing test compounds (the dichloropropenes and chloropicrin) included the chlorine mechanism that is discussed in Appendix A. The reactivity of kerosene was calculated using the mixture of model species given in Table 12, with the mechanisms for these model species given in Appendix B.

## RESULTS AND DISCUSSION

A chronological listing of the environmental chamber experiments carried out for this project is given in Table C-1 in Appendix C. These included experiments with the test compounds of interest for this study and appropriate characterization and control experiments needed for the data to be useful for mechanism evaluation.

### Characterization Results

The results of the individual characterization experiments that are relevant to the experiments for this project are summarized in the “Results” column of Table C-1. The initial characterization experiments relevant this chamber are described in detail by Carter (2004a) or by Carter and Malkina (2005) or Carter et al (2005a), and thus need not be discussed further here. Characterization results specific to this project are discussed below.

#### Arc Light Characterization

The arc light source was used for approximately 2/3 of the experiments discussed in this report. The characterization results for this light source, applicable for runs through EPA245, and the assignments of NO<sub>2</sub> photolysis rates and spectrum used for modeling based on these results, were discussed previously by Carter (2004), but a number of actinometry experiments were carried out subsequently. Figure 4 shows a plot of results of NO<sub>2</sub> actinometry experiments carried out in the EPA chamber using the arc light source with the intensity and configuration used in these experiments. These measurements were made using the quartz tube method of Zafonte et al (1977), modified as discussed by Carter et al (1995b), either inside one of the reactors or in a standardized location in front of the reactors between the reactors and the light. The measurements made in front of the reactor are adjusted by a factor of 0.92 to correct for light intensity differences between this position and the interior of the reactor, as indicated on the figure.

Figure 4 shows that the results of most of the out-of-reactor NO<sub>2</sub> actinometry experiments indicated that the light intensity with this light source did not change during the period since the arc was first employed in its current configuration (around January, 2003) up to the dates of the experiments in this report. The in-reactor measurements carried out through run 216 gave highly consistent results and indicated an NO<sub>2</sub> photolysis rate of 0.260 min<sup>-1</sup>, which is the assigned value derived by Carter (2004) for modeling EPA chamber experiments using this light source in this configuration and power setting. The measurements made around EPA 330-331 were slightly higher, but the results of the measurements in front of the reactor did not indicate any change in overall light intensity, so the assignment was not changed. Therefore, an assigned NO<sub>2</sub> photolysis rate of 0.260 min<sup>-1</sup> was used when modeling all arc light experiments carried out for this project.

The spectrum of the light source was measured periodically using our LI-1800 spectroradiometer, and the results indicated that the spectrum did not change significantly with time, and that the spectrum given by Carter (2004) is also assumed to be applicable for all arc light experiments carried out for this project.

#### Blacklight Characterization

Because of problems with the arc light source during the period of this project, approximately 1/3 of the experiments for this project were carried out using the blacklight light source. Methods for



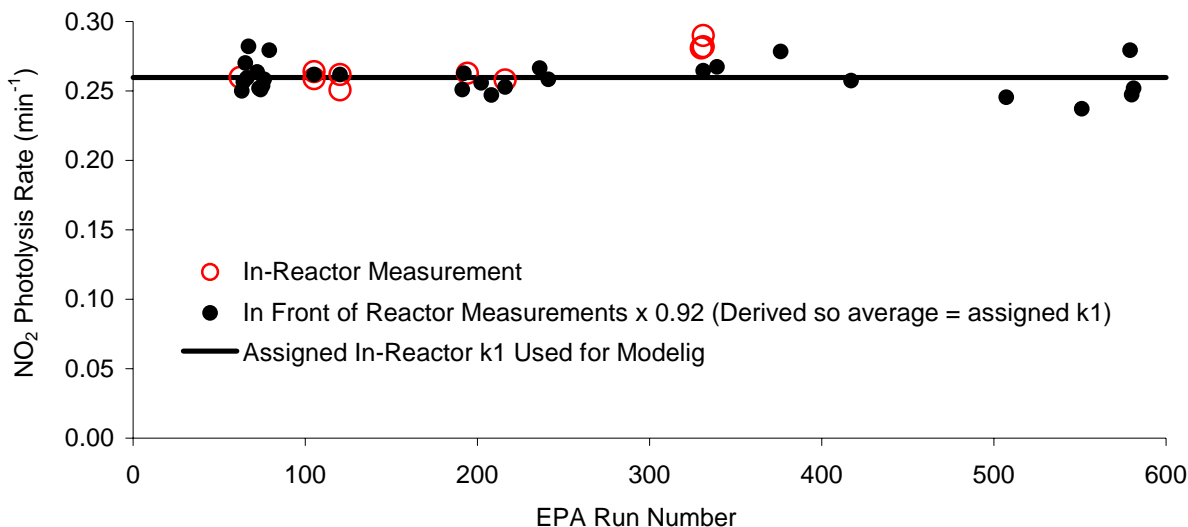


Figure 4. Plots results of NO<sub>2</sub> actinometry experiments vs. EPA run number using the arc light source in its current power setting and configuration.

characterizing the intensity of the blacklight light source were discussed by Carter et al (2005a), though some revisions were made as a result of subsequent measurements. As with the arc light source, NO<sub>2</sub> actinometry measurements were made using the quartz tube method of Zafonte et al (1977), modified as discussed by Carter et al (1995b), with the quartz tube both inside the reactors and also in front of the reactors. As discussed by Carter et al (2005a), the results of these measurements, and other measures of light intensity, indicated a steady decline in light intensity with time, with the results being best correlated with the “blacklight run count”, which is the number of experiments carried out in the chamber using the blacklights, and is thus an indicator of the ageing of the lights due to use. A plot of the results of the in- and out-of-reactor actinometry measurements against run count is shown on Figure 5.

The actinometry measurements made in front of the reactor as shown on Figure 5 are corrected by a factor of 0.698 to give an estimate of the corresponding light intensity inside the reactor. As discussed by Carter et al (2005a), this was derived from near-simultaneous actinometry measurements made both inside and in front of the reactor. Both measurements show similar declines in intensity with time, though the measurements in front of the reactor are more comprehensive because of the larger number of measurements and the larger period of time for which measurements were made.

Light intensity measurements were also made using the QSL-2100 PAR Irradiance Sensor during most chamber experiments, which responds to spherically integrated light in the 400-700 nm range (see Table 2). This should provide a comprehensive indication of relative light intensity changes because such measurements are made during each experiment.. Based on these data, Carter et al (2005a) concluded that the light intensity after about run count 111 (EPA 384) no longer declined but became constant. However, this is not borne out by actinometry and PAR measurements made in subsequent experiments. PAR measurements were found to be sensitive to factors such as the position of the reactor framework and other factors, and were found to change from time to time for unexplained reasons using the arc as well as the blacklight light source. Therefore, we have concluded that the PAR measurements made during the experiments may not be as reliable an indicator of trends in light intensity as previously believed. For this reason, only NO<sub>2</sub> actinometry data are now the primary means used to assess trends in light intensity.

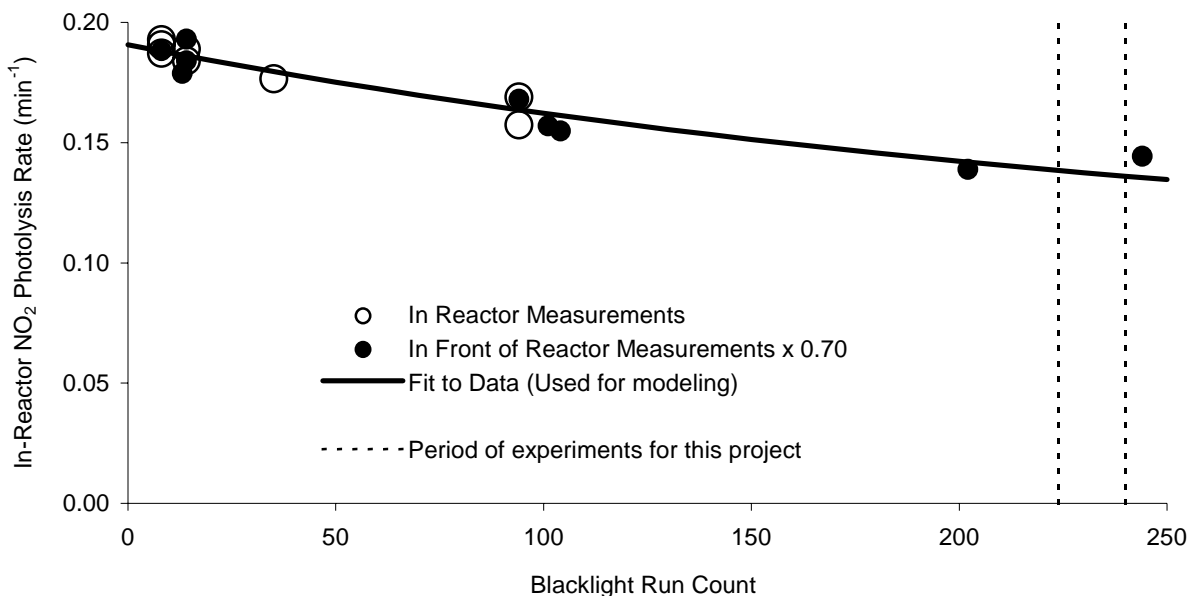


Figure 5. Plots of light intensity data used to assign NO<sub>2</sub> photolysis rates for the blacklight light source.

The actinometry measurements using the blacklight lights source are reasonably well fit by the following empirical expression, where  $k_1$  is the NO<sub>2</sub> photolysis rate in min<sup>-1</sup>:

$$k_1 = 0.0953 \times [1 + \exp(-\text{Blacklight Run Count} \times 0.00355)] \quad (\text{I})$$

The parameters in Equation (I) were derived to minimize sum-of-squares errors in predictions of both the in-reactor actinometry measurements and the in-front-of-reactor measurements corrected by a factor of 0.698. This equation was used to derive the NO<sub>2</sub> photolysis rates used when modeling the blacklight experiments modeled for this project. Figure 5 indicates the range of blacklight run counts that is applicable to the experiments for this project.

The spectrum of the blacklights in this chamber is measured periodically and continues to be essentially the same as the spectrum recommended by Carter et al (1995b) for modeling blacklight chamber runs.

### Chamber Effects Characterization

Except as discussed below, the characterization results for the more recent experiments for this project are consistent with those discussed by Carter and Malkina (2005) and Carter et al (2005a), and the same characterization parameters were used for modeling. The most important chamber effect, and the only chamber effect parameter that was changed when modeling the experiments for this project, concerns the apparent HONO offgasing, which is believed to be responsible for both the chamber radical source and NO<sub>x</sub> offgasing effects (Carter, 2004). This is represented in the chamber effects model by the parameter RN-I, which is the HONO offgasing rate used in the simulations divided by the light intensity as measured by the NO<sub>2</sub> photolysis rate. Figure 6 shows the HONO offgasing parameters that best fit the radical or NO<sub>x</sub> - sensitive characterization experiments carried out in the UCR EPA during the period of the last two sets of reactors. Note that the experiments carried out for this project start at run EPA536, so the applicable characterization data is for the last set of reactors shown on the figure.

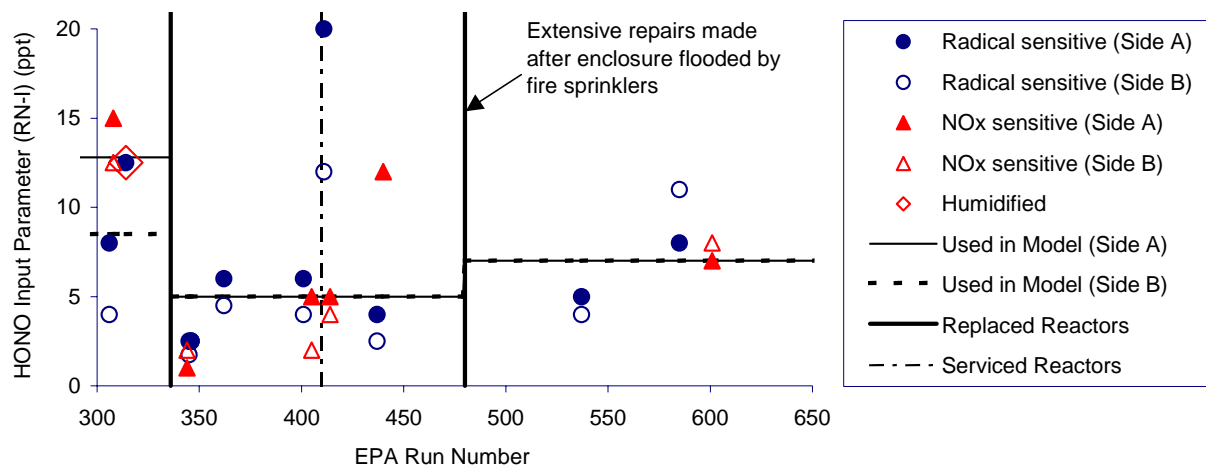


Figure 6. Plots of best fit HONO offgasing parameters against UCR EPA run number. (Data from Carter (2004), with results of newer experiments for this project added.)

The last two reactor replacements were made after run EPA336 and most recently after the enclosure was flooded by fire sprinklers caused by overheating during run EPA480. Replacing the reactors after run 336 resulted in a significant decrease in the apparent HONO offgasing rate, particularly in Reactor A, where characterization runs indicated higher HONO offgasing rates than the other reactor before this run. After run 336 the apparent HONO offgasing rate was the same in both reactors, with the average RN-I value being (excluding an anomalously high run immediately following a reactor servicing) being 5 ppt.

The damage caused by the flooding during run EPA480 necessitated repairs being made to the injection and mixing system as well as replacing the reactors. However, this did not have a significant effect on the apparent HONO offgasing rates, which increased slightly to an average value of 7 ppt. It did have an effect on the background PM results, as discussed in the following section.

For modeling purposes, we use the same chamber effects parameters as used by Carter (2004) Carter and Malkina (2005), and Carter et al (2005a) for all chamber effect parameters except RN-I. For the runs carried out for this project, which were all in the newest set of reactors installed after run 480, the RN-I value used for both reactors was 7 ppt, the average of the measured values for the applicable characterization runs. The values assigned for modeling the runs in the last three sets of reactors are indicated on Figure 6.

The results of the side equivalency test experiments are shown later in this report, where they are compared with the results of the incremental reactivity experiments with added test compounds. These are discussed below in conjunction with the discussion of the incremental reactivity experiments with the added test compounds.

### Background PM Characterization

Although the primary objective of this project was to obtain data on ozone impacts, particulate matter (PM) volume number measurements were made in conjunction with the experiments that were carried out. The results of the initial PM characterization experiments in this chamber have been

discussed by Carter et al (2005a,b). The most useful PM background characterization experiments are pure air irradiations, where small but measurable PM formation is observed. This is apparently due to reaction of OH radicals with some PM precursor, since no PM formation is observed in CO - air or NO<sub>x</sub> - air irradiations, where the presence of the added CO or NO<sub>x</sub> tend to suppress the OH radical levels. Because of this, pure air irradiations continue to be carried out for the purpose of characterizing background PM levels, including experiments around the time of the mechanism evaluation experiments for this project.

Plots of the 5-hour PM volume levels measured in this chamber from the period of the last three sets of reactors, which includes the period of the experiments for this project, are shown on Figure 7. As discussed by Carter et al (2005a,b), for the first two sets of reactors the background PM level was consistently higher in Side A than in Side B, with the background in Side B being quite low. However, for the last set of reactors, used for all experiments carried out for this project, the PM levels were essentially the same on both sides, at about the low range of the level of Side A in the previous sets of reactors. Note that this last reactor change was made at the same time extensive repairs had to be made to the enclosure, sampling, and mixing system because of flood damage caused by a sprinkler system as noted above. The cause of the background PM levels, and the causes in the changes as the reactors were changed, are unknown.

Although the background PM levels in the set of reactors used for this project are not as low as observed previously for Reactor “B”, at least they are now the same in both reactors. This makes it more straightforward to assess the effects of the test compounds on PM levels compared to the base case experiments, at least in a qualitative sense.

## Results of Injection Tests

Tests were performed to determine the extent to which EPTC and kerosene were injected into the gas phase using the injection procedures employed for the experiments. This was not a concern for the chloroprenes, MITC and CS<sub>2</sub> because of the relatively high volatility of these materials, but was a

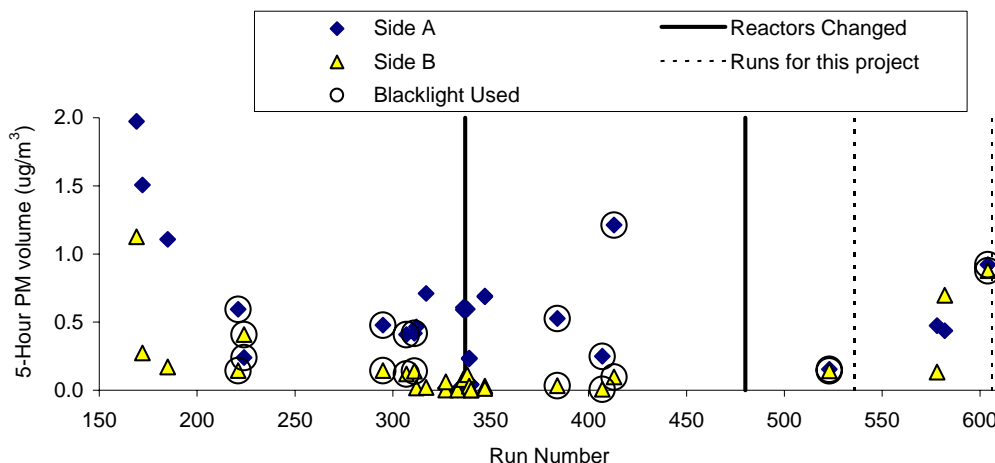


Figure 7. Plots of 5-hour PM volume measured in pure air irradiations in the UCR EPA chamber through the time of the experiments for this project.

concern for the other two. The procedure involved using the same injection method as employed for the experiments (see above), except that instead of going into the reactor the injection lines were connected to a total carbon analyzer, and the flushing continued until the total carbon analyzer signal returned to approximately its pre-injection value. The fraction injected at a particular time was then estimated by the ratio of the integrated total carbon analyzer output up to the given time, divided by the integrated total carbon analyzer output during the entire period until the injection was considered to be complete. Because the initial total carbon reading was generally off scale, it was estimated by extrapolation, assuming exponential decay for the initial period. This has some uncertainty, but the data are not highly sensitive to this extrapolation.

Figure 8 shows results of representative injection tests, indicating estimated fractions of kerosene or EPTC injected as a function of flushing time. The flushing times for the various experiments (or those with the shortest flushing times in the case of EPTC) are also shown on the figure. It is interesting to note that more than half of the kerosene is injected in the first few minutes, but that over two hours is required for the remainder of the material to be injected. This is because kerosene is a mixture of compounds of various volatilities, and the least volatile of the constituents take at least an hour or more to inject. On the other hand, after the initial ~20% of the EPTC is injected the amounts injected increase approximately linearly with time until it is nearly completely injected. This behavior is as expected for a pure compound.

The injection times in the incremental reactivity experiments with kerosene ranged from 1 to 1.5 hours, while those for EPTC ranged from about 1.25-2 hours. This was more than enough for complete injection of EPTC. On the other hand, the data indicate that a two hour or longer injection time would have been better for kerosene, with approximately 90-95% of the kerosene being injected using the procedures employed. Because of this, sensitivity calculations are carried out to determine the effects of removing the 10% heaviest fraction of the kerosene in the environmental chamber simulations, as discussed later in this report.

### OH Radical Rate Constant Determinations

The test compounds MITC and EPTC project are consumed in the atmosphere primarily by reactions with the OH radical, though the possibility of losses of MITC by photolysis and EPTC by

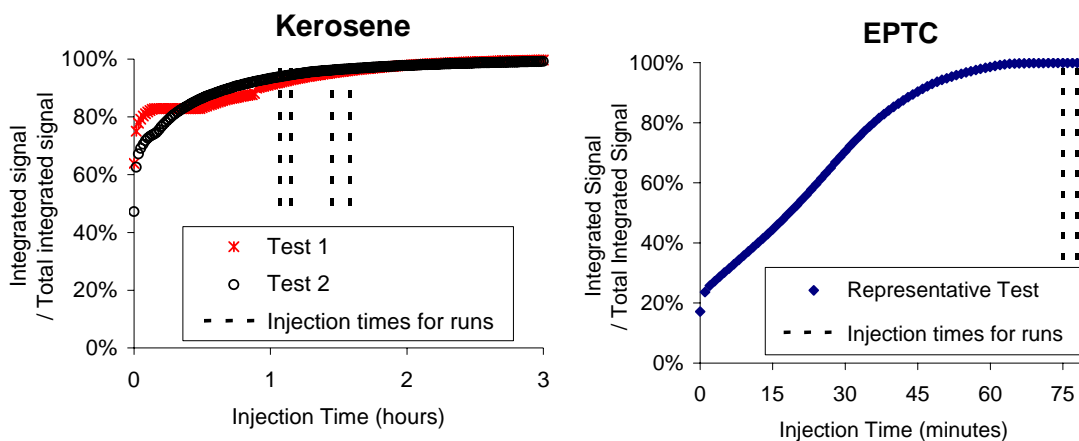


Figure 8. Plots of estimated fractions of kerosene or EPTC injected into the gas phase in representative injection tests.

reaction with NO<sub>3</sub> radicals also needs to be considered. Although measuring OH radical rate constants was not in the work statement of this project, we found that for many of the experiments the GC analysis employed in our laboratory sufficiently precise measurements of these compounds in the gas phase to make a relative rate constant determination feasible. The m-xylene present in the MIR or MOIR/2 surrogate experiments provided a suitable reference compound that is needed for this purpose. Therefore, if it is assumed that loss by reaction with OH radicals is the major factor causing the consumption of the test compound as it is with m-xylene, then the data from the incremental reactivity experiments can be used to derive relative rate constants for their reactions with OH radicals. The results of these determinations are discussed in this section.

If it is assumed that the test compounds react in our experiments only with OH radicals, then the ratio of OH radical rate constants with other compounds present that also only react with OH can be determined from their relative rates of decay. In this case, the kinetic differential equations for the organics can be solved and rearranged to yield

$$\ln\left(\frac{[\text{Test}]_{t0}}{[\text{Test}]_t}\right) - t k_{\text{Test}}^{\text{uni}} = \frac{k_{\text{Test}}^{\text{OH}}}{k_{\text{Test}}^{\text{OH}}} \ln\left[\left(\frac{[\text{Reference}]_{t0}}{[\text{Reference}]_t}\right) - t k_{\text{Reference}}^{\text{uni}}\right] \quad (\text{II})$$

where  $t$  is the irradiation time,  $[\text{Test}]_{t0}$  and  $[\text{Organic}]_t$ ,  $[\text{Reference}]_{t0}$ , and  $[\text{Reference}]_t$  are the initial and time =  $t$  concentrations of the test and reference compounds, respectively,  $k_{\text{Test}}^{\text{OH}}$  and  $k_{\text{Reference}}^{\text{OH}}$  are the test and reference compound's OH rate constant, and  $k_{\text{Test}}^{\text{uni}}$  and  $k_{\text{Reference}}^{\text{uni}}$  are rate constants for any unimolecular loss processes for the organic and reference compound, if applicable. Unimolecular loss processes could be due to losses due to dilution, losses to the walls, or photolysis. Except for the possible loss of MITC due to photolysis as discussed below, unimolecular loss processes are assumed to be negligible for the experiments and compounds studied for this project.

If all unimolecular loss processes are negligible, then plots of  $\ln([\text{Test}]_{t0}/[\text{Test}]_t)$  against  $\ln([\text{Reference}]_{t0}/[\text{Reference}]_t)$  should yield a straight line with intercept of approximately zero and a slope that is the ratio of rate constants. If the test compound undergoes loss by photolysis with a rate of  $k^{\text{phot}}$ , then  $\ln([\text{Test}]_{t0}/[\text{Test}]_t) - t k^{\text{phot}}$  would be plotted against  $\ln([\text{Reference}]_{t0}/[\text{Reference}]_t)$  to yield the same results. Given the known value of  $k_{\text{Reference}}^{\text{OH}}$ , then  $k_{\text{Test}}^{\text{OH}}$  can then be derived. M-Xylene is chosen as the reference compound because it is the most rapidly reacting compound in our reactivity experiments that reacts significantly only with OH radicals, and its OH radical rate constant is well known. The test and reference compound measurement data taken during the incremental reactivity experiments with data suitable for OH radical rate constant determinations given in Table 14 for MITC and Table 15 for EPTC.

In order to take the data from all of the experiments into account in the analysis in a unified manner, the data are fit to Equation (II) by adjusting the ratio of rate constants (which is assumed to be the same for all experiments) and the initial concentrations of the test compounds,  $[\text{Test}]_{t0}$ , for each experiment. (Adjusting  $[\text{Test}]_{t0}$  takes into account effects of measurement errors in the initial reactant concentrations, which can affect the results if data from more than one experiment are combined. It is not necessary to adjust both  $[\text{Test}]_{t0}$  and  $[\text{Reference}]_{t0}$  because the effects of any errors in one initial concentration on the derivation of the rate constant ratio is taken into account in the adjustment of the other.)

Plots of Equation (II) for the data from the MITC and EPTC reactivity experiments, assuming no losses of the test compounds by photolysis or other processes, are shown on Figure 9. Reasonably good fits to the data were obtained using Equation (II) with suitably adjusted initial concentrations and rate constant ratios, relative to m-xylene, of  $0.087 \pm 0.003$  and  $0.92 \pm 0.05$  for MITC and EPTC, respectively. The data for EPTC are somewhat more scattered than those for MITC because of somewhat lower analytical

Table 14. Data used for OH radical rate constant determinations for the MITC reactivity experiments.

Time (min)	m-Xylene	MITC	Time (min)	m-Xylene	MITC
Run EPA587			Run EPA588		
Initial [a]	12.1	179	Initial	12.7	725
-5	12.1	170	-25	12.8	728
45	11.1	183	-3	12.7	711
130	5.5	167	136	4.8	680
163	3.9	162	201	3.6	653
216	3.2	159	242	2.8	636
259	3.0	157	283	2.4	625
300	2.1	154	325	2.1	620
345	1.6	149			
Run EPA589			Run EPA599		
Initial	21.9	1067	Initial	21.2	1725
-15	23.9	1047	-16	22.1	1719
25	20.0	1053	24	20.3	1704
65	14.5	1034	63	16.1	1677
108	12.4	1028	102	13.5	1661
147	11.2	1018	142	12.1	1655
188	10.2	1010	182	11.2	1638
230	9.6	1006	222	10.4	1620
271	9.1	998	262	9.9	1629
314	8.5	975	303	9.4	1610
334	8.3	963			

[a] Initial concentration for the test compound set to minimize sum-of-squares errors of fits of the data to Equation (II) for all the experiments.

precision, but in neither case is there any apparent curvature that could be attributed to significant loss processes for the test compounds other than reaction with OH radicals.

Although the data shown on Figure 9 do not show any curvature that would be indicative of significant unimolecular loss processes for MITC, as discussed above the data of Alvarez (1993) and Alvarez and Moore (1994) indicate that MITC should undergo some loss by photolysis in these experiments. Based on these data and the measured light intensities and spectra of the light sources, we calculate MITC photolysis rates of  $6.45 \times 10^{-5} \text{ min}^{-1}$  for the arc light experiments and  $5.31 - 5.40 \times 10^{-5} \text{ min}^{-1}$  for the blacklight runs. Plots of Equation (II) using  $k_{\text{Test}}^{\text{uni}}$  for MITC set to these photolysis rates are shown on Figure 10. The data are fit by a rate constant ratio of  $0.074 \pm 0.004$ , which is  $\sim 15\%$  lower than the ratio derived assuming no photolysis. However, the qualities of the fits to the data are not significantly changed regardless of whether photolysis is assumed, which means that these data are not useful as evidence that photolysis is occurring to the extent predicted by the data of Alvarez et al (1994).

These relative rate constant measurements can be placed on an absolute basis using the rate constant for the reactions of OH radicals with m-xylene, which is  $2.36 \times 10^{-11} \text{ cm}^3 \text{ molec}^{-1} \text{ s}^{-1}$ , independent of temperature, in the SAPRC-99 mechanism, based on the evaluation of Atkinson (1989). This is essentially the same as the most recent mechanism of Atkinson and Arey (2003), which is  $2.31 \times 10^{-11} \text{ cm}^3 \text{ molec}^{-1} \text{ s}^{-1}$ , independent of temperature. Based on the latter value, we obtain

Table 15. Data used for OH radical rate constant determinations for the EPTC reactivity experiments.

Time (min)	m-Xylene	EPTC	Time (min)	m-Xylene	EPTC
Run EPA581			Run EPA584		
Initial [a]	14.6	81.5	Initial	26.8	143.6
-45	14.2	69.8	-33	26.8	125.9
-5	14.9	80.4	-1	26.7	142.1
34	14.1	87.1	59	23.9	135.5
205	10.0	50.2	109	20.6	116.6
280	8.6	48.9	157	18.3	97.4
365	7.5	49.1	227	18.1	100.8
			319	16.9	92.8
			359	16.7	90.3
Run EPA590			Run EPA586		
Initial	21.4	278.6	Initial	11.0	183.3
-37	21.4	256.5	-45	11.6	197.6
43	21.1	276.8	-3	10.3	166.6
83	19.5	268.9	37	10.3	171.8
168	17.8	235.1	157	8.5	155.0
208	17.0	225.4	199	8.6	147.5
249	16.8	221.3	242	8.3	137.9
293	16.0	215.8	288	8.0	147.0
343	15.3	207.9	327	7.7	124.3
			364	7.6	129.4

[a] Initial concentration for the test compound set to minimize sum-of-squares errors of fits of the data to Equation (II) for all the experiments.

$$k(\text{OH} + \text{MITC}, T \approx 300\text{K}) = 2.00 \pm 0.16 \times 10^{-12} \text{ cm}^3 \text{ molec}^{-1} \text{ s}^{-1}$$

if photolysis is assumed to be negligible, and

$$k(\text{OH} + \text{MITC}, T \approx 300\text{K}) = 1.72 \pm 0.17 \times 10^{-12} \text{ cm}^3 \text{ molec}^{-1} \text{ s}^{-1}$$

assuming upper limit photolysis rates consistent with the data of Alvarez et al (2004). The indicated uncertainties reflect 2 x the standard deviations of the derivation of the rate constant ratio, and do not reflect any uncertainty in the reference rate constant value. We are not aware of any previous measurements of this rate constant.

These OH + MITC rate constants are both significantly higher than the recent value measured by Sommerlade et al (2006), who obtained  $k(\text{OH} + \text{MITC}) = 1.28 \times 10^{-12} \text{ cm}^3 \text{ molec}^{-1} \text{ s}^{-1}$  at 70 torr and 298K. The dotted lines on Figure 9 and Figure 10 indicate where data points need to be for the data to be consistent with that rate constant. However, the initial reaction is postulated to be the addition of OH to MITC, forming a vibrationally excited adduct, so the reaction may well be pressure dependent. If the reaction is not at its high pressure limit at 70 torr, our results, which reflect the rate constant at 740 torr, may not necessarily be inconsistent with the data of Sommerlade et al (2006).

In the case of EPTC, where reaction with OH radicals is expected to be the only significant loss process, the relative rate constants measured in this work, and the absolute OH + m-xylene rate constant of Atkinson and Arey (2003), indicate that



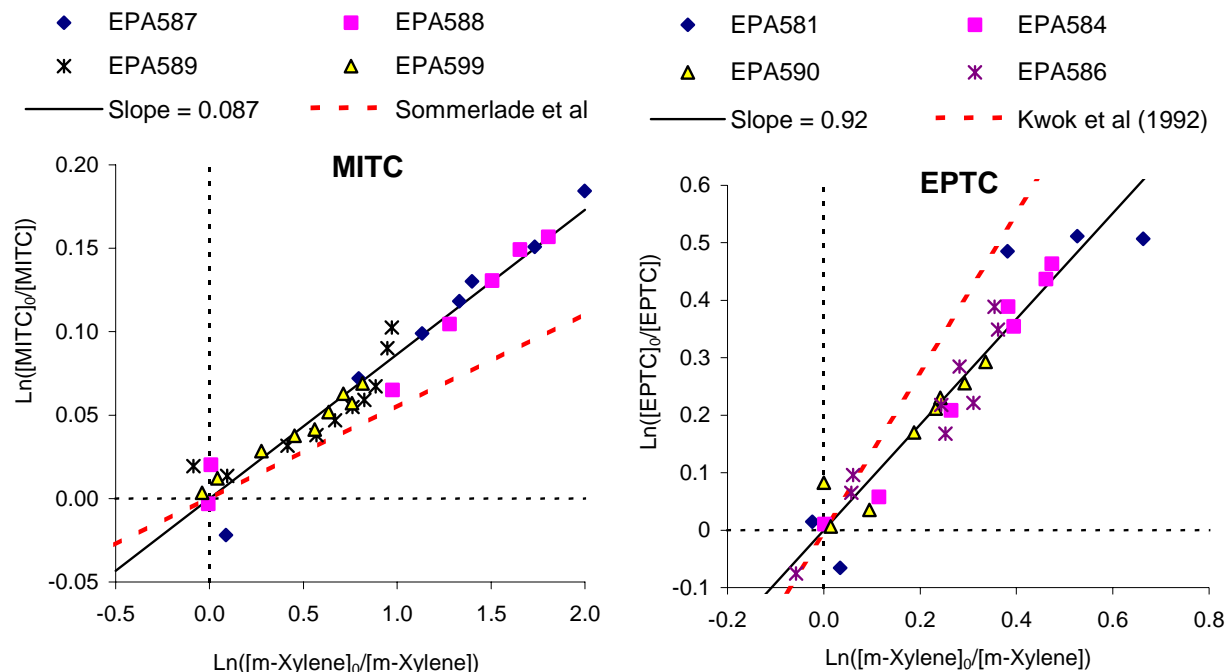


Figure 9. Plots of Equation (II) for the data from the MITC and EPTC reactivity experiments, assuming no losses of the test compounds by photolysis or other processes.

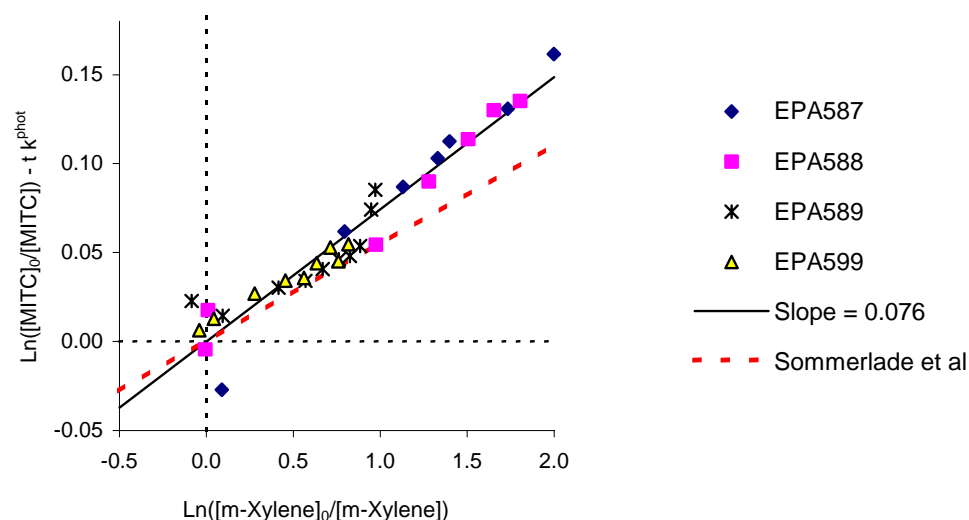


Figure 10. Plots of Equation (II) for the data from the MITC reactivity experiments, assuming that MITC undergoes loss by photolysis with photolysis rates calculated using the absorption cross sections of Alvarez et al (1994) and assuming unit quantum yields.

$$k(\text{OH} + \text{EPTC}, T \approx 300\text{K}) = 2.12 \pm 0.25 \times 10^{-11} \text{ cm}^3 \text{ molec}^{-1} \text{ s}^{-1}.$$

As with MITC, the indicated uncertainty reflects 2 x the standard deviations of the derivation of the rate constant ratio, and does not reflect any uncertainty in the reference rate constant value. This is approximately 33% lower than the value of  $3.18 \pm 0.49 \times 10^{-11} \text{ cm}^3 \text{ molec}^{-1} \text{ s}^{-1}$  reported by Kwok et al (1992). The dotted line on Figure 9 indicates the slope of Equation (II) corresponding to the Kwok et al (1992) rate constant. This discrepancy is somewhat outside the respective uncertainty ranges of the two determinations, but not significantly so.

Although reaction of the 1,3-dichloropropene isomers with OH radicals is probably the most important single loss process under atmospheric conditions, reaction with  $\text{O}_3$ ,  $\text{NO}_3$  and Cl atoms may be non-negligible under the conditions of our experiments. Because of this, determining the OH rate constants for the chloropropenes from the data of our reactivity experiments using the relative rate method discussed may not be a reliable procedure, and strictly speaking would only give lower limits for the rate constant. However, it is of interest to determine the consistency of the data obtained in our reactivity experiments with the rate constants used in the chemical mechanism used in this study.

The dichloropropene and m-xylene data from the dichloropropene reactivity experiments that can be used to derive estimated OH rate constants are summarized in Table 16, and plots of Equation (II), assuming no unimolecular loss processes, are shown on Figure 11 for the two isomers. The figure also shows the lines where the data are predicted to fall using the OH rate constants of Tuazon et al (1988), which are the values used in the mechanism for these compounds. It can be seen that the data are reasonably well fit by straight lines, and the slopes of the lines are consistent with the rate constants of Tuazon et al (1988). This suggests that the reactions of these dichloropropenes with OH radicals is indeed their major fate under the conditions of these experiments.

## Mechanism Evaluation Results

Table 17 lists the initial concentrations and selected results for the incremental reactivity and other ozone mechanism evaluation experiments carried out for this project. The measures of gas-phase reactivity used to evaluate the mechanisms in the incremental reactivity experiments are the effects of the test compound or solvent on  $\Delta([\text{O}_3]-[\text{NO}])$ , or  $([\text{O}_3]_t-[\text{NO}]_t)-([\text{O}_3]_0-[\text{NO}]_0)$ , and IntOH, the integrated OH radical levels. As discussed elsewhere (e.g., Johnson, 1983; Carter and Atkinson, 1987; Carter and Lurmann, 1991; Carter et al, 1993),  $\Delta([\text{O}_3]-[\text{NO}])$  gives a direct measure of the amount of conversion of NO to  $\text{NO}_2$  by peroxy radicals formed in the photooxidation reactions, which is the process that is directly responsible for ozone formation in the atmosphere. This gives a useful measure of factors affecting  $\text{O}_3$  reactivity even early in the experiments where  $\text{O}_3$  formation is suppressed by the unreacted NO. Although this is the primary measure of the effect of the VOC on  $\text{O}_3$  formation, the effect on radical levels is also a useful measure for mechanism evaluation, because radical levels affect how rapidly all VOCs present, including the base ROG components, react to form ozone.

The integrated OH radical levels are not measured directly, but can be derived from the amounts of consumption of reactive VOCs that react only with OH radical levels. In particular,

$$\text{IntOH}_t = \frac{\ln([\text{tracer}]_0/[\text{tracer}]_t) - Dt}{k_{\text{OH}}^{\text{tracer}}} \quad (\text{III})$$

where  $[\text{tracer}]_0$  and  $[\text{tracer}]_t$  are the initial and time t concentrations of the compound used as the OH tracer,  $k_{\text{OH}}^{\text{tracer}}$  its OH rate constant, and D is the dilution rate in the experiments. The latter is small in our chamber and is neglected in our analysis. For most experiments, the base ROG surrogate component

Table 16. Data used for to test the consistency of the results of the dichloropropene reactivity experiments with measurements of the OH + dichloropropene rate constants

Time (min)	m-Xylene	Cis-1,3-DCP	Trans-1,3-DCP	Time (min)	m-Xylene	Cis-1,3-DCP	Trans-1,3-DCP
Run EPA550A				Run EPA555B			
Initial [a]	11.4	60	47	Initial	11.2	26	20
-25	11.5	59	46	-3	11.2	27	21
-5	11.4	59	46	35	9.4	25	18
45	10.1	56	42	73	7.0	22	16
85	7.0	48	34	110	5.7	21	14
124	4.6	40	27	147	5.2	20	13
164	3.3	36	23	183	5.0	18	11
205	2.4	32	19	220	4.7	18	11
258	1.8	28	17	257	4.1	17	10
298	1.7	26	15	294	3.5	17	10
341	1.2	24	13	331	3.3	16	10
				369	3.2	16	10
Run EPA554B							
Initial	23.6	58	44				
7	22.8	58	45				
27	20.4	55	42				
74	13.9	46	33				
115	11.4	43	29				
155	10.3	41	27				
193	10.0	40	26				
233	8.8	39	25				
272	8.4	38	24				
312	8.3	37	22				
352	7.7	36	22				

[a] Initial concentration for the test compound set to minimize sum-of-squares errors of fits of the data to Equation (II) for all the experiments.

m-xylene is the most reactive compound in the experiment that reacts only with OH radicals, and was therefore used as the OH tracer to derive the IntOH data. However, for the non-aromatic surrogate experiments the base ROG component n-octane was used for the OH radical tracer. The m-xylene and n-octane OH radical rate constant used in this analysis were  $2.36 \times 10^{-11}$  and  $\text{cm}^3 \text{ molec}^{-1} \text{ s}^{-1}$  (Atkinson, 1989) and  $8.76 \times 10^{-12}$  and  $\text{cm}^3 \text{ molec}^{-1} \text{ s}^{-1}$  (Atkinson, 1997), respectively.

In experiments with chlorine-containing test compounds, where chlorine atoms may be formed, both the integrated OH and the integrated chlorine levels can be calculated if data are available from two tracers that are consumed by reaction with OH radicals and Cl atoms, provided that the relative rates of consumption by OH or Cl are different for the two tracers. In the case of these experiments, m-xylene is consumed primarily by reaction with OH radicals, while the alkane tracers, such as the n-octane in the base ROG surrogate used in the experiments for this project, or the n-hexane in the “mini-surrogate” in some of the earlier chloropicrin (Carter et al, 1997a,b) runs that are modeled in this report, are consumed to a significant extent by reaction with Cl if sufficient Cl is generated in this experiment. In this case, assuming no losses by unimolecular processes, the integrated chlorine (IntCl) and integrated OH levels can be calculated by

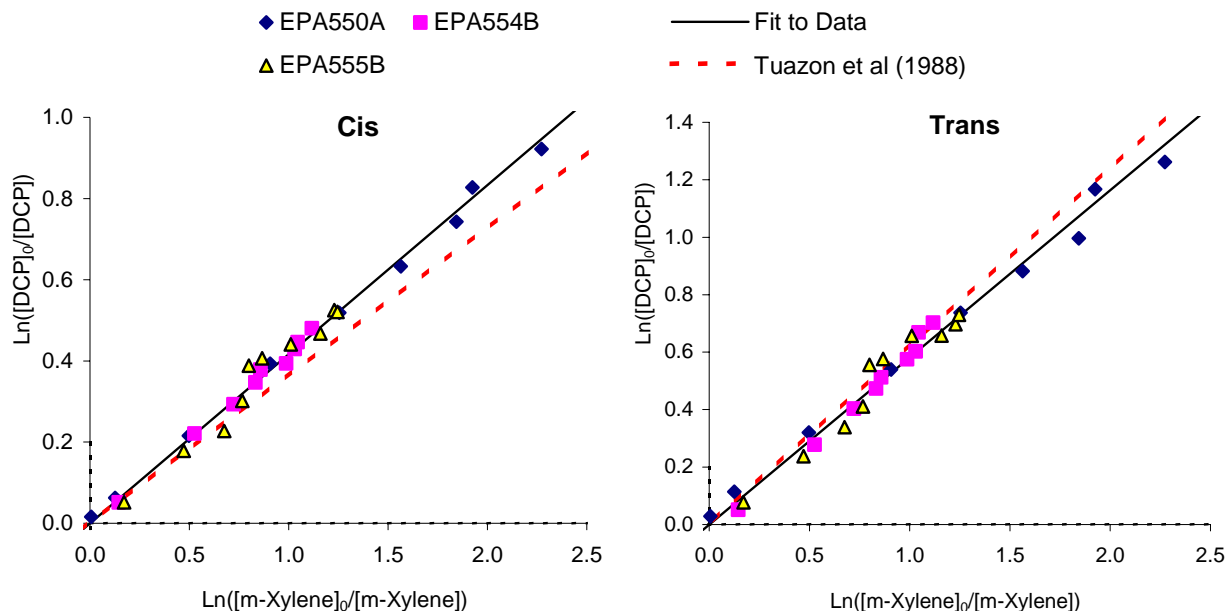


Figure 11. Plots of Equation (II) for the data from the dichloropropene reactivity experiments, assuming no losses of the test compounds other processes.

$$\text{IntCl}_t = \frac{\frac{\text{IntOHunc}_t^{\text{tracer1}}}{k\text{Cl}^{\text{tracer1}}} - \frac{\text{IntOHunc}_t^{\text{tracer2}}}{k\text{Cl}^{\text{tracer2}}}}{\frac{k\text{OH}^{\text{tracer1}}}{k\text{OH}^{\text{tracer2}}}} \quad (\text{IV})$$

$$\text{IntOH}_t = \text{IntOHunc}_t^{\text{tracer2}} - \frac{k\text{Cl}^{\text{tracer2}}}{k\text{OH}^{\text{tracer2}}} \text{IntCl}_t \quad (\text{V})$$

where  $\text{IntOHunc}_t^{\text{tracer1}}$  and  $\text{IntOHunc}_t^{\text{tracer2}}$  are the integrated OH levels calculated without correction for loss by Cl reactions using Equation (III) from the data for tracer1 and tracer2, respectively, and  $k\text{OH}$  and  $k\text{Cl}$  are the OH and Cl rate constants for the tracers. The chlorine atom rate constants used in this analysis are given in Table A-5 in Appendix A.

The side equivalency tests, where equal base ROG -  $\text{NO}_x$  mixtures are simultaneously irradiated without added test compounds, provide a measure of the sensitivity of the experiments to distinguish the effects of the added VOCs. In most cases, the side equivalency for the gas-phase measurements was excellent, with the  $\text{O}_3$  and  $\Delta([\text{O}_3] - [\text{NO}])$  differences being no greater than ~5 ppb and the IntOH differences being less than 5 ppt-min. The results of these tests are summarized on Table 17.

The results for the individual test compounds are discussed in the following sections. However, before discussing the results of the incremental reactivity experiments, it is important to emphasize again that incremental reactivities in the chamber are not necessarily those in the atmosphere. The purpose of the experiments is to test the predictive capabilities of the mechanisms, as discussed in the following section of this report. Although the experiments are designed to represent a range of *chemical* conditions applicable to the atmosphere, it is not practical to duplicate atmospheric conditions exactly, and different aspects of the mechanism have somewhat different relative importances in affecting the results of

Table 17. Summary of initial concentrations and selected gas-phase results of the incremental reactivity experiments.

Run	Test Side	Type [a]	Test VOC Added	Base Run Initial Concentrations		Hours, Light [b]	Final O <sub>3</sub> (ppb)		Δ([O <sub>3</sub> ]-[NO]) Change (ppb)		IntOH Change (ppt-min)
				NO <sub>x</sub> (ppb)	ROG (ppmC)		Test	Base	2 Hr	Final	
Side Equivalency Tests											
549	B	MIR	-	26	0.54	5 a	134	138	1	-3	-5
606	B	MOIR/2	-	23	1.12	5 b	106	106	1	2	-1
Methyl Isothiocyanate (Measured ppm added)											
587	A	MIR	0.17	30	0.58	5 a	134	125	12	6	-3
588	B	MIR	0.72	30	0.56	5 a	166	127	40	40	-4
599	A	MOIR/2	0.99	25	1.03	6 b	174	124	30	49	-5
589	A	MOIR/2	1.05	25	1.15	5 a	184	138	21	46	-5
EPTC (Measured ppm added)											
581	A	MIR	0.078	30	0.58	5 a	129	134	-11	-4	-31
586	A	MIR	0.161	32	0.55	6 a	138	142	-9	-4	
583	B	MOIR/2	0.025	25	1.30	4 a	135	134	2	-1	-6
584	B	MOIR/2	0.119	25	1.23	5 a	130	140	-9	-9	-13
590	B	MOIR/2	0.245	23	1.09	5 a	125	134	-11	-8	-23
Carbon Disulfide (Measured ppm added)											
598	A	MIR	0.35	26	0.57	5 b	98	84	8	13	-2
591	A	MIR	0.55	30	0.55	5 a	164	133	21	28	-8
597	B	MOIR/2	0.63	24	1.09	6 b	131	115	14	15	-4
592	B	MOIR/2	0.65	25	1.11	1 a	75	61		17	0
1,3-Dichloropropenes (Measured ppb added)											
550	A	MIR	104	28	0.54	5 a	184	132	53	51	-13
554	B	MOIR/2	103	22	1.09	5 a	161	139	21	21	-6
555	B	Low Conc. MOIR/2 [c]	48	11	0.57	5 a	98	89	9	8	-2
Kerosene (Calculated ppmC added)											
600	B	MIR		28	0.57	5 b	87	83	-10	4	-23
607	A	MIR		30	0.55	5 b	76	72	-10	2	-23
603	B	MOIR/2		24	1.06	5 b	104	110	-7	-5	-9
602	A	MOIR/2		23	1.08	5 b	96	105	-14	-11	-11

[a] Codes for types of base case experiments for the incremental reactivity experiments are as follows: “MIR”: ~30 ppb NO<sub>x</sub> and ~0.55 ppmC ROG surrogate; “MOIR/2”: ~25 ppb NO<sub>x</sub> and ~1.1 ppmC ROG surrogate.

[b] Hours of irradiation for which O<sub>3</sub> and  $\Delta([O_3]-[NO])$  data are available. Code “a” indicates arc lights used, “b” indicates blacklights.

[c] This was initially intended to be a “MIR” experiment, but due to a NO<sub>x</sub> injection error the base case experiment turned out to be essentially a MOIR/2 experiment with ½ the initial ROG and NO<sub>x</sub> levels.

Table 18. Summary of initial concentrations and selected gas-phase results of the dichloropropene - NO<sub>x</sub> and dichloropropene - NO<sub>x</sub> + propane experiments.

Run	Side	Lt [a]	Initial Concentration (ppm)			O <sub>3</sub> (ppb)		13-DCPs Rct'd (4 Hr)
			NO <sub>x</sub>	13-DCPs	Propane	2 Hr	4 Hr	
547	A	Bl	24	0.40		54	158	34%
547	B	Bl	46	0.40		27	142	30%
551	A	a	23	0.37		111	214	51%
551	B	a	46	0.37		59	233	49%
548	A	a	22	0.38	0.31	120	225	48%
548	B	a	23	0.38	0.12	113	218	49%

[a] Lights used: Bl = blacklights; a = arc lights.

chamber experiments than in model simulations of the atmosphere. This was discussed in more detail by Carter and Malkina (2005), where specific examples of the differences are given.

Measurements were also made of PM formation during these reactivity experiments, allowing effects of these compounds on PM formation to be assessed. These and other PM results are discussed later in this report.

### Methyl Isothiocyanate (MITC)

Experimental and calculated  $\Delta([O_3]-[NO])$  and IntOH data for the MITC incremental reactivity experiments are shown on Figure 12, and data for formaldehyde are shown on Figure 13. The experiments indicate that MITC has a generally positive effect on NO oxidation and O<sub>3</sub> formation in all the experiments, but has a slightly negative effect on OH radical levels except perhaps for the initial period of the experiment. The formaldehyde data indicate that the MITC has no measurable effect on formaldehyde formation, indicating that formaldehyde is not a major product in the oxidation of MITC.

Results of model calculations are also shown on Figure 12 and Figure 13. Note that the model for the base case constituents employs the “adjusted aromatics” mechanism developed by Carter and Malkina (2005) to be consistent with the results of the base case experiments, as discussed above in the “Modeling Methods – Base Mechanism” section. This approach is used in the simulations of all the reactivity experiments carried out for this project. The adjusted mechanism gives reasonably good fits to the results of the base case experiments, except for run EPA699, where the O<sub>3</sub> formation in the base case experiments is slightly underpredicted. The unadjusted mechanism (not shown) tends to underpredict  $\Delta([O_3]-[NO])$  in the MIR runs, but gives qualitatively similar results as the adjusted aromatic mechanism for predictions of changes in  $\Delta([O_3]-[NO])$  or IntOH caused by the addition of MITC.

As discussed above in the “Modeling Methods – Mechanisms for Test Compounds” section, two possible mechanisms for the reaction of MITC with OH radicals are considered, one, designated “Mechanism A” where the HSO radicals formed in this reaction do not react significantly with O<sub>2</sub>, and the other, designated “Mechanism B” where the O<sub>2</sub> reaction is assumed to be sufficiently rapid that it is the major fate of HSO. Mechanism “A” predicts that the net effect of reactions of MITC with OH radicals is the net destruction of O<sub>3</sub>, and thus negative effects of MITC on O<sub>3</sub> formation is predicted. It can be seen that this is clearly inconsistent with the experimental results, where positive effects on O<sub>3</sub> are seen. In addition, this mechanism predicts that MITC has essentially no or slightly positive effects on OH radicals,

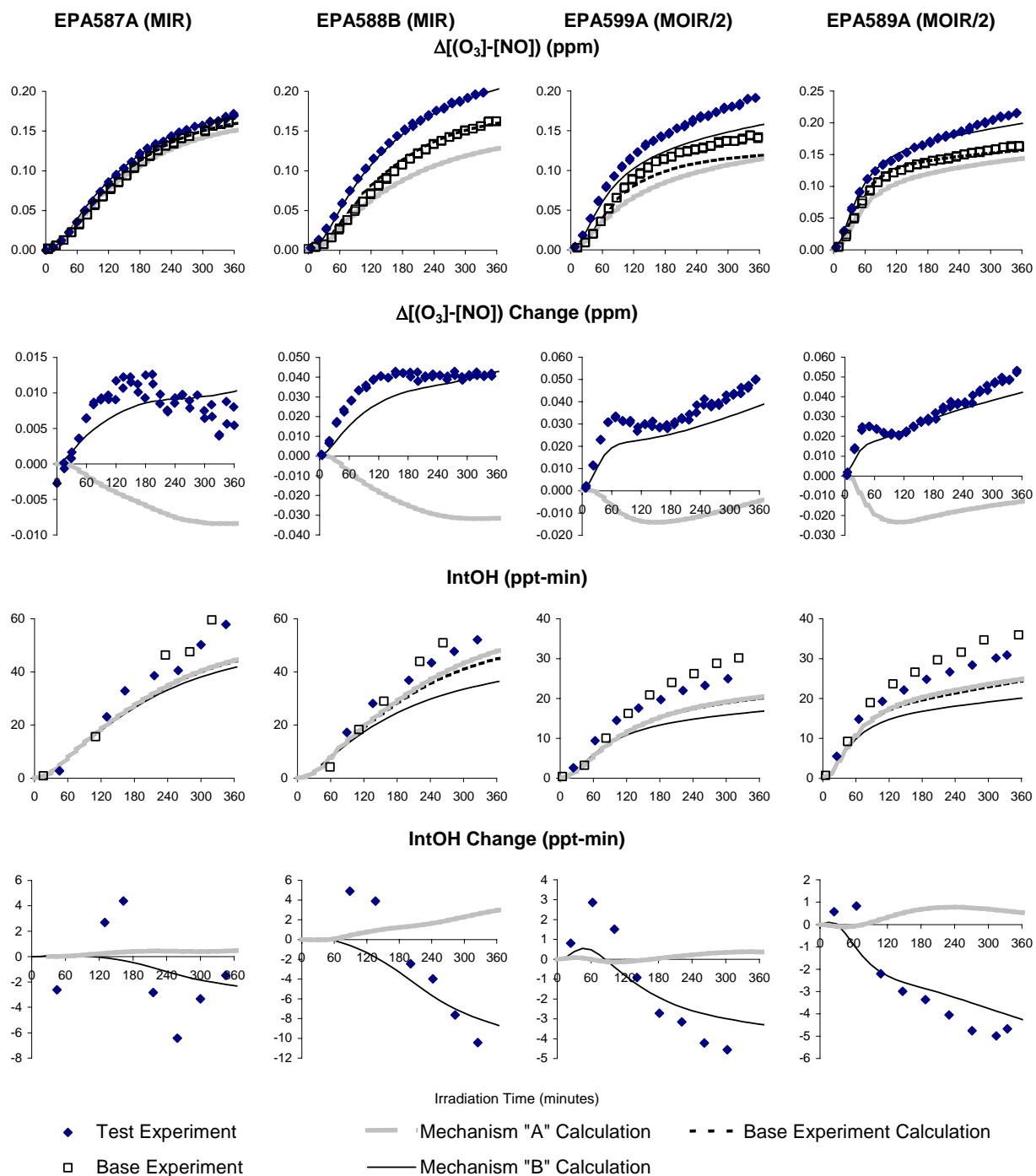


Figure 12. Experimental and calculated concentration-time plots for  $\Delta([O_3]-[NO])$  and IntOH for the incremental reactivity experiments with MITC.

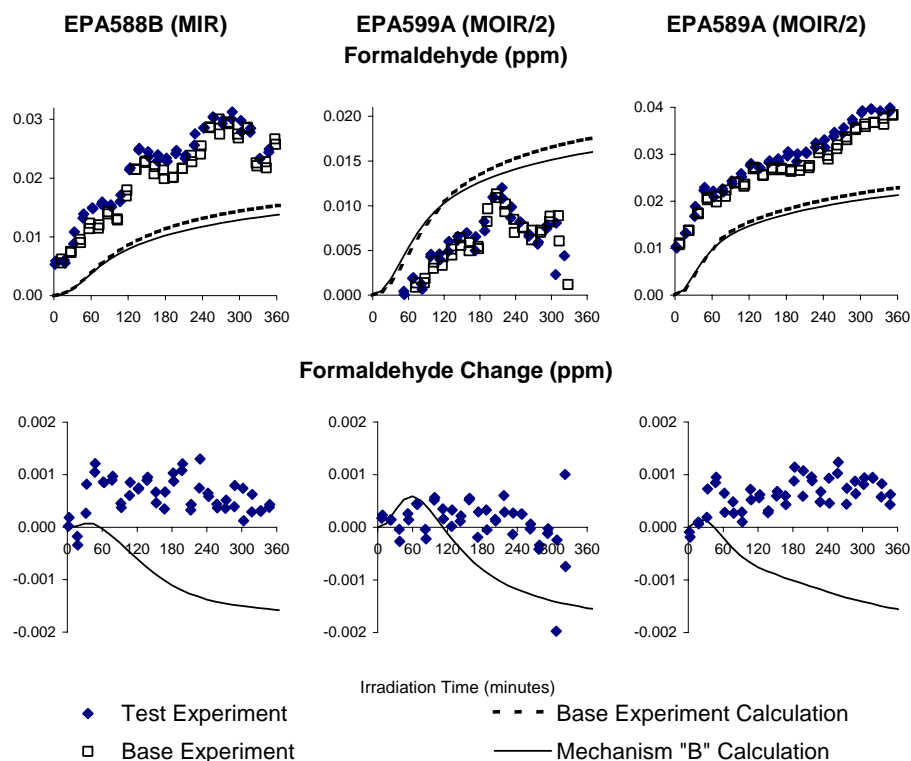
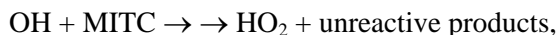


Figure 13. Experimental and calculated concentration-time plots for formaldehyde for the incremental reactivity experiments with MITC that had formaldehyde data.

while experimentally the MITC reduces integrated OH to a measurable extent. Therefore, this mechanism is not considered further.

On the other hand, both the  $\Delta([O_3]-[NO])$  and IntOH incremental reactivity data are reasonably well fit by “Mechanism B”, which assumes that the reaction with  $O_2$ , ultimately forming  $HO_2$ ,  $SO_2$ , and  $O_3$  (from  $O(^3P)$ ), is the major fate of HSO. Note, however, this cannot be taken as definitive evidence that HSO, if formed, indeed reacts with  $O_2$ , since the assumed MITC + OH mechanism is speculative, and may not necessarily be correct. The data are equally well fit by any MITC + OH mechanism where the net effect is



since this is the net effect of “Mechanism B” under the conditions of our experiments. This would be the case, for example, if the HS formed in the initial reaction reacted with  $O_2$  forming  $HO_2$  and  $SO_2$  without the intermediacy of HSO. There may well be other possible mechanisms that have the same net effect.

Figure 14 shows results of additional model simulations of the experiments carried out in order to determine the sensitivity of the results to the photolysis reaction, and also to determine whether mechanisms assuming additional NO to  $NO_2$  conversions would also be consistent with the data. The “no photolysis” calculation assumed that photolysis was negligible, and that the OH reaction consisted of Mechanism “B” with the rate constant increased to  $2.0 \times 10^{-12} \text{ cm}^3 \text{ molec}^{-1} \text{ s}^{-1}$ , the value indicated by the relative rate constant determination in this study if loss photolysis were neglected (see above). It can be



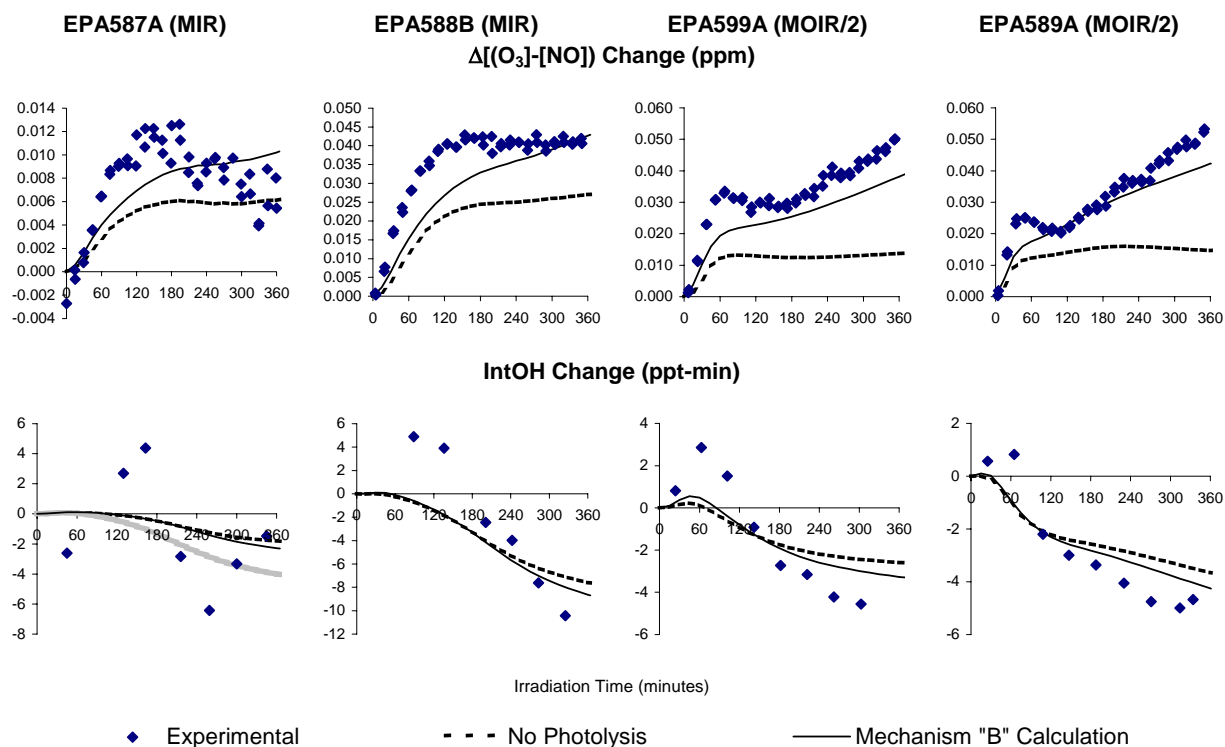


Figure 14. Experimental and alternative model calculations of concentration-time plots for change in  $\Delta([O_3]-[NO])$  for the incremental reactivity experiments with MITC.

seen that this mechanism consistently underpredicts  $\Delta([O_3]-[NO])$  reactivity, indicating that the photolysis, though not the major loss process, has a non-negligible effect on the  $O_3$  reactivity of MITC. It also indicates that the data obtained tend to support the mechanism for the photolysis that is assumed.

The MITC mechanisms discussed assume that the major oxidation products are methyl isocyanide and methyl isocyanate for the photolysis and OH reactions, respectively, and that these are relatively unreactive. However, if the OH reaction were at the methyl group, or if the assumed primary products underwent secondary reaction to any significant extent, then higher levels of formaldehyde formation should be observed in the experiments with MITC. However, this was found not to be the case, as shown in Figure 13, above, which shows formaldehyde measurements and changes in formaldehyde caused by MITC in the incremental reactivity experiments with MITC where formaldehyde data were available. Thus, the formaldehyde measurements in the MITC experiments are consistent with the assumed mechanisms used in this work.

### Carbon Disulfide

Experimental and calculated  $\Delta([O_3]-[NO])$  and IntOH data for the carbon disulfide incremental reactivity experiments are shown on Figure 15. The experiments indicate that carbon disulfide, like MITC, has a generally positive effect on NO oxidation and  $O_3$  formation in all the experiments, but has a slightly negative effect on OH radical levels. Note that the MOIR/2 run EPA592 ended after only two hours of irradiation because of a failure of the arc light, but this was sufficient to give at least some mechanism evaluation results.

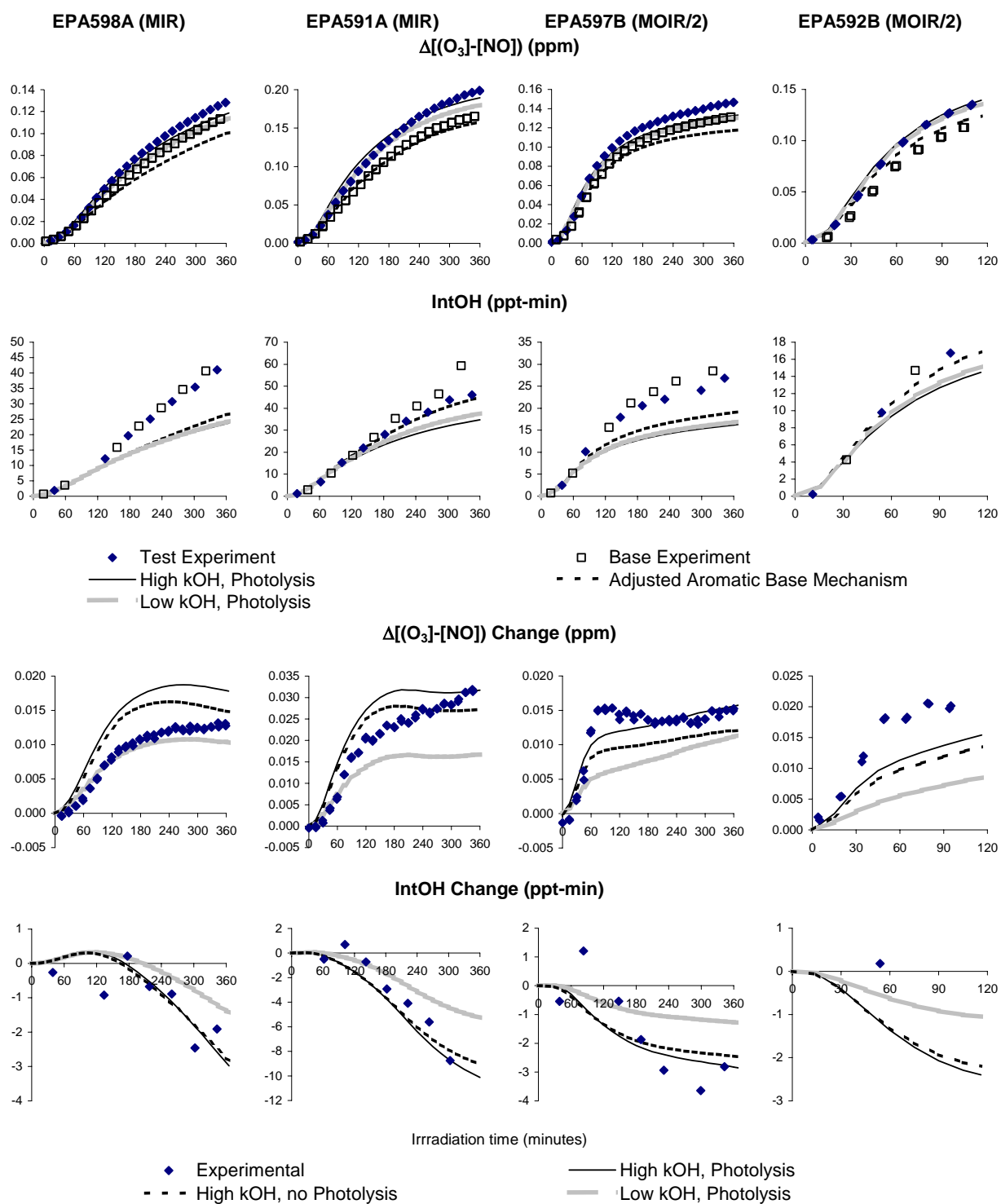


Figure 15. Experimental and calculated concentration-time plots for  $\Delta([O_3]-[NO])$  and IntOH for the incremental reactivity experiments with  $CS_2$ .

Results of model calculations are also shown on Figure 15. Again, the calculations employed the “adjusted aromatics” base mechanism of Carter and Malkina (2005) in order to give satisfactory simulations of the base case experiments, and again the base case experiments were simulated reasonably well except for the consistent underprediction of IntOH that is a characteristic of the current mechanism. However, in this case there is a slight underprediction of the final O<sub>3</sub> in runs EPA597 and EPA598.

Simulations of the added carbon disulfide experiments were carried out with the OH + CS<sub>2</sub> rate constants (kOH) at the minimum and maximum values of 1.2 and 2.76 x 10<sup>-12</sup> cm<sup>3</sup> molec<sup>-1</sup> s<sup>-1</sup> constants, respectively, and the quantum yield for the photolysis reaction ranging from 0 (no photolysis) to 0.012. The results show that the Δ([O<sub>3</sub>]-[NO]) and IntOH incremental reactivities are consistently underpredicted if the low rate constant based on the NASA (2006) recommendation is used, and somewhat better fits are obtained if the higher overall rate constant, derived from the on IUPAC (2006)-evaluated rate constants for the elementary processes, is employed. However, the results of the simulations are variable from run to run, with the Δ([O<sub>3</sub>]-[NO]) incremental reactivities tending to be overpredicted in the MIR experiments and underpredicted in the MOIR/2 runs. It is unclear whether this is run-to-run variability or whether there is some problem with the mechanism not correctly simulating the effects of base case ROG/NO<sub>x</sub> ratios on reactivity.

The simulations where the rate constant was varied were carried out using CS<sub>2</sub> photolysis with the recommended “upper limit” quantum yield of 0.012. Assuming the photolysis is negligible causes a slight reduction in Δ([O<sub>3</sub>]-[NO]) incremental reactivities but has no noticeable effect on IntOH. This is consistent with the fact that the photolysis reaction forms O(<sup>3</sup>P), which forms O<sub>3</sub>, but does form radicals that enhance OH. Because of the variability of the simulation results, the data obtained are not sufficient to provide evidence for or against the photolysis reaction occurring with a quantum yield of 0.012.

### **S-Ethyl N,N-di-n-Propyl Thiocarbamate (EPTC)**

Experimental and calculated Δ([O<sub>3</sub>]-[NO]), IntOH and (where experimental data available) formaldehyde data for the EPTC incremental reactivity experiments are shown on Figure 16, and experimental and calculated changes in concentrations of those species caused by adding EPTC are shown in Figure 17. The experiments indicate that EPTC has a small but generally slightly negative effect on Δ([O<sub>3</sub>]-[NO]) in most of the experiments, and has a strong negative effect on integrated OH radical levels. The strong negative effect on IntOH indicates that significant radical termination processes occur in the EPTC reactions, and this would have a generally negative effect on O<sub>3</sub> reactivity because the reduced radical levels reduces O<sub>3</sub> formation rates from the reactions of the other VOCs that are present. The fact that the effect on NO oxidation and O<sub>3</sub> formation rates is relatively small indicates that strongly negative “indirect” reactivity effect caused by reducing O<sub>3</sub> from the reactions of the base ROG components is compensated, at least to some extent by the NO oxidation and O<sub>3</sub> formation from the reactions of EPTC itself. This type of result is observed for many other compounds that have been studied previously, such as higher molecular weight alkanes, Texanol®, and many other higher molecular weight non-aromatic compounds (e.g., see Carter, 2000a; Carter, 2004; Carter and Malkina, 2005).

Formaldehyde results for the one EPTC experiment with useable formaldehyde data are also shown on Figure 16 and Figure 17. Note that the calibration of formaldehyde is highly uncertain during this period, and the experimental data are corrected to be consistent with the model predictions of the base case experiments. (Experimental and calculated formaldehyde data are generally in good agreement if the formaldehyde data are reliable and the model gives reasonably good simulations of the overall reactivity.) It can be seen that the addition of EPTC causes a reduction in the overall formaldehyde levels. This is attributed to the reduction in overall radical levels caused by the EPTC addition, which reduces rates of

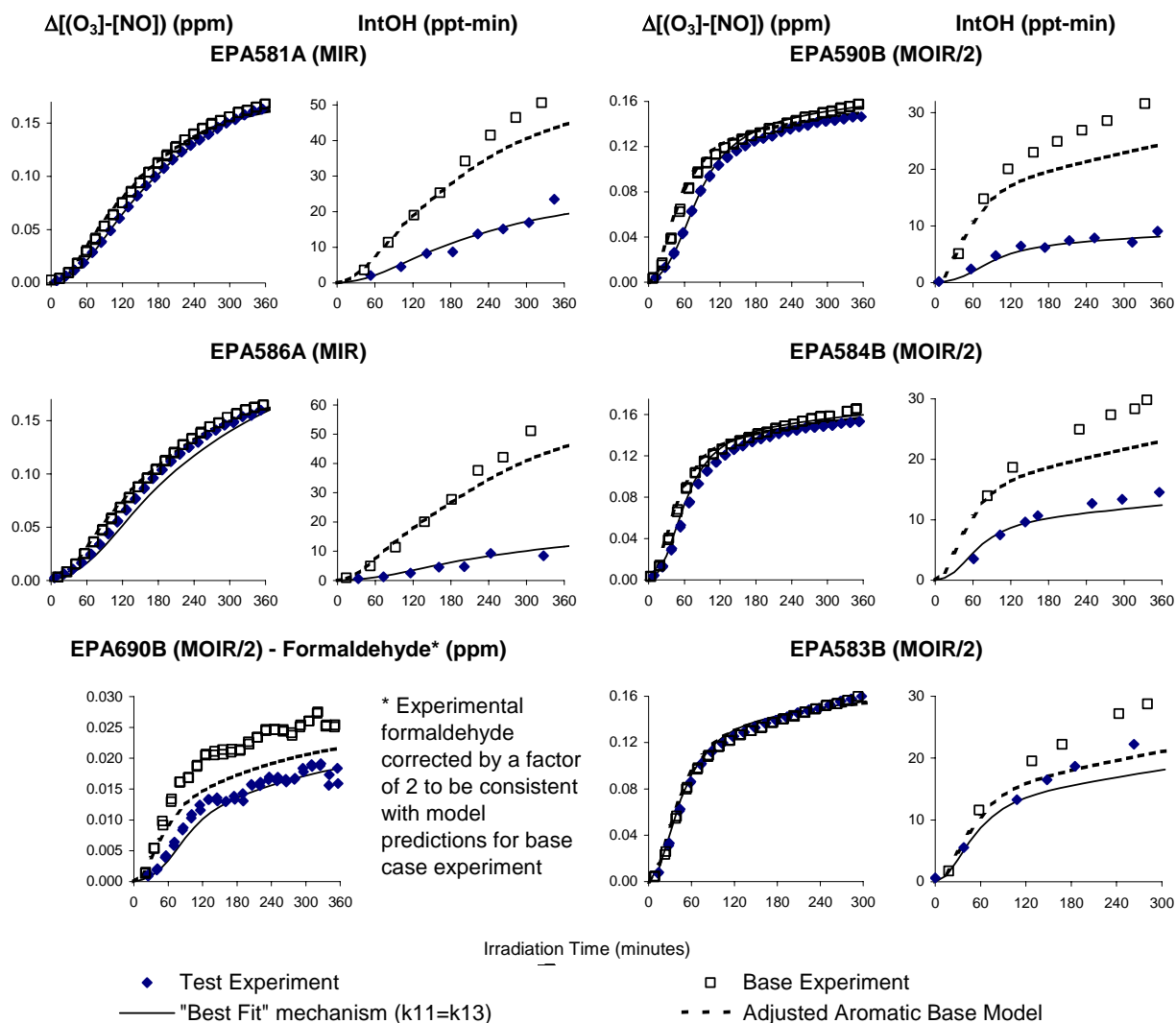


Figure 16. Experimental and calculated concentration-time plots for  $\Delta([O_3]-[NO])$ , IntOH and (where experimental data available) formaldehyde for the incremental reactivity experiments with EPTC.

formaldehyde production from the base ROG constituents (primarily ethylene and propylene). It also indicates that formaldehyde formation from the reactions of EPTC is relatively minor, if it occurs at all.

Results of model calculations are also shown on Figure 16 and Figure 17. As with the other compounds, the model simulations use the “adjusted aromatic” base case mechanism to give the best simulations of the base case conditions (Carter and Malkina, 2005). As discussed above in the “Modeling Methods – Mechanisms for Test Compounds” section, there are a number of uncertainties in the mechanism for the reactions of EPTC with OH radicals, and relative importances of possible competing processes have to be treated as adjustable parameters. Both figures show the test calculation with the version of the mechanism that gave the best fits to the data, while Figure 17 shows results of calculations with other mechanism assumptions, to show the sensitivity of the results to these mechanistic uncertainties.

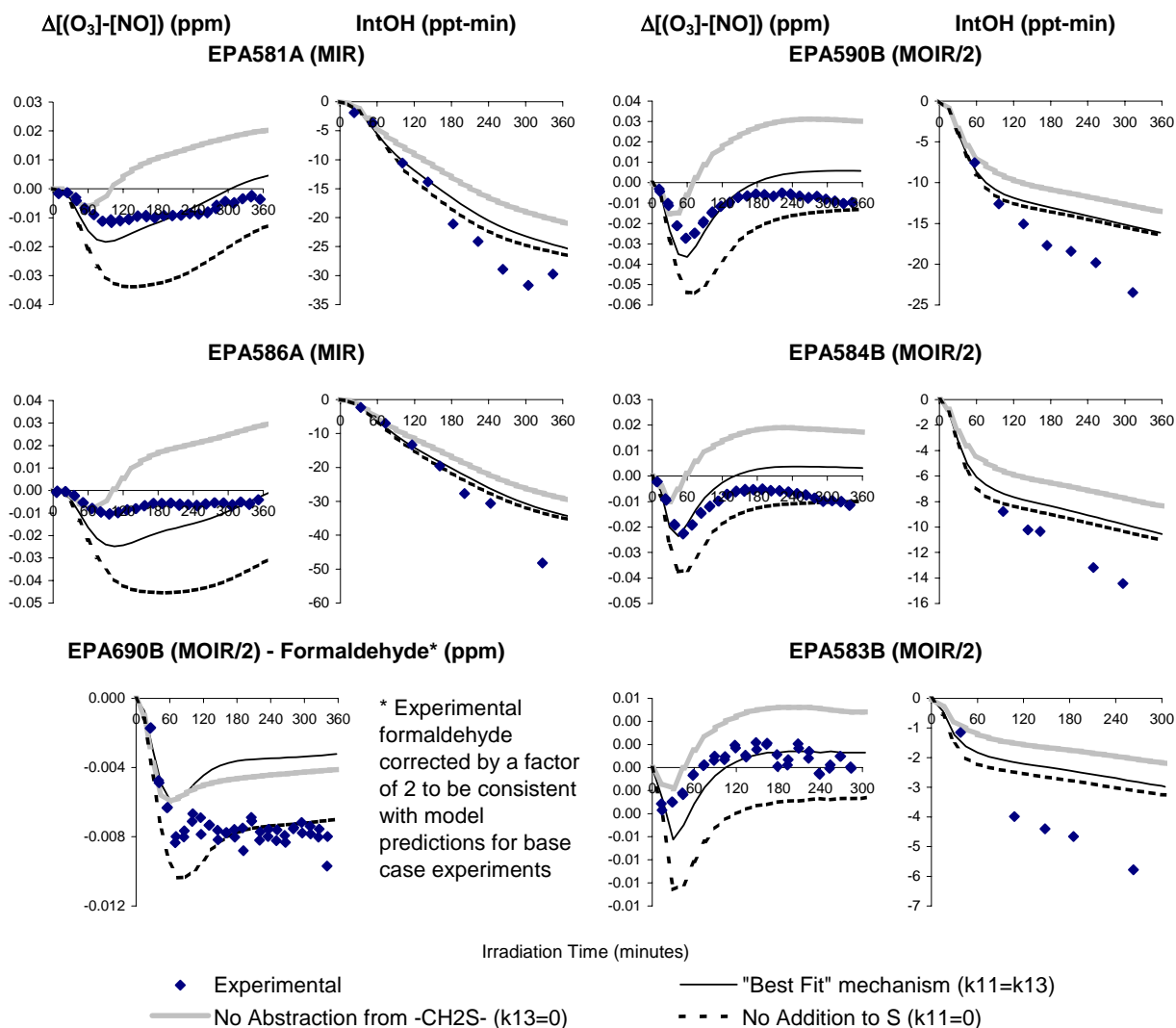
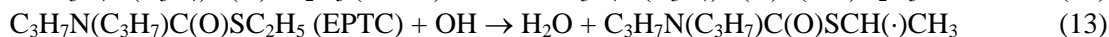
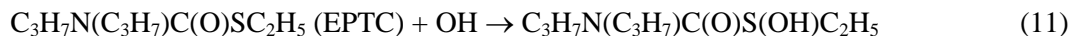


Figure 17. Experimental and calculated concentration-time plots for changes in  $\Delta([O_3]-[NO])$ , IntOH and (where experimental data available) formaldehyde for the incremental reactivity experiments with EPTC

As discussed above, the product data of Kwok et al (1992) are sufficient only to account for approximately 60% of OH + EPTC, and it is uncertain the extent to which the reactions,



account for the remaining ~40%. Results of calculations based on alternative assumptions concerning the relative importances of these two reactions in accounting for the ~40% of the overall reaction are shown on Figure 17. It can be seen that the model simulations are sensitive to what is assumed in this regard, with calculations assuming that Reaction (11) dominates tending to cause  $\Delta([O_3]-[NO])$  reactivity to be overpredicted, while assuming that Reaction (13) dominates has the opposite effect. Generally satisfactory fits are obtained if it is assumed that these two reactions are equally important, i.e., each

occurs about 20% of the time, and therefore this is referred to as the “best fit” mechanism. This is the mechanism that is used for EPTC in the atmospheric impact calculations discussed later in this report.

Note that the simulations are also sensitive to the overall nitrate yield in the reactions of the peroxy radicals formed when OH abstracts from EPTC, but the best results are obtained if the initially estimated 20% yield is used without further adjustment. This is sufficiently uncertain that it would have been adjusted had such adjustments yielded sufficiently improved fits to the data. The mechanism has other uncertainties, but no alternative assumptions regarding these uncertainties were found to yield better fits to the data than the “best fit” mechanism discussed above.

### 1,3-Dichloropropenes

Plots of selected experimental and calculated results for the various mechanism evaluation experiments for the 1,3-dichloropropenes are shown on Figure 18 through Figure 20, where Figure 18 shows the dichloropropene - NO<sub>x</sub> experiments, Figure 19 shows the dichloropropene - NO<sub>x</sub> experiments with added propane, and Figure 20 shows the incremental reactivity experiments. The initial concentrations of these experiments are given in Table 17 and Table 18, above. Significant O<sub>3</sub> formation was observed in all the dichloropropene - NO<sub>x</sub> and dichloropropene + propane - NO<sub>x</sub> experiments, and the addition of the dichloropropenes caused an increase in O<sub>3</sub> formation and NO oxidation in all the incremental reactivity experiments. The relatively rapid O<sub>3</sub> formation and NO oxidation rates in the dichloropropene - NO<sub>x</sub> experiments shown in Figure 18 indicate that these compounds are relatively reactive and have significant internal radical sources, since otherwise the photooxidation rates would have been much slower even with higher levels of dichloropropenes added. On the other hand, the addition of the dichloropropenes caused a reduction in integrated OH in the incremental reactivity experiments, though the reduction was relatively small. The addition of propane had relatively little effect on O<sub>3</sub> formation (see Table 18 and compare the added propane experiments with run EPA551A, which had similar NO<sub>x</sub> and dichloropropene levels), but propane was consumed at a much greater rate than can be attributed to its reaction with OH radicals (see Figure 19).

The results of the experiments provide clear evidence that chlorine atom formation is occurring to a significant extent in the 1,3-dichloropropene oxidation reactions. Propane reacts relatively rapidly with chlorine atoms, and the relatively rapid consumption of propane shown on Figure 19 can be explained by chlorine atom formation. In addition, the n-octane consumption rates in the incremental reactivity experiments are much greater than can be attributed to the OH reaction, which can also be attributed to chlorine reactions. As discussed above, the n-octane and m-xylene consumption data can be used to estimate integrated chlorine levels (See Equation IV), and the results, shown on Figure 20, indicate measurable integrated chlorine levels in the added dichloropropene experiments. Figure 20 also shows that the integrated chlorine levels in the base case experiments are scattered around zero, as expected given the lack of chlorine atom sources.

The results of the model calculations, also shown on the figures, indicates that the model gives reasonably good fits to most of the data if the chloroacetaldehyde product is represented explicitly. ON In initial calculations we attempted the standard SAPRC-99 approach of representing all the higher aldehyde species by the generic RCHO species, whose mechanism is based on that for propionaldehyde, and the results, shown on Figure 18 and Figure 19 indicated that this gives highly unsatisfactory model performance. In particular, this representation resulted in significant underprediction of reactivity in the dichloropropene - NO<sub>x</sub> and dichloropropene - propane - NO<sub>x</sub> experiments, and significant underprediction of the propane consumption rates in the added propane experiments, indicating that chlorine atom formation is being underpredicted. This indicates that the photolysis of chloroacetaldehyde, forming

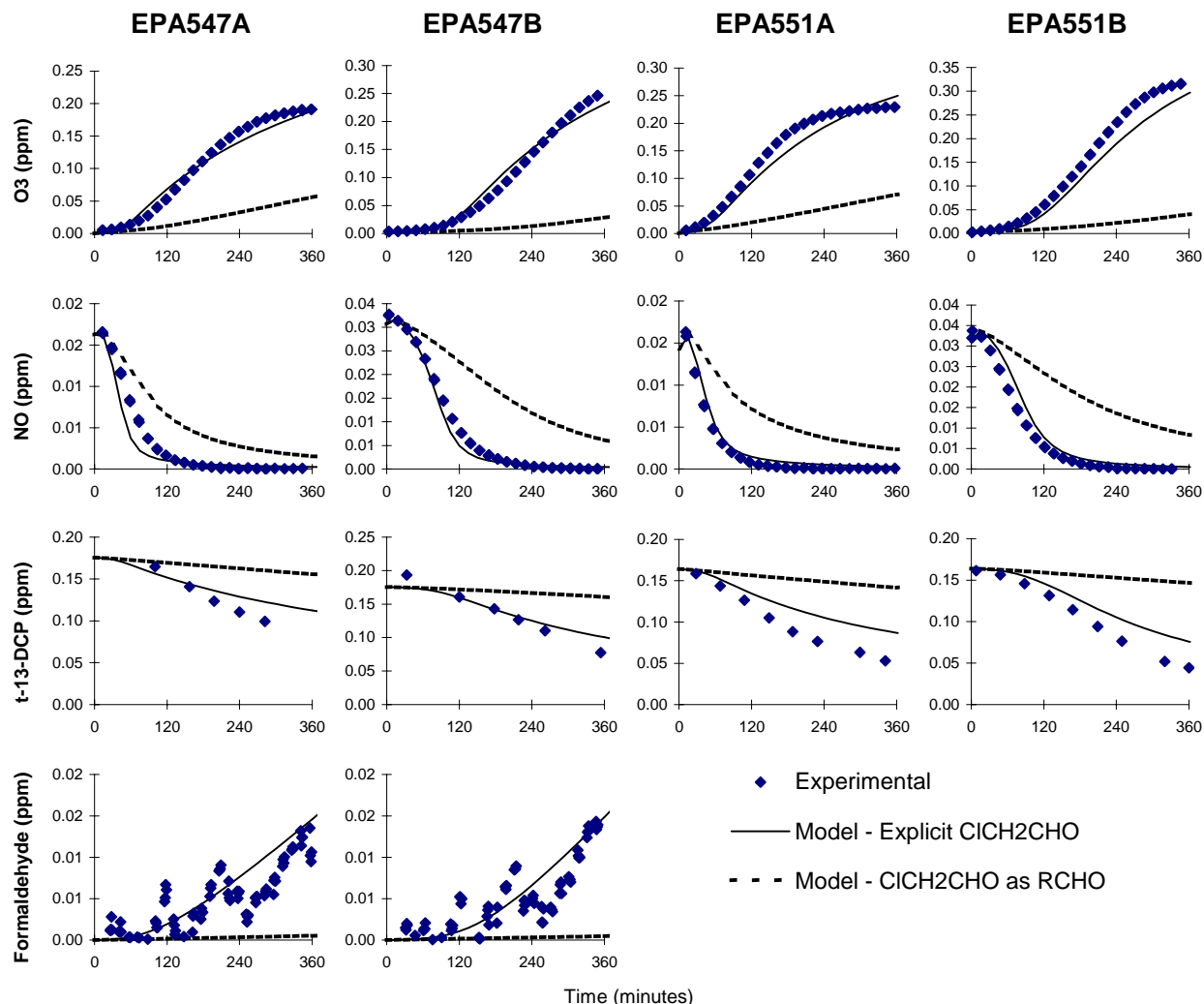


Figure 18. Experimental and calculated concentration-time plots for selected species in the dichloropropene - NO<sub>x</sub> experiments.

chlorine atoms and also other radicals, is a significant process accounting for the reactivity of the 1,3-dichloropropenes.

In order to account for the observed reactivity it was necessary to assume that the chloroacetaldehyde photolyzes with essentially unit quantum yields. This gives an action spectrum resulting in significantly higher photolysis rates than used for RCHO or appropriate for propionaldehyde, as shown on Figure 3, above. Other than this, the mechanism was not adjusted to obtain the fits shown in the figures. However, despite assuming unit quantum yields for chloroacetaldehyde photolysis, the mechanism has a slight tendency to underpredict NO oxidation and O<sub>3</sub> formation rates in a majority (though not all) experiments, and also underpredicts the apparent integrated chlorine levels by about a factor of two. It is possible that the reaction of the dichloropropenes with O<sub>3</sub> could result in higher chlorine yields than assumed in the current mechanism, but the reactions of the dichloropropenes with O<sub>3</sub> is relatively slow, and test calculations assuming 100% chlorine yields do not give significantly different

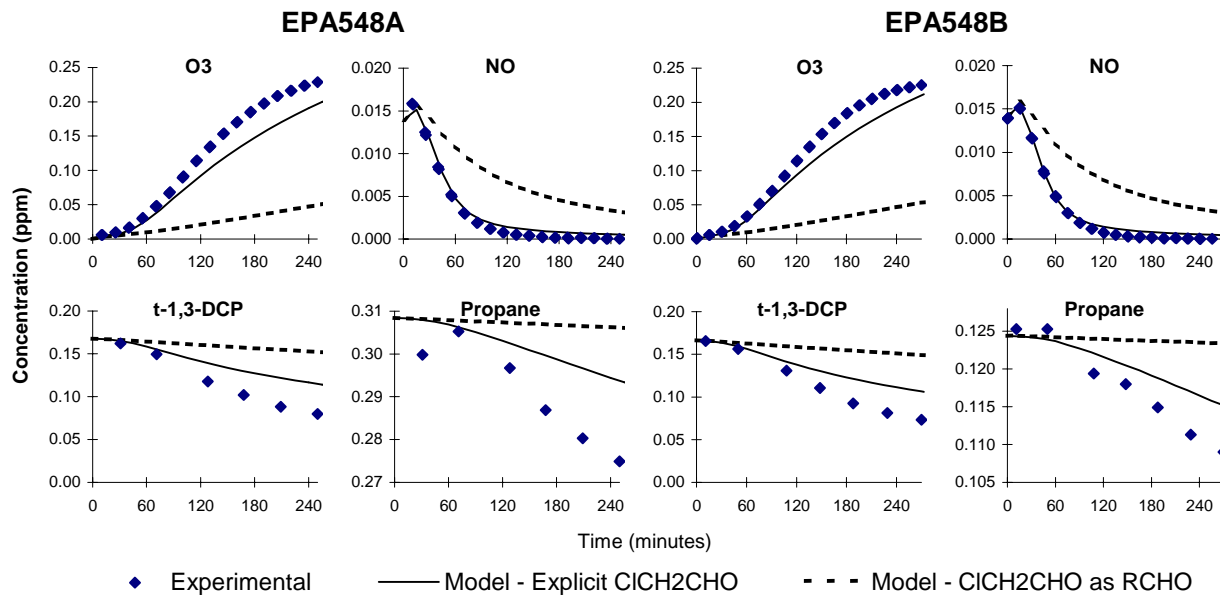


Figure 19. Experimental and calculated concentration-time plots for selected species in the dichloropropene + propane - NO<sub>x</sub> experiments.

predictions than the standard mechanism. Assuming that chlorine atoms are somehow formed in the OH radical reaction actually reduces predictions of reactivity in most of the experiments, and therefore this is unlikely to be the source of the additional apparent reactivity. The photolysis of formyl chloride using the IUPAC (2006)-recommended-absorption cross sections and assuming unit quantum yields has no effect on the calculation because of the low absorption cross sections at atmospherically-relevant wavelengths.

The underprediction of integrated chlorine levels in the incremental reactivity experiments could be attributed to problems with other aspects of the chlorine mechanism or possibly with the assumptions underlying the use of Equation (IV) to predict integrated chlorine. However, as shown in Figure 21 in the following section, the model gives good predictions of integrated chlorine in the incremental reactivity experiments with chloropicrin, which has a much simpler (and therefore less uncertain) mechanism for chlorine formation. This tends to suggest that the chlorine mechanism, and the method used to derive IntCl from the experimental data, may not necessarily have problems. On the other hand, the model also gives good predictions of the integrated OH levels in the higher concentration base case experiments used in the chloropicrin study (Carter et al, 1997a,b), and also predicts O<sub>3</sub> levels in the base case experiments without having to adjust the aromatics mechanism. This is in contrast with the lower concentration base case experiments employed in this study (and the previous coatings study of Carter and Malkina, 2005), where an adjusted aromatics mechanism has to be used, and Integrated OH is consistently underpredicted in the base case experiments. Therefore, the underprediction of integrated Cl in these experiments may be related to problems with the mechanism for the base case experiment. This will need to be revisited when the entire mechanism is updated.

In any case, since we could find no chemically reasonable adjustments to the 1,3-dichloropropene mechanism to improve the performance of the mechanism in simulating the chamber data, so the present mechanism, with its slight tendency towards underprediction in some of the experiments, stands as our current best estimate for predictions of atmospheric reactivity.



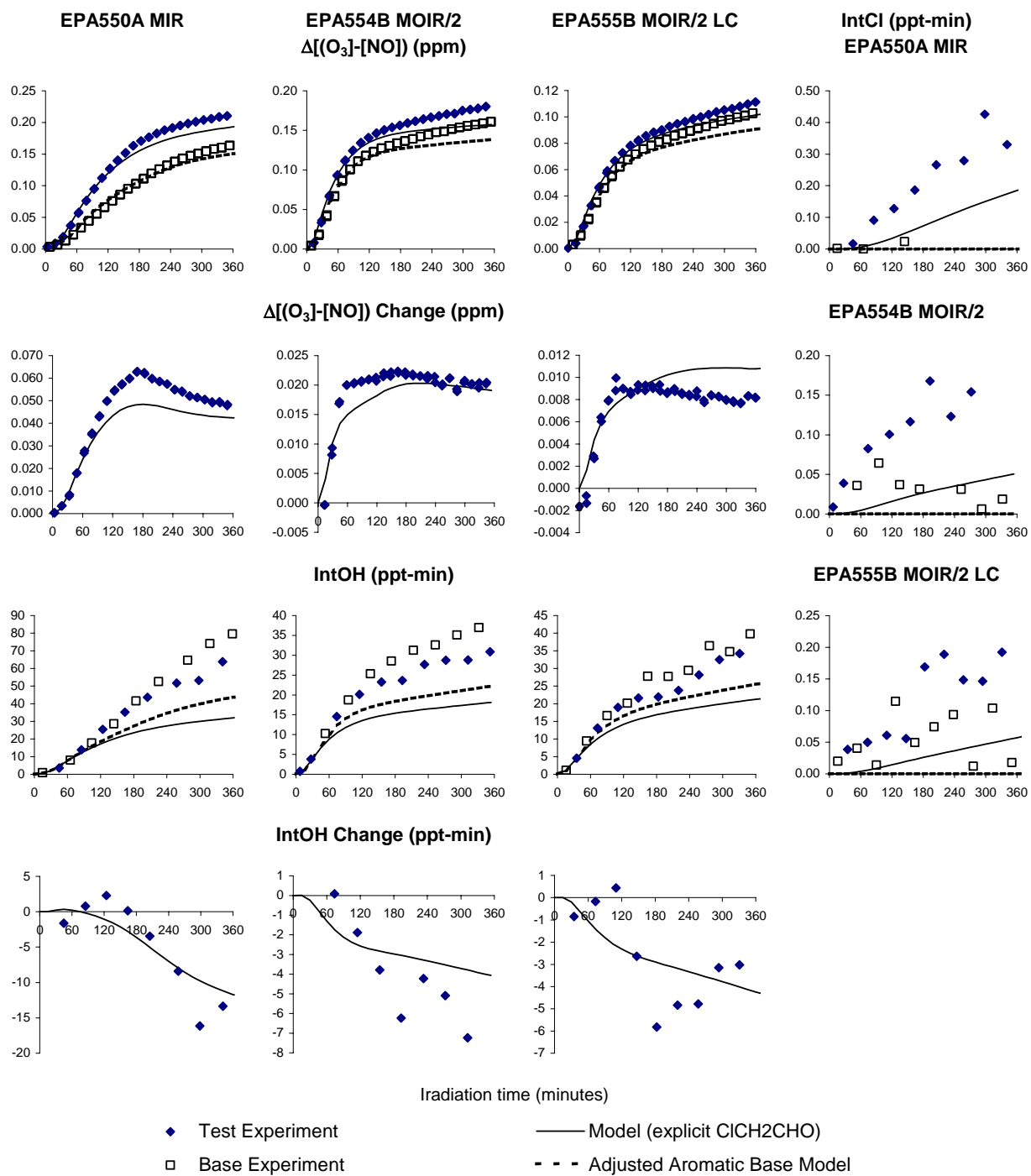


Figure 20. Experimental and calculated concentration-time plots for  $\Delta([O_3]-[NO])$ , IntOH, and IntCl for the incremental reactivity experiments with the dichloropropenes.

## Chloropicrin

As indicated on Table 1 chloropicrin is an important pesticide in California, so estimations of its ozone impact is of relevance to this project. It was not studied experimentally for this project because it was already studied by Carter et al (1997a,b), who also developed a mechanism for this compound that was reasonably consistent with the chamber data obtained. However, the study of Carter et al (1997a,b) used an older version of the SAPRC mechanism that was superseded by SAPRC-99, and an older version of the chlorine mechanism that is superseded by the version given in Appendix A of this report. In addition, since the standard SAPRC-99 mechanism has no representation of chlorine chemistry, the ozone impact of chloropicrin was not calculated using that mechanism, and reactivities of chloropicrin have not been included in the available SAPRC-99 reactivity scales (Carter, 2000a, 2003b).

Therefore, as part of this project, the chloropicrin mechanism is included among the pesticide compound mechanisms given in Table 4, above, and incorporated in the mechanism for atmospheric reactivity calculations. This consists of only a single reaction, representing its photolysis to form  $\text{NO}_2 + \text{CCl}_3\cdot$ , where the latter eventually forms phosgene and Cl atoms after an NO to  $\text{NO}_2$  conversion. The evaluation of this updated mechanism against the results of the chloropicrin chamber experiments of Carter et al (1997a,b) is described in this section.

Carter et al (1997a,b) carried out three types of chloropicrin experiments that are useful for mechanism evaluation. These are (1) chloropicrin -  $\text{NO}_x$  with added ethane or n-butane to evaluate the mechanism in a chemically simple system where an alkane is added to react with the chlorine atoms formed; (2) incremental reactivity experiments with the full surrogate used for this project except at higher reactant concentrations; and (3) incremental reactivity experiments with a three-component “mini-surrogate” of ethene, n-hexane and m-xylene, which tends to be more sensitive to radical initiation effects than the full surrogate. The different types of experiments, and their advantages and disadvantages, are discussed by Carter et al (1997a,b).

Selected experimental and calculated results are shown on Figure 21 and Figure 22, where Figure 21 shows the results for the chloropicrin + propane experiments, and Figure 22 shows the results of the various types of incremental reactivity experiments. Note that in this case the model calculations for the incremental reactivity experiments used the standard SAPRC-99 mechanism for the aromatics in the base ROG mixture, since for these higher concentration experiments the standard mechanism gives better simulations of the base case results than the adjusted aromatics mechanism (Carter, 2000a; Carter and Malkina, 2005). It can be seen that the updated mechanism for chloropicrin and chlorine chemistry gives good simulations of the chloropicrin chamber data, including both the integrated OH and integrated Cl in the incremental reactivity experiments. Therefore the updated mechanism is judged to be suitable for atmospheric reactivity calculations.

## Kerosene

Experimental and calculated  $\Delta([\text{O}_3]-[\text{NO}])$  and IntOH and data for the kerosene incremental reactivity experiments are shown on Figure 23. Like EPTC, the experiments indicate that kerosene has a small but generally slightly negative effect on  $\Delta([\text{O}_3]-[\text{NO}])$  in most of the experiments, and has a strong negative effect on integrated OH radical levels. This result is similar to what is observed for many other higher molecular weight hydrocarbon solvents (e.g., see Carter and Malkina, 2005), and is due to strong radical inhibition effects in the reactions of the higher alkanes, counteracted in part with direct reactivity effects of  $\text{O}_3$  formation from these reactions. The presence of the aromatics may also be contributing to the inhibition of  $\text{O}_3$  in the more  $\text{NO}_x$ -limited MOIR/2 experiments. This is because the reactions of aromatics tend to remove  $\text{NO}_x$  from the system, causing reduced  $\text{O}_3$  formation under conditions where  $\text{O}_3$  is  $\text{NO}_x$ -limited.

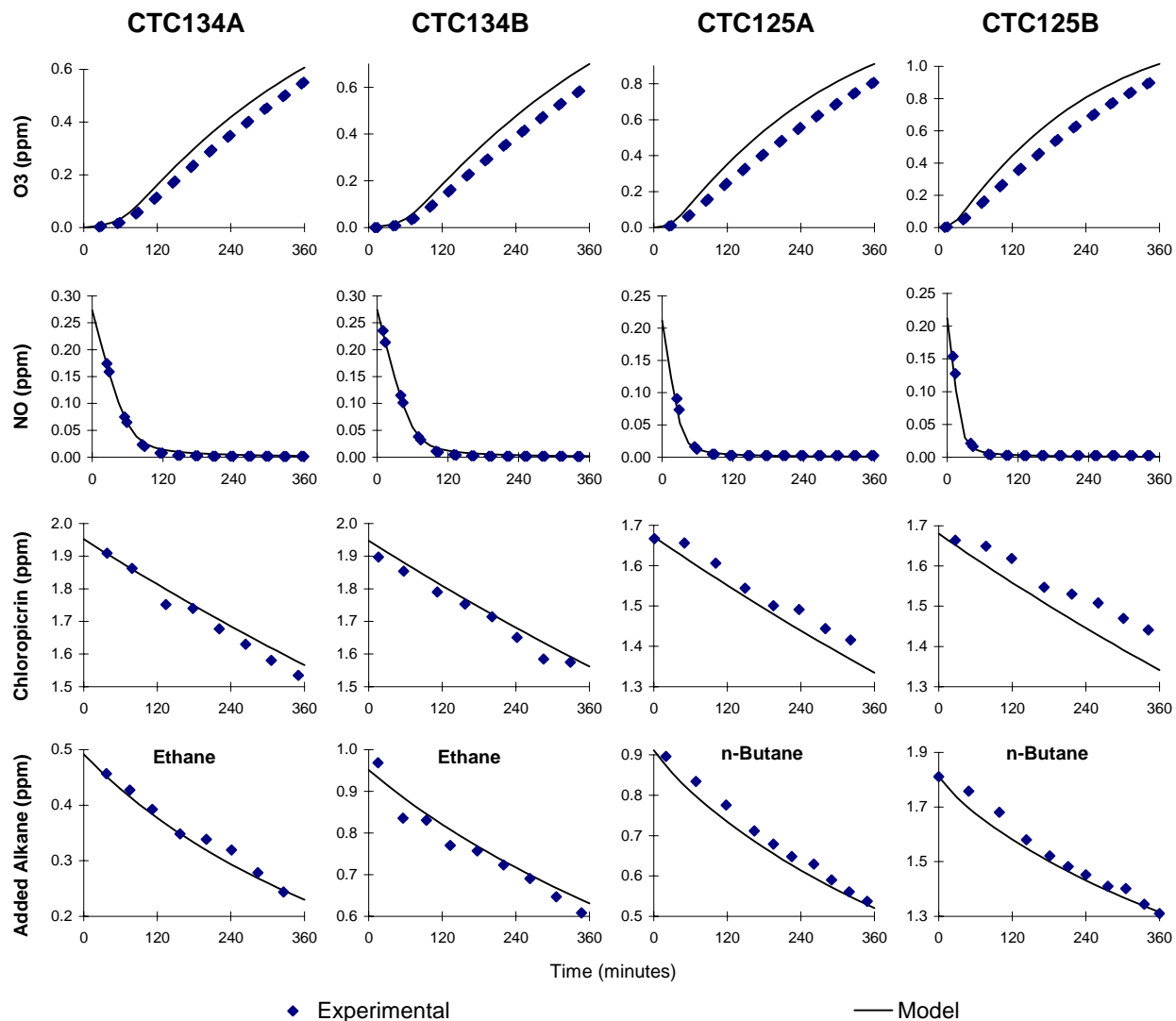


Figure 21. Experimental and calculated concentration-time plots for selected species in the chloropicrin + alkane - NO<sub>x</sub> environmental chamber experiments carried out by Carter et al (1997a,b).

The model calculations shown on Figure 23 indicate that the model performs reasonably well in simulating the reactivity impacts of kerosene addition, though there is a tendency to underpredict the amount of inhibition of IntOH. The latter can be attributed primarily to the underprediction of IntOH in the base case experiments (which is a general characteristic of the SAPRC-99 mechanism, even with aromatics mechanisms adjusted to improve simulations of O<sub>3</sub>), since IntOH is actually simulated quite well in the experiments with added kerosene. Because of this, it is unclear whether modifications to the mechanism or assumed composition would be appropriate to improve the simulations of IntOH reactivities.

One potential problem with the kerosene experiments is the potential for incomplete injection of the less volatile components of the kerosene mixture. Injection tests indicated that the injection times

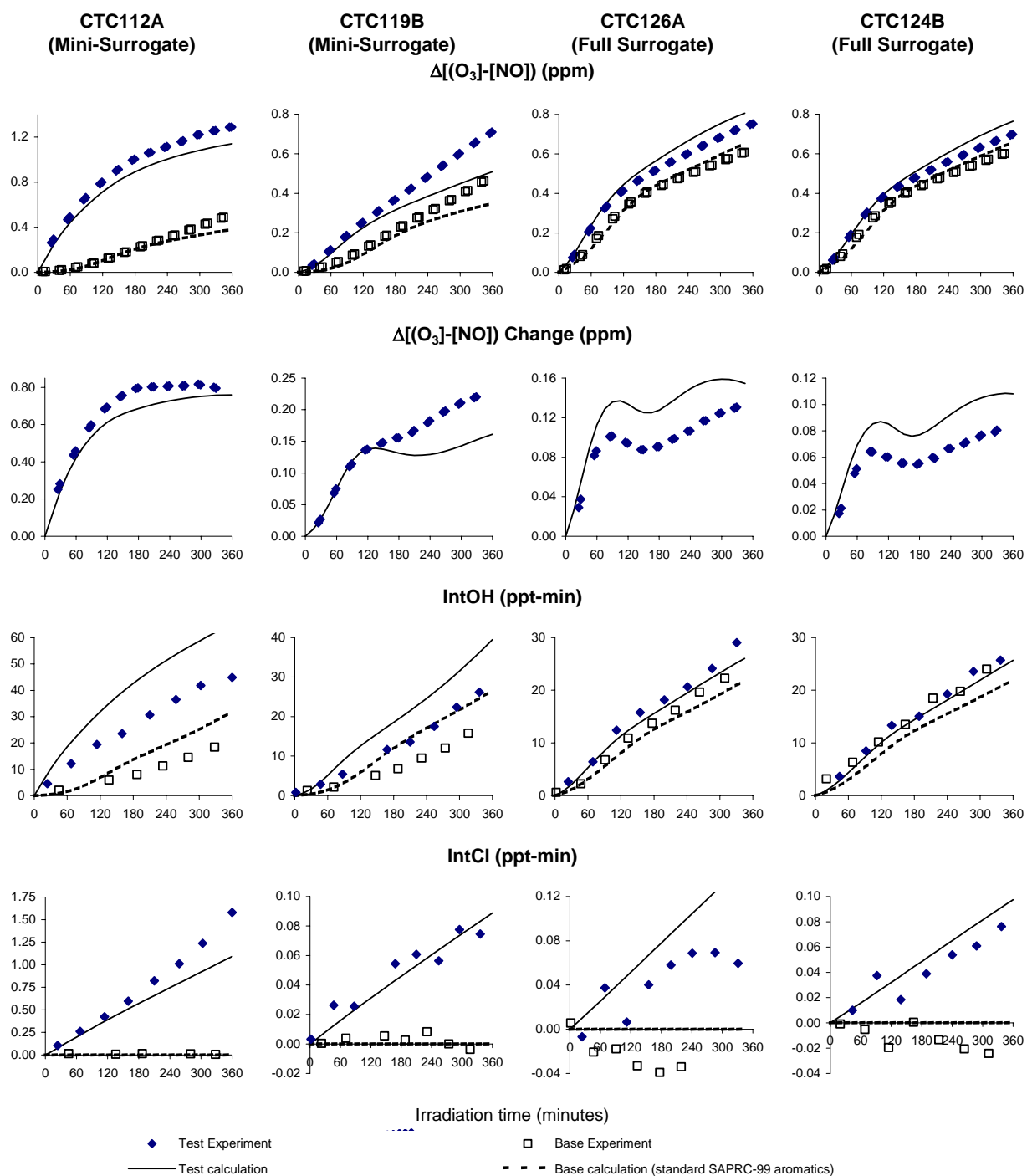


Figure 22. Experimental and calculated concentration-time plots for  $\Delta([O_3]-[NO])$ , Integrated OH, and Integrated Cl in the chloropicrin incremental reactivity environmental chamber experiments carried out by Carter et al (1997a,b).

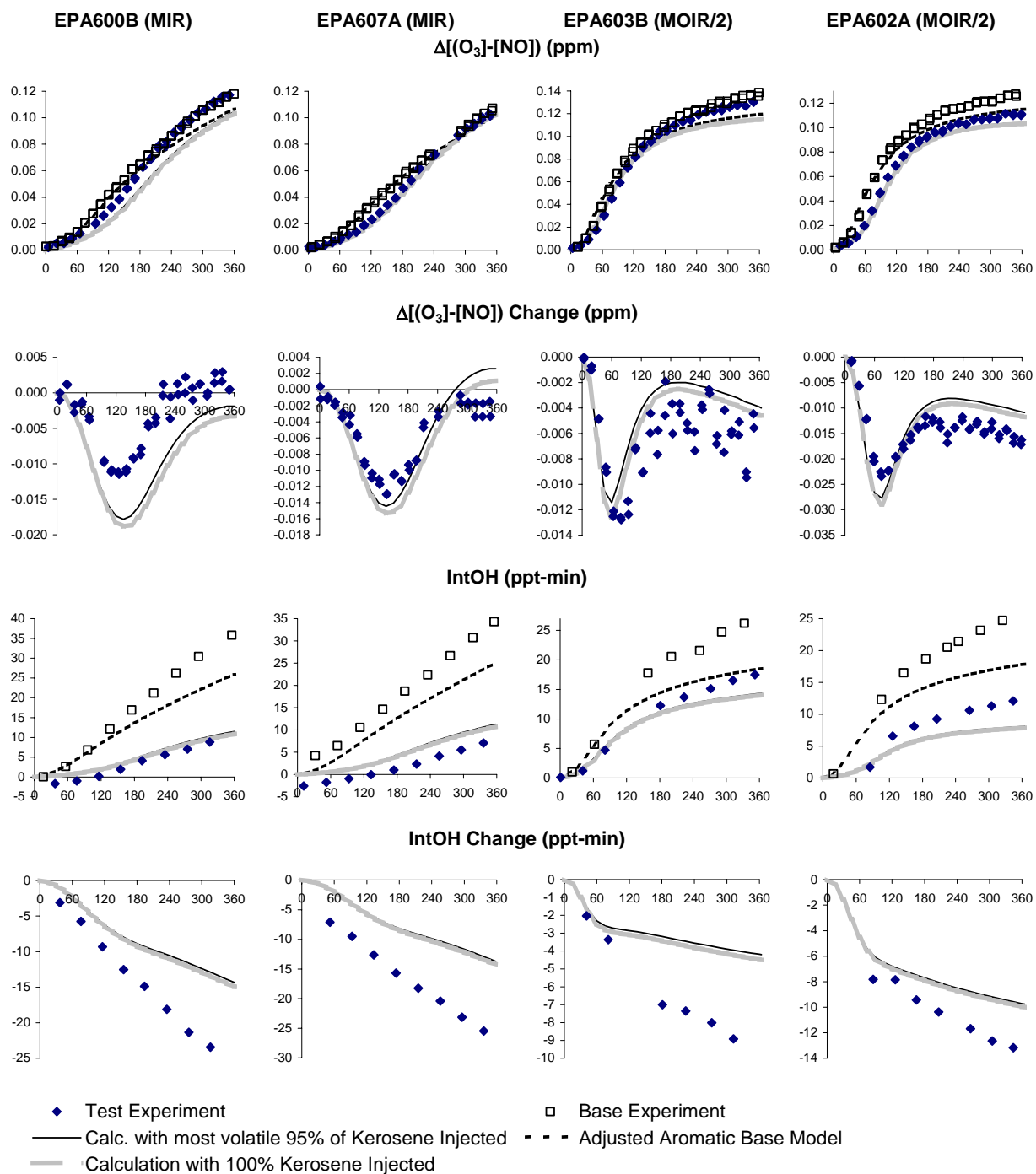


Figure 23. Experimental and calculated concentration-time plots for changes in  $\Delta[\text{O}_3]-[\text{NO}]$  and IntOH for the incremental reactivity experiments with kerosene.

employed in the added kerosene experiments was sufficient to inject an estimated ~95% of the mixture, suggesting that the least volatile ~5% may not be injected. To assess whether this could affect the results of the calculation, Figure 23 shows results of calculations where all the kerosene was assumed to be injected, and where the least volatile 5% of the kerosene mass is removed. [The ordering of volatility was determined by ordering the estimated boiling points, using the carbon number to boiling point relationships used in the hydrocarbon mixture reactivity estimation procedures of Carter and Malkina (2005).] Figure 23 shows that removing this least volatile 5% had very little effect on the reactivity simulations, suggesting that this is not a major factor in using these data for mechanism evaluation.

## PM Impact Results

Selected results of PM number and volume measurements made during the incremental reactivity experiments carried out for this project are summarized on Table 19. (The results are shown for 5 hours for better comparisons among experiments, because not all experiments had data up to 6 hours irradiations.) It can be seen that, contrary to the results of the previous PM measurements reported by Carter et al (2005a) where higher PM levels were consistently formed in reactor side “A” compared to side “B”, consistent results are observed in the base case experiments, regardless of the type of experiment (MIR or MOIR/2) and regardless of reactor side. This is also consistent with the results of the PM background characterization experiments, discussed above, where similar background PM levels are observed in both reactor sides with the current set of reactors, which was installed after the experiments of Carter et al (2005a) were completed. The average 5-hour volume in the base case experiments was  $3.3 \pm 0.9 \mu\text{g}/\text{m}^3$ , which can be compared with the average of  $0.6 \pm 0.3$  for the pure air runs carried out during the period of this project (see Figure 7, above).

The addition of all of the test compounds except for the dichloropropenes was found to cause a significant increase in the PM volume measurements in the experiments. The effect on the PM number depended on the type of compound, with the kerosene having little effect on the PM number, while the sulfur-containing test compounds caused the PM number to approximately double. The addition of the dichloropropenes had negligible effect on PM formation, with the PM number and volume levels in the dichloropropene experiments being essentially the same as in the base case runs. In terms of effect on volume or mass of PM formed relative to the amount added, the relative ordering is kerosene  $\gg$  EPTC  $\approx$  MITC  $>$  CS<sub>2</sub>  $\gg$  1,3-dichloropropenes.

The formation of PM from the sulfur-containing compounds can be attributed, at least in part, to the formation of SO<sub>2</sub>, whose subsequent reaction with OH radicals would ultimately form HSO<sub>4</sub> aerosol. The molar yields of SO<sub>2</sub> from MITC, CS<sub>2</sub>, and EPTC are predicted to be 1, 0.5, and 0.2 in the mechanisms derived for those compounds, as discussed above. The other products predicted to be formed from MITC and CS<sub>2</sub> are not expected to participate in PM formation, so SO<sub>2</sub> is probably the only PM precursor for those compounds. However, it is possible that other products formed in the EPTC formation may also lead to condensable species and PM. In terms of approximate PM formation relative to the moles of compound reacted, the PM yields for CS<sub>2</sub> and EPTC are about half or about the same, respectively as those for MITC. The fact that CS<sub>2</sub> forms about half as much PM on a mole reacted basis as MITC is consistent with the assumption that the SO<sub>2</sub> is the primary PM precursor for those compounds, since the mechanisms predict the yield of SO<sub>2</sub> from CS<sub>2</sub> is about half that as from MITC. However, if SO<sub>2</sub> were the only PM precursor formed from EPTC then this analysis would predict that PM formed from EPTC on a molar basis would be about 20% that from MITC, while in fact about the same amount is formed. This suggests that other compounds formed in the EPTC photooxidation are more important PM precursors than SO<sub>2</sub>.

Table 19. Selected results of PM number and volume measurements made during the incremental reactivity experiments carried out for this project.

Run	Test Side [a]	Type	Added	5-Hour PM Number ( $10^3/\text{m}^3$ )		5-Hour PM Volume ( $\mu\text{g}/\text{m}^3$ )		5 Hr. PM Vol. Incr'l Rct'y [b]
				Test	Base	Test	Base	
<u>Side Equivalency Tests</u>								
549	B	MIR	-	13	13	3.3	3.6	
606	B	MOIR/2	-	12	12	3.0	4.0	
<u>Methyl Isothiocyanate (Measured ppm added)</u>								
587	A	MIR	0.17	18	10	12.5	4.1	18
588	B	MIR	0.72	28	10	27.8	3.6	11
599	A	MOIR/2	0.99	24	9	27.3	3.2	8
589	A	MOIR/2	1.05	20	7	25.2	3.0	7
<u>EPTC (Measured ppm added)</u>								
581	A	MIR	0.08	18	8	9.6	4.1	11
586	A	MIR	0.16	22	14	13.5	5.0	8
583	B	MOIR/2	0.03		10		3.0	
584	B	MOIR/2	0.12	20	10	16.8	3.7	15
590	B	MOIR/2	0.25	21	9	21.2	3.3	9
<u>Carbon Disulfide (Measured ppm added)</u>								
598	A	MIR	0.35	18	6	8.0	1.8	4
591	A	MIR	0.55	19	13	15.1	4.7	7
597	B	MOIR/2	0.63	21	11	14.5	3.3	6
592	B	MOIR/2	0.65					
<u>1,3-Dichloropropenes (Measured ppb added)</u>								
550	A	MIR	104	13	13	3.4	3.5	~0
554	B	MOIR/2	103	13	13	3.5	3.8	~0
555	B	MOIR/2 LC [c]	48	10	10	1.9	1.5	~0
<u>Kerosene (Calculated ppmC added)</u>								
600	B	MIR	1.0	7	8	26.8	1.7	42
607	A	MIR	1.1	12	8	25.7	1.8	36
603	B	MOIR/2	0.5	8	8	17.9	3.9	51
602	A	MOIR/2	1.0	8	8	28.7	2.8	45

[a] This is the reactor where the test compound or mixture was added, except for the side equivalency test experiments, where Side “B” is arbitrarily designated as the “test” side for the purpose of presentation.

[b] PM volume incremental reactivity is in units of  $\mu\text{g}$  PM formed per milligram of VOC added. Calculated as the 5-hour PM volume on the test side minus the average PM volume in the base case experiments ( $3.3 \pm 0.9 \mu\text{g}/\text{m}^3$ ), divided by the amount of  $\text{mg}/\text{m}^3$  test compound added.

[c] This run had lower base case reactant concentrations due to an injection error. See Table 17.

The PM formation observed in the kerosene experiments is significantly higher than the PM formed in the hydrocarbon mixtures studied in the coatings reactivity study, whose PM impacts were relatively modest (Carter et al, 2005). For example, the average 5-hour PM volume reactivity of Aromatic-100 and ASTM-1A, the highest aromatic content hydrocarbon coatings solvents studied by

Carter et al (2005), was only about 5  $\mu\text{g}$  PM per mg VOC injected, or about 12% of the average for kerosene. This can be attributed the fact that this kerosene sample included significant fractions of higher molecular weight compounds, while the coatings solvents tended to be lighter and have less broad carbon number distributions. It is probably the naphthalenes, indans, and tetralins present in the mixture that are particularly important in affecting the PM formation, though the other high molecular weight alkanes and aromatics and alkanes may be contributing to some extent. The compositions assigned to the hydrocarbon mixtures studied in the coatings study included only minor amounts of these bicyclic aromatics (Carter and Malkina, 2005).

## Atmospheric Reactivity Calculations

Calculated atmospheric ozone impacts of the selected pesticide-related compounds and mixtures in the MIR, MOIR, and EBIR incremental reactivity scales are shown in Table 20. This includes all the pesticide-related compounds listed in Table 1 whose mechanisms have already been developed and are already on existing reactivity tabulations (Carter, 2000a, 2003a), and the pesticide-related compounds or mixtures whose mechanisms were developed and evaluated or estimated for this project. The mechanistic uncertainty classifications for the mechanisms used to calculate the reactivities, using the approach adopted previously (Carter, 2000a, 2003a) are also shown. For comparison, Table 20 also gives atmospheric reactivities for the base ROG mixture used to represent reactive organic emissions from all sources in the reactivity modeling scenarios, and of ethane, the compound the EPA has used to define the borderline of negligible reactivity for exemption purposes (Dimitriadis, 1999), and methane, a compound that can be considered as a more conservative borderline for negligible reactivity. As discussed above, the scenarios and methods used were the same as those described previously (Carter, 1994a,b 2000a) and used for the previously reported scales (Carter, 2000a, 2003a). The mechanism is as documented above, with the mechanisms for the test compounds studied in this project in all cases being those that gave the best fits to the chamber data. The compounds are listed in order of descending reactivity in the MIR scale, the scale most commonly used for regulatory applications in California (CARB 1993, 2000). In most cases the ordering in the other scales was similar.

It can be seen that acrolein, the dichloropropenes, and MIBK are the most reactive of the pesticide compounds listed on the table, with calculated ozone impact higher than the base ROG mixture used to represent reactive VOC emissions from all sources. The majority of compounds and mixtures have reactivities between that of the base ROG mixture and ethane, the compound that has been used to define negligible reactivity by the EPA. MITC is the least reactive of the compounds in this group, having ozone impacts only slightly above that of ethane. The non-aromatic thiocarbamates have reactivities in the middle of this range, with pebulate, molinate, and EPTC having very similar reactivities. Thiobencarb has lower reactivities than the other thiocarbamates in part because of its higher molecular weight, but primarily because of its predicted formation of an aromatic aldehyde (represented in the model by the benzaldehyde model species), which the mechanism predicts is an ozone inhibitor. This is also why its reactivity is calculated to decline more rapidly in the lower -  $\text{NO}_x$  MOIR and EBIR scales than is the case for most of the other compounds.

Carbon disulfide is calculated to have a slightly lower reactivity than ethane in all three of the reactivity scales, so it might be considered appropriate for VOC exemption under the standards that has been used by the EPA (Dimitriadis, 1999). However, since  $\text{CS}_2$  is of interest in the pesticide context because it is a by-product, exemption is not relevant in this application, though it may be in others. Note that the uncertainty concerning its photolysis rate is not an important factor affecting predictions of its atmospheric ozone impact. However, the reactivity is very close to ethane and is probably within the uncertainty of the calculation, especially considering the other uncertainties in the  $\text{CS}_2$  mechanism



Table 20. Calculated atmospheric ozone impacts of the selected pesticide-related compounds and mixtures in the MIR, MOIR, and EBIR incremental reactivity scales.

Compound or Mixture	Mass fraction [a]	Incremental Reactivity (gm O <sub>3</sub> / gm VOC)			Unc'y Code [b]	Reactivity Source
		MIR	MOIR	EBIR		
Acrolein	0.7%	7.55	2.76	1.80	3	Carter (2003a)
1,3-Dichloropropenes [c]	11.3%	4.64	1.67	0.98		This work
Trans Isomer (44% of mixture)		5.43	1.89	1.10	3	This work
Cis isomer (56% of mixture)		4.02	1.50	0.89	3	This work
Methylisobutyl ketone (MIBK)	0.8%	4.28	1.81	1.22	2	Carter (2003a)
Base ROG Mixture [d]	-	3.71	1.46	0.85		Carter (2003a)
Glycerine	0.5%	3.26	1.41	0.92	2	Carter (2003a)
Propylene glycol	0.5%	2.74	1.23	0.83	3 [e]	Carter (2003a)
N-Methyl pyrrolidinone	0.5%	2.55	1.23	0.80	2	Carter (2003a)
Chloropicrin	8.6%	2.18	1.09	1.06	2	This work
Pebulate	0.4%	1.84	0.90	0.59	3	This work
S-ethyl N,N-di-n-propyl thiocarbamate (EPTC)	0.5%	1.82	0.92	0.61	2	This work
Kerosene	1.7%	1.71	0.72	0.36	3	This work
Molinate	3.3%	1.68	0.80	0.53	2	This work
Thiobencarb	0.5%	0.72	0.23	0.05	3	This work
MITC (methyl isothiocyanate)	17.8%	0.35	0.22	0.18	2	This work
Ethane [f]	-	0.31	0.20	0.15	1	Carter (2003a)
Carbon disulfide [g,h]	Not Listed	0.25 - 0.28	0.16 - 0.17	0.12 - 0.13	3	This work
Methyl bromide [j]	25.3%	0.017 ≤0.03 [k]	0.010	0.007	6	Carter (2003a)
Methane	-	0.014	0.008	0.006	1	Carter (2003a)

[a] Mass fraction of compound in California pesticide profile. See Table 1.

[b] Uncertainty codes are as follows. Except as indicated, these are taken from Carter (2003a) for compounds whose reactivity is previously calculated, or are assigned for this work.

1. Considered to be relatively uncertain, or some uncertainties but reactivity is not expected to change significantly.
2. Uncertain mechanism may change somewhat if refined, but change is expected to be less than a factor of two.
3. Uncertain and may change if compound is studied (or studied further) or estimation methods are updated. Change in atmospheric reactivity calculations could be as much as a factor of two.
4. Uncertain and is expected to change if compound is studied or estimation methods are updated. It is recommended that uncertainty adjustments be employed in regulatory applications.
5. Non-negligible chance of the estimate being incorrect in significant respects. It is recommended that uncertainty adjustments be employed in regulatory applications.
6. Current mechanism is probably incorrect, but biases in atmospheric reactivity predictions are unknown. Uncertainty adjustments should be employed in regulatory applications.

- [c] The 1,3-dichloropropene mixture employed in this study consisted of 56% of the cis isomer and 44% of the trans isomer, based on analyses after injection into the chamber experiments.
- [d] Mixture used to represent reactive VOC emissions from all sources in the reactivity calculations.
- [e] The uncertainty classification has been increased because of inconsistencies in model predictions of results of recent environmental chamber experiments (Carter et al, 2005a).
- [f] Ethane has been used by the EPA as defining the borderline for “negligible” reactivity for exemption purposes (Dimitriadis, 1999).
- [g] Not on the pesticide profile, but expected to be among the pesticide breakdown products.
- [h] Calculations carried out with the overall quantum yield varied from zero to its upper limit value of 0.012. The lower number shows the results with the zero quantum yield.
- [j] Reactivities of methyl bromide were calculated using a highly approximate “placeholder” mechanism, and are probably too uncertain for most regulatory applications.
- [k] Upper limit MIR (Carter, 2000a, 2003a).

discussed above. Even though methyl bromide has a highly uncertain mechanism, it is clearly less reactive than ethane, even if an upper limit reactivity estimate is used (Carter, 2000a, 2003a). On the other hand, the uncertainty is too great to assess whether it can be considered to be more or less reactive than methane. If this is important, then data would be needed to reduce uncertainties in its mechanism.

Kerosene is a special case among the materials listed in Table 20, being a complex hydrocarbon mixture rather than single compound or mixture of isomers. The CARB had developed a “binning” procedure to estimate MIR values for various hydrocarbon mixtures, depending on its boiling point range and aromatic content (Kwok et al, 2000). Depending its exact boiling point range, kerosene would be either in Bin 15 or Bin 20, whose assigned MIRs are 1.82 and 1.49, respectively. Table 20 indicates that the kerosene sample studied for this project has a calculated MIR of 1.71, which is within that range.

## DISCUSSION AND CONCLUSIONS

This project has been successful in its objective of reducing uncertainties in atmospheric impacts of many types of pesticide-related VOCs used in California, and has resulted in quantitative estimates of ozone impacts of most of the compounds in the California pesticide emissions profile. The major gaps are complex mixtures whose compositions were not specified, or compounds of such low volatility that their availability for participation in gas-phase ozone formation is highly uncertain. There are uncertainties in some of the new ozone impact estimates, as summarized below, and additional data would be useful to reduce these uncertainties. However, for the compounds that were studied experimentally the predictions of the mechanisms developed in this work were sufficiently consistent with the experimental data obtained for this project (or the previous experiments on chloropicrin) that they can be considered a useful basis for estimates of atmospheric ozone impacts. In any case, the level of uncertainty in these estimates is considerably less than would be the case previously, where in most cases quantitative ozone impacts were not available.

Except for kerosene, the compounds studied for this project are representatives of chemical classes whose ozone impacts have not been adequately studied previously. There have been experimental measurements of some of the primary atmospheric rate constants and some limited product data is available in some cases, but in all cases the initially estimated mechanisms did not perform satisfactorily in simulating the chamber data, and adjustments had to be made. In the case of the sulfur-containing compounds the adjustments reflect uncertain aspects of the mechanism where additional study would be useful to reduce uncertainties in the mechanisms, and therefore their predictions of atmospheric ozone impacts. In the case of dichloropropenes, the adjustments reflect the level of detail that is necessary to be included in lumped mechanisms to obtain satisfactory representations of atmospheric reactivities of chlorinated compounds. Although the adjusted mechanisms simulate the data reasonably well, there are some inconsistencies in predictions of some aspects of the data that suggest that further refinements may be appropriate. This is briefly discussed below.

The sulfur-containing compounds studied consisted of methyl isothiocyanate (MITC), carbon disulfide ( $\text{CS}_2$ ), and the representative thiocarbamate S-ethyl N,N-di-n-propyl thiocarbamate (EPTC). In the case of MITC, the expected mechanism predicts the formation of HSO radicals, which can react in the atmosphere either with  $\text{O}_3$ ,  $\text{NO}_2$ , or  $\text{O}_2$ . Although the rate constants for the  $\text{O}_3$  and  $\text{NO}_2$  reactions are known, there is only an upper limit rate constant for the  $\text{O}_2$  reaction, and that upper limit is not low enough to rule out this reaction as the major fate of HSO in the atmosphere. However, the mechanism predictions are consistent with the chamber data only if it is assumed that the reaction occurs with a rate constant near the IUPAC (2006)-recommended upper limit. In effect, these data give a lower limit for this rate constant. It would be useful if there were a direct measurement of this rate constant to put the mechanism developed in this work on a firmer experimental basis.

In the case of carbon disulfide, the mechanism for the atmospheric reactions with OH radicals is highly complex, and despite considerable study (discussed in the IUPAC, 2006 and NASA, 2006 evaluations) the details of the mechanism, and even the overall rate of consumption under atmospheric conditions, has some uncertainty. The rate of atmospheric consumption had to be considered to be at the upper limit of its factor of 2.3 uncertainty to be reasonably consistent with the data, and the best fit mechanism tended to somewhat overpredict the reactivity in the ROG/ $\text{NO}_x$  conditions and underpredict it at higher ROG/ $\text{NO}_x$ . This suggests that the current mechanism may be oversimplifying its atmospheric photooxidation process, at least to some extent. Additional experiments may be useful to reduce the uncertainty in atmospheric ozone impacts predictions, which (based on the discrepancies in the chamber predictions) is probably on the order of  $\pm 50\%$ .

In the case of the representative thiocarbamate EPTC, the existing product data and estimation methods are sufficient to indicate the mechanism for about ~60% of the reaction, but assumptions made concerning the remaining ~40% have significant effects on predicted reactivity. These uncertainties concern the relative importance of addition of OH to the S atom, leading to predicted formation of sulfoxides, or abstraction from the CH<sub>2</sub> next to the S atom, leading to S-centered radicals whose reactions tend to lead to reduced ozone formation. The EPTC reactivity data are best fit if it is assumed that each process has equal importance, and this is used as the basis for estimating mechanisms for the other thiocarbamates on the pesticide list. However, this is a highly indirect determination to serve as a basis for general estimation methods and extrapolations to other molecules. More focused studies and quantitative product yield data on the specific products predicted to be formed in these reactions would be useful in reducing uncertainties for the thiocarbamates for which experimental data are not available.

Despite the clear evidence for chlorine atom involvement in the experiments with the dichloropropenes and need to include chlorine chemistry to model their reactivities, the mechanisms derived for these compounds performed quite well in simulating the chamber data, provided that the chloroacetaldehyde product is represented explicitly and assumed to photolyze with near-unit quantum yield. The model correctly predicts that chlorine atoms play a role in experiments with these compounds, though it somewhat underpredicts integrated chlorine levels derived from rates of consumption of alkane tracer species. The relatively rapid photolysis of chloroacetaldehyde was found to be a major factor affecting the reactivity of these compounds, and is the major source of the chlorine atoms that are clearly present in the system. The standard procedure of using the generic propionaldehyde-based model species to represent all higher saturated aldehydes clearly fails in the case of these chlorinated alkenes, and this may be the case for other halogenated compounds as well. This will need to be taken into account when developing mechanisms for other halogenated compounds.

The mechanism for chloropicrin, developed previously, was updated for this project and was found to give good simulations of the chamber data obtained previously, including overall chlorine levels as indicated by rates of decay of alkane tracers. Chloropicrin has a relatively simple mechanism for chlorine formation, with photolysis forming chlorine atoms in 100% yield being the only significant consumption process, whose rate is well constrained by the available analytical data. The good performance of the mechanism in simulating the chlorine tracer and other data in these experiments therefore not only tends to validate the chloropicrin mechanism, it also lends support to the predictive capability of the overall chlorine mechanism that is presented in Appendix A of this report.

Although no new mechanisms had to be developed to successfully simulate the ozone impacts measured for kerosene, studies with this mixture were useful in extending the range of types of hydrocarbon mixtures for which experimental evaluation data are available. The hydrocarbon mixtures that were previously studied consist primarily of lighter fractions with average carbon numbers of 12 or less, with relatively little contribution of heavier compounds with carbon numbers greater than 13. On the other hand, over 30% of the mass of this kerosene sample had carbon numbers of 14 or greater, of which 5% are aromatics. New procedures, had to be developed to estimate compositions in this higher carbon number range, particularly for aromatics, where contributions by naphthalenes, tetralins, and indans are more important, and the uncertainties in these composition estimation procedures increase with the size of the molecules. With a total aromatic content of almost 18%, the representation of the aromatics is important, and the assumption that the heavier aromatics can be adequately represented by mechanisms of the lighter compounds for which mechanisms were developed is an additional source of uncertainty. Nevertheless, the representation of the composition and mechanisms for this mixture performed as well or better in simulating the chamber data for this mixture as was the case for the lighter hydrocarbon mixtures that were previously studied.

As indicated above, as a result of this project we were able to derive quantitative estimates of the ozone impacts of most of the pesticides in the California pesticide profile in the MIR and other reactivity scales. The results indicate a relatively wide range of ozone impacts of the pesticide compounds, as might be expected considering the wide range of chemicals involved. The most reactive is acrolein, which is about twice as reactive as the base ROG, the mixture of reactive organic gases used to represent emissions from all sources, followed by the 1,3-dichloropropenes and methyl isobutyl ketone, which are also more reactive than this mixture. The least reactive is methyl bromide, which has a highly uncertain mechanism but has an upper limit reactivity below that of ethane, the compound the EPA has used as the borderline for defining negligible reactivity for exemption decisions (Dimitriadis, 1999). Whether it is more or less reactive than methane is uncertain, and would require experimental data to determine. Carbon disulfide may also be somewhat less reactive than ethane (on a mass basis), but the difference between the two is probably within the uncertainty of the CS<sub>2</sub> mechanism. Most of the other pesticides have reactivities between those of ethane and the base ROG.

Except for methyl bromide, whose ozone impact is probably too low to be of major concern, the uncertainty codes for the compounds whose reactivities are given are 3 or less. This classification code refers to compounds whose reactivities are “uncertain and may change if compound is studied (or studied further) or estimation methods are updated. Change in atmospheric reactivity calculations could be as much as a factor of two.” Any mechanisms for the sulfur- or chlorine-containing compounds developed without the data from this project would have been given codes of 5 or worse, where uncertainty adjustments are recommended for regulatory applications.

The pesticide emissions profile includes other complex hydrocarbon mixtures besides kerosene, such as “Aromatic 200”, “Xylene Range Solvent” and “Aliphatic Solvent”. We did not give estimated reactivities for these mixtures because compositional data were not provided. However, the CARB previously developed a “binning” procedure for making MIR assignments for such mixtures (Kwok et al, 2000) which agrees reasonably well with MIRs calculated from detailed compositional data for most categories of hydrocarbons for which such data are available (Carter and Malkina, 2005). The MIR predicted by the bin method for kerosene agreed with the value derived in this study within the range of variability of the method as observed by Carter and Malkina (2005), suggesting that this method is probably appropriate for this type of solvent as well. However, use of detailed compositional data is the preferred method to derive MIRs if such data are available.

Other than these complex mixtures, the only compounds on the California pesticide profile list on Table 1 that do not have reactivity estimates all have estimated vapor pressures of less than ~30 ppb at 25°C. Compounds with such low vapor pressures may not have sufficient volatility to participate in gas-phase reactions. The least volatile of these should probably not be included in VOC emissions profiles at all. However, the semi-volatiles might exist at least to some extent in the gas phase, depending on partitioning and other considerations, and therefore may undergo reaction. However, experimentally studying gas-phase reactions of such compounds would be very difficult in practice, and modeling their atmospheric impacts probably would require appropriate representation of the heterogeneous partitioning processes they probably also undergo. This is beyond the scope of this project, but is an appropriate study for future research.

Although this was not a primary objective of this study, information was also obtained concerning the PM impacts of the representative pesticide materials studied. Kerosene had the greatest PM impact on a mass basis, forming about 5 times more PM on a mass basis than the aromatic-containing hydrocarbon solvents studied for the coatings reactivity project (Carter et al, 2005a). This is consistent with the much higher molecular weight range of the constituents of this mixture. On the other hand, the dichloropropenes had essentially no PM impact, which is also consistent with expectations based on their mechanisms, which predict only high volatility products. Perhaps not surprisingly, all the sulfur-

containing compounds studied had measurable PM impacts, with the impacts of the three being generally comparable. In the case of MITC and CS<sub>2</sub> this can be attributed to the formation of SO<sub>2</sub> in the oxidation mechanisms (which reacts to form non-volatile sulfuric acid), and it is interesting to note that on a mole reacted basis the PM yield from CS<sub>2</sub> was about half that of MITC, consistent with the relative SO<sub>2</sub> yields in the two mechanisms. On the other hand, the SO<sub>2</sub> yield predicted in the EPTC mechanism is not sufficient to account for its PM impact of EPTC on a mole reacted basis, so its photooxidation must involve the formation of other low-volatility products. The other thiocarbamates would probably have comparable PM impacts, but this was not studied.

Finally, it should be noted that the mechanisms for the test compounds are not the only significant source of uncertainty in model predictions of atmospheric ozone impacts. As discussed in previous reports (Carter, 2004, Carter and Malkina, 2005, Carter et al, 2005a), uncertainties in the aromatic photooxidation mechanisms lead to uncertainties in the representation of the base case conditions that would affect predictions of atmospheric reactivity and also complicates the use of incremental reactivity chamber data for mechanism evaluation. We are currently developing an updated version of the SAPRC mechanism, with a major objective of addressing this problem. However, progress to date suggests that at least some of the problems with the aromatics mechanisms may not be resolved in the near term.

Another problem that needs to be addressed is limitations in the environmental chamber database in evaluating certain aspects of the mechanism. Although advances in chamber technology has permitted mechanism evaluation under lower NO<sub>x</sub>, and more atmospherically realistic conditions than previously possible (e.g., Carter, 2004; Carter et al, 2005b), there are still problems with how well current incremental reactivity experiments represent ambient conditions. In particular, some VOCs the magnitude, and even this sign, of the impact of the VOC on ozone formation is different in chamber experiments than in atmospheric simulations. Examples include EPTC and kerosene that was studied for this project, and some of the coatings solvents studied previously (Carter and Malkina, 2005). A modeling analysis indicates that this is due to chamber experiments being much less sensitive to the effects on ozone of the reactions of the VOCs' oxidation products than is calculated to be the case for the atmosphere. This means that an important aspect of the mechanism affecting predictions of ozone in the atmosphere is not being adequately tested, and may not be giving correct predictions in airshed models. This is a particular concern because reactions of products tend to be the most uncertain aspect of the mechanisms of most VOCs, and most mechanisms represent them in a highly simplified manner. This may be applicable to some of the pesticide-related compounds studied for this project, particularly EPTC and kerosene. A project concept to address this has been submitted to the CARB.

## REFERENCES

- Alvarez, R. A. (1993): "Infrared Diode Laser Studies of the Products from the Reaction  $\text{CH}_2(\text{X}_3\text{B}_1) + \text{O}_2$  and from the Near-UV Photolysis of  $\text{CH}_3\text{NCS}$ ," PhD Thesis, University of California, Berkley.
- Alvarez, R. A. and B. Moore (1994): "Quantum Yield for Production of  $\text{CH}_3\text{NC}$  in the Photolysis of  $\text{CH}_3\text{NCS}$ ," *Science*, 263, 205-207.
- Atkinson, R. (1989): "Kinetics and Mechanisms of the Gas-Phase Reactions of the Hydroxyl Radical with Organic Compounds," *J. Phys. Chem. Ref. Data*, Monograph no 1.
- Atkinson, R. (1997): "Gas Phase Tropospheric Chemistry of Volatile Organic Compounds: 1. Alkanes and Alkenes," *J. Phys. Chem. Ref. Data*, 26, 215-290.
- Atkinson, R. and J. Arey (2003): "Atmospheric Degradation of Volatile Organic Compounds," *Chem. Rev.* 103, 4605-
- CARB (1993): "Proposed Regulations for Low-Emission Vehicles and Clean Fuels -- Staff Report and Technical Support Document," California Air Resources Board, Sacramento, CA, August 13, 1990. See also Appendix VIII of "California Exhaust Emission Standards and Test Procedures for 1988 and Subsequent Model Passenger Cars, Light Duty Trucks and Medium Duty Vehicles," as last amended September 22, 1993. Incorporated by reference in Section 1960.
- CARB (2000): "Initial Statement of Reasons for the Proposed Amendments to the Regulation for Reducing Volatile Organic Compound Emissions from Aerosol Coating Products and Proposed Tables of Maximum Incremental Reactivity (MIR) Values, and Proposed Amendments to Method 310, 'Determination of Volatile Organic Compounds in Consumer Products'," California Air Resources Board, Sacramento, CA, May 5.
- Carter, W. P. L. (1994a): "Development of Ozone Reactivity Scales for Volatile Organic Compounds," *J. Air & Waste Manage. Assoc.*, 44, 881-899.
- Carter, W. P. L. (1994b): "Calculation of Reactivity Scales Using an Updated Carbon Bond IV Mechanism," Report Prepared for Systems Applications International Under Funding from the Auto/Oil Air Quality Improvement Research Program, April 12.
- Carter, W. P. L. (2000a): "Documentation of the SAPRC-99 Chemical Mechanism for VOC Reactivity Assessment," Report to the California Air Resources Board, Contracts 92-329 and 95-308, May 8. Available at <http://cert.ucr.edu/~carter/absts.htm#saprc99> and <http://www.cert.ucr.edu/~carter/reactdat.htm>.
- Carter, W. P. L. (2000b): "Implementation of the SAPRC-99 Chemical Mechanism into the Models-3 Framework," Report to the United States Environmental Protection Agency, January 29. Available at <http://www.cert.ucr.edu/~carter/absts.htm#s99mod3>.
- Carter, W. P. L. (2002): "Development of a Next Generation Environmental Chamber Facility for Chemical Mechanism and VOC Reactivity Research," Draft Research Plan and First Progress Report to the United States Environmental Protection Agency Cooperative Agreement CR 827331-01-0, January 3. Available at <http://www.cert.ucr.edu/~carter/epacham>.

- Carter, W. P. L. (2003a): "The SAPRC-99 Chemical Mechanism and Updated VOC Reactivity Scales, Updated and Corrected Data as of February 5, 2003," Available at <http://www.cert.ucr.edu/~carter/reactdat.htm>.
- Carter, W. P. L. (2003b): "Updated Chemical Mechanism for Airshed Model Applications," Research Proposal to the California Air Resources Board, October.
- Carter, W. P. L. (2004): "Evaluation of a Gas-Phase Atmospheric Reaction Mechanism for Low NO<sub>x</sub> Conditions," Final Report to California Air Resources Board Contract No. 01-305, May 5. Available at <http://www.cert.ucr.edu/~carter/absts.htm#Inoxrpt>.
- Carter, W. P. L. (2006): "Current Project Information Page 'Development of an Improved Chemical Speciation Database for Processing Emissions of Volatile Organic Compounds for Air Quality Models,'" <http://www.cert.ucr.edu/~carter/emitdb>. Updated August 12, 2006.
- Carter, W. P. L., R. Atkinson, A. M. Winer, and J. N. Pitts, Jr. (1982): "Experimental Investigation of Chamber-Dependent Radical Sources," *Int. J. Chem. Kinet.*, 14, 1071.
- Carter, W. P. L. and R. Atkinson (1987): "An Experimental Study of Incremental Hydrocarbon Reactivity," *Environ. Sci. Technol.*, 21, 670-679
- Carter, W. P. L. and R. Atkinson (1989): "A Computer Modeling Study of Incremental Hydrocarbon Reactivity", *Environ. Sci. Technol.*, 23, 864.
- Carter, W. P. L., and Lurmann, F. W. (1991) Evaluation of a detailed gas-phase atmospheric reaction mechanism using environmental chamber data. *Atmos. Environ.* 25A:2771-2806.
- Carter, W. P. L., J. A. Pierce, I. L. Malkina, D. Luo and W. D. Long (1993): "Environmental Chamber Studies of Maximum Incremental Reactivities of Volatile Organic Compounds," Report to Coordinating Research Council, Project No. ME-9, California Air Resources Board Contract No. A032-0692; South Coast Air Quality Management District Contract No. C91323, United States Environmental Protection Agency Cooperative Agreement No. CR-814396-01-0, University Corporation for Atmospheric Research Contract No. 59166, and Dow Corning Corporation. April 1. Available at <http://www.cert.ucr.edu/~carter/absts.htm#rct1rept>
- Carter, W. P. L., D. Luo, I. L. Malkina, and J. A. Pierce (1995a): "Environmental Chamber Studies of Atmospheric Reactivities of Volatile Organic Compounds. Effects of Varying ROG Surrogate and NO<sub>x</sub>," Final report to Coordinating Research Council, Inc., Project ME-9, California Air Resources Board, Contract A032-0692, and South Coast Air Quality Management District, Contract C91323. March 24. Available at <http://www.cert.ucr.edu/~carter/absts.htm#rct2rept>.
- Carter, W. P. L., D. Luo, I. L. Malkina, and D. Fitz (1995b): "The University of California, Riverside Environmental Chamber Data Base for Evaluating Oxidant Mechanism. Indoor Chamber Experiments through 1993," Report submitted to the U. S. Environmental Protection Agency, EPA/AREAL, Research Triangle Park, NC., March 20..
- Carter, W. P. L., D. Luo, and I. L. Malkina (1996a): "Investigation of the Atmospheric Ozone Formation Potential of t-Butyl Alcohol, N-Methyl Pyrrolidinone and Propylene Carbonate," Report to ARCO Chemical Corporation, July 8. Available at <http://www.cert.ucr.edu/~carter/absts.htm#arcorpt>



- Carter, W. P. L., D. Luo, and I. L. Malkina (1996b): "Investigation of the Atmospheric Ozone Formation Potential of Trichloroethylene," Report to the Halogenated Solvents Industry Alliance, August. Available at <http://www.cert.ucr.edu/~carter/absts.htm#tcerpt>.
- Carter, W. P. L., D. Luo and I. L. Malkina (1997a): "Investigation of that Atmospheric Reactions of Chloropicrin," *Atmos. Environ.* 31, 1425-1439; See also Report to the Chloropicrin Manufacturers Task Group, May 19. Report available at <http://www.cert.ucr.edu/~carter/absts.htm#clpicrin>.
- Carter, W. P. L., D. Luo and I. L. Malkina (1997b): "Investigation of that Atmospheric Reactions of Chloropicrin," *Atmos. Environ.* 31, 1425-1439.
- Carter, W. P. L., D. Luo, and I. L. Malkina (1997c): "Investigation of the Atmospheric Ozone Formation Potential of Propylene Glycol," Report to Philip Morris, USA, May 2. Available at <http://www.cert.ucr.edu/~carter/absts.htm#pgrept>
- Carter, W. P. L., J. H. Seinfeld, D. R. Fitz and G. S. Tonnesen (1999): "Development of a Next-Generation Environmental Chamber Facility for Chemical Mechanism and VOC Reactivity Evaluation," Research Proposal to the United States Environmental Protection Agency, February 22. (Available at <http://www.cert.ucr.edu/~carter/epacham/proposal.htm>.)
- Carter, W. P. L. and I. L. Malkina (2005): "Evaluation of Atmospheric Impacts of Selected Coatings VOC Emissions," Final report to the California Air Resources Board Contract No. 00-333, March 15. Available at <http://www.cert.ucr.edu/~carter/absts.htm#coatpt>.
- Carter, W. P. L., I. L. Malkina, D. R. Cocker III, and C. Song (2005a): "Environmental Chamber Studies of VOC Species in Architectural Coatings and Mobile Source Emissions," Final Report to the South Coast Air Quality Management District Contract No. 03468, July 5. Available at <http://www.cert.ucr.edu/~carter/absts.htm#scaqcham>.
- Carter, W. P. L., D. R. Cocker III, D. R. Fitz, I. L. Malkina, K. Bumiller, C. G. Sauer, J. T. Pisano, C. Bufalino, and C. Song (2005b): "A New Environmental Chamber for Evaluation of Gas-Phase Chemical Mechanisms and Secondary Aerosol Formation", *Atmos. Environ.* 39 7768-7788.
- Censullo, A., C., D. R. Jones, and M. T. Wills (2002): "Investigation of Low Reactivity Solvents," Final Report for California Air Resources Board Contract 98-310, May 10.
- Cocker, D. R., R. C. Flagan, and J. H. Seinfeld. (2001). "State-of-the-Art Chamber Facility for Studying Atmospheric Aerosol Chemistry," *Environ. Sci. Technol.* 35, 2594-2601.
- Collins D. R., R. C. Flagan, and J. H. Seinfeld (2002). "Improved inversion of scanning DMA data," *Aerosol Science Technology*, 36, 2-9.
- Dimitriades, B. (1999): "Scientific Basis of an Improved EPA Policy on Control of Organic Emissions for Ambient Ozone Reduction," *J. Air & Waste Manage. Assoc.* 49, 831-838
- ExxonMobil (2006): "Analysis of Kerosene". Letter from Steve G. Colgrove, ExxonMobil Process Research Laboratories, P. O. Box 2226, Baton Rouge, LA, 70821, dated September 28, 2006.
- Finlayson-Pitts, B. J. and J. N. Pitts, Jr. (1997): "Tropospheric Air Pollution: Ozone, Airborne Toxics, Polycyclic Aromatic Hydrocarbons, and Particles," *Science*, 276, 1045-1051

- Geddes, J. D., G. C. Miller, and J. E. Taylor, Jr. (1995): "Gas Phase Photolysis of Methyl Isothiocyanate," *Environ. Sci. Technol.* 29, 2590-2594
- Gery, M. W., G. Z. Whitten, J. P. Killus, and M. C. Dodge (1989): "A Photochemical Mechanism for Urban and Regional Scale Computer Modeling," *J. Geophys. Res.*, 94, 12,925.
- Hastie, D. R., Mackay, G. I., Iguchi, T., Ridley, B. A.; and Schiff, H. I. (1983): "Tunable diode laser systems for measuring trace gases in tropospheric air," *Environ. Sci. Technol.* 17, 352A-364A.
- Hynes, A. J., P. H. Wine, and J. M. Nicovitch (1988): "Kinetics and Mechanism for the reaction of OH with CS<sub>2</sub> under Atmospheric Conditions," *J. Phys. Chem.* 92, 3846-2852.
- IUPAC (2006): IUPAC Subcommittee for Gas Kinetic Data Evaluation, data sheets for individual files of reaction data, available at <http://www.iupac-kinetic.ch.cam.ac.uk>. Data sheets accessed through October, 2006.
- Jacobsen, N. W. and R. G. Dickinson (1994): "Spectrometric Assay of Aldehydes as 6-Mercapto-3-substituted-s-triazolo(4,3-b)-s-tetrazines," *Analytical Chemistry* 46/2 (1974) 298-299.
- Jenkin, M. E., S. M. Saunders and M. J. Pilling (1997): "The tropospheric degradation of volatile organic compounds : a protocol for mechanism development," *Atmos. Environ.* 31, 81-104.
- Jenkin, M.E., S.M. Saunders, V. Wagner and M.J. Pilling. (2003): Protocol for the development of the master chemical mechanism MCMv3 (Part B): Tropospheric degradation of aromatic volatile organic compounds," *Atmospheric Chemistry and Physics Discussions*, 2, p1905-1938 (2002). *Atmospheric Chemistry and Physics*, 3, 181-193 (2003)
- Johnson, G. M. (1983): "Factors Affecting Oxidant Formation in Sydney Air," in "The Urban Atmosphere -- Sydney, a Case Study." Eds. J. N. Carras and G. M. Johnson (CSIRO, Melbourne), pp. 393-408.
- Kwok, E. S. C., R. Atkinson, and J. Arey (1992): "Gas-Phase Atmospheric Chemistry of Selected Thiocarbamates," *Environ. Sci. Technol.* 26, 1798-1807.
- Kwok, E. S. C., and R. Atkinson (1995): "Estimation of Hydroxyl Radical Reaction Rate Constants for Gas-Phase Organic Compounds Using a Structure-Reactivity Relationship: An Update," *Atmos. Environ* 29, 1685-1695.
- Kwok, E. S. C., C. Takemoto and A. Chew (2000): "Methods for Estimating Maximum Incremental Reactivity (MIR) of Hydrocarbon Solvents and their Classification," Appendix C to "Initial Statement of Reasons for the Proposed Amendments to the Regulation for Reducing Volatile Organic Compound Emissions from Aerosol Coating Products and Proposed Tables of Maximum Incremental Reactivity (MIR) Values, and Proposed Amendments to Method 310, 'Determination of Volatile Organic Compounds in Consumer Products'," California Air Resources Board, Liu, B. Y. H.; Lee, K. W (1975): "An aerosol generator of high stability," *Am. Ind. Hyg. J.* 1975, 861.
- MCM (2004): The Master Chemical Mechanism website, <http://chmlin9.leeds.ac.uk/MCM/>. Undated. Last accessed 10/2004.

- NASA (2006): "Chemical Kinetics and Photochemical Data for Use in Stratospheric Modeling, Evaluation Number 15," JPL Publication 06-2, Jet Propulsion Laboratory, Pasadena, California, July.
- NIOSH (1994): "Sulfite titration of formaldehyde stock solution: modified Method 3500," NIOSH Manual of Analytical Methods, NMAM, fourth edition, August 15.
- Libuda, H. G., F. Zabel, E. H. Fink, and K. H. Becker (1990): "Formyl chloride: UV absorption cross sections and rate constants for the reactions with chlorine atom and hydroxyl radical," *J. Phys. Chem.*, 94, 5860-5865.
- Peterson, J. T. (1976): "Calculated Actinic Fluxes (290 - 700 nm) for Air Pollution Photochemistry Applications", EPA-600/4-76-025, June.
- Quesenberry, M. S. and Y. C. Lee (1996): "A Rapid Formaldehyde Assay Using Pupalal Reagent: Application under Periodation Conditions," *Analytical Biochemistry*. 234, 50-55.
- Saunders, S.M., M.E. Jenkin, R.G. Derwent and M.J. Pilling (2003): "Protocol for the development of the master chemical mechanism MCMv3 (Part A): Tropospheric degradation of non-aromatic volatile organic compounds," *Atmospheric Chemistry and Physics Discussions*, 2, p1847-1903 (2002). *Atmospheric Chemistry and Physics*, 3, 161-180 (2003)
- Schiff, H. I., Mackay, G. I. and Bechara, J. (1994): "The Use of Tunable Diode Laser Absorption Spectroscopy for Atmospheric Measurements", *Res. Chem. Intermed.* 20, 1994, pp 525-556.
- Scollard, D. J., J. J. Treacy, H. W. Sidebottom, C. Balestra-Garcia, G. Laverdet, G. LeBras, H. MacLeod, and S. Teton (1993): "Rate constants for the reactions of hydroxyl radicals and chlorine atoms with halogenated aldehydes," *J. Phys. Chem.* 97, 4683 - 4688.
- Sommerlade, R, P. Ekici and H. Parlar (2006): "Gas phase reaction of selected isothiocyanates with OH radicals using a smog chamber-mass analyzer system," *Atmos. Environ*, 40, 3306-3315.
- Stockwell, W. R., P. Middleton, J. S. Chang, and X. Tang (1990): "The Second Generation Regional Acid Deposition Model Chemical Mechanism for Regional Air Quality Modeling," *J. Geophys. Res.* 95, 16343- 16376.
- Stockwell, W.R., F. Kirchner, M. Kuhn, and S. Seefeld (1997): "A new mechanism for regional atmospheric chemistry modeling," *J. Geophys. Res.*, 102, 25847-25880.
- Tuazon, E. C., R. Atkinson, A. M. Winer and J. N. Pitts, Jr. (1984): "A study of the atmospheric reactions of 1,3-dichloropropene and other selected organochlorine compounds," *Arch. Environ. Contam. Toxicol.* 13, 691-700.
- Tuazon, E. C., R. Atkinson, S. M. Aschmann, M. A. Goodman and A. M. Winer (1988): "Atmospheric reactions of chloroethenes with the OH radical," *Int. J. Chem. Kinet.* 20, 241-265.
- Wales, P. C. (2002): "Evaluation of Methyl Isothiocyanate as a Toxic Air contaminant. Part A – Environmental Fate", Report to the California Department of Pesticide Regulation, August, 2002. Available at <http://www.cdpr.ca.gov/docs/empm/pubs/mitc/augfinl02/augparta.pdf>.

Wang S. C. and Flagan R. C. (1990): "Scanning Electrical Mobility Spectrometer," *Aerosol Science and Technology*. 13(2): 230-240 1990

Zafonte, L., P. L. Rieger, and J. R. Holmes (1977): "Nitrogen Dioxide Photolysis in the Los Angeles Atmosphere," *Environ. Sci. Technol.* 11, 483-487.

## APPENDIX A. REPRESENTATION OF ATMOSPHERIC CHLORINE REACTIONS

In order to represent the atmospheric reactions of chlorine-containing compounds whose reactions may result in the release of chlorine atoms, it is necessary to include in the mechanism a representation of the reactions of chlorine atoms and the  $\text{ClO}_x$  species they form. Although chlorine chemistry is not part of the standard SAPRC-99 mechanism as documented by Carter (2000a), previous versions of the SAPRC mechanism included chlorine chemistry for the purpose of evaluating mechanisms for trichloroethylene (Carter et al, 1996) and chloropicrin (Carter et al, 1997a,b). However, these mechanisms were developed prior to the development of SAPRC-99 and are therefore somewhat out-of-date.

Therefore, an updated version of atmospheric chlorine chemistry, which was developed as part of our project to update the overall SAPRC mechanism (Carter, 2003), was utilized for modeling the atmospheric reactions of the chlorine-containing pesticides for this project. This mechanism as utilized for this project is documented in this section. Note that the development of the updated SAPRC mechanism is still underway, and portions of the chlorine mechanism, particularly the representation of reactions of Cl with individual VOCs, is subject to change. The final report on the mechanism update project, which is expected around the end of 2006 or early 2007, should be consulted for the final version.

### Mechanism Listing

A list of the model species in the SAPRC-99 mechanism as expanded to represent atmospheric chlorine chemistry is given in Table A-1, with the model species added to represent chlorine reactions underlined. The reactions and kinetic parameters added to the mechanism to represent chlorine chemistry are given in Table A-2, and the absorption cross sections and quantum yields for the added photolysis reactions are given in Table A-3. Footnotes to Table A-2 document the sources of the rate parameters and the mechanisms used, and briefly discuss the applicable assumptions, uncertainties, and other considerations involved in developing the mechanisms for the individual reactions. Note that the other reactions in the mechanism are the same as in the standard SAPRC-99 mechanism as documented by Carter (2000a), so these reactions and their associated documentation are not reproduced here.

Chlorine atoms react rapidly with most reactive VOCs and any complete chlorine mechanism must include a representation of their reactions. This requires knowledge of or ability to estimate the chlorine rate constants for all the VOCs represented in the mechanism, and an ability to estimate or generate mechanisms representing the subsequent reactions that occur. Although we have not yet derived mechanisms for the reactions of chlorine atoms with all types of individual VOCs that can be represented in the current SAPRC-99 mechanism, for the purpose of this project it is necessary to have mechanisms for Cl reactions for all the reactive organic compounds present in the chamber experiments and all the lumped species used to represent the compounds in the base reactive organic gas (ROG) ambient mixture in the atmospheric reactivity simulations. The model species used to represent these compounds are included in the species listing in Table A-1 and their reactions with chlorine atoms are given in Table A-2. [Their other reactions are given with the documentation of the SAPRC-99 mechanism (Carter, 2000a) in the case of the explicitly represented compounds, or in the documentation of the fixed-parameter version of SAPRC-99 (Carter, 2000b) in the case of the lumped model species. The dichloropropenes studied for this project are discussed separately in the main body of this report.] The procedures used to derive these VOC + chlorine reactions and rate constants are discussed further below.

As indicated on Table A-1 and Table A-2, the mechanisms of certain “lumped parameter” model species are derived from mechanisms of mixtures of compounds whose reactions they are designed to

Table A-1. List of model species in the SAPRC-99 mechanism as expanded to represent atmospheric chlorine chemistry. The new model species used to represent chlorine chemistry are underlined.

Type and Name	Description
<u>Species used in Base Mechanism</u>	
<u>Constant Species.</u>	
O2	Oxygen
M	Air
H2O	Water
H2	Hydrogen Molecules
HV	Light
<u>Active Inorganic Species.</u>	
O3	Ozone
NO	Nitric Oxide
NO2	Nitrogen Dioxide
NO3	Nitrate Radical
N2O5	Nitrogen Pentoxide
HONO	Nitrous Acid
HNO3	Nitric Acid
HNO4	Peroxynitric Acid
HO2H	Hydrogen Peroxide
CO	Carbon Monoxide
SO2	Sulfur Dioxide
<u>CL2</u>	Chlorine molecules
<u>CLNO</u>	CINO
<u>CLONO</u>	CIONO
<u>CLNO2</u>	CINO <sub>2</sub>
<u>CLONO2</u>	CIONO <sub>2</sub>
<u>HOCL</u>	HOCl
<u>Active Radical Species and Operators.</u>	
HO.	Hydroxyl Radicals
HO2.	Hydroperoxide Radicals
C-O2.	Methyl Peroxy Radicals
RO2-R.	Peroxy Radical Operator representing NO to NO <sub>2</sub> conversion with HO <sub>2</sub> formation.
R2O2.	Peroxy Radical Operator representing NO to NO <sub>2</sub> conversion without HO <sub>2</sub> formation.
RO2-N.	Peroxy Radical Operator representing NO consumption with organic nitrate formation.
CCO-O2.	Acetyl Peroxy Radicals
RCO-O2.	Peroxy Propionyl and higher peroxy acyl Radicals
BZCO-O2.	Peroxyacyl radical formed from Aromatic Aldehydes
MA-RCO3.	Peroxyacyl radicals formed from methacrolein and other acroleins.
<u>CL.</u>	Chlorine atoms
<u>CLO.</u>	CIO. Radicals
<u>RO2-CL.</u>	Peroxy Radical Operator representing NO to NO <sub>2</sub> conversion with Cl atom formation.
<u>Steady State Radical Species</u>	
O3P	Ground State Oxygen Atoms
O*1D2	Excited Oxygen Atoms
TBU-O.	t-Butoxy Radicals

Table A-1 (continued)

Type and Name	Description
BZ-O.	Phenoxy Radicals
BZNO2-O.	Nitro-substituted Phenoxy Radical
HOCOO.	Radical formed when Formaldehyde reacts with HO <sub>2</sub>
<u>PAN and PAN Analogues</u>	
PAN	Peroxy Acetyl Nitrate
PAN2	PPN and other higher alkyl PAN analogues
PBZN	PAN analogues formed from Aromatic Aldehydes
MA-PAN	PAN analogue formed from Methacrolein
<u>Explicit and Lumped Molecule Reactive Organic Product Species</u>	
HCHO	Formaldehyde
CCHO	Acetaldehyde
RCHO	Lumped C3+ Aldehydes
ACET	Acetone
MEK	Ketones and other non-aldehyde oxygenated products which react with OH radicals faster than $5 \times 10^{-13}$ but slower than $5 \times 10^{-12} \text{ cm}^3 \text{ molec}^{-2} \text{ sec}^{-1}$ .
MEOH	Methanol
COOH	Methyl Hydroperoxide
ROOH	Lumped higher organic hydroperoxides
GLY	Glyoxal
MGLY	Methyl Glyoxal
BACL	Biacetyl
PHEN	Phenol
CRES	Cresols
NPHE	Nitrophenols
BALD	Aromatic aldehydes (e.g., benzaldehyde)
METHACRO	Methacrolein
MVK	Methyl Vinyl Ketone
ISO-PROD	Lumped isoprene product species
<u>Lumped Parameter Products (Mechanisms derived from mixtures as shown on Table A-4)</u>	
PROD2	Ketones and other non-aldehyde oxygenated products that react with OH radicals faster than $5 \times 10^{-12} \text{ cm}^3 \text{ molec}^{-2} \text{ sec}^{-1}$ .
RNO3	Lumped Organic Nitrates
<u>Uncharacterized Reactive Aromatic Ring Fragmentation Products</u>	
DCB1	Reactive Aromatic Fragmentation Products that do not undergo significant photodecomposition to radicals.
DCB2	Reactive Aromatic Fragmentation Products which photolyze with alpha-dicarbonyl-like action spectrum.
DCB3	Reactive Aromatic Fragmentation Products which photolyze with acrolein action spectrum.
<u>Non-Reacting Species</u>	
CO2	Carbon Dioxide
XC	Lost Carbon
XN	Lost Nitrogen
SULF	Sulfates (SO <sub>3</sub> or H <sub>2</sub> SO <sub>4</sub> )
<u>Low Reactivity Compounds or Unknown Products Represented as Unreactive</u>	
H2	Hydrogen
HCOOH	Formic Acid

Table A-1 (continued)

Type and Name	Description
CCO-OH	Acetic Acid
RCO-OH	Higher organic acids
CCO-OOH	Peroxy Acetic Acid
RCO-OOH	Higher organic peroxy acids
<u>HCL</u>	Hydrochloric acid
<u>CLCHO</u>	Formyl Chloride (assumed to be unreactive)
NROG	Unspecified Unreactive Carbon
<u>Species used in Lumped Mechanisms for Base Case and Ambient Simulations</u>	
<u>Primary Organics Represented explicitly</u>	
METHANE	Methane
ETHENE	Ethene
ISOPRENE	Isoprene [a]
<u>Lumped Parameter Species</u> (Mechanisms derived from mixtures as shown on Table A-4) (Used in ambient simulations only)	
ALK1	Alkanes and other non-aromatic compounds that react only with OH, and have kOH between $2 \text{ and } 5 \times 10^2 \text{ ppm-1 min-1}$ . (Primarily ethane)
ALK2	Alkanes and other non-aromatic compounds that react only with OH, and have kOH between $5 \times 10^2 \text{ and } 2.5 \times 10^3 \text{ ppm-1 min-1}$ . (Primarily propane and acetylene)
ALK3	Alkanes and other non-aromatic compounds that react only with OH, and have kOH between $2.5 \times 10^3 \text{ and } 5 \times 10^3 \text{ ppm-1 min-1}$ .
ALK4	Alkanes and other non-aromatic compounds that react only with OH, and have kOH between $5 \times 10^3 \text{ and } 1 \times 10^4 \text{ ppm-1 min-1}$ .
ALK5	Alkanes and other non-aromatic compounds that react only with OH, and have kOH greater than $1 \times 10^4 \text{ ppm-1 min-1}$ .
ARO1	Aromatics with $kOH < 2 \times 10^4 \text{ ppm-1 min-1}$ .
ARO2	Aromatics with $kOH > 2 \times 10^4 \text{ ppm-1 min-1}$ .
OLE1	Alkenes (other than ethene) with $kOH < 7 \times 10^4 \text{ ppm-1 min-1}$ .
OLE2	Alkenes with $kOH > 7 \times 10^4 \text{ ppm-1 min-1}$ .
TERP	Terpenes [a]
<u>VOC compounds in chamber experiments</u> (Used in chamber simulations only)	
ETHANE	Ethane
PROPANE	Propane
N-C4	N-Butane
N-C6	N-Hexane
N-C8	N-Octane
PROPENE	Propene
T-2-BUTE	Trans-2-Butene
TOLUENE	Toluene
M-XYLENE	M-Xylene

[a] Reactions of these biogenic species with chlorine atoms are not represented in the current version of the mechanism because they are unimportant in the simulations discussed here. They will be added in the final version of the updated mechanism, which is in preparation.



Table A-2. Reactions added to the SAPRC-99 mechanism to represent atmospheric chlorine chemistry.

Label	Reaction and Products [a]	Rate Parameters [b]				Notes [c]	
		k(298)	A	Ea	B		
<u>Base Chlorine Mechanism</u>							
Cl01	CL2 + HV = #2 CL.		Phot Set= CL2				1
	CL. + O2 + M = CLO2. + M (ignored)	1.44e-33	1.40e-33	0.00	-3.90		1,2,3
	CLO2. + M = CL. + O2 + M (ignored)	6.23e-13	2.80e-10	3.62			1,3
Cl04	CL. + NO + M = CLNO + M	7.69e-32	7.60e-32	0.00	-1.80		4
Cl05	CLNO + HV = CL. + NO		Phot Set= CLNO-06				1
Cl06	CL. + NO2 = CLONO	1.63e-11	Falloff, F=0.60				4
		0:	1.30e-30	0.00	-2.00		
		inf:	1.00e-10	0.00	-1.00		
Cl07	CL. + NO2 = CLNO2	3.59e-12	Falloff, F=0.60				4
		0:	1.80e-31	0.00	-2.00		
		inf:	1.00e-10	0.00	-1.00		
Cl08	CLONO + HV = CL. + NO2		Phot Set= CLONO				1
Cl09	CLNO2 + HV = CL. + NO2		Phot Set= CLNO2				1
Cl10	CL. + HO2. = HCL + O2	3.46e-11	3.44e-11	0.00	-0.56		1,5
Cl11	CL. + HO2. = CLO. + HO.	9.28e-12	9.41e-12	0.00	2.10		1,5
Cl12	CL. + O3 = CLO. + O2	1.21e-11	2.80e-11	0.50			1
Cl13	CL. + NO3 = CLO. + NO2	2.40e-11					1
Cl14	CLO. + NO = CL. + NO2	1.67e-11	6.20e-12	-0.59			1
Cl15	CLO. + NO2 = CLONO2	2.41e-12	Falloff, F=0.33				1,6
		0:	1.53e-31	0.00	-3.30		
		inf:	7.45e-11	0.00	-0.50		
Cl16	CLONO2 + HV = CLO. + NO2		Phot Set= CLONO2-1				1
Cl17	CLONO2 + HV = CL. + NO3		Phot Set= CLONO2-2				1
Cl18	CLONO2 = CLO. + NO2	3.19e-4	Falloff, F=0.17				7
		0:	4.01e-5	24.90	-0.50		
		inf:	3.87e+16	24.90	5.00		
Cl19	CL. + CLONO2 = CL2 + NO3	1.01e-11	6.20e-12	-0.29			1
Cl20	CLO. + HO2. = HOCL + O2	6.89e-12	2.20e-12	-0.68			1
Cl21	HOCL + HV = HO. + CL.		Phot Set= HOCL-06				1
Cl22	CLO. + CLO. = #.29 CL2 + #1.42 CL. + O2	1.74e-14	1.25e-11	3.89			1,8
Cl23	HO. + HCL = H2O + CL.	7.86e-13	1.70e-12	0.46			1
Cl24	CL. + H2 = HCL + HO2.	1.68e-14	3.90e-11	4.59			1
<u>Chlorine reactions with common organic products</u>							
Cl25	CL. + HCHO = HCL + HO2. + CO	7.32e-11	8.10e-11	0.06			1
Cl26	CL. + CCHO = HCL + CCO-O2.	8.00e-11	8.00e-11				1
Cl27	CL. + MEOH = HCL + HCHO + HO2.	5.50e-11	5.50e-11	0.00			1

Table A-2 (continued)

Label	Reaction and Products [a]	Rate Parameters [b]				Notes [c]
		k(298)	A	Ea	B	
CI28	CL. + RCHO = HCL + #.9 RCO-O2. + #.1 {CCHO + CO + HO2. + R2O2.}	1.23e-10				9
CI29	CL. + ACET = HCL + R2O2. + HCHO + CCO-O2.	2.69e-12	7.70e-11	1.99		4
CI32	CL. + MEK = HCL + #.84 RO2-R. + #.039 RO2-N. + #.136 R2O2. + #.085 CCO-O2. + #.036 RCO-O2. + #.065 HCHO + #.07 CCHO + #.84 RCHO + #.761 XC	3.60e-11				1,10
CI33	CL. + RNO3 = HCL + #.197 NO2 + #.009 HO2. + #.593 RO2-R. + #.202 RO2-N. + #.689 R2O2. + #.045 HCHO + #.3 CCHO + #.029 RCHO + #.003 ACET + #.059 MEK + #.058 PROD2 + #.602 RNO3 + #.527 XC + #.202 XN	1.83e-10				10,11
CI34	CL. + PROD2 = HCL + #.184 HO2. + #.671 RO2-R. + #.116 RO2-N. + #.008 R2O2. + #.007 CCO-O2. + #.022 RCO-O2. + #.237 HCHO + #.109 CCHO + #.789 RCHO + #.051 MEK + #.157 PROD2 + #2.259 XC	1.89e-10				10,11
CI35	CL. + GLY = HCL + #.63 HO2. + #1.26 CO + #.37 RCO-O2. + #-.37 XC	7.32e-11	8.10e-11	0.06		12
CI36	CL. + MGLY = HCL + CO + CCO-O2.	8.00e-11				12
CI37	CL. + CRES = HCL + BALD + RO2-R.	6.20e-11				13
CI38	CL. + BALD = HCL + BZCO-O2.	8.00e-11				14
<u>Chlorine reactions with compounds present in chamber experiments</u>						
c1Cl	CL. + METHANE = HCL + HCHO + RO2-R.	9.95e-14	7.30e-12	2.54		1
c2Cl	CL. + ETHANE = HCL + CCHO + RO2-R.	5.93e-11	8.30e-11	0.20		1
c3Cl	CL. + PROPANE = HCL + #.97 RO2-R. + #.03 RO2-N. + #.482 RCHO + #.488 ACET + #-.09 XC	1.37e-10	1.20e-10	-0.08		10,15
c4Cl	CL. + N-C4 = HCL + #.923 RO2-R. + #.077 RO2-N. + #.495 R2O2. + #.481 CCHO + #.313 RCHO + #.37 MEK + #.16 XC	2.05e-10				1,10
c6Cl	CL. + N-C6 = HCL + #.78 RO2-R. + #.22 RO2-N. + #.811 R2O2. + #.009 CCHO + #.215 RCHO + #.585 PROD2 + #.51 XC	3.40e-10				10,15
c8Cl	CL. + N-C8 = HCL + #.648 RO2-R. + #.352 RO2-N. + #.801 R2O2. + #.088 RCHO + #.561 PROD2 + #2.263 XC	4.60e-10				10,15
etCl	CL. + ETHENE = HCHO + CLCHO + R2O2. + RO2-R.	1.06e-10	Falloff, F=0.60			4
		0:	1.60e-29	0.00	-3.30	
		inf:	3.10e-10	0.00	-1.00	

Table A-2 (continued)

Label	Reaction and Products [a]	Rate Parameters [b]				Notes [c]
		k(298)	A	Ea	B	
prCl	CL. + PROPENE = #.124 HCL + #.971 RO2-R. + #.029 RO2-N. + #.306 RCHO + #.124 METHACRO + #.54 INERT + #.869 XC	2.67e-10				16,17
tbCl	CL. + T-2-BUTE = #.199 HCL + #.921 RO2-R. + #.077 RO2-N. + #.002 R2O2. + #.002 C-O2. + #.737 MEK + #.104 MVK + #.082 ISO-PROD + #.0.238 XC	3.55e-10				16,17
tlCl	CL. + TOLUENE = HCL + BALD + RO2-R.	6.20e-11				18,19
xyCl	CL. + M-XYLENE = HCL + BALD + RO2-R. + XC	1.35e-10				18,19
<u>Chlorine reactions with lumped VOC species in reactivity simulations</u>						
CIL1	CL. + ALK1 = HCL + RO2-R. + CCHO	5.93e-11	8.30e-11	0.20		20
CIL2	CL. + ALK2 = HCL + #.97 RO2-R. + #.03 RO2-N. + #.482 RCHO + #.488 ACET + #.0.09 XC	1.37e-10	1.20e-10	-0.08		10,21
CIL3	CL. + ALK3 = HCL + #.836 RO2-R. + #.07 RO2-N. + #.526 R2O2. + #.094 TBU-O. + #.078 HCHO + #.341 CCHO + #.343 RCHO + #.075 ACET + #.253 MEK	1.87e-10				10,22
CIL4	CL. + ALK4 = HCL + #.831 RO2-R. + #.161 RO2-N. + #.913 R2O2. + #.004 C-O2. + #.004 CCO-O2. + #.002 CO + #.036 HCHO + #.297 CCHO + #.421 RCHO + #.256 ACET + #.078 MEK + #.114 PROD2	2.99e-10				10,22
CIL5	CL. + ALK5 = HCL + #.652 RO2-R. + #.348 RO2-N. + #.887 R2O2. + #.021 HCHO + #.074 CCHO + #.25 RCHO + #.041 ACET + #.038 MEK + #.392 PROD2	3.90e-10				10,22
CIL6	CL. + OLE1 = #.408 HCL + #.864 RO2-R. + #.136 RO2-N. + #.802 R2O2. + #.039 HCHO + #.225 CCHO + #.259 RCHO + #.318 PROD2 + #.223 METHACRO + #.021 MVK + #.042 ISO-PROD + #.0.18 XC	3.97e-10				23,24
CIL7	CL. + OLE2 = #.33 HCL + #.287 RO2-R. + #.134 RO2-N. + #.1.347 R2O2. + #.002 C-O2. + #.577 CL. + #.078 HCHO + #.687 CCHO + #.577 RCHO + #.052 MVK + #.237 ISO-PROD + #.0.381 XC	3.84e-10				23,24
CIL8	CL. + ARO1 = HCL + RO2-R. + #.75 BALD + #.25 PROD2 + #.25 XC	9.52e-11				18,23
CIL9	CL. + ARO2 = HCL + BALD + RO2-R. + #2 XC	1.69e-10				18,23

Table A-2 (continued)

Label	Reaction and Products [a]	Rate Parameters [b]				Notes [c]
		k(298)	A	Ea	B	
<u>Reactions of Peroxy Radical Operator used to represent Cl formation from secondary organic reactions</u>						
Cl39	RO2-CL. + NO = NO2 + CL.	Same k as rxn RRNO				25
Cl40	RO2-CL. + HO2. = ROOH + O2 + #-3 XC	Same k as rxn RRH2				25
Cl41	RO2-CL. + NO3 = NO2 + O2 + CL.	Same k as rxn RRME				25
Cl42	RO2-CL. + C-O2. = #.5 {CL. + HO2.} + #.75 HCHO + #.25 MEOH	Same k as rxn RRN3				25
Cl43	RO2-CL. + RO2-R. = #.5 {CL. + HO2.}	Same k as rxn RRR2				25
Cl44	RO2-CL. + R2O2. = RO2-CL.	Same k as rxn RRR2				25
Cl45	RO2-CL. + RO2-N. = #.5 {CL. + HO2. + MEK + PROD2} + O2 + XC	Same k as rxn RRR2				25

[a] Format of reaction listing: “=” separates reactants from products; “#*number*” indicates stoichiometric coefficient, “#*coefficient* { *product list* }” means that the stoichiometric coefficient is applied to all the products listed.

[b] Except as indicated, the rate constants are given by  $k(T) = A \cdot (T/300)^B \cdot e^{-E_a/RT}$ , where the units of k and A are  $\text{cm}^3 \text{molec}^{-1} \text{s}^{-1}$ ,  $E_a$  are  $\text{kcal mol}^{-1}$ , T is  $^{\circ}\text{K}$ , and  $R=0.0019872 \text{ kcal mol}^{-1} \text{deg}^{-1}$ . The following special rate constant expressions are used:

Phot Set = *name*: The absorption cross sections and quantum yields for the photolysis reaction are given in Table A-5, where “*name*” indicates the photolysis set used. If a “*qy=number*” notation is given, the number given is the overall quantum yield, which is assumed to be wavelength independent.

Falloff: The rate constant as a function of temperature and pressure is calculated using  $k(T,M) = \{k_0(T) \cdot [M] / [1 + k_0(T) \cdot [M] / k_{\text{inf}}(T)]\} \cdot F^Z$ , where  $Z = \{1 + [\log_{10}\{k_0(T) \cdot [M] / k_{\text{inf}}(T)\}]^2\}^{-1}$ , [M] is the total pressure in  $\text{molecules cm}^{-3}$ , F is as indicated on the table, and the temperature dependences of  $k_0$  and  $k_{\text{inf}}$  are as indicated on the table.

Same K as Rxn RRxx: Uses the same rate constant as the reaction in the base SAPRC-99 mechanism with the same label. In this case, it is the corresponding reaction of the model species RO2-R.

[c] Footnotes documenting sources of rate constants and mechanisms are as follows.

- 1 IUPAC (2006) recommendation as of October, 2006. See data sheets at <http://www.iupac-kinetic.ch.cam.ac.uk>.
- 2 Expression given is for  $M=\text{N}_2$ ; IUPAC (2006) gives a slightly different expression for  $M=\text{O}_2$ .
- 3 Reaction is rapidly reversed and can be ignored.
- 4 NASA (2006) Evaluation.
- 5 IUPAC (2006) gives a recommendation for the total  $\text{CL} + \text{HO}_2$  rate constant and for the temperature dependence of the rate constant ratio. Temperature-dependent parameters derived to give best fits to the recommended temperature dependence expression for the temperature range 270-330 K.
- 6 The values of the falloff parameters were adjusted to correspond to the format used in the modeling software, i.e., to remove the  $0.75 - 1.27 \log(F)$  term used in the IUPAC parameterization. Also, F is temperature-independent in this parameterization. The change in calculated rate constants are less than 1% for atmospherically relevant conditions.
- 7 No information could be found concerning the kinetics of this reaction. The temperature- and pressure-dependence expression for the rate constant was estimated from that for the reverse

Table A-2 (continued)

- reaction and the equilibrium constant obtained from the thermochemical data given by NASA (2006) for 298K. The falloff parameters were derived by fitting the falloff expression to the data as a function of temperature and pressure.
- 8 This reaction is not important under most atmospheric conditions, but may be non-negligible under certain situations near Cl<sub>2</sub> emissions sources. The reaction can form either Cl<sub>2</sub> + O<sub>2</sub>, Cl + ClOO, or Cl + OCIO. To avoid introducing new species into the mechanism for this relatively unimportant reaction, OCIO is represented by Cl. ClOO is also represented by Cl because it is expected to rapidly decompose to Cl. The rate expression for the total reaction is derived by fitting an Arrhenius expression to the sum of the temperature-dependent rate constants recommended by IUPAC (2006). The relative product yields are the IUPAC (2006) recommended values for 298K; the temperature dependence of the relative product yields is ignored.
  - 9 Rate constant is average of values listed by Le Crane et al (2005), who also obtained data indicating that abstraction from -CHO occurs ~88% of the time. The rest of the reaction is assumed to occur at the CH<sub>2</sub> group, resulting in ultimate formation of the corresponding alkoxy radical, which is estimated to decompose primarily to acetaldehyde and HCO (Carter, 2000a).
  - 10 Mechanism estimated using the SAPRC-99 mechanism generation system (Carter, 2000a), with rates of initial reactions determined by estimated rates of Cl reactions at various positions. Total rate constant also estimated, unless another footnote indicates otherwise.
  - 11 Mechanism derived using the mixture of organic nitrate compounds used to derive the other mechanistic parameters for the RNO<sub>3</sub> or PROD2 model species. See SAPRC-99 documentation (Carter, 2000a). The mixtures of compounds used, and their Cl atom rate constants, are given in Table A-4.
  - 12 Same rate constant as used for formaldehyde (for glyoxal) or acetaldehyde (for methyl glyoxal). Same mechanism as for OH reaction, except HCl formed.
  - 13 Assumed to have same rate constant as used for toluene, which is average of values tabulated by Wang et al (2005). Mechanism based on assuming reaction only involves abstraction from CH<sub>3</sub>.
  - 14 Same rate constant as used for acetaldehyde. Reaction is assumed to proceed only by abstraction from -CHO.
  - 15 Rate constant from Atkinson (1997) recommendation.
  - 16 Rate constant is average of values tabulated by Wang et al (2002). Value of Wang et al (2002) placed on an absolute basis using the Atkinson (1997)-recommended rate constant for n-heptane.
  - 17 Mechanism used is derived using the SAPRC-99 mechanism generation system (Carter, 2000a), with estimated branching ratios for those reactions whose branching ratios could not be estimated using the methods in the system.
  - 18 Reaction assumed to proceed entirely by abstraction from alkyl group. Benzaldehyde (BALD) assumed to result from reaction at a methyl group, and aromatic ketones, represented by PROD2, assumed to result from reactions at other positions. Fraction of products based on distribution of compounds used to derive the total rate constant.
  - 19 Rate constant average of values tabulated by Wang et al (2005).
  - 20 Rate constant and mechanism based on ethane.
  - 21 Mechanism based on that for propane.
  - 22 Mechanism derived using the mixture of compounds represented by ALK1-5 in the base ROG mixture used in the atmospheric reactivity calculations (Carter, 1994, 2000a). This is the same as used to drive the default parameters in the "fixed parameter" version of SAPRC-99 (Carter, 2000b). The mixtures of compounds used, and their Cl rate constants, are given in Table A-4.

Table A-2 (continued)

- 23 Rate constant is weighed average of those measured or estimated for the mixture of compounds represented by this model species in the base ROG mixture used in the atmospheric reactivity calculations (see Note 22).
- 24 Mechanism used is that derived for 1-pentene (OLE1) or 2-pentenenes (OLE2) using the SAPRC-99 mechanism generation system (Carter, 2000a), with estimated branching ratios for those reactions whose branching ratios could not be estimated. These are taken as representative of the mixture of compounds represented by these lumped species.

Table A-3. Absorption cross sections and quantum yields for the photolysis reactions used in the representation of atmospheric chlorine chemistry.

Phot Set = CL2		Phot Set = CLNO-06				Phot Set = CLNO2		Phot Set = CLONO	
Wl.	Abs.	Wl.	Abs.	Wl.	Abs.	Wl.	Abs.	Wl.	Abs.
280	2.60e-20	280	1.06e-19	348	1.49e-19	280	2.20e-19	280	1.32e-18
290	6.20e-20	282	1.02e-19	350	1.45e-19	290	1.73e-19	285	1.44e-18
300	1.19e-19	284	9.99e-20	355	1.36e-19	300	1.49e-19	290	1.44e-18
310	1.85e-19	286	9.84e-20	360	1.29e-19	310	1.21e-19	295	1.42e-18
320	2.37e-19	288	9.71e-20	365	1.20e-19	320	8.87e-20	300	1.29e-18
330	2.55e-19	290	9.64e-20	370	1.10e-19	330	5.84e-20	305	1.14e-18
340	2.35e-19	292	9.63e-20	375	9.95e-20	340	3.54e-20	310	1.05e-18
350	1.88e-19	294	9.69e-20	380	8.86e-20	350	2.04e-20	315	9.81e-19
360	1.32e-19	296	9.71e-20	385	7.82e-20	360	1.15e-20	320	8.03e-19
370	8.40e-20	298	9.89e-20	390	6.86e-20	370	6.90e-21	325	7.54e-19
380	5.00e-20	300	1.00e-19	395	5.97e-20	380	-	330	5.87e-19
390	2.90e-20	302	1.03e-19	400	5.13e-20			335	5.77e-19
400	1.80e-20	304	1.05e-19	405	4.40e-20			340	4.37e-19
410	1.30e-20	306	1.08e-19	410	3.83e-20			345	3.57e-19
420	9.60e-21	308	1.11e-19	415	3.38e-20			350	2.69e-19
430	7.30e-21	310	1.15e-19	420	2.89e-20			355	2.29e-19
440	5.40e-21	312	1.19e-19	425	2.45e-20			360	1.61e-19
450	3.80e-21	314	1.22e-19	430	2.21e-20			365	1.13e-19
460	2.60e-21	316	1.25e-19	435	2.20e-20			370	9.00e-20
470	1.60e-21	318	1.30e-19	440	2.20e-20			375	6.90e-20
480	-	320	1.34e-19	445	2.07e-20			380	4.10e-20
		322	1.36e-19	450	1.87e-20			385	3.30e-20
		324	1.40e-19	455	1.79e-20			390	2.20e-20
		326	1.43e-19	460	1.95e-20			395	1.50e-20
		328	1.46e-19	465	2.25e-20			400	6.00e-21
		330	1.47e-19	470	2.50e-20			405	-
		332	1.49e-19	475	2.61e-20				
		334	1.51e-19	480	2.53e-20				
		336	1.53e-19	485	2.33e-20				
		338	1.53e-19	490	2.07e-20				
		340	1.52e-19	495	1.78e-20				
		342	1.53e-19	500	1.50e-20				
		344	1.51e-19	527	-				
		346	1.51e-19						

Wavelengths in nm and absorption cross sections in  $\text{cm}^{-2}$ . If no quantum yields are given then unit quantum yields are assumed for all wavelengths.

Table A-3 (continued)

Phot Set = HOCL-06				Phot Sets = CLONO2-1 and CLONO2-2			
Wl.	Abs.	Wl.	Abs.	Wl.	Abs.	QY-1	QY-2
280	4.64e-20	352	1.33e-20	280	1.19e-19	0.400	0.600
282	4.62e-20	354	1.24e-20	285	8.80e-20	0.400	0.600
284	4.68e-20	356	1.17e-20	290	6.41e-20	0.400	0.600
286	4.79e-20	358	1.11e-20	295	4.38e-20	0.400	0.600
288	4.95e-20	360	1.06e-20	300	3.13e-20	0.400	0.600
290	5.13e-20	362	1.02e-20	305	2.24e-20	0.400	0.600
292	5.33e-20	364	9.85e-21	310	1.60e-20	0.386	0.614
294	5.52e-20	366	9.51e-21	315	1.14e-20	0.350	0.650
296	5.71e-20	368	9.19e-21	320	8.31e-21	0.314	0.686
298	5.86e-20	370	8.88e-21	325	6.13e-21	0.279	0.721
300	5.99e-20	372	8.55e-21	330	4.66e-21	0.243	0.757
302	6.08e-20	374	8.22e-21	335	3.67e-21	0.207	0.793
304	6.12e-20	376	7.86e-21	340	3.02e-21	0.171	0.829
306	6.12e-20	378	7.48e-21	345	2.58e-21	0.136	0.864
308	6.07e-20	380	7.08e-21	350	2.29e-21	0.100	0.900
310	5.97e-20	382	6.67e-21	355	2.08e-21	0.064	0.936
312	5.84e-20	384	6.24e-21	360	2.00e-21	0.029	0.971
314	5.66e-20	386	5.80e-21	365	1.80e-21	-	1.000
316	5.45e-20	388	5.35e-21	370	1.59e-21	-	1.000
318	5.21e-20	390	4.91e-21	375	1.41e-21	-	1.000
320	4.95e-20	392	4.47e-21	380	1.21e-21	-	1.000
322	4.67e-20	394	4.05e-21	385	1.37e-21	-	1.000
324	4.38e-20	396	3.64e-21	390	9.10e-22	-	1.000
326	4.09e-20	398	3.25e-21	395	7.60e-22	-	1.000
328	3.79e-20	400	2.88e-21	400	6.40e-22	-	1.000
330	3.50e-20	402	2.54e-21	405	5.40e-22	-	1.000
332	3.21e-20	404	2.22e-21	410	4.40e-22	-	1.000
334	2.94e-20	406	1.94e-21	415	3.60e-22	-	1.000
336	2.68e-20	408	1.68e-21	420	3.20e-22	-	1.000
338	2.44e-20	410	1.44e-21	425	2.30e-22	-	1.000
340	2.22e-20	412	1.24e-21	430	1.90e-22	-	1.000
342	2.03e-20	414	1.05e-21	435	-	-	1.000
344	1.84e-20	416	8.90e-22				
346	1.69e-20	418	7.50e-22				
348	1.55e-20	420	6.30e-22				
350	1.43e-20	422	-				

Wavelengths in nm and absorption cross sections in  $\text{cm}^2$ . If no quantum yields are given then unit quantum yields are assumed for all wavelengths.

Table A-4. List of compounds used to derive mechanistic parameters for the reactions of Cl atoms with lumped parameter species in the SAPRC-99 mechanism.

Group and Compound [a]	Mole Fract.	k(Cl) (cm <sup>3</sup> molec <sup>-1</sup> s <sup>-1</sup> )	Group and Compound	Mole Fract.	k(Cl) (cm <sup>3</sup> molec <sup>-1</sup> s <sup>-1</sup> )
<u>ALK1</u>			<u>ALK5</u>		
<u>Ethane</u>	100%	5.93e-11	2,4-Dimethyl Hexane	11%	4.80e-10
			n-Decane	10%	4.60e-10
<u>ALK2</u>			3-Methyl Hexane	10%	3.50e-10
<u>Propane</u>	59%	1.37e-10	n-Heptane	7%	3.50e-10
Acetylene	41%	(not used)	2,3-Dimethyl Pentane	6%	1.95e-10
			2-Methyl Heptane	6%	3.07e-10
<u>ALK3</u>			4-Methyl Heptane	6%	2.91e-10
n-Butane	68%	2.05e-10	2,4-Dimethyl Heptane	5%	3.40e-10
Isobutane	30%	1.43e-10	Methylcyclohexane	4%	3.26e-10
2,2-Dimethyl Butane	2%	2.20e-10	2,6-Dimethyl Octane	4%	2.81e-10
			n-Nonane	4%	3.82e-10
<u>ALK4</u>			n-Octane	4%	3.84e-10
Iso-Pentane	45%	2.80e-10	Cyclohexane	4%	3.98e-10
n-Pentane	18%	2.90e-10	2-Methyl Nonane	3%	4.56e-10
2-Methyl Pentane	11%	2.80e-10	2-Methyl Hexane	3%	4.99e-10
3-Methylpentane	8%	2.90e-10	2-Methyl Octane	2%	4.41e-10
2,4-Dimethyl Pentane	5%	3.40e-10	4-Methyl Octane	2%	4.42e-10
Methylcyclopentane	5%	2.30e-10	n-Dodecane	2%	6.60e-10
n-Hexane	4%	5.50e-10	4-Methyl Nonane	1.3%	5.01e-10
2,3-Dimethyl Butane	3%	3.90e-10	Ethylcyclohexane	1.0%	4.26e-10
Cyclopentane	2%	3.90e-10	n-Undecane	0.9%	6.02e-10
			3,6-Dimethyl Decane	0.9%	5.74e-10
			2,6-Dimethyl Nonane	0.5%	5.15e-10
			3-Methyl Undecane	0.5%	6.17e-10
			5-Methyl Undecane	0.5%	6.17e-10
			3-Methyl Decane	0.2%	5.59e-10
			4-Methyl Decane	0.2%	5.59e-10
			Ethyl Cyclopentane	0.1%	3.67e-10
			n-Tridecane	0.1%	7.18e-10
<u>ARO1</u>			<u>ARO2</u>		
Toluene	75%	6.20e-11	p-Xylene	23%	1.44e-10
n-Propyl Benzene	11%	2.20e-10	o-Xylene	20%	1.40e-10
Ethyl Benzene	10%	1.69e-10	m-Xylene	20%	1.35e-10
s-Butyl Benzene	2%	2.17e-10	1,2,3-Trimethyl Benzene	14%	2.07e-10
Isopropyl Benzene	2%	1.62e-10	1,3,5-Trimethyl Benzene	13%	2.42e-10
Benzene	(not used)		1,2,4-Trimethyl Benzene	9%	2.07e-10

[a] Underlined compounds are taken as representative of the entire group for the purpose of deriving mechanisms. If no compound is underlined, the mechanism for the lumped group was derived by weighted averages of the parameters for the individual compounds.



Table A-4 (continued)

Group and Compound [a]	Mole Fract.	k(Cl)	Group and Compound	Mole Fract.	k(Cl)
<u>OLE1</u>			<u>OLE2</u>		
Propene	29%	2.67e-10	cis-2-Pentene	14%	3.91e-10
1-Hexene	24%	4.44e-10	<u>trans-2-Pentene</u>	14%	3.91e-10
1-Butene	12%	3.39e-10	trans-2-Butene	11%	3.55e-10
<u>1-Pentene</u>	11%	4.05e-10	Isobutene	10%	3.25e-10
1-Heptene	11%	5.02e-10	cis-2-Butene	9%	3.88e-10
1-Nonene	5%	6.19e-10	2-Methyl-1-Butene	8%	3.82e-10
3-Methyl-1-Butene	3%	3.52e-10	1,3-Butadiene	6%	4.90e-10
1-Octene	2%	5.61e-10	2-Methyl-2-Butene	5%	3.23e-10
1-Undecene	2%	7.35e-10	Cis-2-Hexene	5%	4.50e-10
1-Decene	1%	6.77e-10	Trans-2-Hexene	5%	4.50e-10
			Trans-3-Heptene	4%	5.14e-10
			Trans-4-Nonene	2%	6.30e-10
			Trans-4-Octene	2%	5.72e-10
			Trans-5-Undecene	1.7%	7.47e-10
			Trans-2-Heptene	1.7%	5.08e-10
			Cyclohexene	1.6%	4.95e-10
			Trans-4-Decene	0.7%	6.89e-10
			3,4-Diethyl-2-Hexene	0.2%	6.07e-10
<u>RNO3</u>					
Representative C <sub>5</sub> Nitrate	CH <sub>3</sub> CH <sub>2</sub> CH(CH <sub>3</sub> )ONO <sub>2</sub>			16.7%	4.59e-11
Representative C <sub>6</sub> Nitrate	CH <sub>3</sub> CH(OH)CH <sub>2</sub> CH <sub>2</sub> CH <sub>2</sub> ONO <sub>2</sub>			16.7%	1.40e-10
Representative C <sub>7</sub> Nitrate	CH <sub>3</sub> CH <sub>2</sub> CH(CH <sub>3</sub> )CH(CH <sub>3</sub> )ONO <sub>2</sub>			16.7%	1.40e-10
Representative C <sub>8</sub> Nitrate	CH <sub>3</sub> CH <sub>2</sub> CH <sub>2</sub> CH <sub>2</sub> CH <sub>2</sub> CH(ONO <sub>2</sub> )CH <sub>2</sub> OH			16.7%	2.29e-10
Representative C <sub>9</sub> Nitrate	CH <sub>3</sub> CH <sub>2</sub> C(CH <sub>3</sub> )(ONO <sub>2</sub> )CH <sub>2</sub> CH(CH <sub>3</sub> )CH <sub>3</sub>			16.7%	1.64e-10
Representative C <sub>10</sub> Nitrate	CH <sub>3</sub> CH <sub>2</sub> CH <sub>2</sub> CH <sub>2</sub> CH <sub>2</sub> CH <sub>2</sub> CH <sub>2</sub> CH(ONO <sub>2</sub> )CH <sub>2</sub> CH <sub>3</sub>			16.7%	3.79e-10
<u>PROD2</u>					
Representative C <sub>5</sub> Product	CH <sub>3</sub> C(O)CH <sub>2</sub> CH <sub>2</sub> CH <sub>2</sub> OH			20%	1.20e-10
Representative C <sub>6</sub> Product	CH <sub>3</sub> C(O)CH <sub>2</sub> CH(CH <sub>3</sub> )CH <sub>2</sub> OH			20%	1.36e-10
Representative C <sub>7</sub> Product	CH <sub>3</sub> CH <sub>2</sub> C(O)CH <sub>2</sub> CH <sub>2</sub> CH(CH <sub>3</sub> )OH			20%	1.70e-10
Representative C <sub>8</sub> Product	CH <sub>3</sub> CH <sub>2</sub> C(O)CH <sub>2</sub> CH <sub>2</sub> CH(OH)CH <sub>2</sub> CH <sub>3</sub>			20%	2.30e-10
Representative C <sub>9</sub> Product	CH <sub>3</sub> CH <sub>2</sub> CH <sub>2</sub> CH(OH)CH <sub>2</sub> CH <sub>2</sub> C(O)CH <sub>2</sub> CH <sub>3</sub>			20%	2.89e-10

[a] Underlined compounds are taken as representative of the entire group for the purpose of deriving mechanisms. If no compound is underlined, the mechanism for the lumped group was derived by weighted averages of the parameters for the individual compounds.

represent. The compositions of these mixtures used to derive parameters for the lumped reactive product species RNO3 and PROD2 are derived as discussed in the base SAPRC-99 mechanism documentation given by Carter (2000a), and the compositions of the mixtures used to derive parameters for the lumped emitted VOC species are given in the documentation for the “fixed parameter” version of SAPRC-99 (Carter, 2000b). The parameters and rate constants for the reactions of Cl atoms with these compounds are derived as discussed in the following section.

## Estimation of Chlorine + VOC Mechanisms

Rate constants have been measured for the reactions of chlorine atoms with many types of VOCs, and the recommended or measured rate constants for compounds currently represented in the SAPRC-99 mechanism, or used for deriving rate constant estimation methods, are listed in Table A-5. As indicated in footnotes to the table, most of these are either from the recent IUPAC (2006) evaluation or the review of Atkinson (1997), though for some compounds more recent measurement data are taken from the original references. These rate constants are assigned to the corresponding model species for the purpose of representing their reactions with Cl, and are used as the basis for deriving estimated rate constants for compounds for which measurement data are not available.

Chlorine can react with VOCs either by abstracting a hydrogen to form HCl and the corresponding alkyl radical, or by adding to a double bond. For abstraction reactions, the rate constants can be estimated using group additivity methods, with the rate constant being determined by the sum of the abstraction rate constant assigned to the group, multiplied by substituent correction factors for each non-hydrogen substituent on the group, summed over all groups with hydrogen atoms (e.g., see Kwok and Atkinson, 1995 or Carter, 2000a). Note that the correction factor for methyl substitution is arbitrarily set at unity, with the factors for the other substituents being determined based on differences in rate constants at groups that are only methyl substituted.

For addition to double bonds, we assume that the rate constant is determined only by the number of non-hydrogen substituents about the double bond, with correction factors used for some non-alkyl substituents such as halogens. Although this doesn't affect the rate constant, for the purpose of estimating mechanisms it is also necessary to assign factors for the fractions that react at each position around the double bond. This has to be estimated because we are aware of no data available concerning this,

The group additivity parameters found to give the best fits to the data on Table A-5 are shown on Table A-6 for the abstraction reactions, and on Table A-7 for reactions at double bonds. The “Est'n error” column on Table A-5 shows the extent to which the estimated rate constant agrees with the measured value, with positive numbers indicating overprediction, and vice-versa. If there is no entry in this column it means that the current estimation method is not applicable to those compounds. Except as indicated by footnotes to the tables, the group additivity parameters were determined by minimizing the sum-of-square relative errors in for the compounds listed on Table A-5 for which an estimation error is given. In most cases the estimated rate constants agree with the measured values to better than 25%. However, cases with perfect agreement usually indicate that a parameter was determined only by the data for a single compound, so perfect agreement is not always evidence for the success of the method.

As discussed by Carter (2000a), associated with the SAPRC-99 mechanism is a mechanism generation and estimation system that can be used to derive mechanisms for the reactions of OH radicals (and other species) with large variety of non-aromatic compounds. This involves (1) using group-additivity methods to estimate rates of reaction at various positions of the molecule, from which fractions reacted at the various positions are derived; (2) generating reactions for the radicals formed, using estimated or assigned branching ratios, to derive a fully explicit mechanism; and (3) using the various

Table A-5. Rate constants for reactions with chlorine atoms for organic compounds represented in the SAPRC-99 mechanism, or used to derive parameters for group-additivity estimates, for which measurement data are available.

Compound	Rate Constant Assignment [a]			Note [b]	Est'n Error [c]
	k(298)	A	Ea (deg K)		
Methane	1.03e-13	6.60e-12	1240	1	
Ethane	5.93e-11	8.30e-11	100	1	15%
Propane	1.37e-10	1.20e-10	-40	2	-3%
n-Butane	2.05e-10	2.05e-10	0	1	-5%
n-Pentane	2.80e-10			2	-8%
n-Hexane	3.40e-10			2	-6%
n-Heptane	3.90e-10			2	-3%
n-Octane	4.60e-10			2	-4%
n-Nonane	4.80e-10			2	5%
n-Decane	5.50e-10			2	3%
Isobutane	1.43e-10			2	0%
Neopentane	1.11e-10	1.11e-10	0	2	18%
Iso-Pentane	2.20e-10			2	-7%
2,3-Dimethyl Butane	2.30e-10			2	-6%
2-Methyl Pentane	2.90e-10			2	-8%
3-Methylpentane	2.80e-10			2	-4%
2,2,3-Trimethyl Butane	2.90e-10			2	-29%
2,4-Dimethyl Pentane	2.90e-10			2	-4%
2-Methyl Hexane	3.50e-10			2	-6%
2,2,3,3-Tetramethyl Butane	1.75e-10			2	12%
2,2,4-Trimethyl Pentane	2.60e-10			2	3%
Cyclohexane	3.50e-10			2	6%
Methylcyclohexane	3.90e-10			2	-2%
Ethene	See Table A-2			3	
Propene	2.67e-10			4	-1%
1-Butene	3.39e-10			5	-3%
1-Pentene	4.05e-10			5	-4%
3-Methyl-1-Butene	3.52e-10			6	-4%
3-Methyl-1-Pentene	3.78e-10			6	6%
Isobutene	3.25e-10			6	9%
2-Methyl-1-Butene	3.82e-10			6	10%
cis-2-Butene	3.88e-10			6	-15%
trans-2-Butene	3.55e-10			4	-7%
2-Methyl-2-Butene	3.23e-10			6	7%
Cis 4-Methyl-2-Pentene	4.04e-10			6	0%
1,3-Butadiene	4.90e-10			2	
Isoprene	4.80e-10			2	
Benzene	1.30e-16			7	
Toluene	6.20e-11			8	12%
m-Xylene	1.35e-10			8	3%
o-Xylene	1.40e-10			8	-1%
p-Xylene	1.44e-10			8	-4%
1,3,5-Trimethyl Benzene	2.42e-10			9	-14%
1-Methyl Naphthalene	1.21e-10			9	
2-Methyl Naphthalene	1.05e-10			9	
Acetylene	5.20e-11			3	
Methanol	5.50e-11	5.50e-11	0	1	-34%
Ethanol	1.00e-10	8.60e-11	-45	1	5%
Isopropyl Alcohol	8.60e-11			1	31%

Table A-5 (continued)

Compound	Rate Constant Assignment [a]			Note [b]	Est'n Error [c]
	k(298)	A	Ea (deg K)		
n-Propyl Alcohol	1.62e-10	2.50e-10	130	1	3%
Formic Acid	1.90e-13			1	
Acetic Acid	2.65e-14			1	0%
Formaldehyde	7.23e-11	8.10e-11	34	1	
Acetaldehyde	8.00e-11	8.00e-11	0	1	0%
Propionaldehyde	1.23e-10			10	0%
Acetone	2.69e-12	7.70e-11	1000	11	0%
Methyl Ethyl Ketone	3.60e-11			1	2%
Methyl Chloride	4.89e-13	2.17e-11	1130	11	-7%
Dichloromethane	3.49e-13	7.40e-12	910	11	11%
Chloroform	1.19e-13	3.30e-12	990	11	-7%
Vinyl Chloride	1.27e-10			12	4%
1,1-Dichloroethene	1.40e-10			12	-19%
Trans-1,2-Dichloroethene	9.58e-11			12	8%
Cis-1,2-Dichloroethene	9.65e-11			12	7%
Trichloroethylene	8.08e-11			12	-18%
Perchloroethylene	4.13e-11			12	9%
3-Chloropropene	1.30e-10			13	0%
Chloroacetaldehyde	1.29e-11			14	0%

[a] Rate constants and A factors in units of  $\text{cm}^3 \text{molec}^{-1} \text{s}^{-1}$ . If no A factor or activation energy is given, rate constant is given only for 298K. Otherwise, 298K rate constant is calculated from A factor and activation energy.

[b] Notes:

- 1 IUPAC (2006) recommendation.
- 2 Atkinson (1997) recommendation.
- 3 This reaction is in the pressure falloff region under atmospheric conditions.
- 4 Average of values tabulated by Wang et al (2002). Value of Wang et al (2002) placed on an absolute basis using the Atkinson (1997)-recommended rate constant for n-heptane.
- 5 Average of value of Coquet et al (2000), placed on an absolute basis using the Atkinson (1997)-recommended n-hexane rate constant, and the value of Wang et al (2002), placed on an absolute basis using the Atkinson (1997)-recommended rate constant for n-heptane.
- 6 Value of Wang et al (2002), placed on an absolute basis using the Atkinson (1997)-recommended rate constant for n-heptane.
- 7 Sokolov et al (1998).
- 8 Average of values tabulated by Wang et al (2005).
- 9 Wang et al (2005).
- 10 Average of values listed by Le Crane et al (2005)
- 11 NASA (2006) recommendation.
- 12 From rate constants relative to n-butane from Atkinson and Aschmann (1987), placed on an absolute basis using the n-butane rate constant recommended by IUPAC (2006).
- 13 Average of values tabulated by Albaladejo et al (2003).
- 14 Average of values tabulated by Scollard et al (1993)

[c] (Estimated rate constant - measured rate constant) / measured rate constant.

Table A-6. Group additivity rate constants and factors used for estimating rates of abstraction reactions by Cl atoms.

Group	k(abstract) cm <sup>3</sup> molec <sup>-1</sup> s <sup>-1</sup>	Group	Subst Factor
CH <sub>3</sub>	3.43e-11	-CH <sub>3</sub>	1.00
CH <sub>2</sub>	6.77e-11	-CH <sub>x</sub>	0.95[b]
CH	4.46e-11	-OH	1.07
OH	0 [a]	-CHO	0.40
CHO	6.64e-11	-CO-	0.04[c]
HCO(O)	0 [a]	-O-	1.07[d]
		-C=C	0.95
		-ONO <sub>2</sub>	0.12
		-CH <sub>x</sub> ONO <sub>2</sub>	0.12[b]
		-C=C (arom)	2.03
		-Cl (1 <sup>st</sup> )	0.01
		-Cl (2 <sup>nd</sup> or 3 <sup>rd</sup> )	0.43
		-CH <sub>2</sub> Cl	0.19[d]

[a] Data insufficient to derive a value. Zero assumed.

[b] x = 0 to 2

[b] Assumed to be the same as -CHO

[c] O- Substitution assumed to have same effect as -OH

[d] Based on chloroacetaldehyde only.

Table A-7. Group additivity rate constants and factors used for estimating rates of addition of Cl atoms to double bonds.

Group	k(add)	Add'n to Most Subst. End	Note	Group	Substituent Correction	Note
CH <sub>2</sub> =CH-	2.30e-10	35%	1,2	Alkyl	1	3
CH <sub>2</sub> =C<	2.89e-10	25%	1,4	-Cl	0.58	1
-CH=CH-	2.63e-10	50%	1,5	2 -Cl's	0.68	1
-CH=C<	2.47e-10	25%	1,4	-CH <sub>2</sub> Cl	0.56	1,6
>C=C<	2.47e-10	50%	1,5			

- 1 Addition rate constant and substituent correction factor derived to minimize sum of squares error in predictions of Cl + alkene rate constants. (Optimization for group additivity parameters for abstraction reaction carried out at the same time.)
- 2 Assume same terminal bond addition fraction as used for the reaction of OH with propene (Carter, 2000a).
- 3 All alkyl substituents assumed to have the same factor. Unit factor assigned.
- 4 No information available concerning relative addition rates at the different positions. Assume addition at terminal position occurs about 25% of the time
- 5 Assume equal probability of addition, regardless of substituents.
6. Based on rate constant for 3-chloropropene.

“lumping rules” associated with the SAPRC-99 mechanism to derive the representation of the overall process, and the products formed, in terms of SAPRC-99 model species. This system was designed to designate reactions of many types of VOCs with OH, O<sub>3</sub>, NO<sub>3</sub>, O(<sup>3</sup>P), and (in some cases) by photolysis, and was expanded to cover the reactions of chlorine atoms as discussed below.

Since the reactions of Cl radicals with VOCs are similar to those of OH, this general procedure can be readily adapted to generate mechanisms for Cl + VOC reactions. This requires (1) making group-additivity estimates for all the possible initial reactions of Cl with VOCs, and (2) generating mechanisms for the Cl-containing radicals that can be formed when Cl adds to double bonds. Note that the Cl abstraction reactions form the same radicals as the corresponding reactions with OH, so the procedures for generating the subsequent reactions of those radicals formed have already been developed.

The SAPRC-99 mechanisms generation system was adapted to support the abstraction reactions of Cl atoms with all VOCs for which OH reactions are supported and whose Cl atom rate constants could be estimated using the parameters in Table A-6. This was used to derive the mechanisms for the reactions of Cl atoms with the alkanes used in the incremental reactivity or the added propane chamber experiments, and for the compounds used to derive the rate constants and mechanistic parameters for the lumped parameter model species RNO<sub>3</sub>, PROD2, and ALK1 through ALK5 as indicated in Table A-4. The rate constants and mechanisms so derived are given on Table 2.

Although in principle the enhanced mechanism generation system could also derive mechanisms for the reactions of chlorine atoms with alkenes, in practice this proved difficult, in part because at present the system does not contain the necessary thermochemical or kinetic assignments to estimate reaction rates for many of the halogen-substituted alkoxy radicals predicted to be formed. The only way to deal with this is to make explicit assignments of branching ratios for the Cl-substituted radicals that cannot presently be handled by the system. This can be time consuming for large molecules because of the number of radicals that can be formed. For that reason, assignments were made only to permit the generation of mechanisms for the alkenes present in the chamber experiments (ethene, propene, trans-2-butene, and the 1,3-dichloropropenes), or those chosen to be representative of the lumped model species OLE1 and OLE2. Since both of these lumped species have an average carbon number close to 5, 1-pentene was taken as representative of OLE1 and the 2-pentenenes were taken as representative of OLE2 (the cis and trans isomers give the same generated mechanism).

Table A-8 gives the alkoxy radical branching ratio assignments that were made in order to generate mechanisms for the alkenes in the chamber experiments or used to derive mechanisms for OLE1 and OLE2. The reasons behind the choices are indicated in footnotes to the table. For simplicity, the reaction shown on Table A-8 was assumed to be the dominant process, and competing processes were ignored. This is almost certainly an oversimplification in some cases, and in some cases a competing process may in fact dominate. However, except perhaps for the simulations of the 1,3-dichloropropene NO<sub>x</sub> experiments, the chlorine + alkene reactions are relatively unimportant in the model simulations for this work because the rapid reaction of Cl with alkanes, which are present in higher levels in the incremental reactivity and the ambient simulations, tend to be the major Cl + VOC process.

Another difficulty with extending the mechanism generation procedure to the reactions of Cl atoms with alkenes is that reaction by abstraction, forming HCl and unsaturated radicals, is estimated to be sufficiently important that it cannot be neglected. These SAPRC-99 mechanism estimation and generation procedure as documented by Carter (2000a) does not support reactions of such unsaturated radicals. The approximation made in the SAPRC-99 estimation procedure for the reactions of OH with alkenes (Carter, 2000a) is that reaction occurs only by addition to the double bond, so reactions forming unsaturated radicals (at least for monoalkenes) are neglected. [For isoprene and a few other disubstituted alkenes the reactions are generated by making explicit assignments for the unsaturated radicals formed.]

Table A-8. Branching ratio assignments for chlorine-substituted alkoxy radicals that had to be made in order to generate mechanisms for the reactions of chlorine for the representative alkenes.

Needed for deriving Mechanism of	Reaction Assumed to Dominate	Notes
Propene	$\text{CH}_3\text{CH}(\text{O}\cdot)\text{CH}_2\text{Cl} + \text{O}_2 \rightarrow \text{CH}_3\text{C}(\text{O})\text{CH}_2\text{Cl} + \text{HO}_2\cdot$	1
Propene	$\text{CH}_3\text{CH}(\text{CH}_2\text{O}\cdot)\text{Cl} + \text{O}_2 \rightarrow \text{CH}_3\text{CH}(\text{CHO})\text{Cl} + \text{HO}_2\cdot$	2
2-Butenes	$\text{CH}_3\text{CH}(\text{O}\cdot)\text{CH}(\text{CH}_3)\text{Cl} + \text{O}_2 \rightarrow \text{CH}_3\text{C}(\text{O})\text{CH}(\text{CH}_3)\text{Cl} + \text{HO}_2\cdot$	3
1-Pentene	$\text{CH}_3\text{CH}_2\text{CH}_2\text{CH}(\text{O}\cdot)\text{CH}_2\text{Cl} \rightarrow \cdot\text{CH}_2\text{CH}_2\text{CH}_2\text{CH}(\text{OH})\text{CH}_2\text{Cl}$	4
1-Pentene	$\text{CH}_3\text{CH}_2\text{CH}_2\text{CH}(\text{CH}_2\text{O}\cdot)\text{Cl} \rightarrow \text{CH}_3\text{CH}(\cdot)\text{CH}_2\text{CH}(\text{Cl})\text{CH}_2\text{OH}$	4
1-Pentene	$\text{CH}_3\text{CH}(\text{O}\cdot)\text{CH}_2\text{CH}(\text{Cl})\text{CH}_2\text{OH} \rightarrow \text{CH}_3\text{CH}(\text{OH})\text{CH}_2\text{CH}(\text{Cl})\text{CH}(\cdot)\text{OH}$	4
2-Pentenenes	$\text{CH}_3\text{CH}_2\text{CH}(\text{O}\cdot)\text{CH}(\text{CH}_3)\text{Cl} \rightarrow \text{CH}_3\text{CH}_2\text{CHO} + \text{CH}_3\text{CH}(\cdot)\text{Cl}$	5
2-Pentenenes	$\text{CH}_3\text{CH}(\text{O}\cdot)\text{Cl} \rightarrow \text{CH}_3\text{CHO} + \text{Cl}\cdot$	6
2-Pentenenes	$\text{CH}_3\text{CH}_2\text{CH}(\text{Cl})\text{CH}(\text{O}\cdot)\text{CH}_3 \rightarrow \text{CH}_3\text{CHO} + \text{CH}_3\text{CH}_2\text{CH}(\cdot)\text{Cl}$	5
2-Pentenenes	$\text{CH}_3\text{CH}_2\text{CH}(\text{O}\cdot)\text{Cl} \rightarrow \text{CH}_3\text{CH}_2\text{CHO} + \text{Cl}\cdot$	6
1,3-Dichloropropenes	$\text{Cl}-\text{CH}_2\text{CH}(\text{O}\cdot)\text{CH}(\text{Cl})\text{Cl} + \text{O}_2 \rightarrow \text{Cl}-\text{CH}_2\text{C}(\text{O})\text{CH}(\text{Cl})\text{Cl} + \text{HO}_2\cdot$	7
1,3-Dichloropropenes	$\text{Cl}-\text{CH}_2\text{CH}(\text{Cl})\text{CH}(\text{O}\cdot)\text{Cl} \rightarrow \text{HCOCH}(\text{Cl})\text{CH}_2\text{Cl} + \text{Cl}\cdot$	6

- 1 Assumed to be favored over decomposition on the basis of estimates for  $\text{CH}_3\text{C}(\text{O}\cdot)\text{CH}_3$  and the expectation that Cl-substitution makes radicals less stable
- 2 Assumed to be favored over decomposition on the basis of estimates for  $\text{CH}_3\text{CH}_2\text{CH}_2\text{O}\cdot$  and the expectation that Cl-substitution makes radicals less stable
- 3 Assumed to be favored over decomposition on the basis of estimates for the radical where H- replaces Cl- and the expectation that Cl-substitution makes radicals less stable
- 4 Isomerization is assumed to dominate over competing processes for this radical.
- 5 This decomposition is assumed to dominate based on estimates for similar radicals.
- 6 Decompositions forming chlorine atoms are assumed to be rapid.
- 7 Assumed to be favored over decomposition on the basis of estimates for  $\text{CH}_3\text{C}(\text{O}\cdot)\text{CH}_3$  and the expectation that Cl-substitution makes radicals less stable

However, as part of the project to update the SAPRC mechanism we have enhanced the capability of the mechanism generation system to support reactions of unsaturated radicals, and this was used to permit the generation of Cl atom reactions with alkenes without having to neglect the abstraction processes. These enhancements, and the associated assignments for unsaturated radicals, will be discussed in the report documenting the updated mechanism, which is in preparation. As indicated above, this is not a major factor in the model simulations discussed in this report.

The mechanisms used for the reactions of Cl atoms OLE1 and OLE2 as shown on Table A-1 were therefore based on those for derived for 1-pentene and the 2-pentenenes. However, the rate constants for these reactions were derived from the weighted averages of those for the representative compounds as given on Table A-4.

The measured rate constants for the reactions of Cl atoms with the aromatics are also given in Table A-5, and these were used in the mechanisms for the reactions of Cl with the toluene and m-xylene in the chamber experiments. As shown on Table A-5, the rate constant for the reaction of Cl atoms with

benzene is many orders of magnitude slower than the reactions with alkylbenzenes such as toluene, strongly suggesting that, unlike OH radicals, the addition of Cl to the aromatic ring is negligible under atmospheric conditions. [The data of Sokolov et al (1998) indicate that this is due to the benzene - Cl adduct decomposing much more rapidly than it reacts with O<sub>2</sub>, resulting in no net reaction.] Therefore, for estimation purposes the reactions of aromatics with Cl can be treated as solely an abstraction process from the non-aromatic alkyl groups, and the data on Table A-5 can be used to derive group additivity parameters for aromatic substituents, as shown on Table A-6. These can then be used to estimate Cl atom rate constants for the aromatics used to derive parameters for the ARO1 and ARO2 lumped groups, as shown on Table A-4, from which the Cl atom rate constants for ARO1 and ARO2, shown on Table A-2, can be derived.

The assumption that the reactions of Cl with aromatics proceed only by abstraction from the alkyl group off the rings greatly simplifies the estimation of mechanisms for these compounds. In the case of toluene, the overall process is assumed to be formation of benzaldehyde and HO<sub>2</sub> after an NO to NO<sub>2</sub> conversion, which is represented in terms of SAPRC-99 model species as formation of RO<sub>2</sub>-R· + BALD, where “BALD” is the model species used for aromatic aldehydes. This mechanism is used for all methyl-substituted benzenes, as shown on Table A-2. Since as shown on Table A-4 all the compounds used to derive the parameters for ARO2 are methylbenzenes, this mechanism is also used for ARO2. For ethylbenzene and other alkyl-substituted benzenes, aromatic ketones, such as methyl phenyl ketone from ethylbenzene, are expected to be formed instead of aromatic aldehydes. These are represented by “PROD2” in the mechanism. Since 25% of the compounds used to derive parameters for ARO1 are ethyl and higher monoalkyl benzenes, Table A-2 indicates that the products formed in the reactions of Cl with ARO1 are represented by 0.75 BALD + 0.27 PROD2.

## References

- Albaladejo, J., A. Notario, C. A. Cuevas, B. Ballesteros, and E. Martínez (2003): “A Pulsed Laser Photolysis-Resonance Fluorescence Kinetic Study of the Atmospheric Cl Atom-Initiated Oxidation of Propene and a Series of 3-Halopropenes at Room Temperature,” *J. Atm. Chem*, 45, 35-50.
- Atkinson, R. (1997): “Gas-Phase Tropospheric Chemistry of Volatile Organic Compounds: 1. Alkanes and Alkenes,” *J. Phys and Chem. Reference Data*, 26, 215-290.
- Atkinson, R. and S. M. Aschmann (1987): “Kinetics of the Gas-Phase Reactions of Cl Atoms with Chloroethenes at 298 ± 2 K and Atmospheric Pressure,” *Int. J. Chem. Kinet.* 19, 1097-1105.
- Carter, W. P. L. (1994): “Development of Ozone Reactivity Scales for Volatile Organic Compounds,” *J. Air & Waste Manage. Assoc.*, 44, 881-899.
- Carter, W. P. L. (2000a): “Documentation of the SAPRC-99 Chemical Mechanism for VOC Reactivity Assessment,” Report to the California Air Resources Board, Contracts 92-329 and 95-308, May 8. Available at <http://cert.ucr.edu/~carter/absts.htm#saprc99> and <http://www.cert.ucr.edu/~carter/reactdat.htm>.
- Carter, W. P. L. (2000b): “Implementation of the SAPRC-99 Chemical Mechanism into the Models-3 Framework,” Report to the United States Environmental Protection Agency, January 29. Available at <http://www.cert.ucr.edu/~carter/absts.htm#s99mod3>.
- Carter, W. P. L. (2003): “Updated Chemical Mechanism for Airshed Model Applications,” Research Proposal to the California Air Resources Board, October.



- Carter, W. P. L., D. Luo, and I. L. Malkina (1996): "Investigation of the Atmospheric Ozone Formation Potential of Trichloroethylene," Report to the Halogenated Solvents Industry Alliance, August. Available at <http://www.cert.ucr.edu/~carter/absts.htm#tcerpt>.
- Carter, W. P. L., D. Luo and I. L. Malkina (1997a): "Investigation of that Atmospheric Reactions of Chloropicrin," *Atmos. Environ.* 31, 1425-1439; See also Report to the Chloropicrin Manufacturers Task Group, May 19. Report available at <http://www.cert.ucr.edu/~carter/absts.htm#clpicrin>.
- Carter, W. P. L., D. Luo and I. L. Malkina (1997b): "Investigation of that Atmospheric Reactions of Chloropicrin," *Atmos. Environ.* 31, 1425-1439.
- Coquet, S. and P. A. Ariya (2000): "Kinetics of the Gas-Phase Reactions of Cl Atom with Selected C2–C5 Unsaturated Hydrocarbons at 283 <T< 323 K," *Int. J. Chem. Kinet.* 32, 478-484.
- IUPAC (2006): "Summary of Evaluated Kinetic and Photochemical Data for Atmospheric Chemistry". IUPAC Subcommittee on Gas Kinetic Data Evaluation for Atmospheric Chemistry. Web Version. Available at <http://www.iupac-kinetic.ch.cam.ac.uk>. Accessed January-October, 2006.
- Kwok, E. S. C., and R. Atkinson (1995): "Estimation of Hydroxyl Radical Reaction Rate Constants for Gas-Phase Organic Compounds Using a Structure-Reactivity Relationship: An Update," *Atmos. Environ* 29, 1685-1695.
- Le Crane, J.P., E. Villenave, M. D. Hurley, T. J. Wallington, and J. C. Ball (2005): "Atmospheric Chemistry of Propionaldehyde: Kinetics and Mechanisms of Reactions with OH Radicals and Cl Atoms, UV Spectrum, and Self-Reaction Kinetics of CH<sub>3</sub>CH<sub>2</sub>C(O)O<sub>2</sub> Radicals at 298 K, *J. Phys. Chem. A* 2005, 109, 11837-11850.
- NASA (2006): "Chemical Kinetics and Photochemical Data for Use in Stratospheric Modeling, Evaluation Number 15," JPL Publication 06-2, Jet Propulsion Laboratory, Pasadena, California, July.
- Scollard, D. J., J. J. Treacy, H. W. Sidebottom, C. Balestra-Garcia, G. Laverdet, G. LeBras, H. MacLeod, and S. Teton (1993): "Rate constants for the reactions of hydroxyl radicals and chlorine atoms with halogenated aldehydes," *J. Phys. Chem.* 97, 4683 - 4688.
- Sokolov, O.; Hurley, M. D.; Wallington, T. J.; Kaiser, E. W.; Platz, J.; Nielsen, O. J.; Berho, F.; Rayez, M.-T.; Lesclaux, R.(1998): "Kinetics and mechanism of the gas-phase reaction of Cl atoms with benzene," *J. Phys. Chem. A*, 102, 10671-10681.
- Wang, W., M. J. Ezell, A. A. Ezell, G. Soskin and B. J. Finlayson-Pitts (2002): "Kinetics of Reactions of Chlorine Atoms with a Series of Alkenes at 1 Atm and 298K: Structure and Reactivity," *Phys. Chem. Chem. Phys.* 4, 5813-5820.
- Wang, L., J. Arey, and R. Atkinson (2005): "Reactions of Chlorine Atoms with a Series of Aromatic Hydrocarbons," *Environ. Sci. Technol.* 39, 5302-5310.

## APPENDIX B. MECHANISMS FOR KEROSENE CONSTITUENTS

The mechanisms used for the constituents of kerosene used in the model simulations in this report are given in Table B-1. The mechanisms for most of the alkanes and all of the aromatics are from Carter (2000a). However, a few branched and cyclic alkanes may have been added subsequently to improve representations of complex mixtures, and where applicable these are included on the table. The mechanisms for the added compounds were all generated using the SAPRC-99 mechanism generation and estimation system as documented by Carter (2000a).

Table B-1. Representations of the compounds used to represent the constituents of kerosene in the SAPRC-99 mechanism.

Compound	Reaction and Products [a]	Rate Parameters [b]			
		k(298)	A	Ea	B
n-Hexane	N-C6 + HO. = #.775 RO2-R. + #.225 RO2-N. + #.787 R2O2. + #.011 CCHO + #.113 RCHO + #.688 PROD2 + #.162 XC	5.47e-12	1.38e-12	-0.82	2
n-Heptane	N-C7 + HO. = #.705 RO2-R. + #.295 RO2-N. + #.799 R2O2. + #.055 RCHO + #.659 PROD2 + #1.11 XC	7.02e-12	1.43e-12	-0.95	2
n-Octane	N-C8 + HO. = #.646 RO2-R. + #.354 RO2-N. + #.786 R2O2. + #.024 RCHO + #.622 PROD2 + #2.073 XC	8.70e-12	2.48e-12	-0.75	2
n-Nonane	N-C9 + HO. = #.602 RO2-R. + #.398 RO2-N. + #.777 R2O2. + #.018 RCHO + #.584 PROD2 + #3.055 XC	9.99e-12	2.26e-12	-0.89	2
n-Decane	N-C10 + HO. = #.572 RO2-R. + #.428 RO2-N. + #.772 R2O2. + #.015 RCHO + #.557 PROD2 + #4.045 XC	1.12e-11	2.82e-12	-0.83	2
n-Undecane	N-C11 + HO. = #.553 RO2-R. + #.447 RO2-N. + #.771 R2O2. + #.013 RCHO + #.54 PROD2 + #5.038 XC	1.29e-11			
n-Dodecane	N-C12 + HO. = #.542 RO2-R. + #.458 RO2-N. + #.768 R2O2. + #.011 RCHO + #.53 PROD2 + #6.034 XC	1.39e-11			
n-Tridecane	N-C13 + HO. = #.535 RO2-R. + #.465 RO2-N. + #.766 R2O2. + #.01 RCHO + #.525 PROD2 + #7.03 XC	1.60e-11			
n-Tetradecane	N-C14 + HO. = #.53 RO2-R. + #.47 RO2-N. + #.765 R2O2. + #.009 RCHO + #.521 PROD2 + #8.027 XC	1.80e-11			
n-Pentadecane	N-C15 + HO. = #.527 RO2-R. + #.473 RO2-N. + #.764 R2O2. + #.008 RCHO + #.519 PROD2 + #9.025 XC	2.10e-11			
n-C16	N-C16 + HO. = #.525 RO2-R. + #.475 RO2-N. + #.763 R2O2. + #.008 RCHO + #.517 PROD2 + #10.023 XC	2.30e-11			
2,3-Dimethyl Butane	23-DM-C4 + HO. = #.858 RO2-R. + #.142 RO2-N. + #.918 R2O2. + #.028 HCHO + #.023 CCHO + #.078 RCHO + #1.569 ACET + #.001 MEK + #.132 XC	5.80e-12	1.12e-12	-0.98	2
2-Methyl Pentane	2-ME-C5 + HO. = #.816 RO2-R. + #.184 RO2-N. + #.859 R2O2. + #.004 HCHO + #.011 CCHO + #.661 RCHO + #.346 ACET + #.006 MEK + #.153 PROD2 + #.904 XC	5.30e-12			

Table B-1 (continued)

Compound	Reaction and Products [a]	Rate Parameters [b]			
		k(298)	A	Ea	B
3-Methyl pentane	3-ME-C5 + HO. = #.844 RO2-R. + #.156 RO2-N. + #.989 R2O2. + #.005 HCHO + #.986 CCHO + #.069 RCHO + #.629 MEK + #.036 PROD2 + #.151 XC	5.40e-12			
2,4-Dimethyl Pentane	24-DM-C5 + HO. = #.796 RO2-R. + #.204 RO2-N. + #.1.323 R2O2. + #.333 HCHO + #.016 CCHO + #.562 RCHO + #.483 ACET + #.013 MEK + #.135 PROD2 + #.1.413 XC	5.00e-12			
2-Methyl Hexane	2-ME-C6 + HO. = #.731 RO2-R. + #.269 RO2-N. + #.906 R2O2. + #.022 HCHO + #.048 CCHO + #.236 RCHO + #.137 ACET + #.508 PROD2 + #.1.102 XC	6.89e-12			
3-Methyl Hexane	3-ME-C6 + HO. = #.75 RO2-R. + #.25 RO2-N. + #.924 R2O2. + #.002 HCHO + #.208 CCHO + #.463 RCHO + #.256 MEK + #.235 PROD2 + #.1.266 XC	7.17e-12			
2,4-Dimethyl Hexane	24-DM-C6 + HO. = #.652 RO2-R. + #.348 RO2-N. + #.1.346 R2O2. + #.159 HCHO + #.335 CCHO + #.306 RCHO + #.096 ACET + #.156 MEK + #.293 PROD2 + #.1.492 XC	8.57e-12			
2-Methyl Heptane	2-ME-C7 + HO. = #.659 RO2-R. + #.341 RO2-N. + #.882 R2O2. + #.016 HCHO + #.025 CCHO + #.155 RCHO + #.024 ACET + #.546 PROD2 + #.2.077 XC	8.31e-12			
4-Methyl Heptane	4-ME-C7 + HO. = #.676 RO2-R. + #.324 RO2-N. + #.875 R2O2. + #.002 HCHO + #.004 CCHO + #.377 RCHO + #.115 MEK + #.376 PROD2 + #.2.201 XC	8.59e-12			
2,4-Dimethyl Heptane	24-DM-C7 + HO. = #.598 RO2-R. + #.402 RO2-N. + #.1.176 R2O2. + #.104 HCHO + #.013 CCHO + #.41 RCHO + #.049 ACET + #.073 MEK + #.381 PROD2 + #.2.501 XC	9.99e-12			
2-Methyl Octane	2-ME-C8 + HO. = #.587 RO2-R. + #.413 RO2-N. + #.914 R2O2. + #.002 HCHO + #.064 RCHO + #.014 ACET + #.536 PROD2 + #.3.072 XC	1.01e-11			
4-Methyl Octane	4-ME-C8 + HO. = #.605 RO2-R. + #.395 RO2-N. + #.89 R2O2. + #.001 HCHO + #.034 CCHO + #.127 RCHO + #.006 MEK + #.562 PROD2 + #.2.788 XC	9.70e-12			
2,6-Dimethyl Octane	26DM-C8 + HO. = #.567 RO2-R. + #.433 RO2-N. + #.1.096 R2O2. + #.108 CCHO + #.308 RCHO + #.145 ACET + #.071 MEK + #.276 PROD2 + #.3.887 XC	1.29e-11			
2-Methyl Nonane	2-ME-C9 + HO. = #.551 RO2-R. + #.449 RO2-N. + #.895 R2O2. + #.035 RCHO + #.012 ACET + #.516 PROD2 + #.4.066 XC	1.28e-11			
4-Methyl Nonane	4-ME-C9 + HO. = #.572 RO2-R. + #.428 RO2-N. + #.876 R2O2. + #.001 HCHO + #.019 CCHO + #.14 RCHO + #.004 MEK + #.52 PROD2 + #.3.831 XC	1.14e-11			
2,6-Dimethyl Nonane	26DM-C9 + HO. = #.533 RO2-R. + #.467 RO2-N. + #.1.036 R2O2. + #.001 CCHO + #.221 RCHO + #.12 ACET + #.006 MEK + #.376 PROD2 + #.4.888 XC	1.28e-11			
3-Methyl Decane	3-ME-C10 + HO. = #.526 RO2-R. + #.474 RO2-N. + #.917 R2O2. + #.029 CCHO + #.038 RCHO + #.012 MEK + #.489 PROD2 + #.4.998 XC	1.29e-11			

Table B-1 (continued)

Compound	Reaction and Products [a]	Rate Parameters [b]			
		k(298)	A	Ea	B
4-Methyl Decane	4-ME-C10 + HO. = #.531 RO2-R. + #.469 RO2-N. + #.907 R2O2. + #.001 CCHO + #.08 RCHO + #.003 MEK + #.5 PROD2 + #4.932 XC	1.29e-11			
3,6-Dimethyl Decane	36DM-C10 + HO. = #.494 RO2-R. + #.506 RO2-N. + #1.079 R2O2. + #.001 HCHO + #.088 CCHO + #.11 RCHO + #.055 MEK + #.458 PROD2 + #5.488 XC	1.45e-11			
3-Methyl Undecane	3-ME-C11 + HO. = #.516 RO2-R. + #.484 RO2-N. + #.896 R2O2. + #.025 CCHO + #.033 RCHO + #.011 MEK + #.484 PROD2 + #5.997 XC	1.43e-11			
5-Methyl Undecane	5-ME-C11 + HO. = #.524 RO2-R. + #.476 RO2-N. + #.867 R2O2. + #.01 CCHO + #.059 RCHO + #.504 PROD2 + #5.923 XC	1.43e-11			
3,6-Dimethyl Undecane	36DM-C11 + HO. = #.488 RO2-R. + #.512 RO2-N. + #1.046 R2O2. + #.001 HCHO + #.07 CCHO + #.124 RCHO + #.046 MEK + #.442 PROD2 + #6.579 XC	1.60e-11			
3-Methyl Dodecane	3-ME-C12 + HO. = #.51 RO2-R. + #.49 RO2-N. + #.88 R2O2. + #.023 CCHO + #.03 RCHO + #.009 MEK + #.482 PROD2 + #6.997 XC	1.57e-11			
5-Methyl Dodecane	5-ME-C12 + HO. = #.514 RO2-R. + #.486 RO2-N. + #.863 R2O2. + #.009 CCHO + #.044 RCHO + #.498 PROD2 + #6.942 XC	1.57e-11			
3,7-Dimethyl Dodecane	37DM-C12 + HO. = #.496 RO2-R. + #.504 RO2-N. + #.98 R2O2. + #.055 CCHO + #.11 RCHO + #.03 MEK + #.44 PROD2 + #7.772 XC	1.74e-11			
3-Methyl Tridecane	3-ME-C13 + HO. = #.506 RO2-R. + #.494 RO2-N. + #.871 R2O2. + #.021 CCHO + #.015 RCHO + #.009 MEK + #.493 PROD2 + #7.958 XC	1.71e-11			
6-Methyl Tridecane	6-ME-C13 + HO. = #.512 RO2-R. + #.488 RO2-N. + #.852 R2O2. + #.006 CCHO + #.041 RCHO + #.504 PROD2 + #7.909 XC	1.71e-11			
3,7-Dimethyl Tridecane	37DM-C13 + HO. = #.487 RO2-R. + #.513 RO2-N. + #.98 R2O2. + #.045 CCHO + #.087 RCHO + #.028 MEK + #.44 PROD2 + #8.82 XC	1.88e-11			
3-Methyl Tetradecane	3-ME-C14 + HO. = #.505 RO2-R. + #.495 RO2-N. + #.861 R2O2. + #.02 CCHO + #.013 RCHO + #.008 MEK + #.493 PROD2 + #8.961 XC	1.85e-11			
6-Methyl Tetradecane	6-ME-C14 + HO. = #.51 RO2-R. + #.49 RO2-N. + #.843 R2O2. + #.006 CCHO + #.037 RCHO + #.503 PROD2 + #8.918 XC	1.85e-11			
3-Methyl Pentadecane	3-ME-C15 + HO. = #.504 RO2-R. + #.496 RO2-N. + #.853 R2O2. + #.018 CCHO + #.012 RCHO + #.008 MEK + #.493 PROD2 + #9.964 XC	2.00e-11			
4,8-Dimethyl Tetradecane	48DM-C14 + HO. = #.481 RO2-R. + #.519 RO2-N. + #.962 R2O2. + #.001 CCHO + #.071 RCHO + #.003 MEK + #.473 PROD2 + #9.82 XC	2.02e-11			
7-Methyl Pentadecane	7-ME-C15 + HO. = #.503 RO2-R. + #.497 RO2-N. + #.853 R2O2. + #.022 RCHO + #.5 PROD2 + #9.95 XC	2.00e-11			

Table B-1 (continued)

Compound	Reaction and Products [a]	Rate Parameters [b]			
		k(298)	A	Ea	B
Methyl cyclohexane	ME-CYCC6 + HO. = #.66 RO2-R. + #.34 RO2-N. + #1.146 R2O2. + #.011 HCHO + #.002 CCHO + #.455 RCHO + #.208 PROD2 + #2.328 XC	1.00e-11			
Ethyl cyclohexane	ET-CYCC6 + HO. = #.624 RO2-R. + #.376 RO2-N. + #1.046 R2O2. + #.002 HCHO + #.151 CCHO + #.328 RCHO + #.299 PROD2 + #2.662 XC	1.20e-11			
1-Ethyl-4-Methyl Cyclohexane	1E4MCYC6 + HO. = #.518 RO2-R. + #.481 RO2-N. + #1.339 R2O2. + #.001 CCO-O2. + #.033 HCHO + #.142 CCHO + #.411 RCHO + #.143 PROD2 + #3.703 XC	1.37e-11			
Propyl Cyclohexane	C3-CYCC6 + HO. = #.61 RO2-R. + #.389 RO2-N. + #.864 R2O2. + #.001 RCO-O2. + #.001 HCHO + #.363 RCHO + #.388 PROD2 + #3.242 XC	1.35e-11			
1,4-Diethyl-Cyclohexane	14DECYC6 + HO. = #.508 RO2-R. + #.49 RO2-N. + #1.229 R2O2. + #.002 RCO-O2. + #.021 HCHO + #.226 CCHO + #.333 RCHO + #.209 PROD2 + #4.328 XC	1.55e-11			
1-Methyl-3-Isopropyl Cyclohexane	1M3IPCY6 + HO. = #.535 RO2-R. + #.46 RO2-N. + #1.204 R2O2. + #.004 RCO-O2. + #.006 CO + #.008 HCHO + #.005 CCHO + #.263 RCHO + #.339 ACET + #.293 PROD2 + #3.634 XC	1.51e-11			
Butyl Cyclohexane	C4-CYCC6 + HO. = #.576 RO2-R. + #.423 RO2-N. + #.827 R2O2. + #.024 CCHO + #.179 RCHO + #.467 PROD2 + #4.07 XC	1.49e-11			
1,3-Diethyl-5-Methyl Cyclohexane	13E5MCC6 + HO. = #.429 RO2-R. + #.566 RO2-N. + #1.371 R2O2. + #.003 CCO-O2. + #.002 RCO-O2. + #.006 CO + #.02 HCHO + #.168 CCHO + #.355 RCHO + #.009 MEK + #.09 PROD2 + #5.587 XC	1.72e-11			
1-Ethyl-2-Propyl Cyclohexane	1E2PCYC6 + HO. = #.461 RO2-R. + #.539 RO2-N. + #1.199 R2O2. + #.001 RCO-O2. + #.007 HCHO + #.031 CCHO + #.186 RCHO + #.349 PROD2 + #5.045 XC	1.70e-11			
Pentyl Cyclohexane	C5-CYCC6 + HO. = #.557 RO2-R. + #.443 RO2-N. + #.808 R2O2. + #.016 CCHO + #.147 RCHO + #.456 PROD2 + #5.135 XC	1.63e-11			
1,3,5-Triethyl Cyclohexane	135ECYC6 + HO. = #.417 RO2-R. + #.58 RO2-N. + #1.353 R2O2. + #.003 RCO-O2. + #.005 CO + #.014 HCHO + #.221 CCHO + #.315 RCHO + #.008 MEK + #.116 PROD2 + #6.373 XC	1.90e-11			
1-Methyl-4-Pentyl Cyclohexane	1M4C5CY6 + HO. = #.482 RO2-R. + #.518 RO2-N. + #1.049 R2O2. + #.001 CCO-O2. + #.001 HCHO + #.015 CCHO + #.21 RCHO + #.326 PROD2 + #6.274 XC	1.80e-11			
Hexyl Cyclohexane	C6-CYCC6 + HO. = #.527 RO2-R. + #.473 RO2-N. + #.849 R2O2. + #.093 RCHO + #.461 PROD2 + #6.118 XC	1.78e-11			
1,3-Diethyl-5-Propyl Cyclohexane	13E5PCC6 + HO. = #.433 RO2-R. + #.564 RO2-N. + #1.237 R2O2. + #.003 RCO-O2. + #.002 CO + #.01 HCHO + #.132 CCHO + #.342 RCHO + #.002 MEK + #.188 PROD2 + #7.163 XC	2.05e-11			
1-Methyl-2-Hexyl-Cyclohexane	1M2C6CC6 + HO. = #.462 RO2-R. + #.537 RO2-N. + #1.08 R2O2. + #.001 RCO-O2. + #.004 HCHO + #.009 CCHO + #.128 RCHO + #.38 PROD2 + #7.092 XC	1.94e-11			

Table B-1 (continued)

Compound	Reaction and Products [a]	Rate Parameters [b]			
		k(298)	A	Ea	B
Heptyl Cyclohexane	C7-CYCC6 + HO. = #.515 RO2-R. + #.485 RO2-N. + #.855 R2O2. + #.069 RCHO + #.462 PROD2 + #7.108 XC	1.91e-11			
1,3-Dipropyl-5-Ethyl Cyclohexane	13P5ECC6 + HO. = #.445 RO2-R. + #.553 RO2-N. + #1.158 R2O2. + #.002 RCO-O2. + #.001 CO + #.007 HCHO + #.06 CCHO + #.376 RCHO + #.234 PROD2 + #8.017 XC	2.19e-11			
trans 1-Methyl-4-Heptyl Cyclohexane	1M4C7CC6 + HO. = #.455 RO2-R. + #.544 RO2-N. + #1.059 R2O2. + #.001 HCHO + #.131 RCHO + #.349 PROD2 + #8.242 XC	2.08e-11			
Octyl Cyclohexane	C8-CYCC6 + HO. = #.511 RO2-R. + #.489 RO2-N. + #.847 R2O2. + #.063 RCHO + #.463 PROD2 + #8.099 XC	2.06e-11			
1,3,5-Tripropyl Cyclohexane	135PCYC6 + HO. = #.453 RO2-R. + #.545 RO2-N. + #1.106 R2O2. + #.002 RCO-O2. + #.001 CO + #.005 HCHO + #.415 RCHO + #.258 PROD2 + #8.923 XC	2.33e-11			
1-Methyl-2-Octyl Cyclohexane	1M2C8CC6 + HO. = #.462 RO2-R. + #.538 RO2-N. + #1.035 R2O2. + #.003 HCHO + #.008 CCHO + #.105 RCHO + #.394 PROD2 + #9.08 XC	2.22e-11			
Nonyl Cyclohexane	C9-CYCC6 + HO. = #.509 RO2-R. + #.49 RO2-N. + #.838 R2O2. + #.058 RCHO + #.465 PROD2 + #9.091 XC	2.20e-11			
1,3-Propyl-5-Butyl Cyclohexane	13P5BCC6 + HO. = #.461 RO2-R. + #.538 RO2-N. + #1.045 R2O2. + #.001 RCO-O2. + #.001 CO + #.003 HCHO + #.013 CCHO + #.322 RCHO + #.318 PROD2 + #9.863 XC	2.47e-11			
1-Methyl-4-Nonyl Cyclohexane	1M4C9CY6 + HO. = #.458 RO2-R. + #.541 RO2-N. + #1.018 R2O2. + #.001 HCHO + #.113 RCHO + #.367 PROD2 + #10.209 XC	2.37e-11			
Decyl Cyclohexane	C10CYCC6 + HO. = #.508 RO2-R. + #.492 RO2-N. + #.834 R2O2. + #.055 RCHO + #.467 PROD2 + #10.085 XC	2.34e-11			
Ethyl Benzene	C2-BENZ + HO. = #.19 HO2. + #.786 RO2-R. + #.024 RO2-N. + #.239 PROD2 + #.094 GLY + #.109 MGLY + #.19 CRES + #.498 DCB1 + #.049 DCB3 + #2.338 XC	7.10e-12			
n-Propyl Benzene	N-C3-BEN + HO. = #.19 HO2. + #.786 RO2-R. + #.024 RO2-N. + #.239 PROD2 + #.094 GLY + #.109 MGLY + #.19 CRES + #.498 DCB1 + #.049 DCB3 + #3.338 XC	6.00e-12			
m-Xylene	M-XYLENE + HO. = #.21 HO2. + #.782 RO2-R. + #.008 RO2-N. + #.107 GLY + #.335 MGLY + #.21 CRES + #.037 BALD + #.347 DCB1 + #.29 DCB2 + #.108 DCB3 + #1.628 XC	2.36e-11			
o-Xylene	O-XYLENE + HO. = #.161 HO2. + #.831 RO2-R. + #.008 RO2-N. + #.084 GLY + #.238 MGLY + #.139 BACL + #.161 CRES + #.054 BALD + #.572 DCB1 + #.06 DCB2 + #.145 DCB3 + #1.697 XC	1.37e-11			

Table B-1 (continued)

Compound	Reaction and Products [a]	Rate Parameters [b]			
		k(298)	A	Ea	B
p-Xylene	P-XYLENE + HO. = #.188 HO2. + #.804 RO2-R. + #.008 RO2-N. + #.195 GLY + #.112 MGLY + #.188 CRES + #.083 BALD + #.709 DCB1 + #.012 DCB3 + #2.432 XC	1.43e-11			
1,2,3-Trimethyl Benzene	123-TMB + HO. = #.186 HO2. + #.804 RO2-R. + #.01 RO2-N. + #.065 GLY + #.166 MGLY + #.383 BACL + #.186 CRES + #.044 BALD + #.533 DCB1 + #.077 DCB2 + #.149 DCB3 + #1.904 XC	3.27e-11			
1,2,4-Trimethyl Benzene	124-TMB + HO. = #.186 HO2. + #.804 RO2-R. + #.01 RO2-N. + #.063 GLY + #.364 MGLY + #.079 BACL + #.186 CRES + #.044 BALD + #.733 DCB1 + #.027 DCB3 + #2.73 XC	3.25e-11			
1,3,5-Trimethyl Benzene	135-TMB + HO. = #.186 HO2. + #.804 RO2-R. + #.01 RO2-N. + #.621 MGLY + #.186 CRES + #.025 BALD + #.569 DCB1 + #.097 DCB2 + #.114 DCB3 + #2.273 XC	5.75e-11			
Naphthalene	NAPHTHAL + HO. = #.236 HO2. + #.215 RO2-R. + #.07 RO2-N. + #.479 RCO-O2. + #.084 GLY + #.236 PHEN + #.117 DCB1 + #.049 DCB2 + #.049 DCB3 + #5.601 XC	2.16e-11	1.07e-12	-1.78	
Methyl Naphthalenes	ME-NAPH + HO. = #.236 HO2. + #.155 RO2-R. + #.07 RO2-N. + #.539 RCO-O2. + #.084 GLY + #.038 MGLY + #.236 CRES + #.003 DCB1 + #.076 DCB2 + #.076 DCB3 + #6.259 XC	5.20e-11			
Tetralin	TETRALIN + HO. = #.6 HO2. + #.108 RO2-R. + #.129 RO2-N. + #.163 RCO-O2. + #.084 GLY + #.6 PHEN + #.016 DCB1 + #.046 DCB2 + #.046 DCB3 + #4.446 XC	3.43e-11			
2,3-Dimethyl Naphthalene	23-DMN + HO. = #.236 HO2. + #.094 RO2-R. + #.07 RO2-N. + #.6 RCO-O2. + #.084 GLY + #.076 MGLY + #.236 CRES + #.103 DCB2 + #.103 DCB3 + #6.709 XC	7.68e-11			

[a] Format of reaction listing: “=” separates reactants from products; “#number” indicates stoichiometric coefficient, “#coefficient { product list }” means that the stoichiometric coefficient is applied to all the products listed.

[b] The rate constants are given by  $k(T) = A \cdot (T/300)^B \cdot e^{-E_a/RT}$ , where the units of k and A are  $\text{cm}^3 \text{molec}^{-1} \text{s}^{-1}$ , Ea are  $\text{kcal mol}^{-1}$ , T is  $^{\circ}\text{K}$ , and  $R=0.0019872 \text{ kcal mol}^{-1} \text{deg}^{-1}$ . The following special rate constant expressions are used:

## APPENDIX C. CHAMBER EXPERIMENT LISTING

Table C-1. Summary chamber experiments relevant to this project.

Run [a]	Date	Type [b]	Purpose and Applicable Conditions	Results
		Experiments carried out using arc lights unless indicated otherwise		
536	3/16/06	Pure Air Irradiation	Determination of background effects. No injections made. PM data questionable.	Only ~ 0.3 ppb/hour O <sub>3</sub> formed on both sides. Results generally consistent with predictions using standard chamber model. No PM formation observed, which is consistent with other pure air experiments, so PM data are questionable and were not used.
537	3/17/06	CO - NO <sub>x</sub>	Determination of chamber radical source. ~15 ppb NO <sub>x</sub> and ~35 ppm CO injected into both reactors.	Results consistent with assuming HONO offgasing, NO <sub>2</sub> photolysis rate ratios of 5 and 4 ppt for Sides A and B, respectively, which is in normal range.
547	4/10/06	1,3-Dichloropropenes-NO <sub>x</sub> (Vary NO <sub>x</sub> )	Mechanism evaluation for dichloropropenes in absence of other VOC reactants. ~400 ppb dichloropropenes injected on both sides; 24 ppb NO <sub>x</sub> on Side A and 46 ppb NO <sub>x</sub> on Side B. Blacklight light source used	Results on Table 18 and Figure 18
548	4/11/06	1,3-Dichloropropenes-NO <sub>x</sub> + Propane	Mechanism evaluation for dichloropropenes with added propane to determine the effect of a compound that reacts rapidly with Cl atoms but not OH radicals. ~380 ppb dichloropropenes and 22 ppb NO <sub>x</sub> injected into both sides. 0.3 and 0.12 ppm propane injected into Sides A and B, respectively.	Results on Table 18 and Figure 19
549	4/12/06	MIR Surrogate Side Equivalency Test	Standard MIR surrogate - NO <sub>x</sub> mixture irradiated in both sides to test for side equivalency	Satisfactory side equivalency obtained. Results on Table 17.
550	4/13/06	MIR Surrogate + 1,3-Dichloropropenes	Incremental reactivity experiment using the standard MIR surrogate - NO <sub>x</sub> base case. ~100 ppb dichloropropenes added to Side A	Results on Table 17 and Figure 20.



Table C-1 (continued)

Run [a]	Date	Type [b]	Purpose and Applicable Conditions	Results
551	4/14/06	Dichloropropenes-NO <sub>x</sub> (Vary NO <sub>x</sub> )	Mechanism evaluation for dichloropropenes in absence of other VOC reactants. ~375 ppb dichloropropenes injected on both sides; 23 ppb NO <sub>x</sub> on Side A and 46 ppb NO <sub>x</sub> on Side B. Comparable to run 547 except arc lights used.	Results on Table 18 and Figure 18
554	4/17/06	MOIR/2 Surrogate + 1,3-Dichloropropenes	Incremental reactivity experiment using the standard MOIR/2 surrogate - NO <sub>x</sub> base case. ~100 ppb dichloropropenes added to Side B	Results on Table 17 and Figure 20.
555	4/18/06	MIR Surrogate + 1,3-Dichloropropenes	Standard MIR surrogate - NO <sub>x</sub> experiment with ~50 ppb dichloropropenes added to Side B	Results on Table 17 and Figure 20.
578	5/11/06	Pure Air Irradiation	Determination of background effects. No injections made.	~ 2 ppb O <sub>3</sub> formed on both sides, consistent with previous pure air run and predictions of standard chamber model. Less than 1 µg/m <sup>3</sup> PM formation on both sides.
581	5/17/06	MIR Surrogate + EPTC	Standard MIR surrogate - NO <sub>x</sub> experiment with ~80 ppb EPTC added to Side A.	Results on Table 17, Figure 17, Figure 18, and Table 15.
582	5/18/06	Pure Air Irradiation	Determination of background effects and contamination by EPTC. No injections made.	~0.6 ppb/hour O <sub>3</sub> formed on both sides, somewhat more than observed previously. ~1 µg/m <sup>3</sup> PM formation on both sides, only slightly more than observed previously. Results consistent with predictions of standard chamber model.
583	5/19/06	MOIR/2 Surrogate + EPTC	Standard MOIR/2 surrogate - NO <sub>x</sub> experiment with ~25 ppb EPTC (measured) added to Side B. Not all the intended EPTC was injected, making the amount present somewhat uncertain.	Results on Table 17, Figure 17, and Figure 18
584	5/22/06	MOIR/2 Surrogate + EPTC	Standard MOIR/2 surrogate - NO <sub>x</sub> experiment with 120 ppb EPTC added to Side B.	Results on Table 17, Figure 17, Figure 18, and Table 15.
585	5/23/06	CO-NO <sub>x</sub>	Determination of chamber radical source. ~25 ppb NO <sub>x</sub> and ~40 ppm CO injected into both reactors.	Results consistent with assuming HONO offgassing, NO <sub>2</sub> photolysis rate ratios of 8 and 11 ppt for Sides A and B, respectively, which is higher than other such runs during this period but within the normal range.

Table C-1 (continued)

Run [a]	Date	Type [b]	Purpose and Applicable Conditions	Results
586	5/24/06	MIR Surrogate + EPTC	Standard MIR surrogate - NO <sub>x</sub> experiment with 160 ppb EPTC added to Side A.	Results on Table 17, Figure 17, Figure 18, and Table 15.
587	5/26/06	MIR Surrogate + MITC	Standard MIR surrogate - NO <sub>x</sub> experiment with 170 ppb MITC added to Side A.	Results on Table 17, Figure 12, Figure 14, and Table 14.
588	5/31/06	MIR Surrogate + MITC	Standard MIR surrogate - NO <sub>x</sub> experiment with 770 ppb MITC added to Side B.	Results on Table 17, Figure 12, Figure 13, Figure 14, and Table 14.
589	6/1/06	MOIR/2 Surrogate + MITC	Standard MOIR/2 surrogate - NO <sub>x</sub> experiment with 1.05 ppm MITC added to Side B.	Results on Table 17, Figure 12, Figure 13, Figure 14, and Table 14.
590	6/5/06	MOIR/2 Surrogate + EPTC	Standard MOIR/2 surrogate - NO <sub>x</sub> experiment with 245 ppb EPTC added to Side B.	Results on Table 17, Figure 17, Figure 18, and Table 15.
591	6/6/06	MIR Surrogate + CS <sub>2</sub>	Standard MIR surrogate - NO <sub>x</sub> experiment with ~550 ppb CS <sub>2</sub> added to Side A.	Results on Table 17 and Figure 15.
592	6/7/06	MOIR/2 Surrogate + CS <sub>2</sub>	Standard MOIR/2 surrogate - NO <sub>x</sub> experiment with ~650 ppb CS <sub>2</sub> added to Side B.	Run ended before 2 hours of irradiation because of arc light failure. Results on Table 17 and Figure 15.
		Arc light not operational during this period. Blacklights used for all subsequent runs for this project.		
597	6/15/06	MOIR/2 Surrogate + CS <sub>2</sub>	Standard MOIR/2 surrogate - NO <sub>x</sub> experiment with ~630 ppb CS <sub>2</sub> added to Side B.	Results on Table 17 and Figure 15.
598	6/16/06	MIR Surrogate + CS <sub>2</sub>	Standard MIR surrogate - NO <sub>x</sub> experiment with ~350 ppb CS <sub>2</sub> added to Side A.	Results on Table 17 and Figure 15.
599	6/19/06	MOIR/2 Surrogate + MITC	Standard MOIR/2 surrogate - NO <sub>x</sub> experiment with ~900 ppb MITC added to Side B. Formaldehyde data available for this run to determine if it is formed from MITC.	Results on Table 17, Figure 12, Figure 13, Figure 14, and Table 14.
600	6/20/06	MIR Surrogate + Kerosene	Standard MIR surrogate - NO <sub>x</sub> experiment with ~1 ppmC kerosene added to Side B.	Results on Table 17 and Figure 23.
601	6/21/06	CO - Air	Determination of chamber NO <sub>x</sub> offgasing rate. ~50 ppm CO injected into both reactors.	Results consistent with assuming HONO offgasing, NO <sub>2</sub> photolysis rate ratios of 7 and 8 ppt for Sides A and B, respectively, which is in normal range.

Table C-1 (continued)

Run [a]	Date	Type [b]	Purpose and Applicable Conditions	Results
602	6/22/06	MOIR/2 Surrogate + Kerosene	Standard MOIR/2 surrogate - NO <sub>x</sub> experiment with ~ 1 ppmC kerosene added to Side A.	Results on Table 17 and Figure 23.
603	6/23/06	MOIR/2 Surrogate + Kerosene	Standard MOIR/2 surrogate - NO <sub>x</sub> experiment with ~ 0.5 ppmC kerosene added to Side B.	Results on Table 17 and Figure 23.
604	6/23/06	Pure Air Irradiation	Determination of background effects and contamination by kerosene. No injections made.	Approximately 0.7 ppb/hour O <sub>3</sub> formed on both sides, similar to previous experiment. 1 and 1.5 µg/m <sup>3</sup> PM formed on Sides A and B, respectively.
606	6/26/06	MOIR/2 Surrogate Side Equivalency Test	Standard MOIR/2 surrogate - NO <sub>x</sub> mixture irradiated in both sides to test for side equivalency	Satisfactory side equivalency obtained. Results on Table 17.
607	6/27/06	MIR Surrogate + Kerosene	Standard MIR surrogate - NO <sub>x</sub> experiment with ~ 1 ppmC kerosene added to Side A.	Results on Table 17 and Figure 23.

[a] EPA Chamber run number. Gaps in run numbers reflect experiments carried out for other projects, or experiments that were aborted because of equipment or instrumentation problems, and that are not expected to affect the characterization results.

[b] Unless indicated otherwise, "Surrogate" refers to the 8-component "Full Surrogate" as used in previous environmental chamber incremental reactivity studies in our laboratories, except that formaldehyde was removed and the other ROG components were increased by 10% to yield approximately the same reactivity as discussed by Carter and Malkina (2005). The designation "MIR Surrogate" refers to experiments with 0.55 ppmC base case surrogate and 30 ppb NO<sub>x</sub>. The designation "MOIR/2 Surrogate" refers to experiments with 1.1 ppmC base case surrogate and 25 ppb NO<sub>x</sub>.